Aus dem Lehrstuhl Physiologische Chemie, Biomedizinisches Centrum,
Institut der Ludwig-Maximilians-Universität München
Vorstand: Prof. Andreas Ladurner, PhD

The Regulatory Effects of Glucose Metabolites on the Transcription Factor ChREBP

Transcription Factor ChREBP Directly Senses Metabolic Intermediates

Dissertation
zum Erwerb des Doktorgrades der Naturwissenschaften
an der Medizinischen Fakultät der
Ludwig-Maximilians-Universität zu München

vorgelegt von
Thomas Pysik
aus
Biberach an der Riß
Jahr
2019

Betreuer:	Prof. Andreas Ladurner, PhD
	_____
Zweitgutachter:	Prof. Dr. rer. nat. Alexander Bartelt
Dekan:	Prof. Dr. med. dent. Reinhard Hickel
Tag der mündlichen Prüfung:	16.06.2020

Abstract

From an evolutionary point of view, it was always beneficial to store an excess of sugars, especially glucose in body fat and glycogen, thereby providing thermal insulation, mechanical protection, a stable resource of energy and a constant level of blood glucose. However, the massive increase in carbohydrate consumption over the last century has resulted in an epidemic of diseases linked to metabolism, such as diabetes, obesity, cardiovascular diseases, liver damage and cancer. Since most of these diseases are based on the storage of excessive sugars in the form of fatty acids and lipids, it is fundamental for our health to understand the regulatory mechanisms involved in these processes. Insulin-signaling is one of the best studied systems of how the body copes with increased levels of blood-glucose, keeping it at a constant level. Over the last decade glucose and its metabolites have come into focus of research as a signaling molecule. Studies have shown that increased levels of glucose and glucose-6-phosphate are responsible for the activation of genes involved in lipogenesis and glycolytic pathways. How this signal is sensed by the cell and translated into a physiological response is still not fully understood.

In my PhD project we show the direct interaction of a glucose metabolite with the transcription factor carbohydrate-response element-binding protein (ChREBP), which results in structural changes of the ChREBP glucose-sensing module (GSM). Therefore, ChREBP acts as a cellular receptor for glucose levels and its activation results in the expression of lipogenic and glycolytic target genes. So far, no such intracellular receptor for glucose has been reported. The methods developed in this thesis will help to understand the cellular responses to an increase in glucose levels and the ability to screen for modulators of these responses. Therefore, this work makes an important contribution to our understanding of sugar-mediated fat synthesis and obesity.

Zusammenfassung

Aus evolutionärer Sicht war es immer von Vorteil überschüssigen Zucker, hauptsächlich Glukose, in Form von Fett und Glycogen im Körper zu speichern. Dieser Energiespeicher dient nicht nur als Stabilisator des Blutzuckers, sondern auch der thermischen Isolation sowie mechanischem Schutz. Der massive Anstieg am Verzehr von Kohlenhydraten innerhalb des letzten Jahrhunderts führte jedoch zu einer Epidemie an Stoffwechselerkrankungen wie Diabetes, Fettleibigkeit, Herz-Kreislaufstörungen, Leberschäden und Krebs. Da diesen Erkrankungen meist eine verstärkte Synthese an Körperfetten zugrunde liegt, ist es für die Gesundheit von enormer Bedeutung zu verstehen wie genau die Fettsynthese reguliert wird. Der Insulinabhängige Signalweg zur Steuerung des Blutzuckerspiegels ist einer der best erforschten Mechanismen im Zuckerstoffwechsel. Neben Insulin gerieten über die Jahre jedoch auch Glukose und dessen Abbauprodukte selbst in den Fokus der Erforschung neuer regulativer Signalwege. So zeigten Studien, dass ein Anstieg an intrazellulärer Glukose und Glukose-6-Phosphat für die Aktivierung von im Fettstoffwechsel involvierter Genen verantwortlich sind. Wie Zellen dieses Signal messen und in eine physiologische Antwort umwandeln ist jedoch noch immer nicht vollständig geklärt.

In dieser Arbeit wird eine direkte Interaktion zwischen eines Glukosemetaboliten mit dem Transkriptionsfaktor carbohydrate-response element-binding protein (ChREBP) beschrieben. Diese Interaktion verursacht spezifische Veränderungen in der Proteinstruktur des Glucose-sensing module (GSM) von ChREBP. ChREBP fungiert daher wie ein Rezeptor, oder auch Sensor, für den intrazellulären Glukosespiegel. Ist dieser Sensor aktiviert resultiert dies unter anderem in der Expression von Genen welche für die Lipidsynthese, sowie Glycolyse, benötigt werden. Bis zum heutigen Zeitpunkt war uns kein solcher intrazellulärer Rezeptor für Glukose bekannt. Die in dieser Thesis entwickelten Methoden helfen die zelluläre Antwort auf ansteigende Glukosespiegel zu verstehen und eröffnen die Möglichkeit Modulatoren dieser Antwort zu finden. Aus diesem Grund ist diese Arbeit ein wichtiger Beitrag im Kampf gegen Fettleibigkeit und

die mit ihr einhergehenden Erkrankungen.

Acknowledgments

I would like to acknowledge my supervisor Andreas Ladurner for giving me the opportunity to work on this challenging, but also rewarding project. He gave me the space to develop and follow new approaches and ideas. His support not only pushed the project, but also pushed me to mature as a scientist and colleague.

I thank Daria Zinne and Andrew Bowman. Without their initial research and advice, this work would not have been possible. Mehera Emrich and Hui-Lan Huang for their great work on the *in vivo* site of the project, as well as for fruitful scientific discussion and advise. Nina Heppner and Rebecca Deutsch, two excellent students. It was a great experience and fun working with you. Your natural talent for science made supervision easy. Their work was in great support for this thesis.

Thanks to Joana Veiga and Kasper Rand from the University of Copenhagen having the patience introducing me to the field of HDX-MS. I thank Michaela Smolle for providing state-of-the-art equipment in the BMC core facility for biophysics. As well as the AG Klein and AG Becker for the use of their isotope labs and equipment. I thank all the technicians of the department for being supportive, wherever possible. Anton Eberharter and Christine Werner for providing an environment that allowed me to focus on research.

I thank Carla Margulies, Teresa Burrell, Hui-Lan Huang and Ava Handley for getting me started in the lab and the field of gene regulation and metabolism.

Dejana Mokranjac, Rupa Banerjee, Umut Gunsel for the time sharing a lab with you. Your technical expertise, advice and humor always helped me out when I was stuck.

The group of Andreas Ladurner, as well as the department for great scientific discussions and Christmas parties.

Special thanks to Sandra Esser, Hui-Lan Huang, Rupa Banerjee, Umut Gunsel, Marcel Genge, Petra Robisch and Flavia Söllner for becoming great friends, making the move to Munich something I do not want to miss.

Einen besonderen Dank meinen Eltern und Geschwistern für die unermüdliche Unterstützung und den nötigen Rückhalt. Einen herzlichen Dank an Maike Bühler für den Zusammenhalt der letzten Jahre, sowie Geduld und Verständnis. Diese Arbeit wäre ohne Euere Unterstützung nur schwer möglich gewesen.

LMU LUDWIG-MAXIMILIANS-UNIVERSITÄT MÜNCHEN

Promotionsbüro
Medizinische Fakultät

MMRS

Eidesstattliche Versicherung

Pysik, Thomas

Name, Vorname

Ich erkläre hiermit an Eides statt,

dass ich die vorliegende Dissertation mit dem Titel

The Regulatory Effects of Glucose Metabolites on the Transcription Factor ChREBP

selbständig verfasst, mich außer der angegebenen keiner weiteren Hilfsmittel bedient und alle Erkenntnisse, die aus dem Schrifttum ganz oder annähernd übernommen sind, als solche kenntlich gemacht und nach ihrer Herkunft unter Bezeichnung der Fundstelle einzeln nachgewiesen habe.

Ich erkläre des Weiteren, dass die hier vorgelegte Dissertation nicht in gleicher oder in ähnlicher Form bei einer anderen Stelle zur Erlangung eines akademischen Grades eingereicht wurde.

München, den 06-Jul-2020

Ort, Datum

Thomas Pysik

Unterschrift Doktorandin bzw. Doktorand

Contents

1 Introduction 1

1.1 Transcriptional regulation of metabolism 1

1.1.1 Making the DNA-code accessible for protein expression 1

1.1.2 Transcription factors regulating and regulated by metabolism 3

1.1.3 ChREBP is regulated by glucose levels 8

1.2 Medical relevance of studying ChREBP 9

1.3 Physiological function and phenotypes of ChREBP 10

1.4 Domain architecture and conservation 12

1.4.1 The Glucose Sensing Module is responsive to changes in glucose levels 12

1.4.2 Polymorphism in the GSM is associated with reduction in plasma triglyceride levels 15

1.4.3 The hyperactive brother ChREBP-β 16

1.4.4 The C-terminal basic helix-loop-helix/Zip domain recognizes ChREBP target genes 17

1.5 Regulation of ChREBP activity 18

1.5.1 Cellular localization of ChREBP 19

1.5.2 Protein-Protein interactions 20

1.5.3 Role of post-translational modifications in ChREBP activity 25

1.5.4 Role of metabolites in ChREBP activity 27

2 Aims of this Study 33

3 Materials and Methods 35

3.1 Cloning of expression vectors 35

3.1.1 Standard PCR protocol 35

3.1.2 Agarose Gel Electrophoresis 35

3.1.3 Gel Extraction 36

3.1.4 Restriction Digest 36

3.1.5 Reaction Clean-Up . . . 36
3.1.6 Plasmid Mini-Prep . . . 36
3.1.7 Plasmid Midi-Prep . . . 37
3.1.8 Ligation . . . 37
3.1.9 Transformation . . . 37
3.1.10 Cloning of final expression vector of 14-3-3/GSM . . . 37
3.1.11 Cloning of point mutants . . . 39
3.1.12 Cloning expression vector for Importin-α1 and Δ70 Importin-α1 . . . 40
3.1.13 Cloning expression vector for Glms . . . 41
3.2 Recombinant Protein Expression and Purification . . . 41
3.2.1 Protein Expression . . . 41
3.2.2 Protein Purification . . . 41
3.2.3 Analytical size exclusion chromatography for complex determination . . . 46
3.2.4 Analytical ultracentrifugation for complex size determination . . . 46
3.2.5 Determination of Protein Concentration . . . 47
3.3 Isothermal Calorimetry . . . 48
3.4 Label-Free Microscale Thermophoresis . . . 49
3.4.1 Buffer Screen . . . 49
3.4.2 MST binding experiments . . . 49
3.5 Limited proteolysis . . . 50
3.5.1 Test of different proteases for limited proteolysis . . . 50
3.5.2 Limited proteolysis Glc6P: Titration . . . 50
3.5.3 Limited proteolysis: Competition with AMP . . . 51
3.5.4 Limited Proteolysis W127A GSM-Mutant . . . 51
3.5.5 Limited Proteolysis in Presence of different Metabolites 51
3.6 Hydrogen-Deuterium exchange mass- spectrometry . . . 52
3.6.1 Hydrogen-Deuterium Exchange . . . 52
3.6.2 Liquid Chromatography and Mass Spectrometry . . . 53
3.6.3 Data Analysis . . . 53
3.6.4 Statistical Analysis . . . 54
3.7 Circular-Dichroism Spectroscopy . . . 55
3.8 Metabolite Structures . . . 55

3.9 Scintillation-Proximity Assay 56
3.9.1 SPA experiments for assay set-up 56
3.9.2 Metabolite screening for tritium labeled Glucose-6-phosphate (^{3}H-Glc6P) competition 57
3.9.3 Competition experiments- titration curve 58
3.10 Intrinsic fluorescence 59
3.11 SDS-PAGE 60
3.12 Buffers and Media 61
3.12.1 Buffers for protein purification 61
3.12.2 Working buffers and solutions 61
3.12.3 Buffers and Solvents for HDX-MS 62
3.12.4 Media 62

4 Results 65
4.1 Expression and Purification of 14-3-3/GSM 65
4.1.1 Testing an single chain construct of 14-3-3/GSM for binding to Glc6P 65
4.1.2 Purification of 14-3-3 67
4.1.3 Using the pET-Duet1 expression vector for co-expression of 14-3-3/GSM 69
4.1.4 Purification of 14-3-3/GSM 71
4.2 14-3-3/GSM is a trimeric complex 73
4.3 14-3-3/GSM binds Glc6P 75
4.3.1 Isothermal calorimetry shows binding of Glc6P to 14-3-3/GSM 75
4.3.2 Label-free microscale thermophoresis confirms binding of Glc6P 78
4.4 Binding of AMP to 14-3-3/GSM competes with Glc6P binding . 82
4.4.1 Differences in binding between AMP and Glc6P 82
4.4.2 Mutations of the AMP binding site affects binding of AMP and Glc6P 85
4.4.3 The SNP Q241H does not affect binding of Glc6P or AMP 88
4.4.4 Mutants tested for metabolite binding were able to form a stable complex 88
4.5 Metabolite Specificity 89
4.5.1 Screening for the best scintillation-proximity assay conditions 89

4.5.2 Competition experiments are in line with previous binding assays . . . 92
4.5.3 Scree of biological relevant metabolites for 14-3-3/GSM binding shows highest affinity for Glc6P . . . 92
4.5.4 ITC experiments with different metabolites confirm findings of SPA . . . 96
4.5.5 Chemical space of ligands . . . 98
4.6 Binding of Glc6P causes distinct structural changes . . . 101
4.6.1 Limited proteolysis to detect structural changes . . . 101
4.6.2 Secondary structure composition is not altered by Glc6P binding . . . 107
4.6.3 Binding of metabolites does not affect tryptophan fluorescence . . . 109
4.6.4 Hydrogen-Deuterium Exchange Mass Spectrometry . . . 111
4.7 Potential protein interactions of the 14-3-3/GSM complex . . . 116
4.7.1 Binding of Importin-α in dependence of Glc6P . . . 116
4.7.2 *E.coli* Glms contaminant or relevant interaction partner? 117

5 Discussion 121

6 Summary and outlook 127

7 Appendix 129
7.1 Results . . . 130
7.2 Additional Materials, Chemicals and Laboratory Equipment . . . 131
7.2.1 Equipment . . . 131
7.2.2 Primers . . . 141
7.3 Canonical protein sequences of full length proteins . . . 141
7.3.1 Mounse ChREBP, Q99MZ3 . . . 141
7.3.2 Mouse MondoA, Q2VPU4 . . . 142
7.3.3 *Drosophila melanogaster* (*D. melanogaster*) Mondo/Mio, Q9VID4 . . . 142
7.3.4 Mouse 14-3-3β, Q9CQV8 . . . 143
7.4 Protein sequences for expressed constructs . . . 144
7.5 Vectors generated in support of this work . . . 144

Bibliography 148

List of Tables

1.1 Table of post-translational modifications and their functions . . 27

3.1 PCR reaction mix 35
3.2 Restriction digest 36
3.3 DNA Ligation mix 37
3.4 PCR 1 to introduce point mutation (Sectio A/B) 39
3.5 PCR 2 40
3.6 Primers for site directed mutagenesis 40
3.7 Parameters for determination of protein concentrations 47
3.8 Protease test, reaction mix set-up 50
3.9 LiP W127A reaction mix set-up 51
3.10 List of Metabolite Structures 56
3.11 Table of SPA additives 57

4.1 ChREBP expression vectors based on pET-Duet1 69
4.2 Complex size and elution volumes 73
4.3 Overview of generated mutants 86
4.4 ITC Results for ligands that show binding 96
4.5 Result table CD-spectroscopy 107
4.6 Summary HDX experiments in presence of Glc6P and AMP . . 116

7.1 ITC Result table mutants 130
7.2 Table of laboratory equipment used 132
7.3 Table of chemicals and consumables 138
7.4 Metabolites used for binding experiments 140
7.5 Table of additional primers used in this thesis 141
7.6 Table of vectors created during this PhD 147

List of Figures

1.1 Key steps of gene transcription and translation 2
1.2 Regulation of transcription factors by insulin and glucose 4
1.3 Mammalian SREBP pathway 5
1.4 ChREBP target genes are involved in a variety of glycolytic and lipogenic pathways 8
1.5 Transcriptional regulation of FAS 9
1.6 Domain organization of ChREBP 12
1.7 Sequence alignment of mouse ChREBP-α, MondoA and *Drosophila* Mondo GSM 14
1.8 The GSM is partially disordered 15
1.9 Distribution of Q241H in the old world 16
1.10 Domain Comparison between ChREBP-α and ChREBP-β . . . 17
1.11 Orientation of the bHLH/Zip domains 18
1.12 Overview of ChREBP activity and localization 19
1.13 Phosphorylation independent interaction of 14-3-3 with the α2-helix of ChREBP 22
1.14 Overview of post-translational modifications regulating ChREBP activity 26
1.15 Structure of AMP bound to 14-3-3/GSM 29
1.16 Hinge model of ChREBP activation 31

3.1 Vectormap 14-3-3/GSM 38
3.2 Schematic representation of cloning strategy 39
3.3 Basics of an ITC experiment 48

4.1 Single chain construct of 14-3-3/GSM reveals binding of Glc6P 66
4.2 Purification of 14-3-3 68
4.3 Test Expression and purification of ChREBP pet-Duet constructs 70
4.4 Purification of 14-3-3/GSM 72
4.5 SEC and AUC indicate that 14-3-3/GSM is a trimeric complex . 74

4.6 ITC shows binding of Glc6P to 14-3-3/GSM 76
4.7 Analysis of samples before and after ITC shows mild aggregation 78
4.8 Buffer screen for MST measurements 79
4.9 MST analysis shows binding of Glc6P to 14-3-3/GSM 81
4.10 Binding of AMP and Glc6P to 14-3-3/GSM 83
4.11 Binding kinetics of AMP and Glc6P 84
4.12 Truncated GSM shows distinct differences in binding compared to full-length GSM 85
4.13 Mutations of the AMP binding site affects metabolite binding . . 87
4.14 SNP Q241H does not affect metabolite binding 88
4.15 Analytical size exclusion chromatography of mutants 89
4.16 Design of the scintillation proximity assay 90
4.17 Determination of SPA conditions 91
4.18 SPA titration experiment 93
4.19 Metabolite screen for ChREBP binding 95
4.20 ITC of 14-3-3/GSM and metabolites identified in SPA 97
4.21 Structure of tested metabolites in SPA and ITC 99
4.22 Critical functional-groups and positions for binding 100
4.23 Testing of different proteases for limited proteolysis 102
4.24 Metabolite titrations for limited proteolysis 103
4.25 LiP of W127A 104
4.26 LiP of W127A 106
4.27 CD-spectra of 14-3-3/GSM 108
4.28 Effect of ligand binding on intrinsic fluorescence 110
4.29 Peptide coverage of the GSM under HDX-MS conditions 111
4.30 Deuterium uptake in presence of AMP compared to control . . . 113
4.31 Deuterium uptake in presence of Glc6P compared to control . . 115
4.32 Test for interaction between 14-3-3/GSM and Importin 118
4.33 Test for interaction of 14-3-3/GSM and Glms 119

5.1 Model of regulation of ChREBP activity by metabolite binding . 122

List of Abbreviations

^{3}H-AMP	tritium labeled adenosine 5'-monophosphate	90
^{3}H-Glc6P	tritium labeled Glucose-6-phosphate	XI
A_{280}	absorption at a wavelength of 280nm	77
aa	amino acid	55
Acc1	acetyl CoA carboxylase 1	10
AUC	analytical ultracentrifugation	46
bHLH/Zip	basic helix-loop-helix/Zip	5
cAMP	cyclic-AMP	82
ChoRE	carbohydrate response element	8
ChREBP	carbohydrate-response element-binding protein	I
cpm	counts per minute	92
D. melanogaster	*Drosophila melanogaster*	XII
D_2O	dideuterium monoxide, heavy water	62
DTT	dithiothreitol	46
E. coli	*Escherichia coli*	37
EDTA	ethylenediaminetetraacetic acid	90
F2,6bP	fructose-2,6-bisphosphate	30
Fasn	fatty acid synthase	10
Glc6P	glucose-6-phosphate (G6P)	13
GlcNAc	N-acetylglucosamine	26
GRACE	glucose-response activation domain	12
GSM	glucose-sensing module	I
H_2O	water	

HEPES	4-(2-hydroxyethyl)-1-piperazineethanesulfonic acid	62
IC_{50}	half maximal inhibitory concentration	59
IPTG	isopropyl-β-D-thiogalactoside	69
ITC	isothermal calorimetry	75
K_D	equilibrium constant of dissociation	48
K_{off}	dissociation constant	82
K_{on}	association constant	82
LID	low-glucose inhibitory domain	12
Lpk	liver type pyruvate kinase	10
Mlx	Max-like protein X	17
MST	micro scale thermophoresis	78
Mw	molecular weight	46
NES	nuclear export signal	13
NLS	nuclear localization signal	13
OD_{600}	optical density at a wavelength of 600nm	41
OGT	O-GlcNAc transferase	24
PKA	protein kinase A	25
PP2A	protein- phosphatase 2A	28
PPP	pentose phosphate pathway	27
RT	room temperature	58
SDS-PAGE	sodium dodecyl sulfate-polyacrylamide gel electrophoresis	60
SEC	size exclusion chromatography	67
SNP	single-nucleotide polymorphism	88
SPA	scintillation proximity assay	62
wt	wild type	85
X5P	xylulose-5-phosphate	20

1 Introduction

1.1 Transcriptional regulation of metabolism

1.1.1 Making the DNA-code accessible for protein expression

Each cell of an organism contains the same genetic information (with some exceptions). By regulating the expression of this information in a spatial and temporal manner, different cell types are established during the development of an organism. DNA is thus the blue-print of life. To make this information usable for the expression of proteins, the RNA polymerase II enzyme reads the information encoded by DNA and transcribes it into the messenger molecule RNA (mRNA). For access and migration of the RNA polymerase, additional factors are required (see Figure 1.1B). The synthesized mRNA is then further processed and translated by the ribosome into a chain of amino acids, the building blocks of proteins (see Figure 1.1A and C).

To make sure only a specific set of DNA (genes) is transcribed into protein, the initiating process of RNA synthesis has to be tightly regulated. The main regulatory mechanism is the accessibility of RNA polymerases to the transcription start sit. For the majority of genes this access is impaired by chromatin (DNA wrapped around nucleosomes) [Cramer, 2019, Fuda et al., 2009]. To target RNA polymerase to the transcription start site, nucleosomes have to be (partially) removed and/or the affinity for the polymerase has to be increased to enable the initiation of transcription [Cramer, 2019, Lorch and Kornberg, 2015, Knezetic and Luse, 1986, Lorch et al., 1987]. There are three major mechanism described in how the cell achieves the opening of DNA and the recruitment of the RNA polymerase:

First, the TATA box which can be found upstream of transcription start sites is a short T and A rich DNA motif. This motif is recognized by a TATA box binding protein, resulting in initiation of the recruitment and assembly of the RNA Pol II complex [Burley, 1996]. Other core promotor DNA elements work similarly.

A

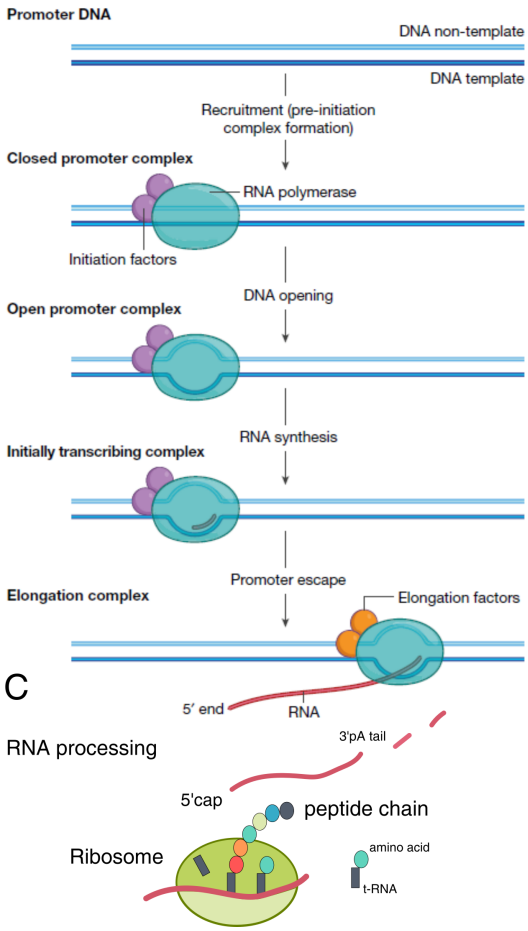

B

Transcription phase	Factor (no. of subunits)	Function
Initiation	TFIIB (1)	Bridges between Pol II and promoter DNA
	TFIID (14)	Contributes to promoter DNA recognition and includes TBP
	TFIIE (2)	Activates TFIIH and stabilizes the open promoter complex
	TFIIF (2)	Stabilizes TFIIB and the PIC
	TFIIH (10)	Catalyses DNA opening and Pol II CTD phosphorylation, and stimulates promoter escape
	Mediator (about 35)	Bridges between transcription factors and the PIC, stimulates CDK7 and can function in early elongation regulation
Elongation	DSIF (2)	Enables Pol II pausing and active elongation, and recruits elongation and 3′ processing factors
	Capping enzymes (3)	Catalyses 5′ RNA cap formation, and prevents pre-mRNA degradation by 5′ exonucleases
	NELF (4)	Stabilizes promoter-proximally paused Pol II
	P-TEFb (2)	Triggers activation of promoter-proximally paused Pol II by phosphorylating Pol II and elongation factors
	SEC (6)	Contains P-TEFb and ELL, a positive elongation factor
	SPT6 (1)	Recognizes phosphorylated CTD linker, and stimulates elongation
	PAF (5 or 6)	Stimulates elongation, and recruits chromatin-modifying enzymes
	CHD1 (1)	Remodels nucleosomes co-transcriptionally, and is ATP-dependent
	FACT (2)	Histone chaperone that facilitates nucleosome passage
	SET1 complex (7)	Histone methyltransferase that targets histone H3 lysine-4
	SET2 (1)	Histone methyltransferase that targets histone H3 lysine-36
	TFIIS (1)	Stimulates RNA cleavage, improves RNA proofreading and restarts arrested Pol II with backtracked RNA
Termination	CPSF (14)	Recognizes poly-adenylation sequence, cleaves pre-mRNA and dephosphorylates transcription machinery
	CStF (5)	Binds Pol II CTD and contributes to RNA binding
	XRN2 complex (3)	'Torpedo' nuclease complex that degrades cleaved, nascent RNA from the 5′ end and terminates Pol II transcription

Figure 1.1: **Key steps of gene transcription and translation**
A: Schematic representation of key steps in transcription. Binding or RNA polymerase, opening of DNA and elongation of RNA. B: Additional factors required for initiation, elongation and termination. C: Schematic representation of mRNA translation by the ribosome to a polypeptide chain. Single amino acids are transported by t-RNA to the ribosome, where the growing peptide chain is transferred onto the new arrived amino acid. Modified from [Cramer, 2019], permission granted by Springer Nature.

Second, CpG islands are often found in genes required for all cell types (house keeping genes)[Deaton and Bird, 2011, Cramer, 2019]. The enrichment of C and G in promotor regions has an inhibitory effect on the occupancy by nucleasome complexes, making the DNA accessible for the RNA pol II machinery [Fenouil et al., 2012, Deaton and Bird, 2011].

Third, specific DNA sequences (motifs) that can be recognized by transcription factors (TFs). These factors can either recruit directly the RNA polymerase machinery to target promotors [Dynan and Tjian, 1983], or recruit additional pro-

tein (complexes) such as histone acetyltransferases, regulating the chromatin environment and therefore accessability for RNA polymerases [Cramer, 2019]. To fulfill this function TFs possess a DNA recognizing domain, such as helix-loop-helix or zinc-finger domains and a so-called transactivation domain [Kadonaga et al., 1988]. In contrast to the DNA binding domain, the transactivation domain is often disordered and of low complexity, promoting the recruitment and interaction with additional proteins involved in transcription initiation and promotor accessibility [Cramer, 2019]. In 2018 Lambert *et al.* cataloged over 1600 human TFs. TFs themselves are often regulated by expression, localization, post-translational modifications (such as phosphorylation) and interaction with other proteins or small molecules, such as hormones [Filtz et al., 2014, Payvar et al., 1981, Cramer, 2019]. The following section will give a brief introduction to such regulatory mechanism of transcription factors, with a focus on expression of lipogenic and metabolic genes.

1.1.2 Transcription factors regulating and regulated by metabolism

Many enzymes are regulated by fasting and feeding cycles. The activity of these enzymes can be influenced by several mechanisms such as, post-translational modifications, degradation, compartmentalization and allosteric control. Another mechanism of regulation can be the expression of the required enzymes themselves. This mechanism is of particular importance in *de novo* lipogenesis and triacylglycerol synthesis [Wang et al., 2015]. To express these proteins only when needed, transcription factors have to be integrated into the cellular sensor and signaling pathways. The following sections provide an overview of the diversity, complexity, and cellular integration of these mechanisms.

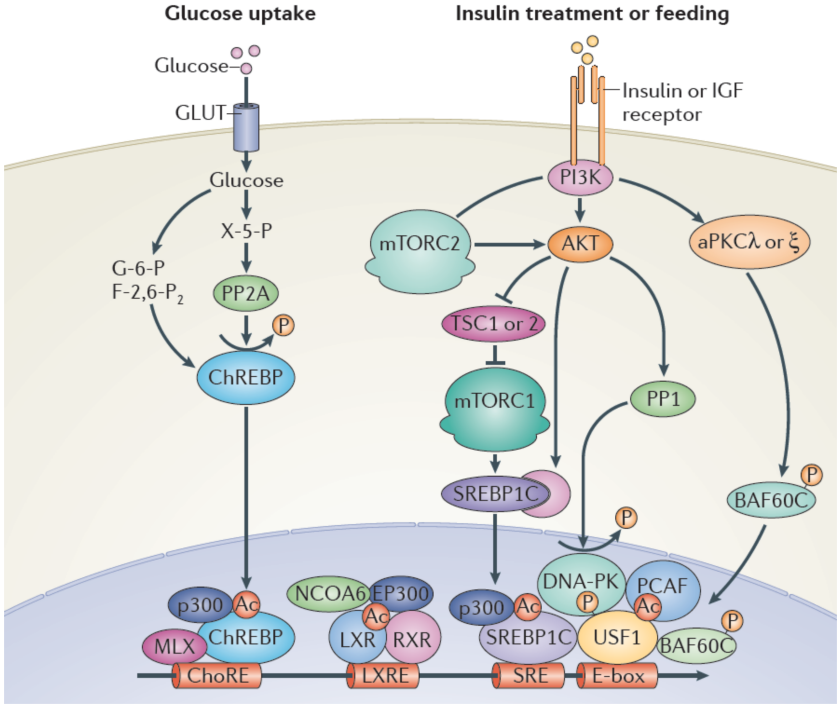

Figure 1.2: **Regulation of transcription factors by insulin and glucose**
Insulin signaling and glucose uptake trigger a variety of transcription factors, resulting in the expression of enzymes required for *de novo* lipogenesis and TAG synthesis. Binding of insulin triggers the activation of downstream kinases such as AKT, and mTOR, resulting in the activation of SREBP(1C) and USF1. ChREBP is regulated by an increase in cellular glucose levels, resulting in dephosphorylation and subsequent activation of ChREBP. In addition of dephosphorylation, also glucose metabolites itself have an stimulating effect on ChREBP activity. LXR is regulated by binding of intracellular oxysterols, resulting in the formation of an active complex together with RXR. atypical protein kinase C (aPKC), mTOR complex (mTORC), DNA-dependent protein kinase (DNA-PK), protein phosphatases (PP1 and PP2), upstream stimulatory factor 1 (USF1), sterol regulatory element-binding protein 1C (SREBP1C), carbohydrate-responsive element-binding protein (ChREBP), liver X receptors (LXRs), E-box (5'-CATGTG-3'), sterol regulatory element (SRE; 5'-TCACNCCAC-3'), carbohydrate response element (ChoRE; 5'-CAYGNGN5CNCRTG-3'), LXR response element (LXRE; 5'-AGGTCAN4AGGTCA-3'), fructose-2,6-bisphosphate (F-2,6-P2), glucose-6-phosphate (G-6-P), glucose transporter (GLUT), insulin-like growth factor (IGF), Max-like protein X (MLX), nuclear receptor coactivator 6 (NCOA6), p300/CBP-associated factor (PCAF), retinoic acid receptor (RXR), tuberous sclerosis (TSC), xylulose 5-phosphate (X-5-P). Figure from [Wang et al., 2015], permission granted by Springer Nature.

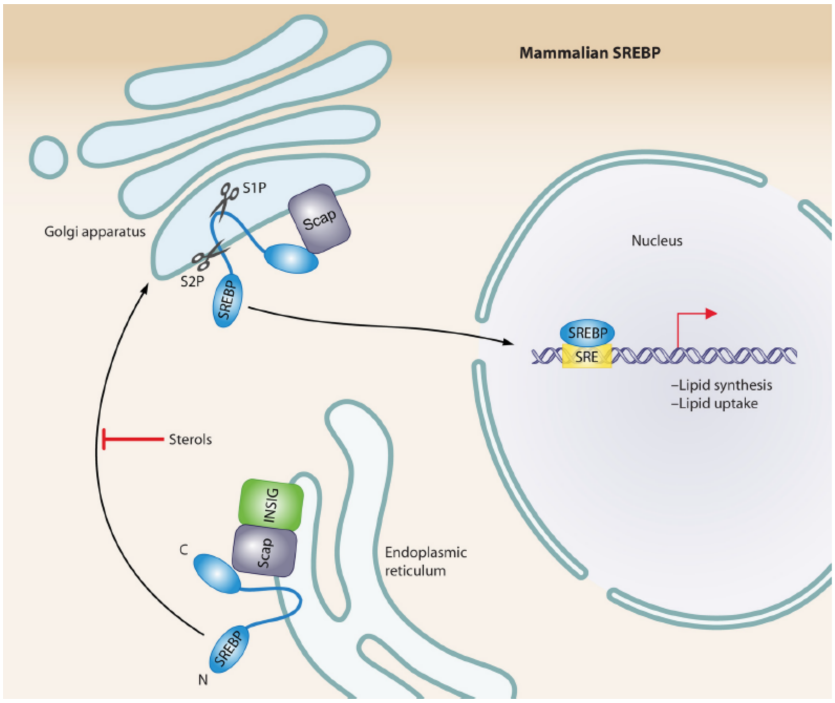

Figure 1.3: **Mammalian SREBP pathway**
Sterol binds to the sterol sensing domain of Scap in the ER, resulting in the binding of SREBP-Scap complex to Insig, anchoring of the complex in the ER. Under low sterol conditions SREP-Scap no longer interact with Insig and are transported to the Golgi apparatus where SREBP is cleaved by the site 1 and site 2 protease. The N-terminus of SREBP is released and enters the nucleus where it binds to SRE sites, activating genes required for lipid synthesis and uptake. Figure from [Bien and Espenshade, 2010], permission granted by ASM.

SREBP regulates cholesterol and fatty acid synthesis by a feedback regulatory system

Cholesterol and fatty acids are fundamental building blocks of biological membranes. However, an overexpression can have toxic effects. Therefore, cellular levels have to be tightly regulated. This is achieved by the membrane bound TF sterol regulatory element-binding protein (SREBP). SREBP is part of the basic helix-loop-helix/Zip (bHLH/Zip) TF-family [Hua et al., 1993] and is expressed as an inactive ER-membrane bound protein [Wang et al., 1994]. Under low cholesterol conditions the membrane bound TF becomes proteolytically released from the membrane, activating the expression of genes required for lipid synthesis [Wang et al., 1994, Yokoyama et al., 1993]. The SREBP pathway [Brown and Goldstein, 1997] is not only a great example for the regulation of TFs by localization, its target genes are also partially overlapping with ChREBP [Linden et al., 2018]. As mentioned, SREBP is expressed as a membrane protein and

forms a complex with the membrane protein Scap (SREBP cleavage-activatiog protein) in the ER membrane [Hua et al., 1996] (see Figure 1.3). When cholesterol levels are high, sterol binds to the sterol-sensing domain [Radhakrishnan et al., 2004] of Scap, causing a conformational change resulting in binding to the Insig protein and retention of the complex in the ER [Sun et al., 2005]. Under low cholesterol conditions, Scap does not interact with Insig, allowing the binding of COPII (coating protein complex II), which triggers the transport of SREBP-Scap complex to the Golgi [Sun et al., 2005]. In the Golgi, the N-terminal bHLH transcription domain of SREBP is released by a two step proteolytic reaction. First, the Golgi- located Site-1 protease (S1P) cleaves SREBP in the lumen [Duncan et al., 1997]. Second, the membrane bound protease S2P releases the N-terminal domain of SREBP from the membrane [Duncan et al., 1998]. This allows the translocation of the transcription factor into the nucleus, where it binds to specific sterol regulatory element sequences (SRE) in the promotors of target genes [Hua et al., 1993], resulting in the upregulation of sterol synthesis (reviewed in more detail in [Ye and DeBose-Boyd, 2011, DeBose-Boyd and Ye, 2018]). SREBPs, in particular the isoform SREB1C, are also integrated into the insulin signaling pathway by regulatory input from AKT and mTORC1. Phosphorylation of SREB1C increases the affinity of the SREB1C-SCAP complex for proteins involved in COPII mediated transport from the ER to the Golgi apparatus where they undergo cleavage (see Figure 1.2) [Yellaturu et al., 2009].

LXR is a nuclear hormone receptor

The liver X receptor belongs to the superfamily of nuclear hormone receptors and is activated by binding to oxysterols, derivatives of cholesterol [Janowski et al., 1996, Chen et al., 2007]. Its transcriptional activity is dependent on the formation of a heterodimer with retinoid x receptors (RXR) (see Figure 1.2), also a member of the nuclear receptor family [Willy et al., 1995, Svensson et al., 2003, Hong and Tontonoz, 2014]. The heterodimeric complex binds to DNA by recognition of the LXRE motif. If no oxysterols are bound to LXR (and/or retionid acid to RXR) co-repressors (e.g. nuclear co-repressor1, NCO1) bind to the heterodimer, which inhibits the transcription of target genes. Upon binding of oxysterols, the conformation of LXR-RXR is changing and the co-repressors are released, allowing the binding of nuclear receptor co-activators such as EP300 and activating signal co-integrator 2 (NCOA6) (see Figure 1.2) [Wang et al., 2015, Mouchiroud et al., 2014, Lee et al., 2008]. Target genes of LXR are in-

volved in the uptake, excretion, metabolism and transport of cholesterol, as for example the membrane bound transporter ABCA1 [Peet et al., 1998]. Resulting in the transport of cholesterol and phospholipids to apolipoproteins [Wagner et al., 2003, Wang et al., 2015]. Interestingly most activating ligands of LXR are sterols that inhibit the SREBP pathway, showing the high connection between the two pathways [Hong and Tontonoz, 2014]. LXR binding sites (LXRE motif) are also found in promotor regions of FAS (fatty acid synthase), ACC (acetyl-CoA carboxylase), as well as in the promotor regions of SREB1C and ChREBP [Schultz et al., 2000, Joseph et al., 2002, Poupeau and Postic, 2011], resulting in direct lipogenic gene transcription, as well as indirect by regulating SREB1C and ChREBP [Wang et al., 2015, Poupeau and Postic, 2011]. In 2007 Mitro *et al.* described LXR as a sensor of glucose. Their study shows direct binding of glucose and glucose-6-phosphate to LXR, resulting in the expression of LXR target genes [Mitro et al., 2007]. However, these findings are challenged due to its low affinity towards glucose and the hydrophilic nature of glucose-6-phosphate which was added to the media in their study (discussed in [Lazar and Willson, 2007]).

USFs are regulated by phosphorylation and acetylation

Upstream stimulatory factors (USFs) are also part of the bHLH/Zip family of transcription factors. USF1 and USF2 bind to E-boxes as homo- or heterodimers [Sirito et al., 1992]. USFs have major roles in a variety of cellular functions and are broadly regulated (mainly by phosphorylation) (see [Horbach et al., 2015]). In this section we will focus on the regulation by insulin and the involvement of USFs in metabolism (see Figure 1.2). USFs are bound under fed and starved conditions to the E-box in promotor regions of their target gene (for example of FAS) [Wong et al., 2009]. Mass spectrometry analysis of liver samples from fed and starved mice showed changes in phosphorylation and acetylation of USF1 in dependency to the metabolic state [Wong et al., 2009]. Further analysis hinted to DNA-PK as the responsible kinase for phosphorylation at S262 under fed conditions. This phosphorylation is regulated by high insulin levels, causing the translocation of the phosphatase PP1 to the nucleus where DNA-PK is activated by dephosphorylated. DNA-PK then phosphorylates USF1 at S262, resulting in the recruitment of PCAF and subsequent acetylation of USF1 at K237. This acetylation enhances the transcriptional activity of USF1 [Wong et al., 2009] and recruitment of additional chromatin relaxing factors, such as the LipoBAF com-

plex [Zhang et al., 2016]. Under starved condition USF1 is kept in a deacetylated state by interaction with HDAC9 [Wong et al., 2009].

1.1.3 ChREBP is regulated by glucose levels

ChREBP is also part of the bHLH/Zip transcription factor family, recognizing the carbohydrate response element (ChoRE), existing of two E-boxes separated by 5 nucleotides. As shown in Figure 1.2, ChREBP activity is dependent on glucose levels. Post-translational modifications and localization are described as the major effectors in regulating ChREBP, which will be discussed in more detail later. Part of this thesis will be to elucidate the possibility of ChREBP acting as a nuclear receptor for glucose-(metabolites). As shown in Figure 1.4, ChREBP target genes are involved in a variety of lipogenic and glycolytic pathways.

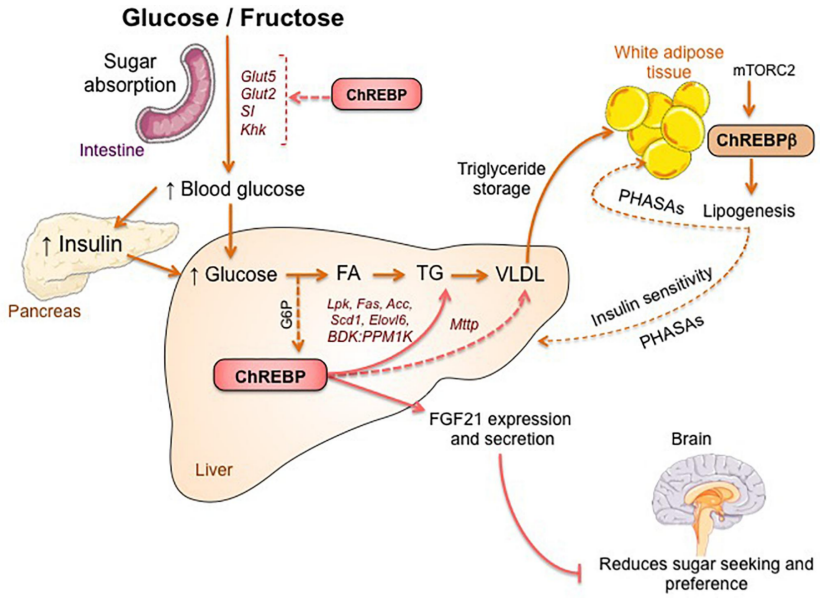

Figure 1.4: **ChREBP target genes are involved in a variety of glycolytic and lipogenic pathways**
ChREBP regulates the expression of target genes involved in lipogenesis and glucose metabolism in different tissue (target genes are highlighted in red). Figure from [Ortega-Prieto and Postic, 2019]

It has to be mentioned that target genes are often under regulation of an entire set of transcription factors, allowing several levels of regulation. One particular example for the transcription factors discussed in this thesis is the FAS promotor containing a ChoRE, LXRE and SER motif (see Figure 1.5).

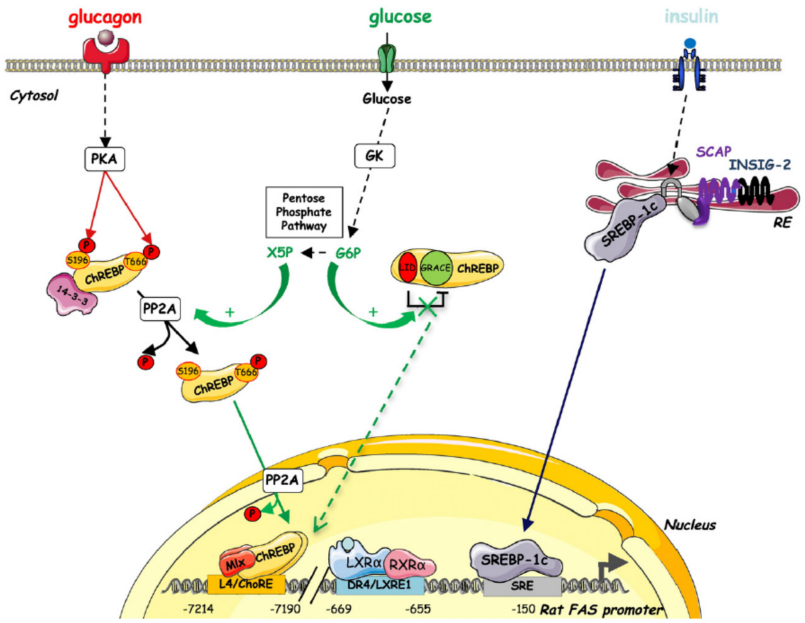

Figure 1.5: **Transcriptional regulation of FAS**
FAS expression is regulated by ChREBP, LXR and SREBP-1c. Insulin triggers transport of SREBP1C to the Golgi apparatus where it is activated by proteolytic cleavage and translocates to the nucleus binding to SRE motifs of target genes, such as FAS. LXR directly binds to the LXRE motif where it is activated by glucose (?) or insulin mediated signaling. ChREBP translocates under high glucose conditions to the nucleus where it binds to ChoRE motifs. Translocation is promoted by dephosphorylation of ChREBP by PP2A, or direct sensing of glucose-6-phosphate. Binding of Glc6P results in the intramolecular release of inhibitory effects. Red arrows indicate inhibitory mechanism, green arrows indicate activating mechanism of ChREBP regulation. Figure from [Poupeau and Postic, 2011], permission granted by Elsevier BBA.

1.2 Medical relevance of studying ChREBP

According to the World Health Organization (WHO) more than 1.9 billion people are overweight or obese. Obesity has tripled since 1975 and the majority of the world population now lives in countries where obesity kills more people than underweight[1]. Overweight comes with a variety of health consequences, such as diabetes, osteoarthritis, cancer and cardiovascular diseases.

Although obesity could be prevented by a change in energy intake and a reduction in sugars as the main energy source, as well as promoting a more active lifestyle, the socio- economic situation of individuals often works against such anticipated health-beneficial changes. In addition, the broad and cheap availability of sugar enriched foods catalyze the obesity epidemic.

[1] https://www.who.int/news-room/fact-sheets/detail/obesity-and-overweight

This epidemic is not only affecting individuals in their daily life, but has also become a major cost factor of healthcare systems. Due to the pace of increased sugar consumption, the human body has not been able to evolutionary adapt to such a major change in availability of energy resources. Therefore, it becomes fundamental to understand how the human body copes with such changes in energy intake, lean lifestyle and its biological and medical consequences.

Over the last decades more and more signaling networks and molecules, such as insulin, have been discovered. Also gene transcription itself, including regulatory elements such as transcription factors have come into the focus of research. One of these transcription factors, regulating genes mainly involved in glucose metabolism and lipid synthesis, is the carbohydrate-response element-binding protein (ChREBP). How ChREBP is regulated is in the center of this thesis.

1.3 Physiological function and phenotypes of ChREBP

ChREBP is a bHLH/Zip transcription factor that, together with its interaction partner Mlx, was found to bind to specific DNA sequences in response to glucose levels. One of the recognized DNA sequences contains two E-boxes with a particular 5 nucleotide spacing (CACGTGnnnnnCACGTG). These are called ChoREs [Shih et al., 1995, Stoeckman et al., 2004, Ma et al., 2005]. ChoREs are found in promotor regions of genes involved in glycolytic, glyconeogenic and lipogenic pathways. The most prominent targets are liver type pyruvate kinase (Lpk) [Yamashita et al., 2001], fatty acid synthase (Fasn)[Iizuka et al., 2004] and acetyl CoA carboxylase 1 (Acc1)[Iizuka et al., 2004], reviewed in [Iizuka et al., 2013].

ChREBP is widely expressed in a variety of tissue, however most abundant in organs and tissue involved in lipogenesis such as liver, kidney, brown and white adipose tissue [Iizuka et al., 2004]. Interestingly its paralogue MondoA, targeting genes mainly involved in glycolysis, is expressed predominantly in skeletal muscle [Sans et al., 2006]. Although whole body ChREBP knock-out mice (ChREBP-/-) are viable, they show alterations in for example free fatty acid compositions. Feeding of diets containing a high content of simple carbohydrates resulted in hypothermia, a further decline in free fatty acids, finally culminating in death within a week [Iizuka et al., 2004]. In contrast, ChREBP liver-knock-out (KO) mice were viable on a high sugar diet, however these mice exhibited insulin

sensitivity [Jois et al., 2017]. Mice with an intestine specific ChREBP-KO manifest weight loss when on a high fructose diet, suggesting nutrient malabsorption [Kim et al., 2017].

Although more work has to be done in understanding these physiological phenotypes, it demonstrates the significance of ChREBP function in coping with sugar rich diets. In humans several studies showed a positive correlation between ChREBP expression levels and glucose intolerance/ diabetes, reviewed in [Abdul-Wahed et al., 2017].

Experiments in *Drosophila. melanogaster* underline the importance of ChREBP (in *D. melanogaster* called Mondo) and its target genes in response to sugary diets. Larvae lacking the obligatory binding partner Mlx (in *Drosophila* named Bigmax) show a markebly reduced survival on diets containing sucrose, glucose or fructose. This could be rescued by changing the food sources [Havula et al., 2013]. Experiments in our lab by Hui-Lan Huang, using *Drosophila* Mondo-KO lines could confirm these findings (unpublished data).

By specific neuronal knockdowns of the *Drosophila* ChREBP homolog Mondo, Docherty *et al.* demonstrated that Mondo functions as a regulator in feeding and nutrient storage [Docherty et al., 2015]. ChREBP/Mondo is also present in *Caenorhabditis elegans* (MML-1), where it was shown to promote expression of target genes involved in longevity. How MML-1 is regulated in *C. elegans* has still to be elucidated. However, response to insulin-like signals and caloric restriction also suggest a function as metabolic sensor. In addition ChIP-seq showed enrichment of genes that function in carbohydrate metabolism, suggesting a similar function to mammalian Mondo [Johnson et al., 2014, Nakamura et al., 2016]. N-terminal domain swap experiments of the glucose sensing module (see Section 1.4.1) between mammalian paralogues MondoA and ChREBP (also named MondoB), with the *D. melanogaster* homologue Mondo were shown to be functional in luciferase assays [Li et al., 2006].

These findings not only show the importance of the physiological role of Mondo proteins in regulating sugar metabolism and homeostasis, their conservation across organism are an indication for a fundamental mechanism of gene regulation and sugar signaling.

1.4 Domain architecture and conservation

ChREBP is part of the basic helix-loop-helix transcription factor family. Its architecture can be roughly divided into three parts: The N-terminal GSM, the central prolin- rich region and the C- terminal DNA- binding basic helix- loop-helix/Zip domain (Figure 1.6A).

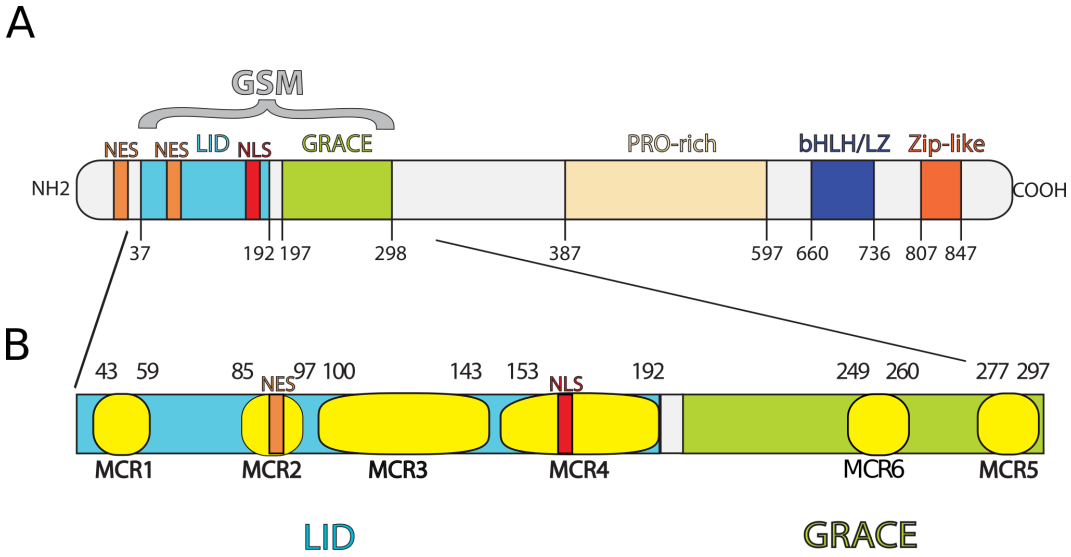

Figure 1.6: **Domain organization of ChREBP**
A: Schematic representation of ChREBP domain architecture. N-terminal glucose sensing module (GSM), prolin-rich region and C-terminal basic helix-loop-helix/Zip domain for DNA binding. B: Detailed view of the GSM, highlighting mondo conserved regions (MCRs) in yellow located. The GSM can be further divided in LID (blue) and GRACE (green) domain. Also located in the LID are a nuclear export sequnece (NES) and nuclear localizatio sequence (NLS). Boundaries based on [McFerrin and Atchley, 2012].

1.4.1 The Glucose Sensing Module is responsive to changes in glucose levels

The ChREBP N-terminal region is evolutionary conserved across Mondo proteins (see Figure 1.7). Li *et al.* were able to systematically truncate ChREBP and establish structure function relationships of these conserved regions by using a luciferase system as a readout [Li et al., 2006]. These studies showed that the first 297 amino acids are composed of a low-glucose inhibitory domain (LID) and glucose-response activation domain (GRACE). As shown in Figure 1.6B the LID spans from 37-192 and GRACE from 197-297. The absence/deletion

of the LID results in a constantly active construct independent of glucose levels, whereas the deletion of the GRACE domain results in an inactive construct [Li et al., 2006]. Therefore, the N-terminal region was named glucose sensing module (GSM). Up to this day the exact mechanism of how this module is sensing glucose levels is not understood in detail. However, several mechanisms have been suggested, which will be discussed in this chapter.

Mondo conserved regions (MCRs) are conserved across Mondo proteins and species (see alignment Figure 1.7). Four of these MCRs are located in the LID (MCR1-4). MCR5 and MCR6 are located in the GRACE domain, due to its only recent discovery MCR6 is actually N- terminal of MCR5 (see Figure 1.6B) [Li et al., 2006, Li et al., 2008, Davies et al., 2008, Davies et al., 2010, McFerrin and Atchley, 2012]. A number of mutation studies, using cellular readouts such as luciferase expression and/ or target gene expression, in combination with pull-down experiments revealed several features of these MCRs. One of the two nuclear export signals (NESs) is located in MCR2 and is responsible for nuclear export by Crm1 [Davies et al., 2008, Eilers et al., 2002]. MCR3 is the best characterized MCR. It contains a binding site for 14-3-3 (117-137aa), therefore also playing a role in cellular localization [Eilers et al., 2002, Merla, 2004]. Interestingly, this interaction is not dependent on phosphorylation of ChREBP, as first assumed, and was finally crystallized by Ge *et al.* in 2012 [Sakiyama et al., 2008, Ge et al., 2012](PDB:4GNT). Undisruptive mutations for 14-3-3 binding of MCR3 in addition to experiments altering nuclear shuttling showed that nuclear localization cannot be the only function of MCR3 in response to changing glucose levels [Li et al., 2008, Davies et al., 2008]. This argument is supported by Sato *et al.*, describing the 14-3-3/ MCR3 interface as a binding site for AMP, resulting in the cytoplasmic localization of ChREBP [Sato et al., 2016]. MCR4 contains a bipartite nuclear localization signal (NLS) and interacts with Importin-α. This NLS overlaps with a second, weaker 14-3-3 binding site [Ge et al., 2011]. MCR6 is the most recent described conserved region. Based on sequence similarities with other Glc6P binders MCR6 is suggested to be a potential glucose-6-phosphate (G6P) (Glc6P) binding site [McFerrin and Atchley, 2012]. So far no specific functions were described for MCR1 and MCR5. However, mutation studies demonstrated their overall importance for glucose response in luciferase assays [Davies et al., 2010, Li et al., 2006].

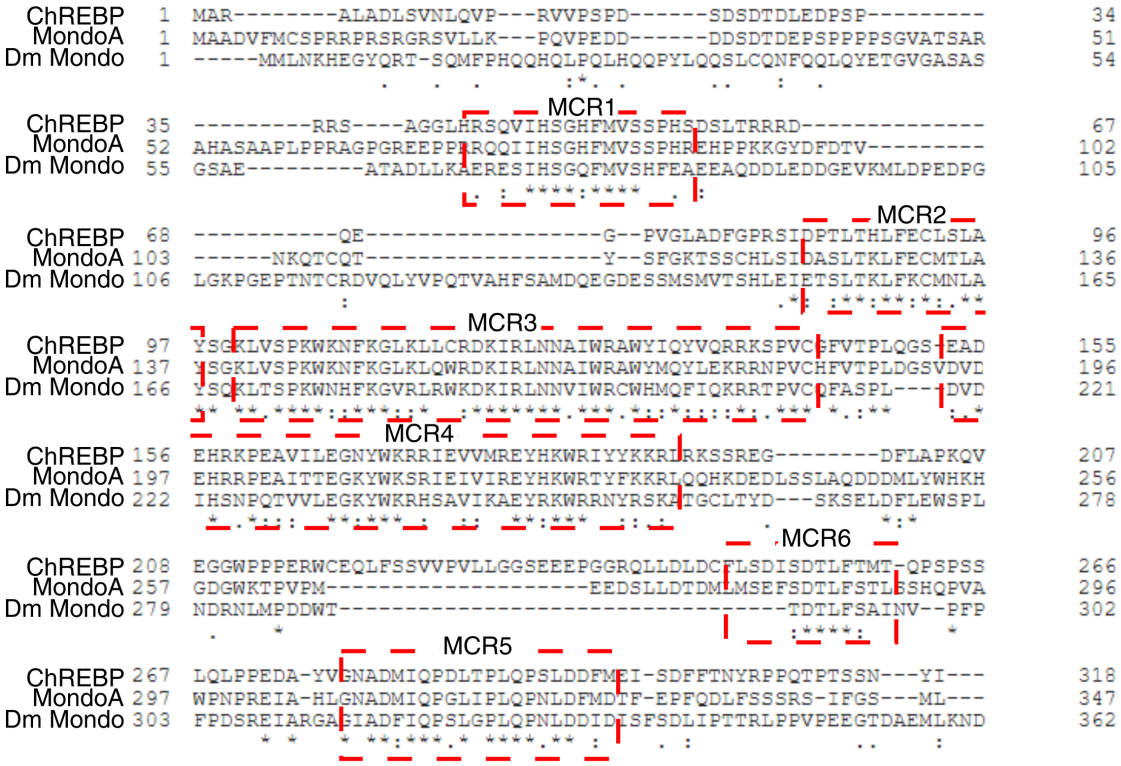

Figure 1.7: **Sequence alignment of mouse ChREBP-α, MondoA and *Drosophoal* Mondo GSM**
Mondo conserved regions (MCRs) are highlighted in red boxes. Asterisks indicate identical amino acids, dots indicate amino acid similarity across organisms.

Although the N-terminal region is functionally described in different domains and modules, it has to be mentioned that this naming is not meant from a structural point of view. So far no overall domain- fold or structural feature was described for this region. In fact, secondary structure predictions and predictions for disordered regions (using PSIPRED[2]) describe the N- terminal region as rather unstructured (illustrated in Figure 1.8).

[2]http://bioinf.cs.ucl.ac.uk/psipred

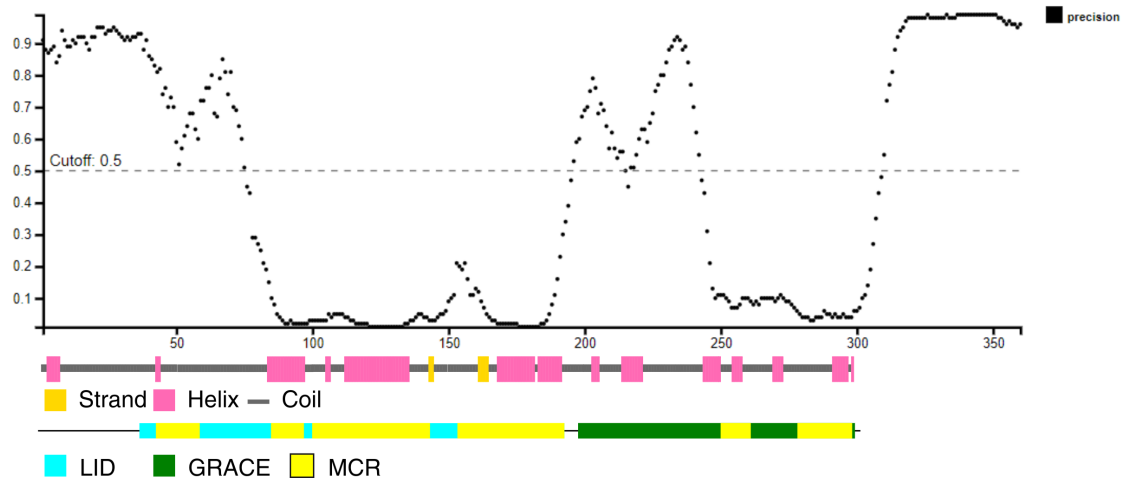

Figure 1.8: **The GSM is partially disordered**
Prediction of disordered regions of the GSM show two disordered patches (values above 0.5 are considered as disordered). Secondary structure prediction of the GSM is shown below the plot, together with information about their location within the GSM. Scale according to aa positions in plot. Disordered region and secondary structure were generated using PSIPRED.

1.4.2 Polymorphism in the GSM is associated with reduction in plasma triglyceride levels

Genome-wide association studies by Kooner *et al.* linked a single nucleotide polymorphism (SNP) in the conserved GSM region of ChREBP to reduced triglyceride levels [Kooner et al., 2008]. The described SNP is a missense mutation of Gln 241 to His. The observed low triglyceride levels in association with the Q241H polymorphism might be due to a reduction in ChREBP activity. Kooner *et al.* speculate that because of an increase in excessive sugar consumption, the *Chrebp*-gene might be a plausible candidate for a 'thrifty gene', allowing adaptation to a new environment [Kooner et al., 2008]. A concept that was supported by Nakayama *et al.* in 2011 [Nakayama et al., 2011]. By assessing the phenotypic consequences of Q241H in populations in Asia and Oceania, they not only confirmed previous findings of decreased plasma triglycerides, but also described the SNP as an adaptation to a nomadic lifestyle. By determining the world wide distribution of the H-allele , they found a high prevalence in central asian populations, including Mongolians, Uyghurs and Tibetans (see Figure 1.9) [Nakayama et al., 2011]. The traditional foods of these ethnic groups is rich in protein and dietary products, but limited in simple sugars such as glucose. To provide the body, especially the brain and erythrocytes with glucose the available

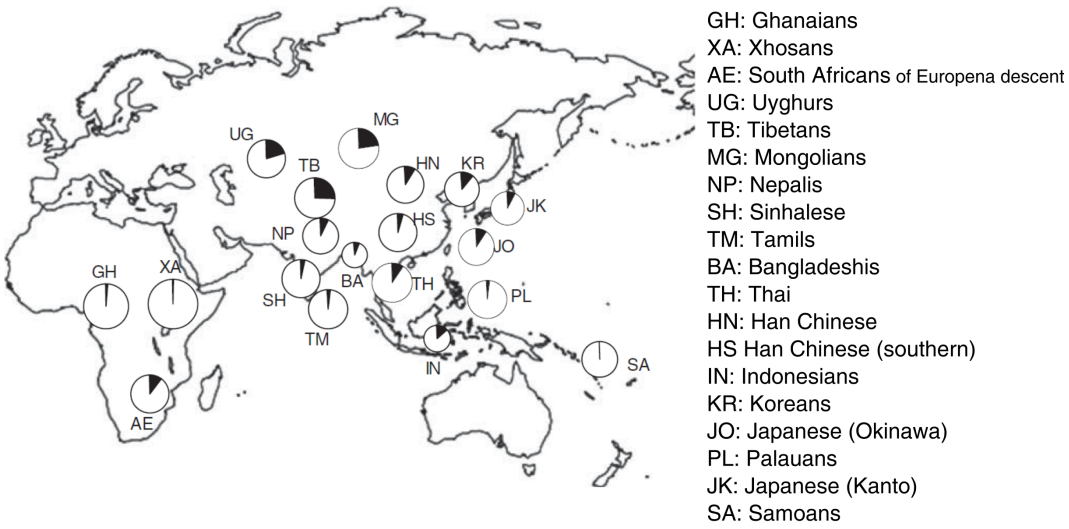

Figure 1.9: **Distribution of Q241H in the old world**
Allele frequencies of the H allele are indicated in black areas of the pie charts. Figure from [Nakayama et al., 2011], permission granted by Springer Nature.

energy resources have to be converted to glucose. It is therefore speculated, that a reduction in ChREBP activity is beneficial for these populations, since scarce glucose is not deposited in fat [Nakayama et al., 2011]. However, experimental evidence showing a reduced activity for the Q241H variant of ChREBP is still lacking.

1.4.3 The hyperactive brother ChREBP-β

In 2012, Herman *et al.* described a novel isoform of ChREBP, named ChREBP-β. The expression of this isoform is regulated by ChREBP(-α), binding to a ChoRE located close to exon1b, upstream of exon1a of the *Chrebp* gene [Herman et al., 2012]. This alternative mRNA expression leads to a splicing variant of 687aa size(see Figure 1.10). This shorter variant lacks most of the LID domain and is therefore constantly active and located in the nucleus. Although, ChREBP-β exhibits lower mRNA levels, its activity is described to be 20fold higher than ChREBP-α [Herman et al., 2012]. Based on the difference in activity and regulation of expression, the current model for the role of ChREBP-β is a feed-forward mechanism. Under high glucose conditions, the constantly expressed isoform ChREBP-α becomes activated, expressing lipogenic target genes and ChREBP-β. ChREBP-β enhances the expression of (additional) target genes [Herman et al., 2012]. How this signal is turned off again is not well understood

to this date. The most likely model is rapid degradation via the ubiquitin- proteasome pathway [Guinez et al., 2011, Ido-Kitamura et al., 2012, Abdul-Wahed et al., 2017].

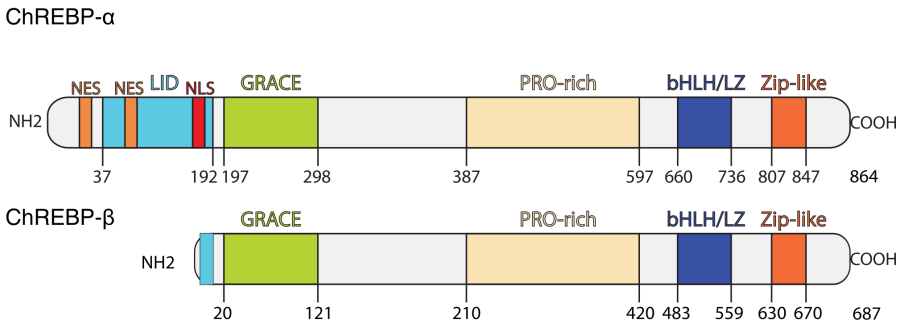

Figure 1.10: **Domain Comparison between ChREBP-α and ChREBP-β**
Use of an alternative transcription start site results in a splice variant of ChREBP, lacking most of the LID. This isoform (ChREBP-β) is constantly activ and predominantly located in the nucleus. Based on [Poupeau and Postic, 2011, Herman et al., 2012].

1.4.4 The C-terminal basic helix-loop-helix/Zip domain recognizes ChREBP target genes

The target sequence for ChREBP was defined as two imperfect E-boxes with a particular spacing of 5 nucleotides [Shih et al., 1995]. E-boxes are known to be recognized by dimeric bHLH/Zip domains [Atchley and Fitch, 1997, Ferré-D'Amaré et al., 1993]. Since members of the bHLH/Zip family must form dimers to bind to their target DNA, Cairo *et al.* used a yeast two- hybrid approach to screen systematically for potential dimerisation partners of ChREBP. Max-like protein X (Mlx) was the only bHLH/Zip member that showed interaction [Cairo et al., 2001]. In 2004 Stockman *et al.* described Mlx as the obligatory heteromeric partner of ChREBP for E-box binding [Stoeckman et al., 2004]. Structural modeling, in combination with mutation studies suggest the formation of ChREBP/Mlx heterodimers recognizing a single E-box. Formation of a heterotetrameric complex recognizing ChoRE is driven by interactions of the two Mlx subunits bound to two separate E-boxes or E-box like sequences (see Figure 1.11) [Ma et al., 2007].

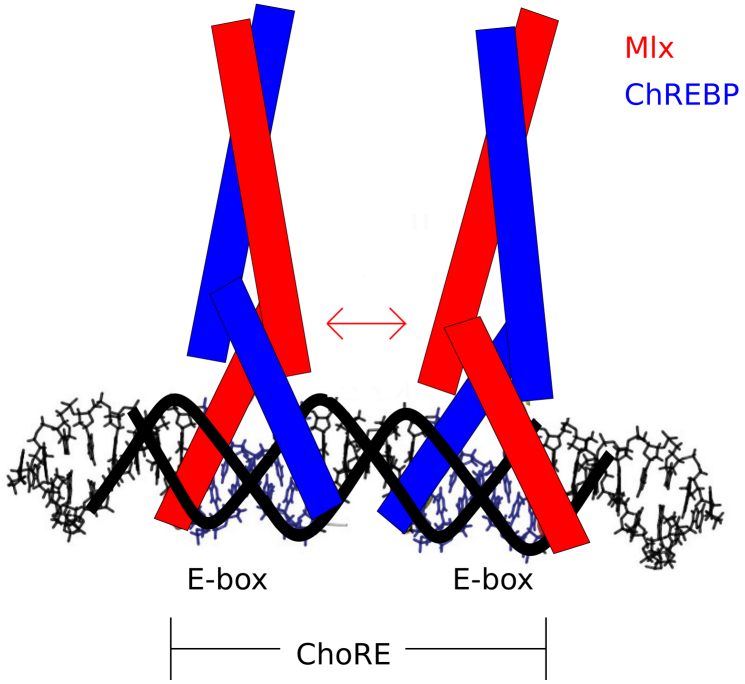

Figure 1.11: **Orientation of the bHLH/Zip domains**
Two heterodimers of ChREBP bHLH/Zip (blue) and Mlx bHLH/Zip (red) bound to DNA containing a ChoRE sequence. Arrow represents postulated stabilizing interactions of the Mlx-loops. Based on Ma *et al.* [Ma et al., 2007].

1.5 Regulation of ChREBP activity

ChREBP is regulated by a variety of mechanism, such as post-translational modifications, protein-protein interactions, localization and metabolites. Latter is the focus of this work. A first overview of ChREBP regulation is shown in Figure 1.12. A more detailed view will be given in the following sections.

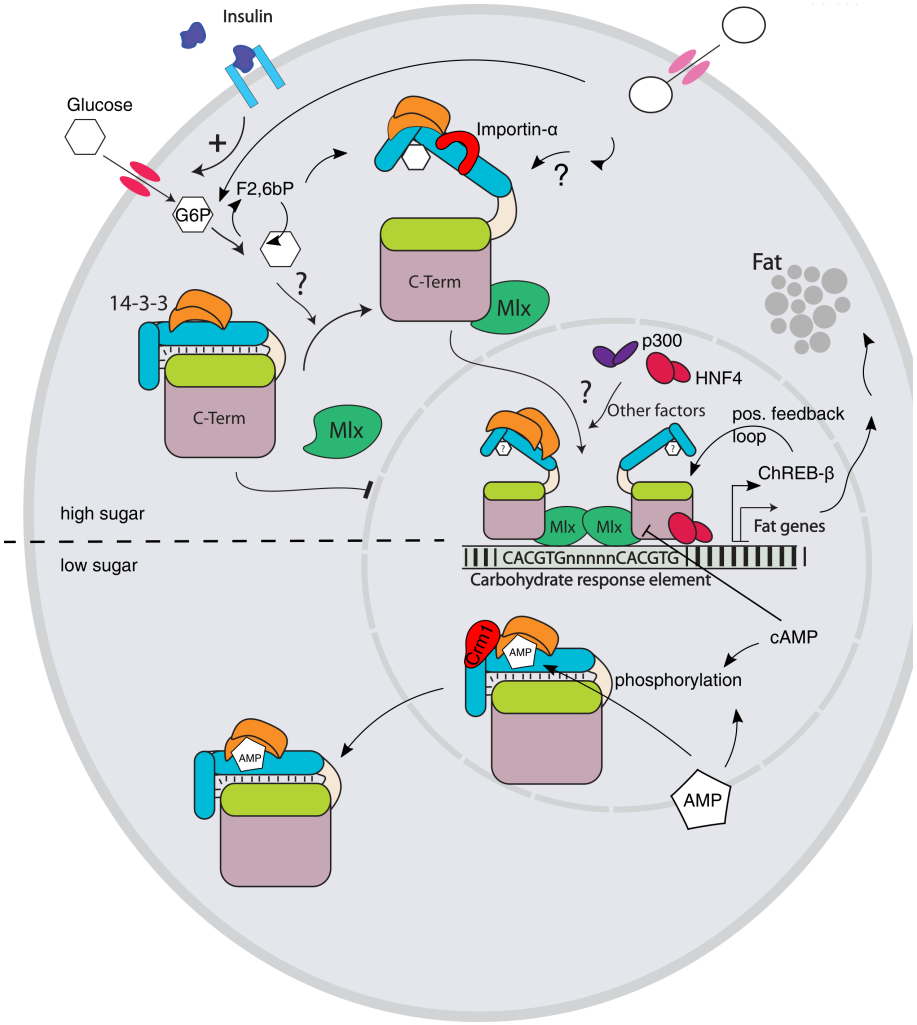

Figure 1.12: **Overview of ChREBP activity and localization**
Under high sugar conditions, ChREBP localization to the nucleus is mediated by sugar-metabolites and Importin-α. Nuclear accumulation of ChREBP results in complex formation on ChoRE motifs together with HNF4α, p300 and unknown other factors. Activating the expression of the isoform ChREBP-β and target genes involved in lipogenesis. Expression of ChREBP-β creates an positive feedback loop, further increasing expression of target genes. Under low glucose conditions, levels of cAMP and AMP are increased and trigger the inhibitory phosphorylation of ChREBP. In addition, binding of AMP promotes the interaction with 14-3-3 and the subsequent nuclear export by Crm1. Modified from A. Ladurner

1.5.1 Cellular localization of ChREBP

Under low glucose conditions ChREBP is mainly localized in the cytoplasm. Therefore, localization is one of the main aspects in ChREBP regulation.

Kawaguchi *et al.* identified two phosphorylation sites (S196 and T666) critical for ChREBP regulation and localization. Mutating these sites to Ala has

not only increased nuclear localization of ChREBP, but also increased the expression of target genes in cultured primary hepatocytes. These findings describe the mechanism of cellular localization as the main regulatory mechanism for ChREBP activity. The phosphorylation causing nuclear export is triggered by an increase in cAMP mediated PKA activity, whereas dephosphorylation is regulated via xylulose-5-phosphate (X5P) activared PP2A. Although these findings were confirmed by Stoeckmann *et al.*, and Dentin *et al.* [Stoeckman et al., 2004, Dentin et al., 2005], the relevance of phosphorylation for ChREBP localization was challenged later.

Merla *et al.* were not able to reproduce the effect on nuclear localization using S196A and T666A mutants in Cos-7 and 293T cells, however additional experiments showed that ChREBP is actively exported by CRM1, suggesting a dynamic flux between cytoplasm and nucleus [Merla, 2004]. Tsatsos *et al.* showed that cAMP levels are constant under low and high glucose levels in hepatocytes, again questioning the role of phosphorylation in nuclear localization. In addition, the initially discussed mutants did not have an influence on ChREBP localization nor regulation of activity by changes in glucose levels, contradicting the model of phosphorylation mediated localization of ChREBP [Tsatsos and Towle, 2006].

More strikingly, although glucose causes an increase in nuclear ChREBP, trapping ChREBP in the nucleus by the use of mutations or export inhibitors do not increase activity under low glucose conditions. Again suggesting a different mechanism than localization in regulation of ChREBP [Davies et al., 2008]. Certain mutations of the nuclear export signals NES1 and NES2 are also reported to decrease ChREBP activity under high glucose conditions, although ChREBP is enriched in the nucleus and still able to bind DNA. This suggests that NES1 and NES2 may have additional roles in glucose sensing [Fukasawa et al., 2010]. Taken together, ChREBP is constantly shuttling between cytoplasm and nucleus, although glucose causes an enrichment in nuclear localization, the increase in localization is not the cause for an increase in ChREBP activity itself. These findings suggest additional regulating mechanisms [Davies et al., 2008].

1.5.2 Protein-Protein interactions

ChREBP is shown to interact with a variety of proteins. These interactions were shown to be important for regulation of activity, function and localization. The most prominent interaction partners are highlighted in this section.

14-3-3, a key player in ChREBP activity

14-3-3 is one of the best studied ChREBP interaction partners. The interaction was first described in 2004 by Merla *et al.*, using a yeast two hybrid screen. Besides 14-3-3β, also 14-3-3γ, ϑ and ζ were found to bind to the N-terminal region of ChREBP and the bHLH/Zip region. The interaction of 14-3-3 with the GSM was first described to be dependent on phosphorylation mediated by PKA on S140 and S196, facilitating the binding of 14-3-3 together with CRM1, resulting in nuclear export and cytoplasmic localization [Sakiyama et al., 2008]. The role of phosphorylation in 14-3-3 binding was challenged by Li *et al.*, showing that *in vivo* changing glucoes levels do no affect 14-3-3/ChREBP interaction. In addition, mutation of S140 to alanine did not affect interaction with 14-3-3 proteins. Indicating the interaction is of constitutive nature [Tsatsos and Towle, 2006, Li et al., 2008]. It is suggested that MCR3 has additional functions to 14-3-3 binding, since single mutations in ChREBP MCR3 (R128A) or deletion of MCR3 causing a loss of 14-3-3 binding also lead to failiure of ChREBP responce to glucose levels. It has been claimed that the interaction of 14-3-3 with MCR3 is essential for controlling subcellular localization, but also harbors an additional role independent of the localization in glucose response [Li et al., 2008]. A weaker second binding site for 14-3-3 was described in the MCR4 α3-helix. Interestingly this binding site is masking the NLS for Importin binding. This second 14-3-3 interaction is strengthened by phosphorylation [Ge et al., 2011]. By obtaining a high-resolution crystal structure, Ge *et al.* were able to show the interaction of 14-3-3β with the α2-helix of MCR3. As suggested by previous publications, this interaction is independent of phosphorylation. However, a sulfate group was located in the 14-3-3/MCR3 interface potentially mimicking phosphorylation of the 14-3-3 substrate (see Figure 1.13) [Li et al., 2008, Ge et al., 2012].

In 2016 Sato *et al.* crystallized the same complex again, this time the 14-3-3/MCR3 complex contained a bound AMP, replacing the sulfate by the phosphogroup of AMP. The binding of AMP results in a higher affinity of 14-3-3 to ChREBP and therefore nuclear export during starvation when AMP levels are high [Sato et al., 2016].

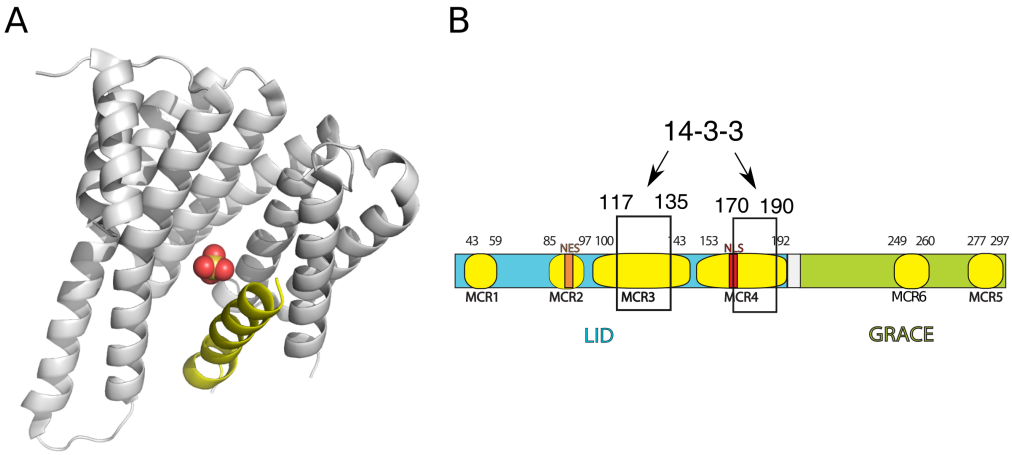

Figure 1.13: **Phosphorylation independent interaction of 14-3-3 with the α2- helix of ChREBP**
A: X-ray crystall structure of 14-3-3 (grey) binding the α2- helix of ChREBP MCR3 in a phosphorylation indepnendent manner. A sulfate (sphere structure) might support this interaction, mimicking phosphorylation. B: Position of the described binding sites in the ChREBP GSM of 14-3-3 [Ge et al., 2011, Ge et al., 2012]. For the second binding site no structure is resolved.

CRM1 is involved in nuclear shuttling

In 2002 Eilers *et al.* described a CRM1 (exportin)-dependent nuclear export signal (NES) in the ChREBP family member MondoA. This NES is conserved in ChREBP (located in MCR2). By using fluorescence microscopy and constructs altering CRM1 and 14-3-3 binding, they could show that CRM1 and 14-3-3 control the sub-cellular localization of MondoA [Eilers et al., 2002]. Using leptinomycin-b to specifically inhibit CRM1 dependent nuclear export Merla *et al.* observed an accumulation of ChREBP in the nucleus, supporting the model of CRM1 mediated export. Interestingly, deletion of the NES still resulted in the CRM1 dependent cytoplasmic localization of ChREBP, which suggests the (additional) use of NES in 14-3-3 [Merla, 2004].

Formation of a stable complex of 14-3-3/ChREBP and CRM1 was also reported to be dependent on phosphorylation of ChREBP S140. Although the authors claim the pulldown of the entire complex, only the western-blot for 14-3-3/ChREBP interaction is shown in their publication [Sakiyama et al., 2008]. Based on the reported data an involvement of CRM1 in ChREBP trafficking can be assumed. If CRM1 is exporting ChREBP due to direct binding to the NES located in the GSM and/or the NES of 14-3-3, or involvement of additional (unknown) adapter-proteins is not known at this point. Additionally, the impor-

tance of the different NESs seems to differ between cell types [Merla, 2004]. In 2010 a second NES was described at position 5-15 (now NES1). Mutation studies showed, that NES1 and NES2 are required for binding to CRM1 [Fukasawa et al., 2010]. Replacing the NES2 with a classical NES from the Rev HIV-I protein resulted in a loss of glucose response [Li et al., 2008]. Mutations of NES2 result in nuclear accumulation and failure to activate gene expression. These findings indicate additional functions of NES2 in ChREBP regulation beside CRM1 mediated export [Davies et al., 2008].

Importin-α competes with 14-3-3 for ChREBP binding

Using pull-down assays, Sakiyama *et al.* showed direct interaction between ChREBP and Importin-α, locating the nuclear localization sequence for Importin binding between 158-173aa. Phosphorylation of S140 and S196 reduce the interaction with Importin and the ChREBP NLS, but increase interaction of ChREBP with 14-3-3. Suggesting a competition between 14-3-3 (masking the NLS) and Importin for ChREBP binding[Sakiyama et al., 2008]. This NLS, located in MCR4, redefined as a bipartite NLS encompassing the residues 158-190 by Ge *et al.* was also found to be a secondary binding site for 14-3-3 [Ge et al., 2011]. Its close proximity to the phosphorylation site S196 might explain the role of phosphorylation in trafficking [Kawaguchi et al., 2001, Ge et al., 2011]. Importin is not able to compete off 14-3-3 completely due to the presence of the primary 14-3-3 binding site in MCR3. If 14-3-3 binds to this site as a monomer, or as dimer with one empty binding pocket is not known [Ge et al., 2011]. However, since 14-3-3 is predominantly a dimer (reviewed in [Sluchanko and Gusev, 2012]), and binding to MCR3 is crucial for CHREBP response to high glucose levels [Li et al., 2008], it has to be assumed that under high glucose conditions at least one 14-3-3 monomer is bound to MCR3, whereas MCR4 is occupied with Importin.

Max-like protein X, an obligatory interaction partner

As described in Section 1.4.4 and [Cairo et al., 2001, Stoeckman et al., 2004], Mlx is the obligatory interaction partner of the C-terminal ChREBP region. Deletion of Mlx in *Drosophila* results in lethality during development when larvae are raised on high sugar food. Strikingly, this could be rescued by a change to protein rich food sources [Havula et al., 2013]. Eilers *et al.* also

described a role for Mlx in nuclear localization of the ChREBP paralogue MondoA. MondoA was only able to localize to the nucleus, when both MondoA and Mlx were overexpressed, suggesting a C-terminal export signal in the Zip-like region of Mondo proteins, which is overwritten by interaction with Mlx [Eilers et al., 2002]. Due to the high conservation between MondoA and ChREBP (as for example demonstrated by McFerrin *et al.* [McFerrin and Atchley, 2012]), it has to be assumed that ChREBP is regulated in a similar fashion. Although bHLH/Zip transcription factors are known to homodimerize or heterodimerize with a variety of family members, ChREBP is only reported to heterodimerize with Mlx [Cairo et al., 2001, Stoeckman et al., 2004, Ma et al., 2007]. Mlx, however, is also found in complex with Mad1, Mnt and itself, suggesting additional cellular functions in gene regulation [Cairo et al., 2001, Billin et al., 1999].

Additional protein interactions of ChREBP

A variety of additional ChREBP interacting proteins have been reported. For example the binding of sorcin to the N-terminal region, resulting in a cytoplasmic localization. In pancreatic β-cells sorcin binding is released and ChREBP accumulates in the nucleus [Noordeen et al., 2012] upon Ca^{2+} influx. However, the complex involvement of Ca^{2+} in β- cell signaling and for example its function in vesicle fusion, resulting in an increase of glucose transporters, have to be kept in mind when talking about Ca^{2+} and sorcin as regulator of ChREBP activity (reviewed in Sabatini *et al.* [Sabatini et al., 2019]).

In 2009 Burke *et al.* showed the co-occupation of the L-PK promotor by ChREBP, HNF4α and CBP/ p300 in a glucose dependent manner. Exact regions of protein-protein interactions are not known, however Bricambert *et al.* showed that p300 acetylates ChREBP at K672, increasing the transcriptional activity of ChREBP [Bricambert et al., 2010]. The formed complex is reported to be disrupted by increasing levels of cAMP [Burke et al., 2009]. Interestingly HNF4α was also found to bind E-boxes in the ChREBP gene, having an influence on ChREBP(-β) expression [Meng et al., 2016]. The recruitment of the histone acetyl transferase p300 was also shown to cause acetylation of histone H4, influencing the chromatin landscape of promotor regions [Cha-Molstad et al., 2009].

O-GlcNAc transferase (OGT) interacts and transfers N-acetylglucosamine (GlcNAc) on ChREBP. This modification is reported to have a stabilizing function on ChREBP, upregulating gene expression of target genes and protecting ChREBP from proteosomal degradation [Sakiyama et al., 2010, Guinez et al.,

2011]. The protein-protein interaction between OGT and ChREBP is stronger under low glucose conditions, suggesting a "ready to be activated state" [Guinez et al., 2011]. Since the building blocks for GlcNAcylation require an energy rich cellular state OGT is considered as a nutrient sensor [Guinez et al., 2011]. Yang *et al.* showed presence of GlcNAc modification at Thr517 and Ser839 is important for dimerization with Mlx and glucose- dependent regulation of ChRBEP by influencing nuclear trafficking [Yang et al., 2017]. Interestingly, FoxO1 was shown to connect insulin signaling pathways with GlcNAc of ChREBP. How this inhibition of OGT is achieved is still not understood [Ido-Kitamura et al., 2012].

1.5.3 Role of post-translational modifications in ChREBP activity

ChREBP was reported to be post-translationally modified by a variety of research groups, a summary of these modifications can be found in Table 1.1 and illustrated in Figure 1.14. The most prominent modification is the phosphorylation by protein kinase A (PKA) in the N-terminal region. Under low glucose conditions PKA phosphorylates ChREBP at Ser196, promoting the binding of 14-3-3 and nuclear export/ cytosolic retention [Kawaguchi et al., 2001]. However, Sakiyama *et al.* showed that single mutants of S140A and S196A were still able to bind 14-3-3 [Sakiyama et al., 2008]. Although these mutants enriched in the nucleus, under both low and high glucose conditions, an increase in the expression of target genes was only observed under high glucose conditions. Indicating additional mechanism of transcriptional activation [Sakiyama et al., 2008]. The model of Kawaguchi *et al.* was further challenged by Tsatsos and Towle, who showed that ChREBP phosphorylation was not affected in response to changing glucose levels, this was also the case for the C-terminal phosphorylation sites S626 and T666. If the observed differences are due to experimental and/or tissue specific mechanisms in ChREBP regulation is still not fully understood. An additional inhibitory modification of ChREBP is the phosphorylation at S568, in the prolin-rich region, by AMPK [Kawaguchi et al., 2002]. AMPK is activated under low glucose conditions by increasing levels of AMP (reviewed in [Kahn et al., 2005], the phosphorylation results in a reduction of DNA binding by ChREBP.

The inhibitory phosphorylations are removed by the activation of the phosphatase PP2A, which is regulated by the pentose phospate pathway intermediate

X5P [Kabashima et al., 2003, Kawaguchi et al., 2001].

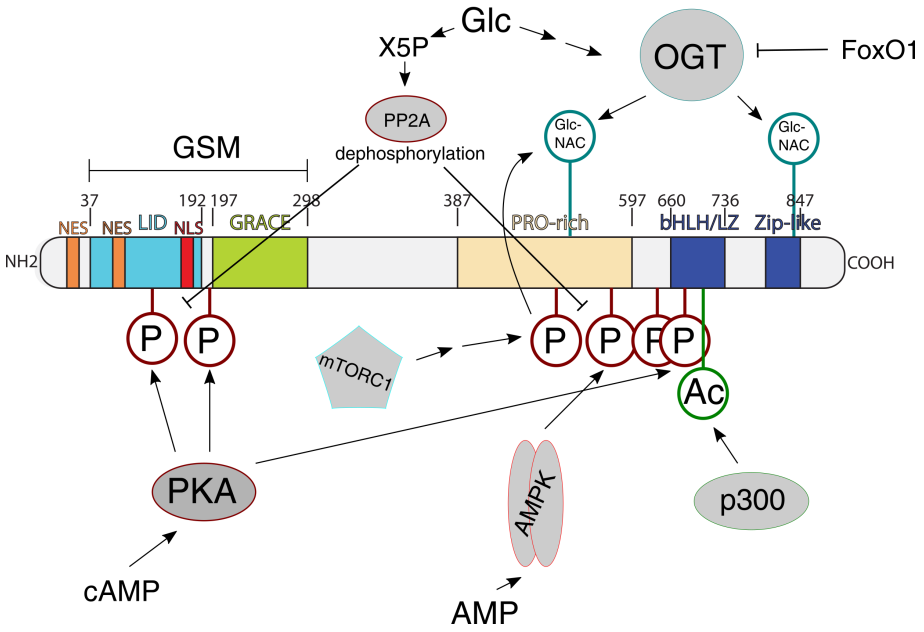

Figure 1.14: **Overview of post-translational modifications regulating ChREBP activity**
Metabolic cues regulate ChREBP activity by post-translational modifications. High glc levels increase concentrations of X5P and UDP-N-acetyl-glucosamine. X5P activates the phosphatase PP2A. OGT transfers GlcNAc to the C-terminus of ChREBP. Acetylation by p300 increases DNA affinity. Under starvation cAMP and AMP levels are high and activate kinases that phosphorylate ChREBP on various positions, causing nuclear export and inactivation. P= phosphorylation, Ac= acetylation, GlcNAc= N-acetylglucosamine.

The post-translational modification of proteins with N-acetylglucosamine (GlcNAc) is seen as a readout of the nutritional state of the cell, integrating nutrient regulation with transcription and signaling (reviewed in [Hart, 2019]). These modifications by OGT on ChREBP are all in the C-terminal region. Although these modifications are not crucial for ChREBP transcriptional activity, they lead to an increase in target gene expression by stabilisation of ChREBP and its interaction with DNA. N-acetylglucosamine (GlcNAc) was also shown to protect ChREBP from degradation via the proteasomal pathway [Sakiyama et al., 2010, Guinez et al., 2011, Yang et al., 2017]. Ido-Kitamura *et al.* demonstrated that overexpression of constantly active FoxO1 leads to a reduction of GlcNAc on ChREBP, suggesting a link between insulin signaling and ChREBP activity [Ido-Kitamura et al., 2012].

Under high glucose conditions ChREBP is in complex with p300 at promotors of ChREBP target genes. P300 acetylates ChREBP in the bHLH/Zip region at

residue K672, promoting the recruitment to ChoRE of target genes [Bricambert et al., 2010].

Position	Modification	Function	Reference
140, Ser	Phosphoryl.	14-3-3 interaction, cytosolic localization	[Sakiyama et al., 2008]
196, Ser	Phosphoryl.	Modified by PKA, cytosolic retention	[Kawaguchi et al., 2001, Davies et al., 2008, Tsatsos and Towle, 2006, Sakiyama et al., 2008]
514, Ser	Phosphoryl.	Modified by mTORC1, enhances Glc-NAc of T517	[Yang et al., 2017]
517, Thr	GlcNAc	Modified by OGT, stabilization, upregulation of target genes, protection against degradation, Mlx dimerization	[Sakiyama et al., 2010, Guinez et al., 2011, Yang et al., 2017]
568, Ser	Phosphoryl.	Modified by AMPK, influence on DNA binding	[Kawaguchi et al., 2002]
626, Ser	Phosphoryl.	Modified by PKA, inhibition of DNA binding	[Kawaguchi et al., 2001]
666, Thr	Phosphoryl.	Modified by PKA, loss of DNA binding	[Kawaguchi et al., 2001]
672, Lys	Acetylation	Modified by HAT/p300, increased recruitment and transcriptional activity	[Yang et al., 2017, Bricambert et al., 2010]
839, Ser	GlcNAc	Modified by OGT, stabilization, upregulation of target genes, protection against degradation, Mlx dimerization	[Sakiyama et al., 2010, Guinez et al., 2011, Yang et al., 2017]

Table 1.1: Table of post-translational modifications and their functions

1.5.4 Role of metabolites in ChREBP activity

Over the last couple of years, a variety of metabolites have been reported to influence ChREBP activity. In this section we will give an overview of metabolites and how they might be involved in the regulation of ChREBP.

Xylulose 5-phosphate, activation of ChREBP by dephosphorylation

X5P is a intermediate of the pentose phosphate pathway (PPP) and therefore increases under elevated glucose conditions. X5P has been shown to activate

protein- phosphatase 2A (PP2A) in the liver [Nishimura and Uyeda, 1995]. Subsequently, Doiron *et al.* showed that addition of xylitol to hepatocytes leads to an increase in ChREBP target gene expression, such as LPK. This was shown to be in a PP2A- dependent manner, without affecting Glc6P levels [Doiron et al., 1996]. The link between the PPP, PP2A and ChREBP activity by dephosphorylation of S196 and T666 was first suggested by Kawaguchi *et al.* [Kawaguchi et al., 2001]. It was later shown that addition of X5P to cytosolic extract resulted in dephosphorylation of S196 and subsequent nuclear translocation. In nuclear extract the addition of X5P is sufficient to remove phsophorylation at T666 and S568, activating the DNA-binding activity of ChREBP [Kabashima et al., 2003].

However, the model of X5P as the key metabolite in the regulation of ChREBP activity is challenged, since ChREBP activation is independent of X5P in cells where the PPP only plays a minor role or PP2A is not abundant [Li et al., 2010, da Silva et al., 2006]. In addition, the model of ChREBP regulation by phosphorylation, and therefore the involvement of the X5P-PP2A axis, has been challenged as already mentioned in Section 1.5.3. The X5P model also cannot explain regulation of ChREBP in organisms where the (de)phosphorylation sites are not conserved, such as *D. melanogaster* and *C.elegans* [Li et al., 2010]. However, it cannot be excluded that X5P plays a role in lipogenic tissue or be part of a regulatory networks including additional regulatory signals [Li et al., 2010, Sakiyama et al., 2010].

AMP modulates localization by regulating interactions with 14-3-3

Under low glucose conditions or a high fat diet AMP levels increase and activate AMPK, resulting in the subsequent phosphorylation of ChREBP at Ser568, altering the ability of DNA binding. [Kawaguchi et al., 2002]. In 2016 Sato *et al.* showed an additional role of AMP in regulation of CREBP. AMP causes the sequestering ChREBP in the cytosol by promoting 14-3-3 interaction. The increase in ChREBP affinity for 14-3-3 is achieved by direct binding of AMP in the protein-protein interface of 14-3-3 and the ChREBP α2- helix (see Figure 1.15) [Sato et al., 2016]. Although Sato *et al.* experimentally showed the binding of AMP (also reproduced in this thesis) based on the size of the suggested binding pocket and the poor electron density for AMP in their crystal structure, it is questionable how accurate the current structure of the AMP bound 14-3-3/ChREBP complex is. The electron density and binding site are shown in Figure 1.15B and C. So far, AMP is the only metabolite that was shown to directly bind ChREBP.

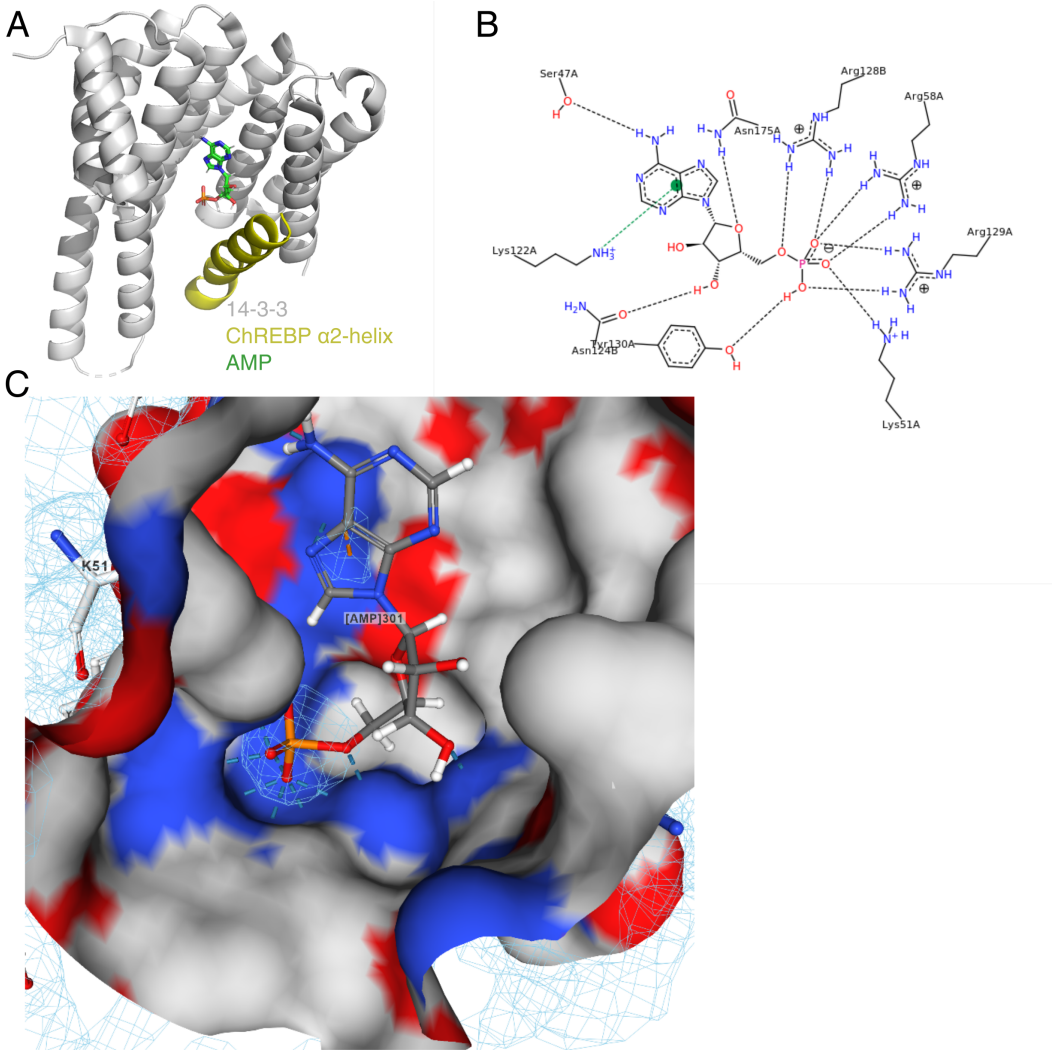

Figure 1.15: **Structure of AMP bound to 14-3-3/GSM**
A: Crystal structure of AMP bound to the complex of 14-3-3 and the α2-helix of ChREBP, located in MCR3 (117-137aa) B: Residues involved in ligand binding. Chain A= 14-3-3, Chain B= ChREBP. C: Binding pocket with the electron densities for the ligand (mesh). Structure published by Sato *et al.* PDB: 5F74 [Sato et al., 2016]

cAMP activates the kinase PKA

It has been suggested that to regulate ChREBP activity cAMP, much like AMP, activates specific kinases under low glucose conditions. In this particular case the kinase PKA [Kawaguchi et al., 2001]. As described in Section 1.5.3, the importance of these phosphorylation sites in ChRBEP regulation are under debate. An additional explanation for the inhibitory effect of cAMP was presented in 2009 by Burke *et al.* [Burke et al., 2009], where the recruitment of HNF4α, CBP and ChREBP to the promotor region of LPK was shown to be necessary to fully activate LPK transcription. Increase in cAMP antagonises the glucose dependent recruitment of this complex, thereby inhibiting gene expression, an effect first descibed by Bergot *et al.* in 1992 [Bergot et al., 1992]. Although Burke *et al.* showed the cAMP-PKA pathway is required for this repression, it is not because of phosphorylation of previously described PKA target sites on HNF4α or ChREBP. Leading to the speculation of CBP as a potential target for phsophorylation by PKA. Under low glucose conditions this physphorylation of CBP results in the disruption of the ChREBP-HNF4α -CBP complex [Burke et al., 2009].

Fructose-2,6-bisphosphate regulates ChREBP in liver cells

By altering fructose-2,6-bisphosphate (F2,6bP) levels in liver cells, Arden *et al.* could show that ChREBP activity and nuclear localization is increased by the presence of this key regulatory metabolite. Although the authors do not exclude the role of other metabolites in ChREBP regulation, they also speculate if ChREBP activity is influenced not by a single metabolite, but rather a ratio of metabolites. In liver cells F2,6bP is the limiting factor, whereas Glc6P or X5P might be the limiting factor in pancreatic cells [Arden et al., 2012]. How F2,6bP regulates ChREBP in detail is still unclear.

Glucose-6-phosphate is a central metabolite in the regulation of lipogenic genes

The correlation between Glc6P levels and the upregulation of lipogenic genes has been widely reported [Foufelle et al., 1992, Prip-Buus et al., 1995, Girard et al., 1997]. By altering abundance and activity of enzymes involved glycolysis, increasing amounts of evidence has emerged, describing Glc6P as a major regulator of ChREBP activity [Prip-Buus et al., 1995, Arden et al., 2012, Iizuka et al.,

2013, Li et al., 2010, Hoogerland et al., 2019, Dentin et al., 2012]. The central role of the primary glucose metabolite Glc6P in cell metabolism, however makes it difficult to demarcate whether the activation is directly regulated by Glc6P, or a secondary effect caused by shifts in metabolic flux (discussed in Arden *et al.* [Arden et al., 2012]). How Glc6P regulates ChREBP is still not known. The presence of the GSM (see Section 1.4.1) suggests a hinge-like model where, upon direct binding of Glc6P, the inhibitory effect of the LID might be released (see Figure 1.16) [Davies et al., 2010]. This mechanism is further supported by the newly described MCR6, as a potential Glc6P binding site regulating ChREBP in an allosteric manner [McFerrin and Atchley, 2012]. However, so far no experimental evidence exist for this model, other than a sequence similarity to Glc6P binding enzymes.

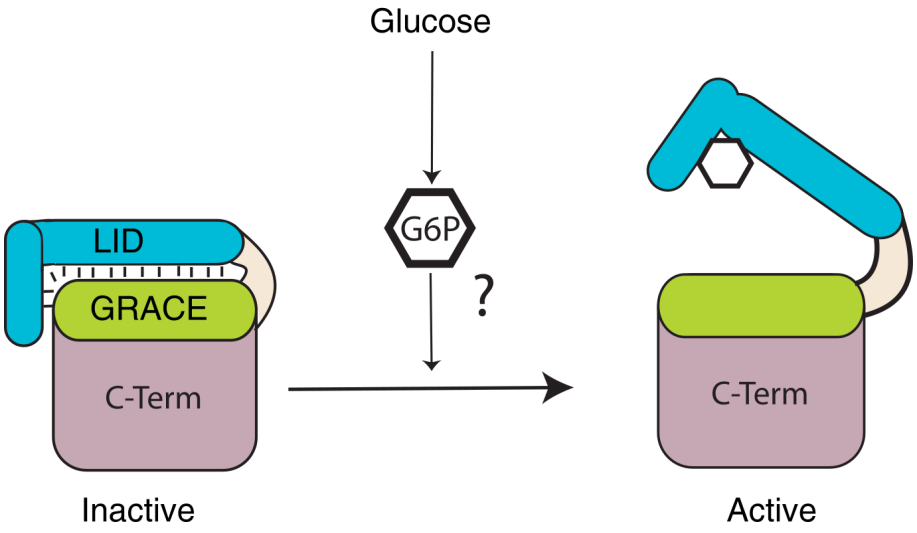

Figure 1.16: **Hinge model of ChREBP activation**
Upon binding of Glc6P or a different glucose metabolite the inhibitory effect from the LID is lifted from the GRACE domain and ChREBP become active. Model based on [Davies et al., 2010]

2 Aims of this Study

Research of ChREBP demonstrate its central physiological importance in energy homeostasis and metabolism. Although functional studies and characterization of ChREBP *in vivo* showed its activity is dependent on glucose levels, a detailed understanding of regulatory mechanisms are still absent. Over the last two decades several regulatory pathways of ChREBP activity were described. However, these mechanism are still under debate and questioned in their physiological relevance.

One reason for the limited understanding of ChREBP regulation is the lack of direct biochemical assays. This is due to the fact that the transcription factor is very challenging to express and purify in quantities sufficient for biochemical assays. Therefore, most assays in the published literature were performed *in vivo* and hereby can only provide an indirect readout on the ChREBP regulatory network. Although these assays hinted towards an involvement of glucose-(metabolites) in ChREBP activity, the complex cellular environment and the central position of glucose in cell metabolism makes it impossible to test and thus asses for a direct interaction between metabolites and Glc6P.

The central hypothesis of my thesis is related to showing the potential direct interaction of sugar metabolites and ChREBP, and testing whether this alters its activity. Such data would for the first time describe a nuclear receptor-like protein for glucose metabolites. In this scenario, glucose metabolites itself act as signaling molecules. Fundamentally changing the knowledge of how eukaryonta sense carbohydrates.

Therefore, the aim of my thesis is to establish biochemical and biophysical assays to evaluate if glucose metabolites can bind in a receptor-like fashion directly to ChREBP. The designed assays shall give *in vitro* information about specificity, dynamicity and functionality of ChREBP as a potential sensor of glucose-metabolites. To do so, the following aims have to be achieved:

- ChREBP, and/or domains of ChREBP have to be expressed and purified in sufficient amounts and purity.

- Suitable binding assays have to be developed and set-up.
- A variety of relevant metabolites have to be tested for potential binding.
- Characterize structural changes as a potential consequence of ligand binding.
- Define the metabolite binding site.

Finally, the obtained results have to be set into context of our own and reported *in vivo* studies.

3 Materials and Methods

3.1 Cloning of expression vectors

3.1.1 Standard PCR protocol

	Volume [µL]	Final conc.
Primer Fwd (10 µM)	1	0.2 µM
Primer Rev (10 µM)	1	0.2 µM
Betain 5 M	10	1 M
template	0.5	0.2 ng/µL
dNTPs	1	200 µM
5x Phusion buffer	10	1x
Phusion polymerase	0.2	8 mU/µL
MQ	Up to 50 µL	

Table 3.1: PCR reaction mix

The following PCR protocol was used to amplify the target DNA:
Initial Denaturation (95°C, 3 min), denaturation (95°C, 30 sec), annealing (55°C, 30 sec), elongation (72°C, 1 min/kbp), cycles 34, store at 12°C.

3.1.2 Agarose Gel Electrophoresis

To separate DNA fragments agarose gel electrophoresis was performed. Small DNA fragments migrate faster through the gel-matrix towards the anode than larger fragments. The *NEB* 2-log DNA standard was run in parallel to the samples to determine the fragment sizes.
The agarose gels were prepared from a 1% agarose-solution (w/v) in TAE Buffer (see Section 3.12). 15 µL of 0.25 mg/mL Ethidium Bromide was added to the still liquid gel for later visualization of DNA. The solidified gel was covered with 1x TAE buffer and run at 100 V for 20 min. Afterwards the gel was analyzed under UV-light.

3.1.3 Gel Extraction

DNA-fragments of interest were cut from the gel under UV-light. To extract the DNA form the gel, manufacturers protocol. In brief, the gel was heated in gel extraction buffer, loaded on a spin column and eluted with ddH_2O.

3.1.4 Restriction Digest

For digestion of DNA, all restriction enzymes were purchased from *NEB*. If possible "high-fidelity" enzymes were chosen. Reaction buffer was choosen based on the manufactures recommendation. The restriction digest mixture (Table 3.2) was incubated for at least 2 hours at 37°C.

Component	Amount/Volume [µL]
Buffer (10x)	5
Restriction enzyme 1	2
Restriction enzyme 2	2
DNA	2 µg Plasmid or 30 µL PCR product(no spec. conc.)
ddH_2O	up to 50 µL

Table 3.2: Restriction digest

3.1.5 Reaction Clean-Up

To purify DNA from enzymatic reactions, such as restriction digests or PCR reactions, the *MinElute Reaction Cleanup Kit, Quiagen*, was used. All steps were carried out according to manufactures recommendations. For eluting the DNA ddH_2O was used.

3.1.6 Plasmid Mini-Prep

For small scale purification of bacterial plasmids 4 mL of LB containing the appropriate antibiotics were inoculated with a colony and incubated at 37°C overnight at 165 rpm. The next day the culture was pelleted and the plasmid was purified using a *mi-Plasmid Miniprep kit, Metabion International AG*, according to manufacturers recommendations. In brief, the pellet was lysed, cell debris removed, applied to a spin column and after washing steps eluted in ddH_2O. Purified DNA was stored at -20°C.

3.1.7 Plasmid Midi-Prep

For purification of bacterial plasmids in a larger scale, 50 mL of LB containing the appropriate antibiotics were inoculated and incubated overnight at 37°C at 165 rpm. The next day the culture was pelleted and the plasmid was purified using the vacuum based *PureYield Plasmid Midiprep System, Promega*. DNA was eluted in 600 µL ddH_2O.

3.1.8 Ligation

DNA of interest (PCR insert) was ligated into a vector, digested with the same restriction enzymes as the insert. The molar ratio between vector and insert was 1:3. The reaction mix, containing the T4 Ligase (Table 3.3) was incubated for 1-2 hours at room temperature, or at 4°C overnight.

Component	Amount/Volume [µL]
T4 Ligase Buffer (10x)	1 µL(1x)
Vector	50 ng
Insert	3x vector conc.
T4 Ligase	1 µL
ddH_2O	up to 10 µL

Table 3.3: DNA Ligation mix

3.1.9 Transformation

To transform DNA into *Escherichia coli* (*E. coli*), chemical competent lab strains of DH5alpha were used. 1 µL of Ligation mix or 0.2 µL of purified DNA were gently mixed with 50 µL of competent cells and incubated for 15 min on ice. Afterwards a heat-shock of 35 seconds at 42°C is applied, followed by a 2 min incubation on ice. 250 µL of LB is added and the cells are incubated for 30 min at 37°C and 600 rpm on a thermoshaker. Afterwards 100 µL are streaked on a LB plate containing the appropriate antibiotics or 50 µL were used to inoculate a liquid culture overnight.

3.1.10 Cloning of final expression vector of 14-3-3/GSM

Mouse 14-3-3 beta/alpha was obtained from mouse cDNA using the primer set 205853 and 205855 (see Table 7.5). The obtained construct was cloned

into pET-M11 using AgeI and XbaI restriction sites (done by previous lab members, resulting in the clone CL3248). For expression of 14-3-3 in complex with ChREBP-GSM the *E. coli* expression vector pET-Duet1 (*Novagen*) was modified by adding a ChREBP sequence in combination with TEV protease cleavage site followed by a 6xHis-tag C-terminal of the ChREBP insert of the second multiple cloning site. Described features were introduced by using the primers 206407 and 206457. For the final version of the expression plasmid CL3776, ChREBP cDNA was obtained from the lab of Cathrin Postic, Paris (lab clone number CL3237). The GSM of ChREBP was cloned into the modified pet-Duet1 vector using the restriction sites NdeI and KpnI (2nd MCS), which were introduced by PCR to the insert by using the primer pair 206407/206815. 14-3-3 was cloned from the plasmid CL3248 (see above) using primer 2021 and 2018. The resulting PCR fragment was ligated into pET-Duet1 using NcoI and EcoRI restriction sites. For both inserts the correctness was controlled by sequencing (*GATC Biotech AG*). The final plasmid was catalogued as CL3776 (for vectormap see Figure 3.1).

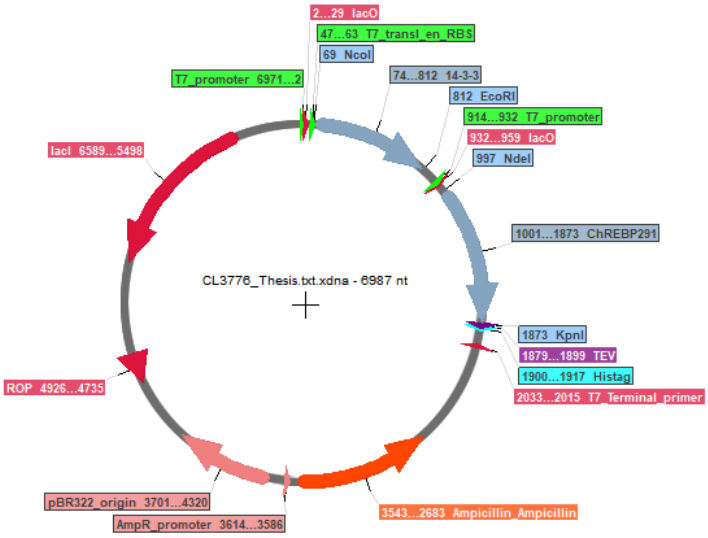

Figure 3.1: **Vectormap of 14-3-3/GSM(CL3776)**
Features of the expression vector pET-Duet1 containing the cDNA sequences for 14-3-3 and GSM 1-291. Map generated using *SerialCloner*.

3.1.11 Cloning of point mutants

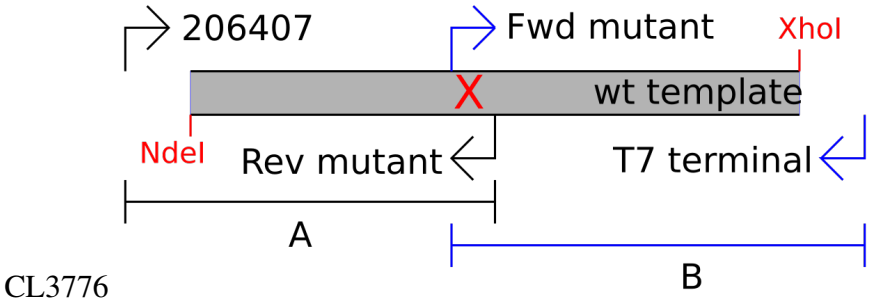

Figure 3.2: **Schematic representation of cloning strategy**
Arrows indicate direction of primers. Mutant primers contain mutated codons resulting in the translation to a different aa (red mark).

Figure 3.2 shows the basic principle of the site directed mutagenesis. The gene of interest is split into two fragments and the mutation is introduced by using primers containing the mutated sequence. After the first PCR (Table 3.4), fragment A and B are purified and mixed in a 1:1 ratio (approx. 1 µL each). The PCR is repeated using the primers 206407 and T7 terminal (Table 3.5). The PCR product is extracted and digested with the appropriate restriction enzymes together with the vector. After ligation the vector is transformed into *E. coli* DH5alpha.

PCR protocol for generation of point mutants:
Initial denaturation (95°C, 3min), denaturation (95°C, 30 sec), annealing (55°C, 30 sec), elongation (72°C, 1 min/kbp), cycles 34, store at 12°C.
Primers used for point mutations tested in this thesis are listed in Table 3.6

	Volume [µL]	Final conc.
Primer Fwd (10 µM)	1	0.2 µM
Primer Rev (10 µM)	1	0.2 µM
Betain 5 M	10	1 M
Template	0.2	0.2 ng/µL
dNTPs	1	200 µM
5x Phusion buffer	10	1x
Phusion polymerase	0.2	8 mU/µL
MQ	Up to 50 µL	

Table 3.4: PCR 1 to introduce point mutation (Sectio A/B)

	Volume [µL]	Final conc.
Primer Fwd (10 µM)	1	0.2 µM
Primer Rev (10 µM)	1	0.2 µM
Betain 5 M	10	1 M
Fragment A	1	0.2 ng/µL
Fragment B	1	0.2 ng/µL
dNTPs	1	200 µM
5x Phusion buffer	10	1x
Phusion polymerase	0.2	8 mU/µL
MQ	Up to 50 µL	

Table 3.5: PCR 2

Identifier	Mutation	Seq (5'-3')
206407 fwd	*wt* Fwd	gattatcatatggca cga gcaCTG GCGGATCTATCCG
TP2033 fwd	14-3-3, S47A	ggaatctactcGCTgttgcctacaagaacgtgg
TP2034 rev	14-3-3, S47A	ccacgttcttgtaggcaacAGCgagtagattcc
TP2035 fwd	14-3-3, K51A	ctgttgcctacGCGaacgtggtaggtgccc
TP2036 rev	14-3-3, K51A	gggcacctaccacgttCGCgtaggcaacag
TP2037 fwd	14-3-3, R58A	gtg gtaggtgcccgcGCCtcttcctggcgtgtc
TP2038 rev	14-3-3, R58A	gacacgccaggaagaGGCgcgggcacctaccac
TP2031 fwd	GSM, W127A	cggctgaacaacgccatcGCCagagcctggtacattcag
TP2032 rev	GSM, W127A	ctgaatgtaccaggctctGGCgatggcgttgttcagccg
TP2027 fwd	GSM, Q241H	gagcctgggggccggCAccttctagacctggactgc
TP2028 rev	GSM, Q241H	gcagtccaggtctagaagGTGccggcccccaggctc
T7 terminal	*wt* for pET-vectors	CTAGTTATTGCTCAGCGG

Table 3.6: Primers for site directed mutagenesis

3.1.12 Cloning expression vector for Importin-α1 and Δ70 Importin-α1

Template for Importin was obtained from Origen (MR208487 NM_ 010655). For cloning, the standard PCR protocol with the primer set TP2069/ TP2070 for Importin-α1 and TP2071/TP2070 for Δ70 Importin-α1 was used (see Table 7.5). The PCR product was analyzed on a 1% agarose gel, gel extracted and digested using NcoI-HF and EcoRI-HF (*NEB*). In parallel the expression vector pET-M11 (Novagen) was linearized with the same restriction enzymes. Afterwards the inserts were ligated into the pET-M11 vector using T4-ligase (*NEB*). 1 µL of the ligation mix was transformed into *E. coli* DH5alpha and platen on LB plates containing the appropriate antibiotics (kanamycin). The next day colonies were picked and 2 mL LB-kanamycin inoculated for later plasmid mini-prep. Plas-

mids were sequenced and added to the database. Importin-α1= CL4165 and Δ70 Importin-α1 = CL4192.

3.1.13 Cloning expression vector for Glms

Glms was cloned by PCR from the genomic DNA of the lab stock *E. coli* DH5alpha into pET-M11, as described in 6.1.4. For PCR the primerset 207201/207202 were used, encoding the restriction sites NcoI and KpnI for introducing the insert into the vector. Clone was sequenced and deposited in the database as CL3963.

3.2 Recombinant Protein Expression and Purification

3.2.1 Protein Expression

Several *E. coli* strains were tested for protein expression: BL21 pRIL, BL21, BL21 solubl, Bl21 pLys, BL21gold and Rosetta, also in combination with the *Takara Chaperon Plasmid set, Cat. 3340* for the expression of additional chaperons. In the end expression with BL21pRIL gave the most consistent results.
The *E. coli* strain Bl21 pRIL was transformed with expression vectors using heat shock. Overnight cultures were grown at 37°C in LB-medium, supplemented with chloramphenicol and ampicillin. 2 L of PSB media (Section 3.12.4) were inoculated with 20 mL overnight culture and grown at 37°C for the first hours. optical density at a wavelength of 600nm (OD_{600}) was monitored during the entire growth. At an OD_{600} of 0.4-0.5 the cultures were cooled down to 20°C followed by induction of expression by the addition of 0.1 mM IPTG at an OD_{600} of 0.7-0.8. Cultures were harvested the next morning by centrifugation using a Beckman Coulter Avanti J-20XP centrifuge in combination with a JLA 8.100 rotor at 4000 rpm. The pellets were frozen and stored at -20°C.

3.2.2 Protein Purification

Detailed buffer compositions can be found in Section 3.12, if not listed separately.

Test-Expression and Purification of different ChREBP fragments

4 mL of either LB, TB, PSB or PSB+Glc+$MgSO_4$ were inoculated with BL21pRIL transformed with the vectors listed in Table 1. Cultures were grown at 37°C at

170 rpm to an OD_{600} of 0.5-0.7. Afterwards expression was induced by 0.1 mM IPTG and kept overnight at 16°C. The next morning, cultures were harvested by centrifugation and tested for expression by following instructions of the Protino 96 Ni-IDA purification protocol for native conditions (*Macherey-Nagel, catalogue 745300.1*). Fractions of whole cell lysate (5 µL) and the elution (10 µL) were loaded on 14%-SDS-PAGE gel for analysis.

Purification of 14-3-3 in Complex with ChREBP GSM

All steps were performed on ice or in the cold room. Three *E. coli* pellets of two liter cultures (approx.15 g each) were resuspended in 50 mL lysis buffer, each supplemented with one tablet of complete protease inhibitor (*Roche*) and 2.5 µg/mL lysozyme. For lysis a Bransons sonifier with a coin shaped rod was used (6x1 min pulse, 2 min break, duty cycle 70%, output control 5). Afterwards the lysate was centrifuged for 1 h using a JA 25.50 rotor at 20 000 rpm and 4°C (*Beckman Coulter*).
For affinity chromatography the supernatant was loaded onto a self-packed Ni-NTA (*Qiagen*) column (column volume 10 mL) with a flowrate of 5 mL/min, using an akta pure system. The column was washed with at least 5 CV of lysis buffer. Column bound protein was eluted using 50% and 100% of elution buffer. Fractions containing the target proteins were pooled and dialyzed for 5-6 h in Ion Exchange buffer A (IEX A) using dialysis tubing with an 12000 MWCO (*Roth, Germany*). To cleave off the C-terminal His-tag 1.25 mg of in-house purified His-tagged TEV protease was added into the dialysis tubing. After dialysis the His-tag, as well as TEV protease were removed by running the sample over an 5 mL HisTrapHP column (*GE-Healthcare*). The flow-through was collected and applied onto a HiTrapQ column using IEX A as a running buffer[1]. For further separation of the protein sample a gradient elution was chosen (1-35%, 1% per CV), using IEX B as an elution buffer. Fractions of the first major peak were pooled an concentrated using an centrifugal concentrator tube (Amicon Ultra 15 mL, 10,000 MWCO). The concentrated protein then was applied onto a pre-equilibrated HiLoad-Superdex 200 pg 26/60 (*GE-Healthcare*), using the gel filtration buffer. Fractions of the major peak were pooled and dialyzed overnight in dialysis buffer. After dialysis the sample was again concentrated. By centrifugation (10 min, 15000 g, 4°C) at a table-top centrifuge potential pro-

[1] for upscaled purifications a self-packed 15SourceQ column was used, with a bed volume of 15 mL

tein aggregates were removed. Concentrations were measured using a nanodrop (*NanoDrop 2000C Thermo-Scientific*) and aliquots of adequate volumes were frozen in liquid nitrogen and stored at -80°C for later use.

Purification of 14-3-3 in complex with ChREBP GSM for scintillation proximity assays

All steps were performed on ice or in the cold room. An *E. coli* pellet expressing 14-3-3/GSM (clone CL3776) was resuspended in lysis buffer (50 mL for 1 l culture), supplemented with one tablet of complete protease inhibitor (*Roche*) and 2.5 µg/mL lysozyme. For lysis a bransons sonifier with a coin shaped rod was used (6x1 min pulse, 2 min break, duty cycle 70%, output control 5). Afterwards the lysate was centrifuged for 1 h using a JA 25.50 rotor at 20 000 rpm and 4°C.
For affinity chromatography the supernatant was loaded onto a self-packed Ni-NTA column (*Qiagen*) (column volume 10 mL) with a flowrate of 5 mL/min using an akta pure system. The column was washed with at least 5 CV of lysis buffer. Column bound protein was eluted using 50% and 100% of elution buffer. To reduce the salt concentration, the fractions were pooled and diluted with ion-exchange buffer A (IEX A) in a 1:3 ratio. The protein solution was loaded onto a HiTrapQ column using IEX A as a running buffer and finally eluted with IEX B using a gradient from 0-35% B over 35 column volumes. The appropriate fractions were pooled and concentrated for size exclusion chromatography using a HighLoad-Superdex200pg (26/60) and gel filtration buffer. Fractions of the main peak were pooled and dialyzed overnight in dialysis buffer. The next morning the protein was concentrated to appropriate concentrations using an Amicon concentrator tube with a cut off of 10 kDa. Protein and buffer aliquots were frozen in liquid nitrogen and stored at -80°C for later use.

Purification of 14-3-3 in complex with ChREBP GSM for MST

As described in Section 3.2.2 (Purification of 14-3-3 in Complex with ChREBP GSM). For samples tested with MES buffer pH 6.5 HEPES was replaced with MES pH6.5 in all purification steps. For samples tested with HEPES buffer pH 7 same buffers were used as in Section 3.2.2 however, pH was adjusted to 7 in all purification steps by using HCl.

Purification of 14-3-3

Lysis was performed as described in Section 3.2.2 (Purification of 14-3-3 in Complex with ChREBP GSM). For affinity chromatography a 5 mL Protino Ni-NTA column (*Macherey-Nagel*) was used. To remove the His-tag the, pooled fraction of elution was dialyzed in IEX A buffer together with TEV-protease. After 5-6 hours of dialysis the sample was run again over a 5 mL Protino Ni-NTA column, using IEX A as a running buffer. The flow through was collected and concentrated to a volume suitable to load onto a HiLoad Superdex 200pg 26-60 column (*GE-Healthcare*). Fractions containing protein of interest were pooled and dialyzed overnight in dialysis buffer. The next morning the sample was again concentrated. By centrifugation (10 min, 15000 g, 4°C) in a table-top centrifuge potential protein aggregates were removed. Concentrations were measured using a nanodrop (*Nanodrop 2000C, Thermo Scientific*) and aliquots of adequate volumes were frozen in liquid nitrogen and stored at -80°C for later use.

Purification of 14-3-3 and GSM point mutants

Mutants were expressed and purified identical to *wt* Section 3.2.2 (Purification of 14-3-3 in Complex with ChREBP GSM) for ITC experiments.

Purification of 14-3-3 for HDX-MS

For comparison of 14-3-3 without GSM and 14-3-3 with GSM it was necessary to purify 14-3-3 with an identical peptide sequence as in 14-3-3/GSM. Therefore an untagged 14-3-3 had to be purified as the following: 14-3-3 was expressed using the same vector as for 14-3-3/GSM, however the second MCS was empty (CL3636). For a first capture step, the pellet was lysed in Buffer A (50 mM MES, 50 mM NaCl, 1 mM β-ME, pH= 6) containing complete EDTA free protease inhibitor(*Roche*) using sonification as described before. The lysate then was centrifuged for 1 h, 4°C at 20000 rpm and the supernatant was run over a HiTrap Q 5 mL colum (*GE-Healthcare*). Proteins were eluted by a gradient of buffer B (50 mM MES, 2 M NaCl, 1 mM β-ME, pH6). Fractions were analyzed on SDS-PAGE, pooled and dialyzed for 3 h in 20 mM HEPES, 50 mM NaCl, 1 mM β-ME pH 7,5. Afterwards the sample was concentrated using centrifuge concentrator with a cut-off of 10 kDa and again loaded on a ion exchange column (MonoQ, *GE-Healthcare*) and eluted with a gradient of buffer B (20 mM

HEPES, 1 M NaCl, 1 mM beta-ME pH7,5). Fractions were again analyzed on SDS-PAGE and pooled. For final purification the protein was again concentrated and loaded on a HiLoad Superdex 200pg 16/60 (*GE-Healthcare*) using Gel filtration buffer (20 mM HEPES; 150 mM NaCl, 1 mM beta-ME). Sample was dialyzed overnight in dialysis buffer (10 mM HEPES, 50 mM NaCl, 1 mM β-ME). The next day samples were concentrated to 75 µM (monomeric concentration) and aliquoted. For storage samples were frozen with liquid nitrogen and kept at -80°C.

Purification of Importin-α1 and Δ70 Importin-α1

Cell pellet of a 2 L culture was resuspended and lysed in 50 mL lysis buffer by sonication (6x1 min, 2 min break, duty cycle 70%, output 5). Afterwards the lysate was centrifuged for 1 h at 20000 rpm (JA 25.50) and 4°C. The supernatant was run over a HisTrap 5 mL column (*GE-Healthcare*) using an akta system and eluted by a gradient of elution buffer. 1.25 mg TEV protease was added to pooled fractions containing Importin and incubated for 3.5 h at 4°C. To remove protease, as well as His-tag and uncleaved target protein, the protein solution was again run over a 5 mL HisTrap and the flow through was collected. The flow through then was concentrated using a 10000 MWCO concentrater (*Millipore*) and loaded on a HiLoad Superdex 200 16/60 (*GE-Healthcare*)equilibratd with gel filtration buffer. Fractions were pooled, aliquots were frozen by liquid nitrogen and stored at -80°C. For buffer compositions see Section 3.12.1.

Expression and purification of the single chain MBP-14-3-3-GSM construct

Vector pMal-cR1 (CL3903), containing the single chain 14-3-3-39ChREBP251 insert of interest, was transformed into *E. coli* Bl21 and grown overnight at 37°C. The next day 2 L of PSB were inoculated with 20 mL of overnight culture and grown to an OD_{600} = 0.7. Expression was induced with 0.1 mM IPTG and the culture was incubated overnight at 16°C under constant shaking and harvested the next morning.
Pellets were resuspended and lysed in lysis buffer (50 mM Tris, 0.5 M NaCl, 0.1 mM EDTA, 10 mM β-ME, pH= 7.5) as described previously. The by centrifugation cleared lysate was applied on a self packed dextrose column (diameter 26 mm and ca. 6 cm bed height, packed by Andrew Bowman) and eluted using a gradient (0-100%) of elution buffer (50 mM Tris, 0.5 M NaCl, 10 mM Maltose,

0.1 mM EDTA, 10 mM β-ME, pH= 7.5). Fractions were collected, analyzed on SDS-PAGE and dialyzed overnight in 50 mM Tris, 100 mM NaCl, 10 mM β-ME, pH= 7.5.

3.2.3 Analytical size exclusion chromatography for complex determination

Size exclusion buffer contained 20 mM HEPES, 150 mM NaCl, 0.5 mM dithiothreitol (DTT), pH 7.5 with KOH was used to equilibrate a Superdex 200 Increase 10-300 column (*GE Healthcare*). To generate the standard curve the LMW Gel filtration Kit (*GE Healthcare*)17-0442-01 was used according to manufacturers recommendations. 100 µg of 14-3-3/GSM and 14-3-3 were prepared (based on parameters from Table 3.7) in a total sample volume of 150 µL and loaded onto an 500 µL loop for injection onto the column. Elution volumes were determined manually and a standard curve was calculated by a linear fit to standards in the linear range of the column using SciDavis[2]. Theoretical molecular weight (Mw) of complexes of interest were calculated based on protein sequence (see Table 3.7 and Appendix Section 7.4).

3.2.4 Analytical ultracentrifugation for complex size determination

14-3-3/GSM was purified in the same buffer as used for the analytical ultracentrifugation (AUC) run itself (10 mM Hepes, 50 mM NaCl, pH 7.5-KOH). Concentration was calculated to obtain an A_{280} = 0.7 with a path length of 1,2 cm. 400 µL of buffer and protein solution were loaded in SV sample cells containing two windows. SV run was performed in a XL-I analytical ultracentrifuge (*Beckman Coulter*) set to 20°C at a speed of 45000 g. Absorbance was recorded in continuous scans form 5,94-7,18 cm at 0.003 intervals (142 scans in total).
For analysis, parameters of buffer and protein composition were calculated by Sednterp[3] (20130813 BETA, DBstructure 20120320): vbar was set to 0.73, as expected for proteins. Buffer density ρ= 1.001 g/L and buffer viscosity to η= 0.01016. Raw absorbance data was loaded into SEDFIT version 16.1c[4] and

[2]http://scidavis.sourceforge.net/
[3]http://rasmb.org/sednterp/
[4]http://www.analyticalultracentrifugation.com/

timestamp corrected. To calculate the c(s) distribution following parameters were chosen: resolution(100), smin (2.0), smax (20), fractional ratio (floating, selected), baseline (selected), Fit RI Noise (selected), confidence level F-ratio (0.95).

3.2.5 Determination of Protein Concentration

Determination of protein concentration was done using as nanodrop (*NanoDrop 200C, Thermo-Scientific*) in combination with the Nanodrop2000 Software V1.6.198 (*Thermo Fischer*). By measuring the absorbance of the protein solution at A_{280} the concentration can be calculated using the Beer-Lambert law:

$$A = \epsilon \cdot c \cdot d \tag{3.1}$$

Where A is the absorption at a wavelength of 280nm , ε is the molar extinction coefficient in M^{-1} cm^{-1}, c the concentration in M and d the pathlenght in cm.
The molar extinction coefficient was calculated by using the ProtParam tool provided by the Swiss-Institute of Bioinformatics[5]. For the used constructs in this thesis the following parameters were determined:

Protein	Expression vector	ε= molar extinction coefficient (M-1 cm-1)	Mw (Da)
14-3-3 (monomer)	CL3248	27515	28301.64
His-TEV-14-3-3	CL3248	29005	30815.24
14-3-3(mono)/ GSM	CL3776	79675	61981.94
14-3-3(mono)/ GSM-TEV-His	CL3776	79675	62861.84
14-3-3(dimer)/ GSM	CL3776	107190	90020.33
14-3-3(mono)/ GSM W127A	CL4013	74175	61866.81
Glms	CL3963	46550	70091.85
Importin-α1	CL4165	47815	57928.1
Δ70 Importin-α1	CL4192	47815	49972.11

Table 3.7: Parameters for determination of protein concentrations

[5]https://web.expasy.org/protparam/

3.3 Isothermal Calorimetry

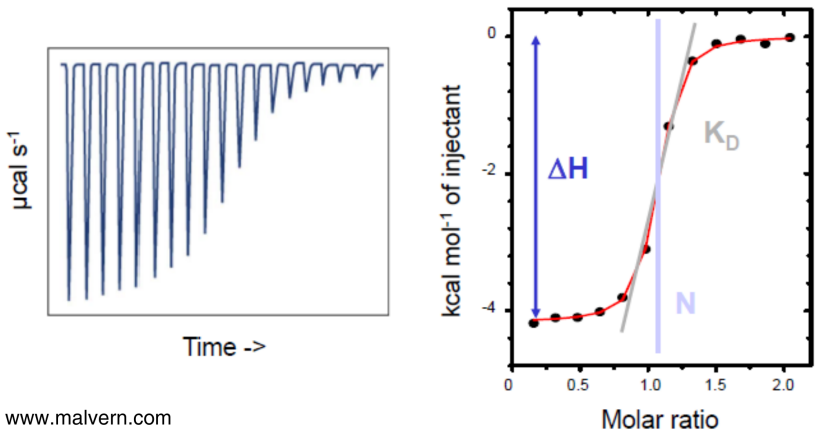

Figure 3.3: **Basics of an ITC experiment**
By detecting the heat released from an binding event, the affinity equilibrium constant of dissociation (K_D), stiochiometry (N) and binding enthalpy (ΔH) are extracted.

For isothermal calorimetry a MicroCal PEAQ-ITC instrument (*Malvern*) was used. The instrument was controlled by MicroCal PeaQ-ITC control software V1.21 (*Malvern-Panalytical*). For all experiments a cell temperature of 25°C was used. Sample cell was filled with protein from 30-100 µM. Ligands were dissolved to a stock concentration of 10 mM in the identical buffer as the protein (buffer from final dialysis). The ligand then was further diluted to a working concentration, usually 300 µM-450 µM. Reference power was set to 10 µcal/s. For experiments with 19 injections an injection volume of 2 µL was chosen, for experiments with 13 injections 3 µL of ligand were injected into the cell. In both cases the first injection of 0.4 µL was later excluded from analysis. For determination of binding parameters the MicrocalPeaq-ITC analysis software V1.21(Malvern-Panalytical) was used. The baseline was manually adjusted if needed.
By integration of the heat signal the K_D, stochiometry and binding enthalpy can be extracted (see Figure 3.3). Based on these values, Gibbs free energy (ΔG) and entropy (ΔS) can be calculated:

$$\Delta G = RT \cdot lnK_D \tag{3.2}$$

$$\Delta G = \Delta H - T\Delta S \tag{3.3}$$

Where R= 1.985 kcal $K^{-1}mol^{-1}$ and T is temperature in Kelvin.
For analysis of samples before and after ITC runs sample was removed from the sample cell and the OD_{600} or A_{280} was measured on a nanodrop (*Thermo-Scientific*). Samples for A_{280} were diluted 1:2 in sample buffer or 4 M Urea before measurement. To remove aggregates, samples were centrifuged for 10 min at 15000 g.

ITC of Point Mutants

30 µM of (1:1 complex) of 14-3-3/GSM mutant was loaded into the sample cell (equals 22 µM 2:1 complex stoichiometry) and 300 µM of Glc6P or AMP were titrated in thirteen 3 µL injections. If necessary baseline was adjusted and for evaluation a 2:1 protein complex was assumed, therefore the concentration was manually changed to 22 µM during analysis. Measurements for the *wt* were performed under identical conditions.

3.4 Label-Free Microscale Thermophoresis

3.4.1 Buffer Screen

1.15 µM of 14-3-3/GSM (assuming 2:1 complex, equals 1.5 µM of 1:1 complex) was prepared in standard dialysis buffer. The protein was then diluted 1:1 with the different buffers (200 mM stock), resulting in a protein concentration of 750 nm and 100 mM of buffer. For easy handling buffers were prepared in a 96 deep-well plate and stored at 4°C. For each conditions 4 capillaries (premium coated, *Nanotemper*) were loaded (quadruplets) and measured in a Monolith NT. LabelFree MicroScale Thermophoresis (*Nanotemper, Germany*) using 20% LED power and 20%MST power. For analysis Fnorm was calculated from the cold region (-1s to 0s) and hot region (19s to 20s). Fnorm then was plotted as seen in Figure 3.7

3.4.2 MST binding experiments

1.5 µM of 14-3-3/GSM (purified at an pH of 7 in HEPES buffer) complex (assuming 1:1 stoichiometry) was prepared and added to a dilution series of ligands (either Glc6P, Glc or Glc1P, dissolved in identical buffer as protein) for a final protein concentration of 750 nM. The final concentration of ligands tested ranged

from 2 mM to 61 nM. For measurements samples were loaded in premium coated capillaries and an LED power of 20% and MST power of 60% (“high”) was used. Thermophoresis signal was calculated for cold region (-1 s to 0 s) and hot region (19 s to 20 s). Measurements were carried out in replicates for Glc6P. For ligands showing no binding, also other MST conditions were tested. For uniformity only same conditions are shown in this thesis.

3.5 Limited proteolysis

3.5.1 Test of different proteases for limited proteolysis

Protease stocks were prepared at a concentration of 1 mg/mL in protease dilution buffer (20 mM Hepes, 50 mM NaCl, 10 mM MgSO4, pH to 7.5 with KOH). For long time storage stocks were frozen in liquid nitrogen and kept at -80°C. For the digest a dilution series of proteases was generated (1:10, 1:100, 1:1000) using protease dilution buffer. 7 µL of 22 µM 14-3-3/GSM were preincubated with 2 µL of Glc6P (10 mM in H_2O) for 5 min on ice. For samples containing no Glc6P only H_2O was added as a control to the protein. Afterwards 3 µL of different protease dilutions were added to each sample. Reactions were mixed and incubated for 30 min on ice. The digest was stopped by adding 4 µL of 4x SDS-LB and incubation at 95°C for 5 min. For analysis samples were loaded on 14% SDS-PAGE gels together with negative controls (no protease) and the highest concentration of the protease used to identify bands coming from the protease itself. For set-up of the digest see Table 3.8.

	Pipetting Vol	Final concentration
14-3-3/GSM (22 µM)	7 µL	13 µM
Glc6P (10 mM) or H_2O	2 µL	1.7 mM
Protease (1:10/1:100/1:1000)	3 µL	0.025 µg/µL 0.0025 µg/µL 0.00025 µg/µL

Table 3.8: Protease test, reaction mix set-up

3.5.2 Limited proteolysis Glc6P: Titration

A 1:2 dilution series of Glc6P in dialysis buffer was prepared, starting from a final assay concentration of Glc6P at 1.7 mM to 1.7 µM. Equal volumes of lig-

and dilutions were pipetted to a constant concentration of 14-3-3/GSM (13 µM) and incubated on ice for 10 min. The limited proteolysis was started by adding chymotrypsin (final 0.0025 µg/µL in protease buffer) and stopped after 30 min (see Section 3.5.1). Digest was analyzed on 14%SDS-PAGE gel, stained with coomassie.

3.5.3 Limited proteolysis: Competition with AMP

A 1:2 AMP dilution series was generated from 1250 µM to 10 µM (final assay conc) in dialysis buffer. 14-3-3/GSM (12.5 µM) was preincubated with 50 µM Glc6P for 5 min on ice and added to the AMP dilution series. After an additional incubation of 10 min chymotrypsin was added (0.0017 µg/µL). Digest was stopped after 60 min an analyzed on an 18%SDS-PAGE gels stained with coomassie.

3.5.4 Limited Proteolysis W127A GSM-Mutant

As previously described, *wt* and mutant proteins were preincubated with ligands or buffer for 5 min on ice. Digest was started by adding chymotrypsin. After 60 min on ice, reaction was stopped by adding 4xSDS-LB. Digest was analyzed on 18%SDS-PAGE and stained with coomassie. For reaction set-up see Table 3.9.

	Pipetting Vol	Final concentration
wt or W127A (20 µM)	7 µL	12 µM
Glc6P (10 mM)/ AMP (10 mM) or buffer	2 µL	1.7 mM
Protein buffer	Up to 12 µL total	
Chymotrypsin (1:100)	1 µL	0.8 µg/mL

Table 3.9: LiP W127A reaction mix set-up

3.5.5 Limited Proteolysis in Presence of different Metabolites

Chymotrypsin and trypsin were dissolved in protease dilution buffer (Section 3.12.2) to 1 mg/mL and stored at -80°C. 17.5 µM of 14-3-3/GSM complex were incubated with different metabolites, using a final concentration of 1.7 mM for 10 min. Afterwards, the protein-metabolite mixtures was incubated on ice for various time points with chymotrypsin (2.5 µg/mL) or trypsin (2.5 µg/mL or

0.25 µg/mL). To achieve adequate pipetting volumina, stock solutions of protease were first diluted 1:100 or 1:1000 in protease dilution buffer. To stop the digestion 10 µL of the proteolysis solution were mixed with 4 µL of 4x SDS-LB and incubated for 5 min at 95°C. For analysis of the digestion pattern the samples were loaded onto 18% SDS-PAGE gels and stained with coomassie. All metabolites, as well as proteins were diluted in dialysis buffer.

Mass-Spectrometry Analysis of GSM Fragments

The band of interest (30 kDa) as well as the undigested control band of GSM were cut from the SDS-PAGE gel and submitted to the biochemistry core facility of the Max Planck institute of Biochemistry, Martinsried, Germany for analysis by MS/MS (ref. Oribi2974). Peptide positions were plotted against log-intensities by Naga Nagaruna.

3.6 Hydrogen-Deuterium exchange mass-spectrometry

All experiments were performed in the lab of Kasper Rand, University of Copenhagen. The majority of analysis, as well as experimental design was planned and realized by Joanna Veiga, University of Copenhagen. The findings resulted in her Master Thesis [Veiga, 2019]. During two research stays in Copenhagen I was preparing the samples, as well as measuring the labeled proteins together with Joana. For a detailed methodology I therefore refer to the Master Thesis of Joana and focus in this thesis on a more brief description of the parts I mainly was involved in. The main text, overall structure and information in this section is mainly generated by Joana Veiga
For a description of used buffers see Section 3.12.

3.6.1 Hydrogen-Deuterium Exchange

14-3-3/GSM and 14-3-3 were diluted into sample buffer (10 mM HEPES, 50 mM NaCl, 1 mM β-ME, pH 7.5) to a concentration of 20 µM. AMP and Glc6P were added to the protein complex, in a concentration resulting in a 95% binding (Kd for Glc6P 3 µM for AMP 7 µM). For labeling the protein-ligand solutions were diluted 1:10 in deuterated sample buffer. Giving a deuterium content of

90% during labeling. Labeling reactions were incubated for various timepoints (25 sec, 1 min, 10 min, 60 min, 8 h) at 25°C. For quenching of labeling reaction the sample was diluted 1:2 in ice cold quench buffer (300 mM phosphate buffer, pH 2.3) and immediately frozen at -80°C. The total amount of protein injected onto the system is 30 pmol (equals entire labeling reaction).

3.6.2 Liquid Chromatography and Mass Spectrometry

Frozen samples were quickly thawed in a table top centrifuge and injected into a UPLC system, kept at 0°C (*NanoAcquity, Waters*). The protein was digested on-line in an in-house pepsin column (*20 mm x2 mm, Thermo Scientifix)*. After digest at room temperature the peptides were trapped on a *Vanguard Column (C18, 1.7µm, 1mm x 100 mm, Waters*) and desalted for 3 min with solvent A (200 µL/min)(seeSection 3.12.3). In a next step the peptides were seperated by a *Acquity UPLC column (C18, 1.7µm, 1mm x 100mm, Waters)* in a gradient from 5-40% of solvent B. Eluted peptides were analyzed by a *Synapt G2-Si, Waters* ESI-Q-TOF mass spectrometer, where the MS was set in positive ionization mode and the peptides were separated by ion mobility for enhanced peak capacity. To identify peptides, non-deuterated samples were injected and analyzed with identical chromatography settings. These peptides also were fragmented by collision-induced dissociation, using argon, in either data dependent (DDA) or data independent acquisition (DIA). For maximum labeled controls proteins were incubated overnight in 90% deuterated buffer under denaturing conditions.

3.6.3 Data Analysis

MS/MS data was processed with *ProteinLynx Global Server (PLGS version 3.0, Waters)* to identify peptides. For correct identification DDA had to have PLGS Ladder Score above 1.0, below 15 ppm mass error for the precursor ion, in addition to a manual inspection of the fragment spectrum in PLGS. DIA peptides were identified by*DynamX (version 3.0, Waters)*. Peptides had to be fragmented at least 1 time, 0.2 fragmentations per amino acid, and below 10 ppm mass error for the precursor ion. Further, the peptides had to be identified in two out of three acquired MS/MS files. Lastly, the presence of a signal for the precursor ion was verified in *DynamX* along with analysis of deuterium uptake of all positively identified peptides. Maximum labeled controls were used to calculate the back exchange (BE) for all peptides with a maximum labeled control by the following

equation:

$$BE(\%) = (1 - \frac{m_{MX} - m_{0\%}}{m_{MAX} - m_{0\%}}) \cdot 100\% \tag{3.4}$$

Where m_{MX} is the mass of the maximum-labeled peptide, $m_{0\%}$ is the mass of the non-deuterated peptide and m_{MAX} is the theoretical maximum deuterium uptake (excluding N-terminus and prolines).
The calculated back exchange was used to obtain the average back exchange of ChREBP and 14-3-3.*HX-Express 2.0* was used to analyze peptides showing bimodal isotopic patterns in dependence of deuteration.

3.6.4 Statistical Analysis

For statistical analysis *Excel, Microsoft Corp.* was used. To determine if the difference between uptake points of two states is significant a cutoff value was determined. By obtaining a confidence interval significance was assigned. Since triplicate measurements were obtained, absolute difference was chosen to represent the data, and the standard deviation of differences (also named propagated SD, in this case) was calculated as:

$$SD = \sqrt{SD_A^2 + SD_B 12} \tag{3.5}$$

$SD_A{}^2$ and $SD_B{}^2$ are the average of SD across all timepoints of state A and state B.
A significance threshold for all peptides of GSM was used to define a significant difference, the difference charts were set to 0.32 Da, 0.34 Da, or 0.31 Da for differences in HDX between the control (C1C) and Glc6P (C1G) states, the control and AMP (C1A) states, or C1G and C1A states, respectively, corresponding to the two-tail 98% confidence interval (CI) calculated according to:

$$\frac{t_{n-1} \cdot SD}{\sqrt{n}} \tag{3.6}$$

Where t_{n-1} is the correspondent student t value for n ($t_{98\%,n=3}$=6.965, the number of replicate samples (n=3).
For 14-3-3, the significance thresholds were set to 0.35 Da, 0.34 Da, 0.35 Da and 0.33 Da for differences in absolute HDX between the C1C and P14 states, the C1C and C1G states, the C1C and C1A states, and the C1G and C1A states, respectively, according to the same calculations as for ChREBP. Due to the dimer- formation of 14-3-3 peptides could not be distinguished between the two

monomers, making it difficult to interpret data for 14-3-3. Therefore this data is not included in this thesis, however Joana Veiga discussing her finding in her Master Thesis [Veiga, 2019].

3.7 Circular-Dichroism Spectroscopy

Protein was purified as for ITC experiments (Section 4.1.4). 10 µM of complex in dialysis buffer were diluted 1:4 in ddH_2O to a final concentration of 2.5 µM (1:1 complex) and the CD spectra was recorded using a Jasco instrument. Afterwards 7 µL of 10 mM Glc6P was added (0.34 mM final) to the cuvette and a second spectra was recorded. Calculation of α-helical percentage was based on [Scholtz et al., 1991]. To calculate the theoretical percentage amino acid (aa) were counted manually from the PDB file 5wfx(A) and the psipred[6] prediction for the GSM. 73aa of 246aa are non-helical in 14-3-3(monomer). 242 of 291aa are non-helical based on the psipred prediction for the GSM. The experiments were conducted by Frits Kamps, DZNE Munich.

3.8 Metabolite Structures

Metabolite structures were derived from the pubchem database[7], downloaded as 3D structures in sdf file-format and illustrated by using pymol. Downloaded files are listed in Table 3.10.

[6] http://bioinf.cs.ucl.ac.uk/psipred/
[7] pubchem.ncbi.nlm.nih.gov

Name	Identifier
2DGlc6P	440992
6PG	91493
AcAc	6971017
ADP	6022
AMP	6083
ATP	5957
cAMP	6076
CMP	6131
dAMP	12599
F6P	439160
F1,6bP	445557
F2,6bP	105021
G1P	65533
Glc6P (G6P)	439284
Gal6P	439404
Glc	5793
GlcN6P	439217
GMP	136661904
M6P	447096
NAcGlcN	439174
R5P	439167
Rib	5779
UDP-Glc	8629
UDP-NAc-GlcN	445675
X5P	439190

Table 3.10: List of Metabolite Structures

3.9 Scintillation-Proximity Assay

3.9.1 SPA experiments for assay set-up

Buffer additives

90 µL of different assay buffers (1x containing 20 mM HEPES, 100 mM NaCl, 0.5 mM TCEP, pH= 7.5 plus additives) were pipetted in duplicates into a 96-well plate (*Isoplate-96, white, Perkin Elmer*). To each well 0.075 mg His-TAG YSI beads (*Perkin Elmer*) and 10 µL of protein complex (4.45 µM stock 2:1 complex) or buffer was added. The plate was incubated for 1 h, 1100 rpm at 4°C. After incubation 0.2 µCi of 3H-Glc6P or 3H-AMP was added and again incubated for 10 min at RT under shaking. For measurement the plate was transferred to the MicroBeta2 Microplate counter (*Perkin Elmer*, AG Klein BMC), where the plate

was settled for 30 min in the dark before each well was measured for 1 min (3H SPA program). The final assay volume was 120 µL. Additives were added to 2x assay buffer and diluted to 1x to a final concentrations as seen in Table 3.11.

Additive	final conc.
BSA	0.20%
NP-40	0.01%
Triton X-100	0.01%
Triton X-114	0.01%
Tween-20%	0.01%
Blocking Solution	2.00%
Smart Block	2.00%
BSA block	2.00%
MgCl2	1 mM
CaCl2	1 mM
NaCl	100 mM
Kcl	50 mM
EDTA	2 mM

Table 3.11: Table of SPA additives

Testing for ligand concentrations

Protein-bead mixture was prepared as described in the section above using SPA assay buffer (see Section 3.12). Ligands were added at various concentrations as described in 4.5.1. After 10 min incubation at RT plate was allowed to settle for 30 min in the plate reader, afterwards the signal was measured.

Testing for protein concentration

Dilution series of protein was generated and incubated with constant amounts of beads (0.075 mg) and a constant ligand concentration of 0.2 µCi/well. After incubation at RT under constant shaking signals were measured as described before.

3.9.2 Metabolite screening for ^{3}H-Glc6P competition

Potential ligands (ref to list with metabolites) were dissolved to 1.2 mM stock concentrations in 1x SPA-buffer (Section 3.12.2), aliquoted and stored at -80°C. A 96-multititer plate (Isoplate-96, white, *Perkin Elmer*) was set up with 0.05 mg/well Copper His-TAG YSI beads (*Perkin Elmer*) and 0.125 µM 14-3-3/GSM (1:1

complex, 93 µM 2:1 complex) in 1x SPA buffer. To determine non-specific binding control wells were set-up without protein, the difference in volume was adjusted by adding protein buffer only. Unlabeled metabolites were added to the wells in a final concentration of 10 µM (2-10times above the KD of G6P). This mixture was incubated for 1h at 4°C under constant shaking 1100 rpm on an Eppendorf TermoMixerC to avoid settling of the YSI beads. Afterwards 0.2 µCi of radioligand, D-[6-3H]6-phosphate disodium salt (3H-G6P) (*Hartmann Analytic, Germany*) was added to the wells. This equals a Glc6P concentration of 27nM/well. The plate was closed with TopSeal-A Plus foil (*Perkin Elmer*) following a 10 min incubation at room temperature (RT) under constant shaking the plate was transferred to a MicroBeta2 Microplate counter (*Perkin Elmer*, AG Klein-BMC) and incubated for 1h before measurement. To read the SPA signal, the following settings were used: *Name: tpysik H-3 SPA, Cassette type 96wells, 8 by 12, quench correction: off, assay type: SPA, Paralux used: No, Counting time: 1 min , Detector normalization: None, Window 5-360*. The total assay volume per well was 120 µL and each metabolite was tested in 3 wells for binding and non-specific binding. In 2- independent experiments. The set-up was tested for potential radioligand depletion as well as signal stability during the measurement.
Assay analysis: The mean counts per minute (cpm) were calculated for each metabolite to obtain the values for binding (well containing protein) and non-specific binding (well containing no protein). To calculate specific binding:

$$specificbinding = (mean\,binding) - (mean\,nonspecific\,binding) \quad (3.7)$$

To calculate the normalized binding, or fractions of 3H-Glc6P bound, the following equation was used:

$$3H\text{-}Glc6P\;bound = \frac{cpm\;competitor}{cpm\;buffer\;ctrl.} \quad (3.8)$$

To calculate fraction of competitor bound:

$$Fraction\;Comp.\;bound = 1 - 3H\text{-}Glc6P\;bound \quad (3.9)$$

3.9.3 Competition experiments- titration curve

A 96-multititer plate (Isoplate-96, white, Perkin Elmer) was set up with 0.05 mg/well Copper His-TAG YSI beads (Perkin Elmer) and 0.125 µM 14-3-3/GSM (1:1

complex, 93 µM 2:1 complex) in 1x SPA buffer. To determine non-specific binding control wells were set-up without protein, the difference in volume was adjusted by adding protein buffer only. 10 µL unlabeled metabolites (AMP, Glc6P, R5P) were added to the wells in a final concentration from 500 µM to 50 pM (1:10 dilution series). Ligands were dissolved and diluted in 1x assay buffer. This mixture was incubated for 1h at 4°C under constant shaking 1100rpm on an Eppendorf ThermoMixerC to avoid settling of the YSI beads. Afterwards 0.2µCi of radioligand, D-[6-3H]6-phosphate disodium salt (^{3}H-Glc6P) (*Hartmann Analytic, Germany*) was added to the wells. This equals a Glc6P concentration of 27 nM/well. The plate was closed with TopSeal-A Plus foil (*Perkin Elmer*) following a 10 min incubation at RT under constant shaking, the plate was transferred to a MicroBeta2 Microplate counter (*Perkin Elmer*, AG Klein-BMC) and incubated for 1 h before measurement. To read the SPA signal
To determine the half maximal inhibitory concentration (IC_{50}) and Ki, the normalized specific binding was plotted in QtiPlot[89] and analyzed by using *"Fit Boltzman (Sigmoidal)"*, allowing the determination of IC_{50}.
For calculation the Kd for Glc6P the following equation was used[DeBlasi et al., 1989]

$$Kd = IC_{50} - [L] \tag{3.10}$$

Where L is the concentration of radioligand.
The Ki of AMP and R5P were caluclated by the Cheng Prusoff equation [Cheng and Prusoff, 1973].

$$Ki = \frac{IC_{50}}{\frac{[L]}{Kd} + 1} \tag{3.11}$$

Where L is the concentration of radioligand and KD the dissociation constant for the radioligand.

3.10 Intrinsic fluorescence

A protein stock concentration of 2 µM was prepared by diluting protein in dialysis buffer. Metabolites (Glc6P and AMP) were solubilized to 10 mM in dialysis buffer. A dilution series 1:2 was prepared for AMP and Glc6P with final assay concentrations of 5 mM to 40 nM. Protein and ligand was mixed 1:1

[8] https://intranet.cells.es/Members/cpascual/docs/unofficial-qtiplot-packages-for-windows
[9] https://www.qtiplot.com/index.htmL

resulting in a 1 µM protein concentration and incubated for 10 min at RT. Final assay volume was 10 µL. Fluorescence was measured in *Corning 4514 multi-well plate* (384wells) using a *Tecan infinite pro 1000*. Excitation wavelength 280 nm and Emission spectra from 300-410 nm were recorded. For denaturation proteins were either incubated for 5 min at 95°C or 5% SDS (final conc.) was added to the protein solution.

3.11 SDS-PAGE

sodium dodecyl sulfate-polyacrylamide gel electrophoresis (SDS-PAGE) was used to analyze proteins and protein fragments based on their molecular mass (based on [Laemmli, 1970]. For running gels, a Mini-Protean Tetra Vertical Electrophoresis cell (*Bio-Rad*) was used. Depending on protein size, either a 4-20% MP TGX Stain-Free precast gels (*Bio-Rad*) or self-cast gels were used. For self-cast gels the separating and stacking gel were prepared as the following (from Mocranjac Group, BMC Munich).

Separating gel: 12-18% (w/v) acrylamide:bis-acrylamide mix (37.5:1), 375 mM Tris-Cl (pH 8.8), 0.1% (w/v) SDS, 0.05% (w/v) APS, 0.05% (v/v) TEMED. Stacking gel: 6% (w/v) acrylamide:bis-acrylamide mix (37.5:1), 60 mM Tris-Cl (pH 6.8), 0.1% (w/v) SDS, 0.07% (w/v) APS, 0.35% (v/v) TEMED.
To analyze protein samples, precast or self-cast gels were covered with SDS-Running buffer (50 mM Tris-Cl, 384 mM glycine, 0.1% (w/v) SDS, pH 8.3) and protein sample were denatured by incubation at 95°C, 5 min in Leammli buffer (final 60 mM Tris-Cl pH 6.8, 10% (v/v) glycerol, 2% (w/v) SDS, 0.01% (w/v) bromphenol blue and 3% β-ME.)
Gels are run for 55 min, 200 V for 14% self-cast gels, and 20 min, 300 V for 4-20% precast gradient gels. After separation of the protein sample, proteins are stained by incubation in coomassie (0.1% (w/v) coomassie blue R250, 40% (v/v) methanol, 10% (v/v) acetic acid. By running a protein standard along the samples, the size of the proteins of interest can be determined.

3.12 Buffers and Media

3.12.1 Buffers for protein purification

Lysis buffer

50 mM HEPES Na salt, 500 mM NaCl, 30 mM Imidazole, 1 mM β-ME in milliQ water. The pH of the buffer was set to 7.5 at 4°C using KOH/NaOH.

Elution buffer

50 mM HEPES Na salt, 500 mM NaCl, 500 mM Imidazole, 1 mM β-ME in milliQ water. The pH of the buffer was set to 7.5 at 4°C using KOH/NaOH.

Ion-exchange buffer A

20 mM HEPES·Na salt, 50 mM NaCl, 20 mM Imidazole, 1β-ME in milliQ water. The pH of the buffer was set to 7.5 at 4°C using KOH/NaOH.

Ion-exchange buffer B

20 mM HEPES·Na salt, 1 M NaCl, 20 mM Imidazole, 1 mM β-ME in milliQ water. The pH of the buffer was set to 7.5 at 4°C using KOH/NaOH.

Gel filtration buffer

Gel filtration buffer: 20 mM HEPES·Na salt, 150 mM NaCl, 0.5 mM TCEP in milliQ water. The pH of the buffer was set to 7.5 at 4°C using KOH/NaOH.

Dialysis/ITC buffer

Dialysis/ ITC buffer: 10 mM HEPES·Na salt, 50 mM NaCl, 0.5 mM TCEP in milliQ water. The pH of the buffer was set to 7.5 at 4°C using KOH/NaOH.

3.12.2 Working buffers and solutions

50x TAE

242.g Tris base dissolved in MQ. Slowly add 57.1 mL glacial acid and 100 mL EDTA (pH 8, 0.5 M). Bring volume up to 1 L with milliQ water.

10x PBS

$Na_2HPO_4 \cdot 7\,H_2O$ 25.6 g/L, NaCl 80 g/L, KCl 2 g/L, KH_2PO_4 2 g/L. Add water and autoclave

2x scintillation proximity assay (SPA)-buffer

40 mM HEPES Na salt, 200 mM NaCl, 1 mM TCEP, 4 mM EDTA. The pH of the buffer was set to 7.5 at 4°C using KOH/NaOH.

Protease Dilution buffer

20 mM HEPES, 50 mM NaCl, 10 mM $MgSO_4$, pH 7.5 using KOH.

3.12.3 Buffers and Solvents for HDX-MS

100x $HXMS^-$

1 M 4-(2-hydroxyethyl)-1-piperazineethanesulfonic acid (HEPES), 100 mM β-ME. pH 7.5 using KOH

$HXMS^-$

100x $HXMS^-$ diluted 1:100 in **H20!**, 50 mmol NaCl (total vol. 1 mL)

$HXMS^+$

100x $HXMS^-$ diluted 1:100 in dideuterium monoxide, heavy water (D_2O), 50 mmol NaCl (total vol. 1 mL)

Mobile Phase

Solvent A: 0.23% Formic acid in MQ water
Solvent B: 0.23% Formic acid in Acetonitrile

3.12.4 Media

LB-Media

For cloning and teste expression Bactotryptone 10 g/L, Bacto yeast extract 5 g/L, NaCl 10 g/L, add ddH_2O and adjust pH to 7 with NaOH and autoclave.

PSB-Media

For protein expression. Bacto Tryptone 10 g/L, Casamino Acids 2 g/L, yeast extract 2 g/L, NaCl 5 g/L, NH_4Cl 1 g/L, KH_2PO_4 3 g/l, $Na_2HPO_4 \cdot 2H_2O$ 7.5 g/L, Glucose$\cdot H_2O$ 4.4 g/L and 0.2 g/L $MgSO_4 \cdot 6H_2O$. Fill up with ddH_2O and autoclave. Usually a 10x solution was prepared

TB-Media

For test expression Dissolve yeast extract 24 g/L, tryptone 12 g/L, Glycerol 4 mL/L in water and autoclave. Cool solution down and add 100 mL of sterile 10x PBS.

4 Results

4.1 Expression and Purification of 14-3-3/GSM

For most biochemical and biophysical assays large quantities of pure protein are needed. So far, it was difficult to express and purify ChREBP from *E.coli* based expression systems. Therefore, a major goal of this thesis was to optimize ChREBP expression, as well as purification. This section describes how the most stable construct was identified, expression conditions were optimized and how the purification of the complex was achieved. A more detailed description of the single steps, as well as buffer compositions can be found in Section 3.2 an Section 3.12.1.

4.1.1 Testing an single chain construct of 14-3-3/GSM for binding to Glc6P

To obtain a stable complex of 14-3-3 and the ChREBP GSM, we first forced the formation of the complex by linking 14-3-3 with the GSM, using a short 6aa spacer (Figure 4.1). The expressed construct was then purified by using a self packed dextrose column, binding the MBP-tag of our construct. The bound fraction was eluted by a gradient of maltose and the fractions were analyzed on SDS-PAGE together with -IPTG, +IPTG, supernatant (SN) and pellet (P). As shown in Figure 4.1B, the protein could be purified. However, coomassie staining also shows contamination with other proteins, degradation products and most likely endogenous MBP. To test if this protein(-mixture) is able to bind Glc6P isothermal calorimetry was performed. As shown in Figure 4.1C, a clear binding signal was observed. Due to the absence of MCR6 in the tested construct, it can be excludes that this conserved region is the site of interaction with Glc6P, as previously suggested by McFerrin *et al.* [McFerrin and Atchley, 2012]. This raises the question about the site of binding for Glc6P.

For binding, a low stoichiometry (N) of 0.18 was observed. This is most

likely the result of an incorrect determination of protein concentration due to the amount of impurities and degradation products. The Master student Nina Heppner tried for her thesis to improve the purity by changing the purification protocol, as well as the construct itself. For example she included a C-terminal His-tag and varying the linker length between 14-3-3 and GSM. These changes only resulted in minor improvements in purity (for details see thesis of Nina Heppner [Heppner, 2016]).

We therefore speculated co-expression of 14-3-3 and GSM, without a covalent linker, could help to increase the purity. In support of this theory is the fact, that 14-3-3 is reported to form dimers [Chaudhri et al., 2003, Jones et al., 1995] and binding as such to ChREBP [Sakiyama et al., 2008]. This complex formation is not possible with the tested single chain constructs. Therefore, new constructs were designed and tested for expression (see Section 4.1.3).

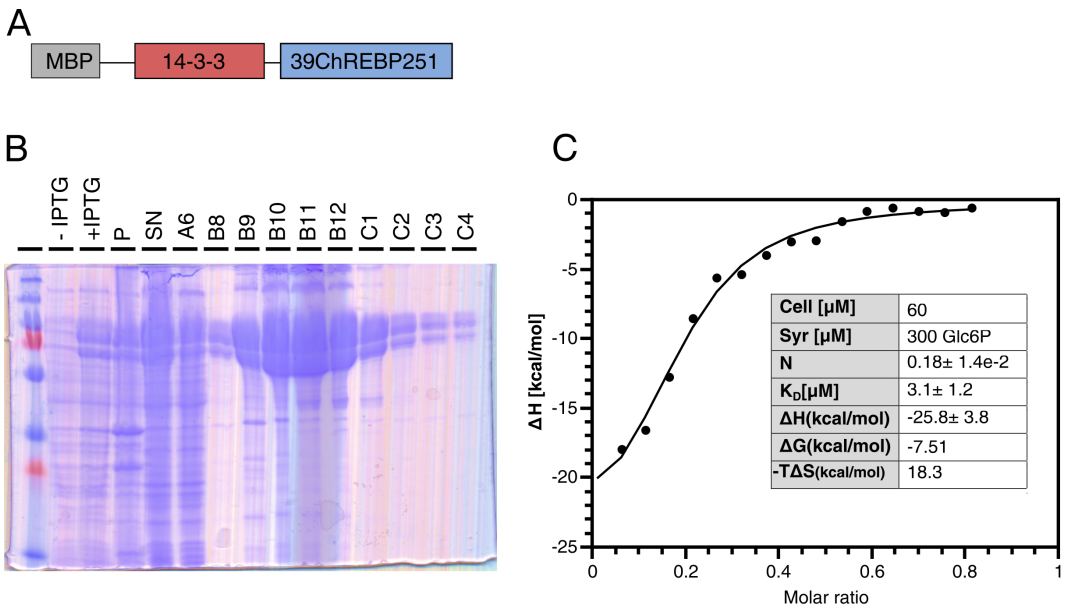

Figure 4.1: **Single chain construct of 14-3-3/GSM indicates binding of Glc6P**
A: Schematic representation of the designed construct, containing an N-terminal maltose binding protein (MBP)-tag linked to 14-3-3 and partial GSM (from aa 39-251). The GSM is linked with a 6aa spacer to the C-terminus of 14-3-3. B: Fractions of the dextrose column based purification were analyzed on SDS-PAGE. The gel shows high amount of proteins, together with degradation products and impurities. C: Isothermal calorimetry binding profile of Glc6P to the purified protein.

4.1.2 Purification of 14-3-3

Since the goal was to express and purify the GSM together with 14-3-3, the 14-3-3 protein was needed as a control in downstream applications.

E. coli pellets of 2 L cultures were resuspended in lysis buffer and lysed. The lysate was centrifuged and the supernatant loaded onto a HisTrap using an akta pure system. Bound protein was eluted with step elutions using elution buffer containing 0.5 M imidazole. Flow through and elutions were analyzed by SDS-PAGE (see Figure 4.2A). Fractions containing the proteins of interest (grey area under the curve Figure 4.2A) were pooled and incubated with His-TEV protease for 4-6 hours in the coldroom, to remove the N-terminal His-tag. At the same time, the protein solution was dialyzed to reduce the amount of imidazole in the buffer. After dialysis the protein solution was again passed over a Ni-NTA column to remove His-TEV protease, uncleaved 14-3-3 and cleaved off His-tag. Afterwards, protein was concentrated for size exclusion chromatography (SEC) on a Superdex 200pg 26/60 column (Figure 4.2B). Since most downstream applications require both, protein and potential ligands in identical buffers, fractions containing 14-3-3 were pooled and dialyzed overnight in dialysis buffer (10 mM HEPES, 50 mM NaCl). Afterwards, protein and dialysis buffer were snap frozen by liquid nitrogen and stored at -80°C. The SDS-PAGE in Figure 4.2B shows that 14-3-3 can be purified from *E. coli* with only minor impurities. The total amount of protein that could be purified from one purification was between 30-40 mg.

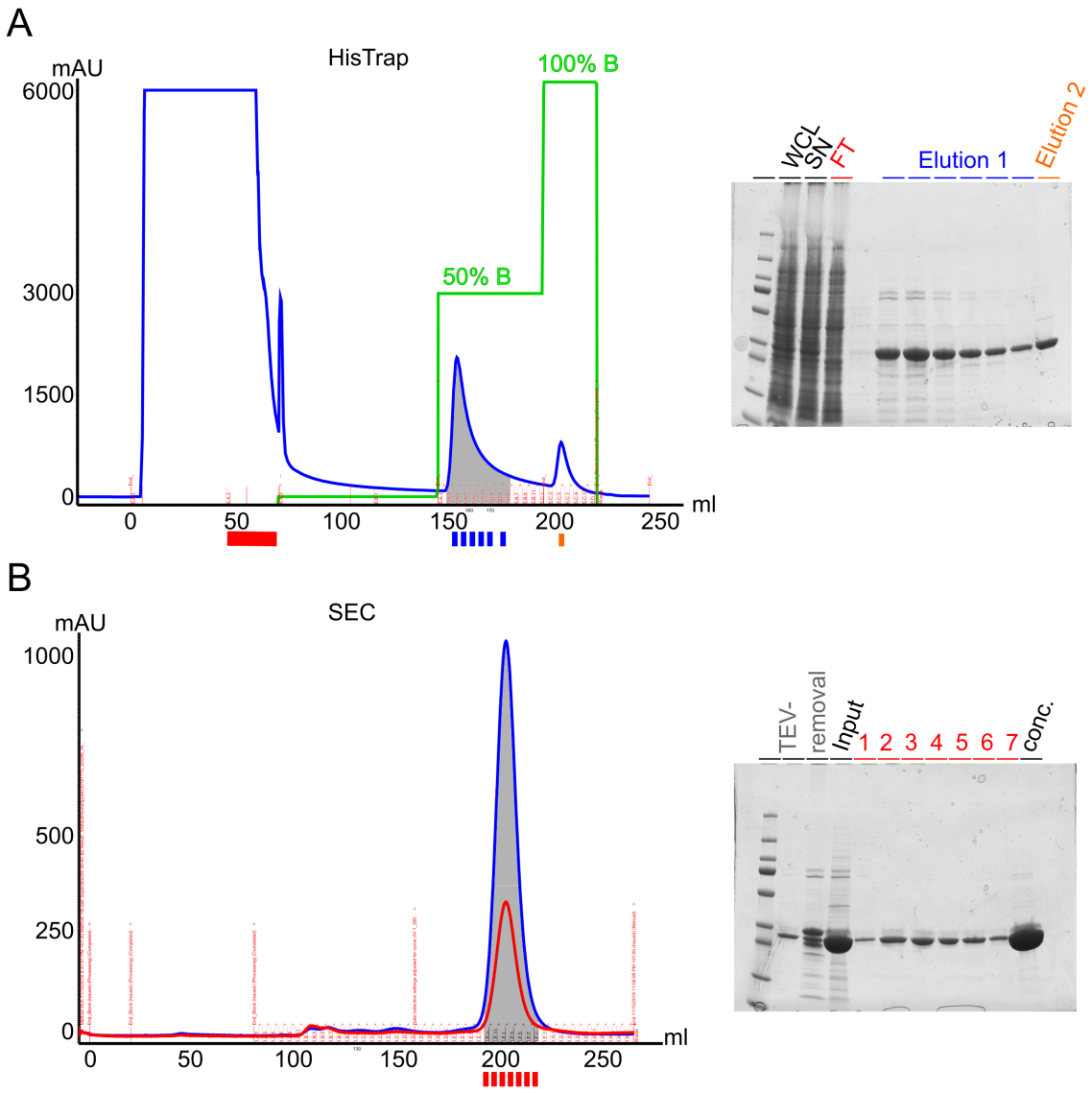

Figure 4.2: **Purification of 14-3-3 by different chromatographic methods**
A: His-Trap of tagged 14-3-3. Fractions of flow-through, together with fractions from elutions (marked by colored bars below the chromatogram) were analyzed by SDS-PAGE. As shown by the gel, 14-3-3 can be affinity- purified. B: Chromatogram of size exclusion chromatography (HiLoad Superdex 200) and final purified construct (SDS-PAGE last lane). Bars under the chromatograms indicate fractions that are loaded onto the SDS-PAGE for analysis. Grey area under the curve shows fractions that were pooled and used for downstream applications

4.1.3 Using the pET-Duet1 expression vector for co-expression of 14-3-3/GSM

As mentioned in Section 4.1.1, expression of the 14-3-3/GSM complex is challenging. To search for constructs that can be expressed and purified in *E.coli*, the important ChREBP interaction partner 14-3-3β was cloned together with different fragments of the ChREBP-GSM into the pET-Duet1 expression vector (*Novagen*). Only ChREBP was tagged with a C-terminal His6-tag for later affinity purification. The cloned constructs are listed in table 4.1. After confirmation of the correct constructs by sequencing, the vectros were tested for expression of the target genes. To test for expression, the plasmids were transformed into

Clone	Cloning Site 1	Cloning Site 2 ChREBP-TEV-His fragment	Mw ChREBP -fragment [kDa]
CL3773	14-3-3	1-261	31,6
CL3774	14-3-3	1-271	32,6
CL3775	14-3-3	1-281	33,7
CL3776	14-3-3	1-291	34,8
CL3777	14-3-3	1-301	35,8
CL3778	14-3-3	1-321	38,2
CL3779	14-3-3	1-351	41,0
CL3780	14-3-3	1-381	44,2
CL3771	Mlx125-222 (13,6kDa)	660-747	11,3
CL3676	14-3-3	1-251	30,4

Table 4.1: ChREBP expression vectors based on pET-Duet1

E. coli Bl21 pRIL and cultivated in either TBS-, LB-, PSB- or PSB media supplemented with extra glucose. After induction of expression at an OD_{600} of 0.7 with 0.1 mM isopropyl-β-D-thiogalactoside (IPTG), the cultures were incubated over night at 16°C. The next day, cells were harvested and analyzed for expression using a 96well protino-Ni-IDA purification kit.

From each sample the whole cell lysate (5µl), as well as elution fraction (10µl) were analyzed on 14%-SDS-PAGE gels. As shown in Figure 4.3, most of the expressed clones expressed 14-3-3 (28 kDA) and fragments of ChREBP. The experiment also showed that PSB+ $MgSO_4$+ Glc media yielded denser cultures with more target protein expressed, compared to the other media tested (see Figure 4.3 bottom panel). One of the best expressed clones was vector CL3776. This vector contained almost the entire GSM (1-291), which is the region of interest in this thesis. Therefore we decided to base future experiments on this expression

construct. For simplification, this construct will be called 14-3-3/GSM from now on.

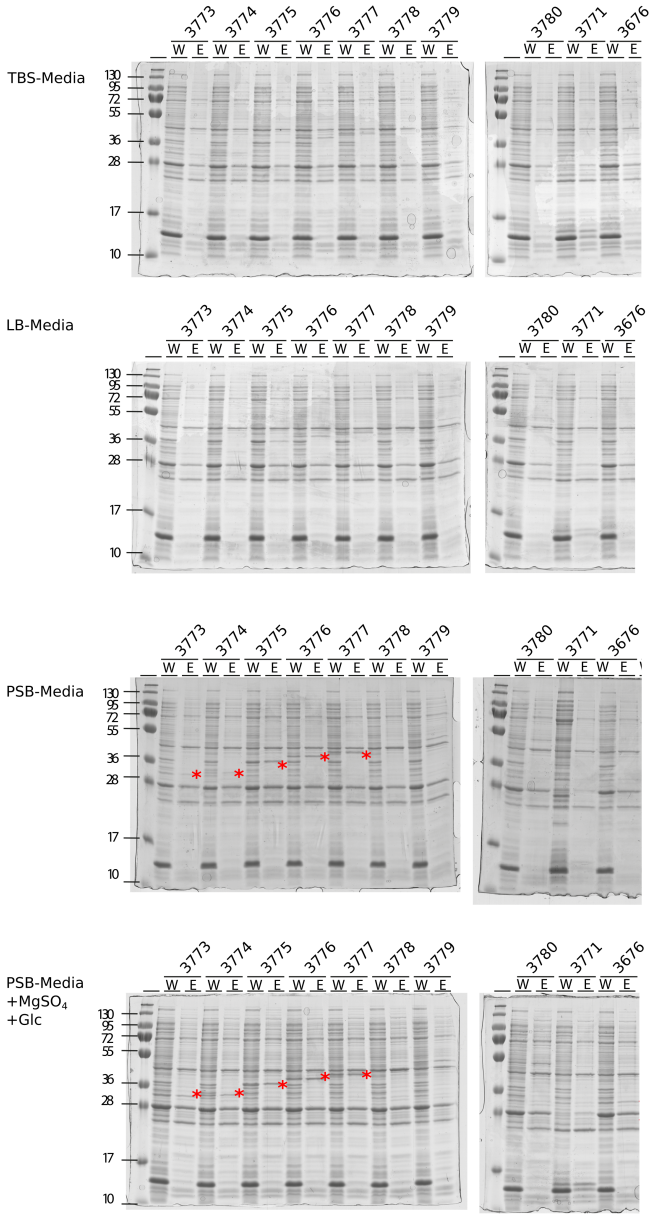

Figure 4.3: **Test expression and purification of pet-Duet1 vectors containing 14-3-3 and different ChREBP fragments**
For expressed fragments, see vector number in Table 4.1. W= whole cell lysate E= elution. Red asterisks indicate for ChREBP fragments that could be purified and identified based on Mw.

4.1.4 Purification of 14-3-3/GSM

For the purification of 14-3-3/GSM *E. coli* pellets of cultures between four and six liters were resuspended in lysis buffer and lysed by sonification. The lysate was centrifuged and the supernatant loaded onto a self-packed Ni-NTA column, using an äkta pure system. Bound protein was eluted by step elutions, using elution buffer containing 0.5 M imidazole. Flow through and elutions were analyzed by SDS-PAGE (see Figure 4.4A, colored bars under the chromatogram reflect fractions loaded on SDS-PAGE). Fractions containing the proteins of interest (grey area under the curve, Figure 4.4A) were pooled and incubated with His-TEV protease for 4-6 hours in the coldroom to remove the His-tag. At the same time, the protein solution is dialyzed into ion exchange A buffer (IEXA). After dialysis the protein solution is run over a Ni-NTA column to remove His-TEV protease, His-tag and uncleaved target protein (Figure 4.4B). Afterwards proteins are further purified by ion exchange chromatography, using Q-sepharose as an anion exchanger (Figure 4.4B small graph), concentrated and loaded on a HiLoad Superdex 200pg column for size exclusion chromatography (Figure 4.4C). Since for most downstream applications it is crucial to have the protein and ligand in identical buffers, fractions containing 14-3-3/GSM complex are pooled and dialyzed overnight in dialysis buffer. Afterwards, the protein and dialysis buffer is snap frozen by liquid nitrogen and stored at -80°C. The SDS-PAGE in Figure 4.4C shows that 14-3-3/GSM can be purified from *E. coli* with only minor impurities. The total amount of protein that can be purified from one purification was between 40-60 mg.

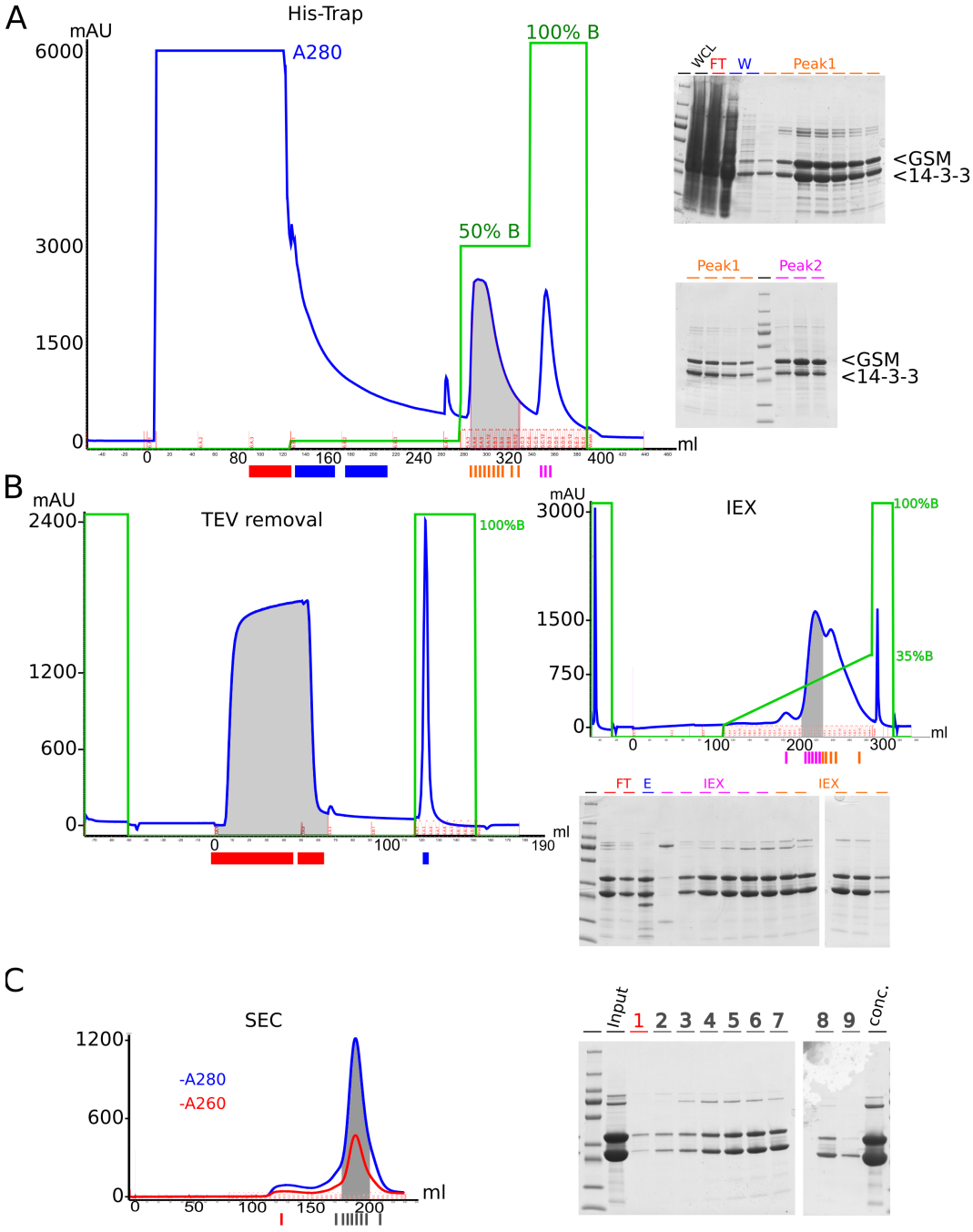

Figure 4.4: **Purification of 14-3-3/GSM complex by different chromatographic methods**
A: His-Trap of tagged GSM in complex with 14-3-3. As shown by the SDS-PAGE 14-3-3 is forming a stable complex with GSM and can be co-purified. B: Chromatogram of TEV removal and ion exchange. C: Chromatogram of size exclusion chromatography (HiLoad Superdex 200) and final purified construct (SDS-PAGE last lane). Bars under the chromatograms indicate fractions that are loaded onto the SDS-PAGE for analysis. Grey area under the curve shows fractions that were pooled and used in downstream processes.

4.2 14-3-3/GSM is a trimeric complex

14-3-3 isoforms are known to form homo- or hetero-dimers[Chaudhri et al., 2003, Jones et al., 1995], also Ge *et al.* [Ge et al., 2011] described two potential 14-3-3 binding sites in ChREBP. To determine the stoichiometry of the purified complex, purified 14-3-3 and 14-3-3/GSM were run over a Superdex Increase 200 10-30 size exclusion chromatography column. The elution volumes are compared to a standard-curve, generated by elution of proteins of known size. Based on theoretical molecular weight, the predicted elution volume was calculated and compared to the experimentally observed elution volumes (see Table 4.2 and Figure 4.5A,B). As shown in Figure 4.5B and summarized in Table 4.2, 14-3-3 elutes close to the calculated molecular weight of a dimer. 14-3-3/GSM elutes close to the calculated volume for a 14-3-3homodimer bound to one GSM (14-3-3_2/GSM). In addition, sedimentation velocity analytical ultracentrifugation was performed (SV-AUC). With this method two major populations were detected (sed. coefficient 3.6 and 5 Figure 4.5C). Calculating the molecular weight of these populations results in sizes of 55.2 kDA and 98.7 kDa. Most likely, these values reflect free 14-3-3dimer and 14-3-3dimer bound to GSM. A sed. coefficient of 3.75 was previously reported for the dimeric isoform 14-3-3ζ [Woodcock et al., 2017]. Based on the observations made by size exclusion chromatography, as well as analytical ultracentrifugation it is concluded that 14-3-3 binds as a dimer to GSM. In addition, on SDS-PAGE the band for 14-3-3 always stains stronger compared to GSM, despite its smaller size. The experimentally determined stoichiometry of the complex is in line with the reported binding-characterizations of 14-3-3 to ChREBP by Sakiyama *et al.* [Sakiyama et al., 2008] and [Ge et al., 2011, Ge et al., 2012]. For simplicity, this complex is called **14-3-3/GSM** from now on.

Complex	Mw [kDa]	Calculated elution volume [ml]	Observed elution volume [ml]
14-3-3_2	57	15.7	15.5
14-3-3/GSM	62	15.6	14.6
14-3-3_2/GSM	90	14.9	14.6
14-3-3_2/GSM_2	124	14	14.6

Table 4.2: Complex size and elution volumes

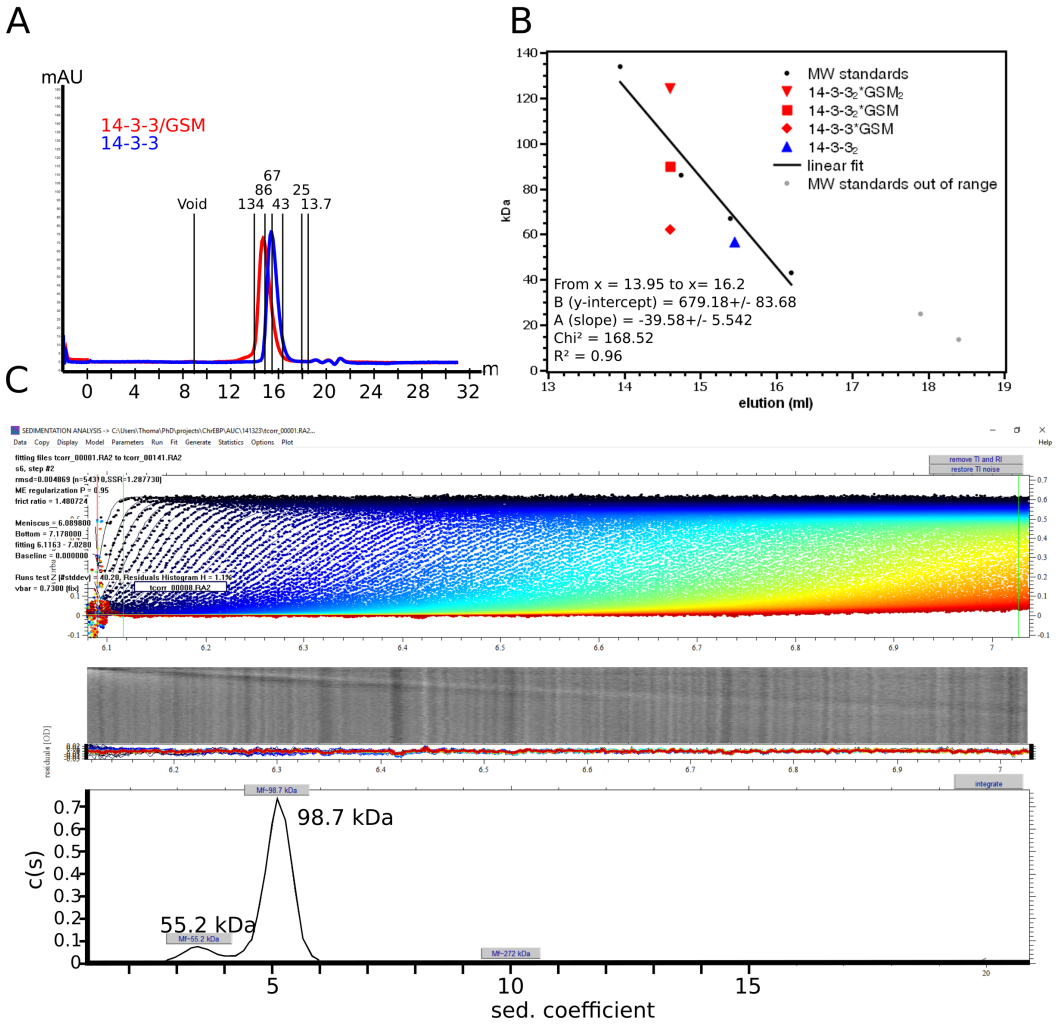

Figure 4.5: **SEC and AUC indicate that 14-3-3/GSM is a trimeric complex**
Size characterization of 14-3-3/GSM complex. A: Elution volume of 14-3-3 (blue) and 14-3-3/GSM (red) in comparison to known molecular weight standards, indicated by horizontal lines. Numbers are Mw in kDa. B: Standard curve based on A, 14-3-3/GSM (red) is blotted with a theoretical Mw of a complex containing monomeric 14-3-3 (diamond), dimeric 14-3-3 (square) and dimeric 14-3-3 with a dimeric GSM (triangle). Mw of 14-3-3 (blue triangle) is calculated as dimer. C: AUC-SV run of 14-3-3/GSM. Top panel shows fit of raw data. Bottom panel shows analysis of sedimentation coefficient and calculated molecular weight.

4.3 14-3-3/GSM binds Glc6P

4.3.1 Isothermal calorimetry shows binding of Glc6P to 14-3-3/GSM

Previous reports indicate that Glc6P may regulate ChREBP function in living cells (see Section 1.5.4). As mentioned, we could confirm this assumption by first ITC experiments using a single chain 14-3-3-ChREBP construct as a proof of concept (Section 4.1.1). To further investigate Glc6P binding to the ChREBP GSM, we again used isothermal calorimetry (ITC) as an *in vitro* assay in combination with our optimized 14-3-3/GSM complex. ITC is the gold standard for detecting molecular interactions and binding events. 14-3-3/GSM is loaded into the sample cell and Glc6P is titrated to the protein sample in a series of injections. The released heat of binding is recorded and binding parameters are calculated. As shown in Figure 4.6A (black graph), heat is released because of Glc6P binding to the protein complex. The thermodynamic signature, as well as binding stoichiometry are shown in Figure 4.6B and D. Based on the slope in Figure 4.6C, Glc6P binds with an K_D of 2µM.

Due to the heat of dilution, injections of a mismatched buffer into the sample cell could create a false positive binding signal. To exclude this possibility, we run a sample of Glc6P against buffer as a control. No false-positive binding is detected (see Figure 4.6A, top panel). Since in our hands the GSM only can be purified together with 14-3-3, the possibility of Glc6P binding to 14-3-3 without the involvement of the GSM, needs to be excluded. Therefore Glc6P was injected into 14-3-3 only. Figure 4.6A (red graph) shows also in this case that no binding curve can be detected. Therefore it is concluded, that Glc6P is binding to the complex of 14-3-3/GSM with a K_D in the low µM range. This binding is driven by enthalpy, resulting in a reduction of entropy (most likely caused by unfavorable structural changes).

If one molecule of Glc6P is binding to one binding site in 14-3-3/GSM, a stoichiometry of N= 1 is expected. However, binding of Glc6P is with N= 0.6 below this expected value. Several factors could explain a binding stoichiometry N<1. The most obvious is a lower protein concentration than determined. This can be caused for example by an error in measurement of the absorbance or wrongly calculated extinction coefficient, where latter is based on the assumption of an complex of dimeric 14-3-3 and monomeric GSM. Since AUC shows a fraction of free 14-3-3 (Figure 4.5C) and SDS-PAGE shows slight contamination with other

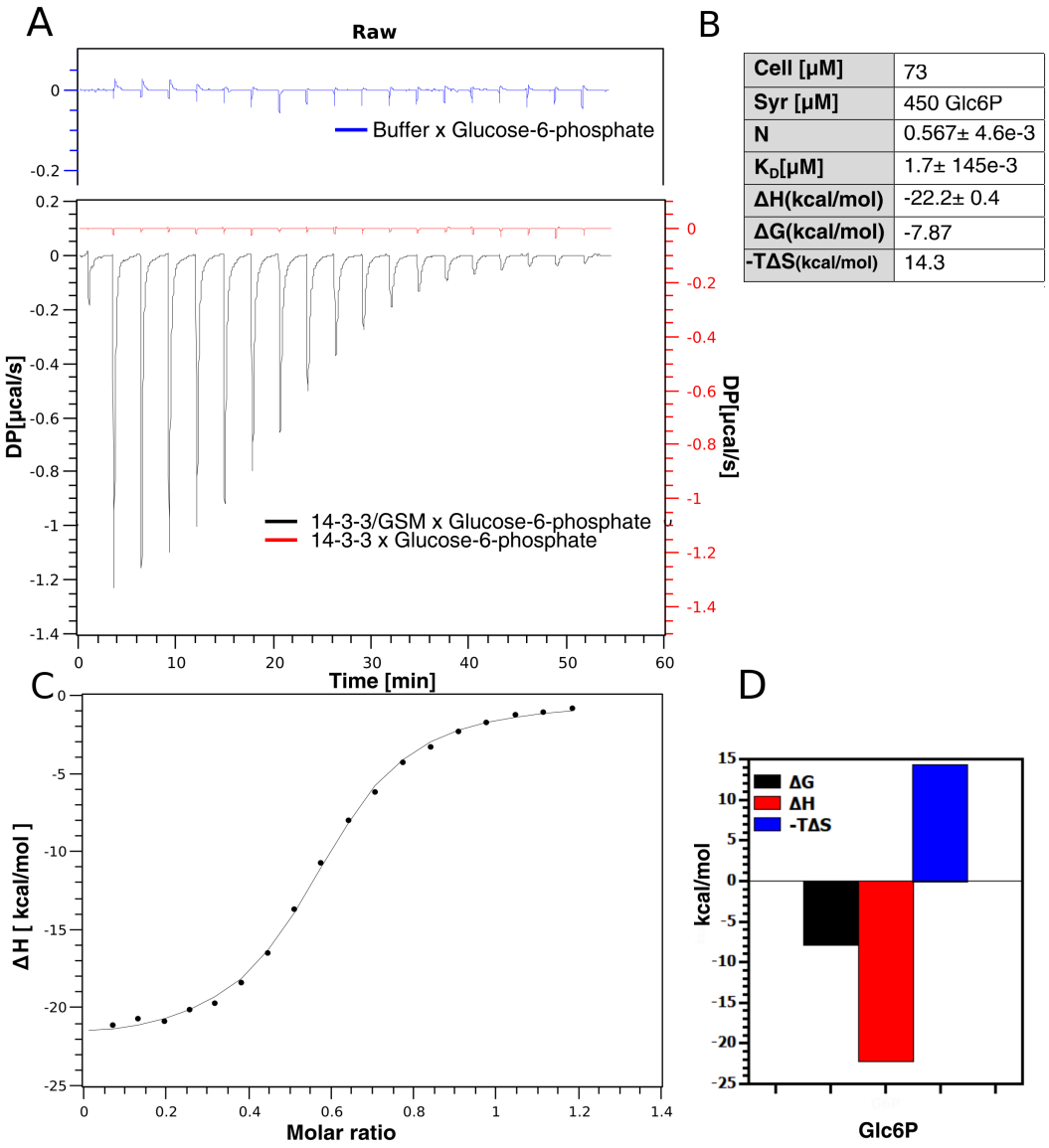

Figure 4.6: **ITC shows binding of Glc6P to 14-3-3/GSM**
A: Titration of Glc6P in buffer (blue) and Glc6P against 14-3-3 (red) show no binding in the ITC raw signal. Glc6P titration in 14-3-3/GSM complex shows binding (black). Integration of the heat signal is shown in C. B: Binding parameters for Glc6P to 14-3-3/GSM. D: Signature-plot of Glc6P binding.

proteins (Figure 4.4), these factors might contribute to an error in absorbance based calculation of protein concentration. Second, some of the protein is not active due to instability, modifications or misfolding. Since our own observations are that ChREBP is a rather unstable protein, this explanation is quite likely. The fact that ITC measurements are conducted at 25°C, under constant stirring of the sample, it is quite likely that the ITC run itself can cause aggregation of protein. To investigate this possibility, samples were taken before and after an ITC run and analyzed. To estimate for aggregates, the OD_{600} of the protein samples were measured by using a nanodrop. Figure 4.7A shows that ITC measurements cause an increase in OD_{600} , and therefore indicate for aggregation. These findings were confirmed by also measuring the absorbance at A_{280}nm (Figure 4.7B). The small decrease of signal for absorption at a wavelength of 280nm (A_{280}) samples before and after ITC can be explained by dilution of the protein sample by ligand-containing buffer. OD_{600} and absorbance of the "after ITC" samples are decreased after centrifugation, which is a measure that protein (aggregates) are pelleted. Treatment with urea brought the absorbance value back to its initial values by solubilization of the aggregate.

Because of the analysis of proteins before and after ITC runs, as well as the presence of free 14-3-3 in AUC, we concluded that the binding stoichiometry of Glc6P to 14-3-3/GSM is N<1 due to protein aggregation in the sample cell and the presence of additional free 14-3-3, resulting in a lower complex concentration than expected.

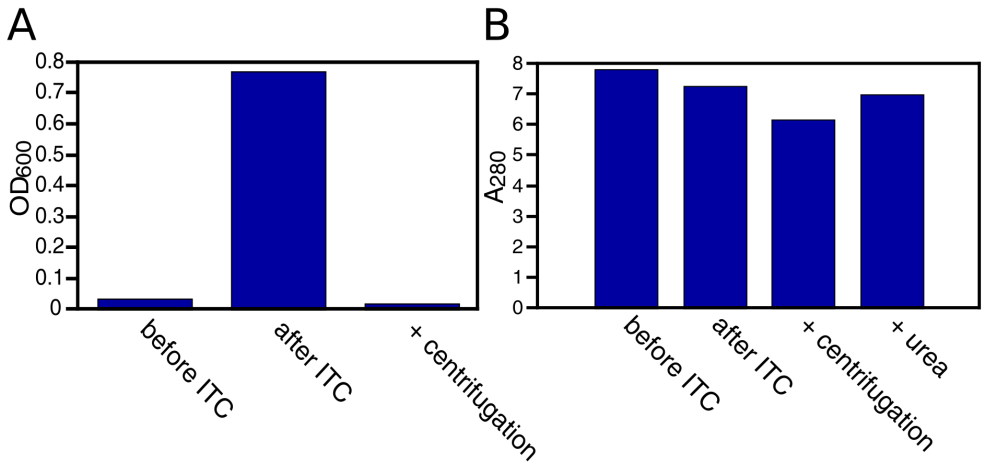

Figure 4.7: **Analysis of samples before and after ITC shows aggregation**
A: OD_{600} was measured before and after an ITC run. Aggregates, which are measured by an increase in OD_{600} signal, can be removed by centrifugation. B: A_{280} before and after ITC run. By centrifugation protein is removed. Treatment with urea results in similar absorption than after ITC

4.3.2 Label-free microscale thermophoresis confirms binding of Glc6P

To confirm the observed binding of Glc6P to the 14-3-3/GSM complex by using an independent method, label free micro scale thermophoresis (MST) was chosen. Since this method is based on changes in the hydration shell of proteins upon ligand binding, the choice of the correct buffer is essential. We tested a series of assay buffers to determine the one with the lowest noise. To do so, a set of four capillaries were filled with the identical protein-buffer mixture, using different buffers for each set. MST traces were recorded and normalized fluorescence *"Fnorm"* of each capillary and buffer was plotted (see Figure 4.8A). Buffers that showed the lowest noise between measurements (capillaries with the same protein-buffer mixture) were MES buffer (pH= 6.5) and HEPES (pH= 7).

To test whether under these buffer conditions the protein complex still binds Glc6P, the proteins were purified as described before in Section 4.1.4 , but HEPES buffer was replaced with MES pH 6.5 or pH was adjusted to 7 instead of 7.5. Purified proteins were then subjected to ITC experiments (Figure 4.8B). MES buffer interfered with binding of Glc6P, where HEPES pH 7 showed a K_D of 2µM, which is in line with previous experiments. The fitted binding parameters for the sample containing MES buffer are too inaccurate for the determination of a K_D value. Based on these results, we chose to carry out the MST binding

experiments with HEPES buffer at a pH of 7.

We belief the reason why MES buffer is interfering with binding is due to its structural similarity to phosphorylated sugars. An effect we also observed for macrodomains, where crystal structures showed MES to mimic the binding of ADP-ribose (personal communication with A. Ladurner). After optimization of

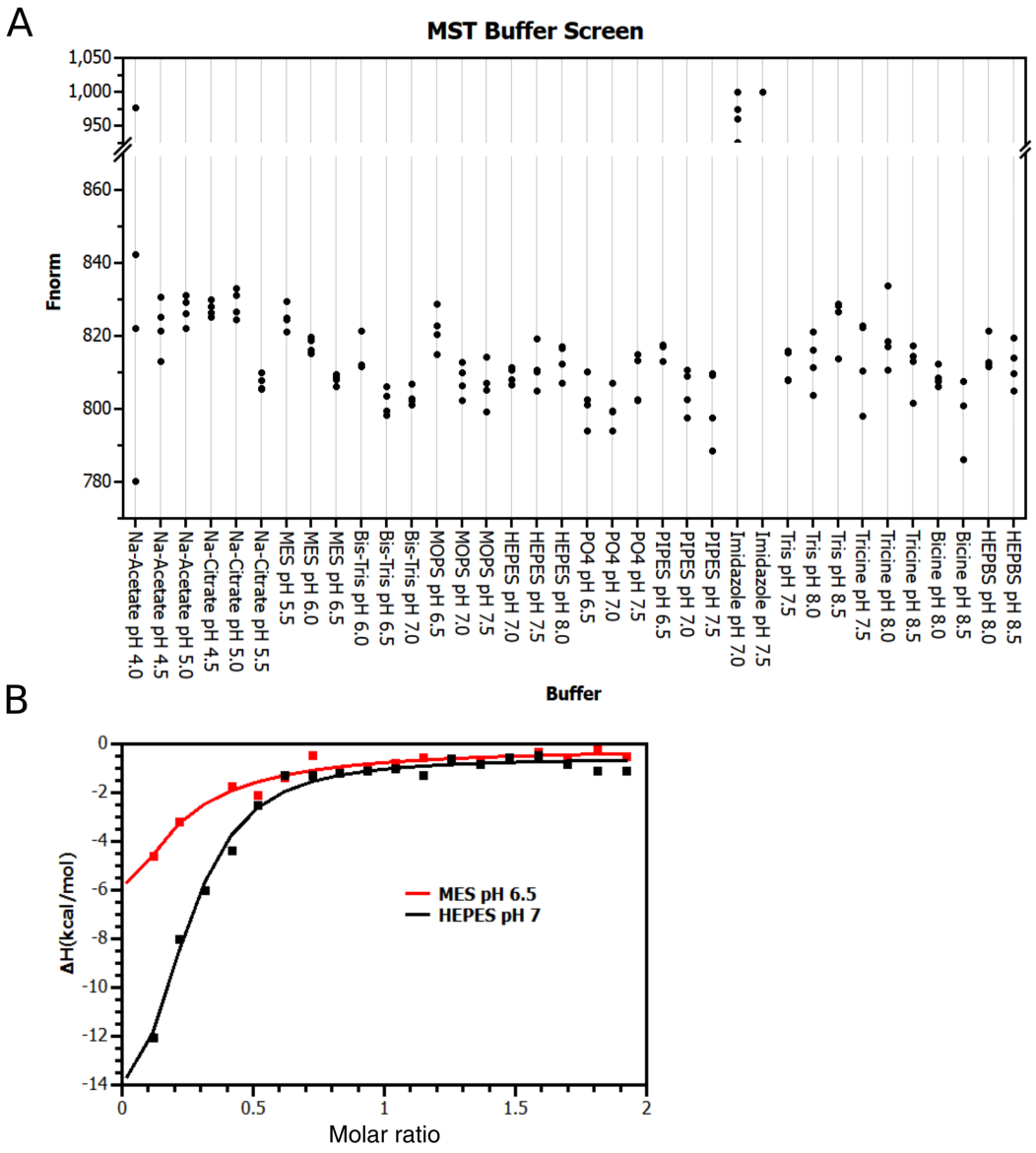

Figure 4.8: **Buffer screen to find best MST conditions**
A: Each datapoint represents one capillary (four of each buffer). Buffers with close clustering of the individual capillaries were MES pH 6.5 and HEPES pH 7. B: ITC experiment of 14-3-3/GSM purified with indicated buffers and tested for Glc6P binding. HEPES pH 7 resulting in a K_D of 2µM.

buffer conditions, we performed binding experiments. Glc6P was dissolved in

assay buffer and a dilution series was generated. Protein was added at a constant concentration and MST traces were recorded (Figure 4.9D). The thermophoresis signal was first plotted in a dose response curve (Figure 4.9A), showing a decrease in fluorescence with increasing Glc6P concentration. Next, a binding curve was generated (Figure 4.9B) and the K_D was calculated. In line with previous ITC experiments (Section 4.3.1), the K_D was approximately 2µM. To eliminate the possibility of false positive binding by some effects of ligand titration, we chose Glc1P and Glc as negative controls. As shown in Figure Figure 4.9A, these metabolites did not show a dose response. Additionally, we tested whether the high concentration of Glc6P could have any effect on the pH of the assay buffer. The pH was tested with test stripes, showing no difference between 2 mM Glc6P and buffer (Figure 4.9E). An additional control for this possibility was the use of Glc1P as a negative control. In summary, we were able to confirm the binding of Glc6P to 14-3-3/GSM in an independent biophysical assay, resulting in a comparable K_D to the ITC experiments. In addition, the specificity of 14-3-3/GSM for Glc6P binding was tested by including Glc and Glc1P as controls.

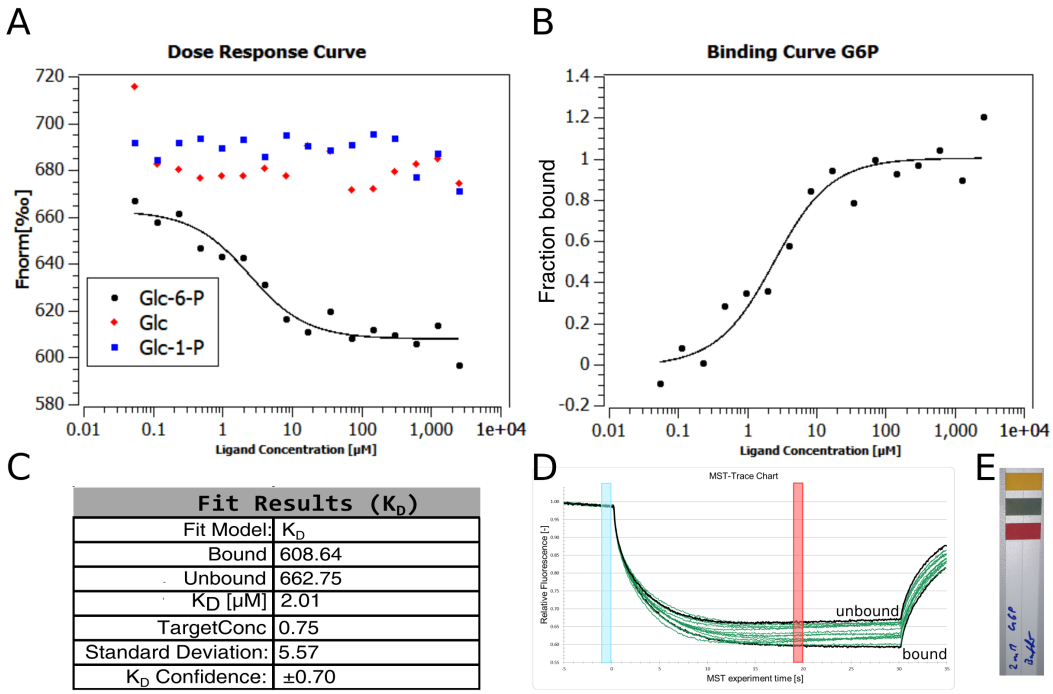

Fit Results (K_D)	
Fit Model:	K_D
Bound	608.64
Unbound	662.75
K_D [µM]	2.01
TargetConc	0.75
Standard Deviation:	5.57
K_D Confidence:	±0.70

Figure 4.9: **MST shows binding of Glc6P to 14-3-3/GSM**
A: Dose response curve of MST experiments of 14-3-3/GSM and different metabolites. B: Binding curve of Glc6P. C: Binding parameters for Glc6P binding. D: MST traces of Glc6P, blue and red boxes indicate regions that were used for evaluation. E: pH indicator strip shows no difference between 2 mM Glc6P and buffer only.

4.4 Binding of AMP to 14-3-3/GSM competes with Glc6P binding

It has previously been reported, that the binding of AMP to the 14-3-3/α2-helix of the GSM interface is strengthening the interaction of 14-3-3 to ChREBP. Promoting its nuclear export and cytoplasmic retention [Sato et al., 2016]. The ITC experiments for AMP binding in this study were set-up in an indirect fashion, investigating the affinity of the α2-helix peptide to 14-3-3 in absence and presence of AMP in the sample cell. Not the binding of the metabolite itself. Therefore we decided to test in this thesis, if AMP can bind directly to 14-3-3/GSM complex, the same as for Glc6P. As shown in Figure 4.10A, AMP can directly bind to the 14-3-3/GSM complex with a K_D of 5μM, slightly above Glc6P. Binding of AMP to 14-3-3/GSM is less enthalpic than Glc6P. To test whether binding of one or the other metabolite is exclusive, 14-3-3/GSM was preincubated with AMP in the ITC-sample cell at a concentration at which 14-3-3/GSM is saturated by AMP. Under these conditions binding of Glc6P was strongly reduced (Figure 4.10A dashed line, black square). As a negative control 14-3-3/GSM was preincubated with cyclic-AMP (cAMP), which is not binding to the complex. In this case Glc6P was able to bind as expected (see Figure 4.10A). The competition between AMP and Glc6P could have two indications. First, both metabolites bind to the same or overlapping site. Second, binding of AMP may cause conformational changes that block the binding of Glc6P. If latter is the case, it should be possible to mutate the AMP binding site and still maintain Glc6P binding.

4.4.1 Differences in binding between AMP and Glc6P

Comparing the ITC-binding experiments between AMP and Glc6P, a difference in the peak-shape of the raw- ITC curve was observed (Figure 4.11A). With AMP injections reaching faster the baseline than with Glc6P. Often this can be an indication of differences in association constant (K_{on}) and dissociation constant (K_{off}) between ligands [Burnouf et al., 2012]. To investigate this possibility, the program *KinITC*[1] was used to calculate the K_{on} and K_{off} rates for AMP and Glc6P binding. As shown in Figure 4.11, Glc6P binding is at a lower on rate and dissociation when compared to AMP. Resulting in an overall lower K_D for

[1] https://www.affinimeter.com/site/kinitc-2/

A

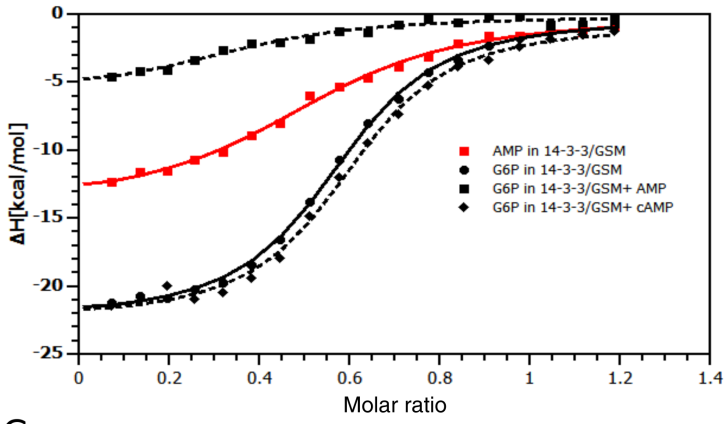

B

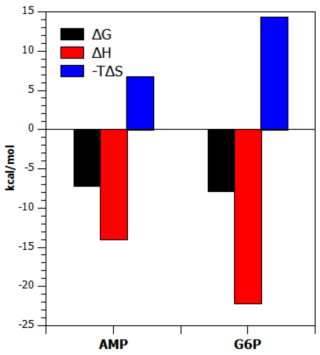

C

Cell [µM]	Syr [µM]	N	K_D [µM]	ΔH (kcal/mol)	ΔG (kcal/mol)	-TΔS (kcal/mol)
73	450 G6P	0.57± 4.6e-3	1.7± 145e-3	-22.2± 0.4	-7.87	14.3
73	450 AMP	0.53± 1.4e-2	4.81± 915e-3	-14.0± 0.8	-7.26	6.7
73 & 80 cAMP	450 G6P	0.59± 8.7e-3	1.56± 256e-3	-21.7± 0.7	-7.92	13.8
73 & 80 AMP	450 G6P	0.37± 3.2e-2	6.18± 3.39	-5.72± 1.1	-7.11	-1.39

Figure 4.10: **Binding of AMP and Glc6P to 14-3-3/GSM**
A: Binding of AMP to 14-3-3/GSM (red) in comparison to Glc6P (black solid). Presence of AMP blocks Glc6P binding (black square, dashed line). Presence of cAMP does not inhibit Glc6P binding (black diamond, dashed line). B: Signature plot of AMP and Glc6P binding. C: Result table from A.

Glc6P (Figure 4.11[2]).

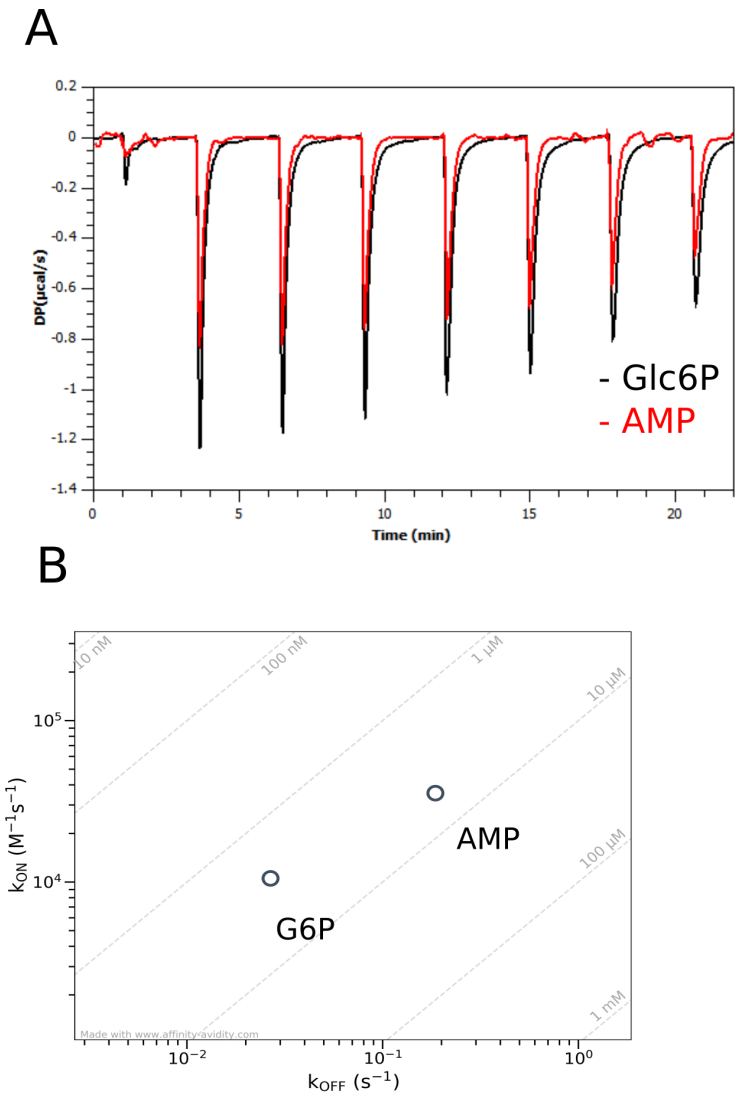

Figure 4.11: **Binding kinetics of AMP and Glc6P**
A: Overlay of ITC-raw data for AMP (red) and Glc6P (black) binding shows differences in the time needed to reach baseline. B: Plot of K_{on} and K_{off} show AMP is binding faster than Glc6P, however K_{off} rate is higher as well.

Interestingly, using a GSM fragment from 81-291aa (deletion of MCR1 and partially MCR2), which is still able to bind 14-3-3, the differences in binding kinetics between AMP and Glc6P are diminished/absent (see Figure 4.12A). Additionally, the free enthalpy ΔH of binding was significantly reduced for Glc6P, but only minor affected for AMP (Figure 4.12B and D), when compared to the full-length construct. This does not only show that the N-terminal MCR1 and

[2]plot generated using https://affinity-avidity.com/

MCR2 are not directly involved in metabolite binding, it also indicates a conformational change in this region, resulting in an increase in enthalpy for Glc6P binding. For example, additional protein-protein or intramolecular interactions upon binding to Glc6P. Hydrogen deuterium exchange (HDX) experiments (Section 4.6.4) also show a reduction in deuterium uptake, compared to the control sample, only for the Glc6P bound state in this region. It therefore can be assumed that the binding of Glc6P results in a protein-ligand complex that is distinct from the AMP bound state. It has to be noted that purification of this truncated construct of the GSM was less efficient than compared to the wild type (*wt*) full length construct (Figure 4.12C). Therefore a direct comparison to *wt* has to be taken with caution.

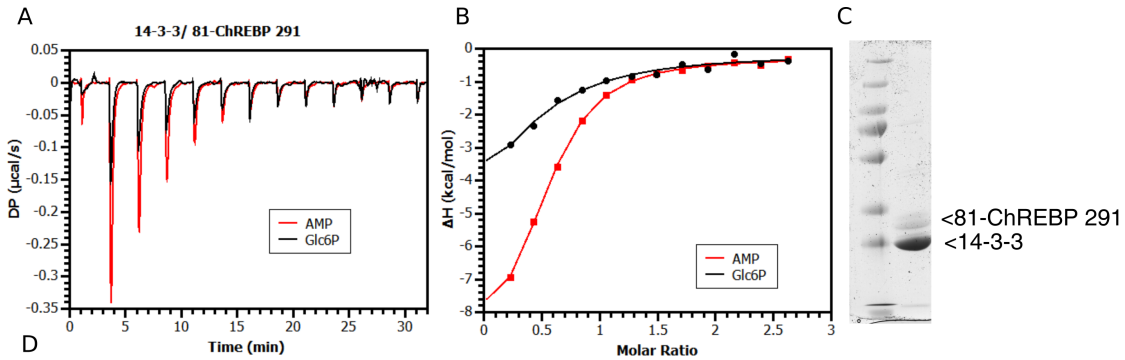

D

	Syr (µM)	Cell (µM)	N (sites)	KD (µM)	ΔH (kcal/mol)	ΔG (kcal/mol)	-TΔS (kcal/mol)	Offset (kcal/mol)	Red. Chi-Sqr. (kcal/mol)²
AMP	300	22	0.509	2.72	-9.22	-7.59	1.63	-0.258	2.60E-03
Glc6P	300	22	0.421	9.90	-6.75	-6.83	-7.90E-02	-0.172	1.80E-02

Figure 4.12: **Truncated GSM shows distinct differences in binding compared to full-length GSM**
A: Overlay of ITC-raw data for AMP (red) and Glc6P (black) binding show only minor differences in the time needed to reach baseline. B: Normalized binding of AMP and Glc6P. C: SDS-PAGE o the purified construct shows a less intense band for GSM compared to *wt* purifications. D: Result table for ITC experiments shows a reduction in ΔH for Glc6P, compared to *wt*. Values for AMP are similar to *wt*.

4.4.2 Mutations of the AMP binding site affects binding of AMP and Glc6P

The potential binding site of AMP in the 14-3-3/GSM complex was crystallized by Sato *et al.* [Sato et al., 2016] (PDB 5F74). However, this structure has to be seen with caution since only an electron density for the phosphate rather

for AMP could be observed, which questions the correctness of the structure (Figure 1.15). In addition, the crystallization buffer contained high amounts of sulfate and therefore it can not be excluded that this structure is solely based on a sulfate sitting in the potential binding site.

Based on this structure we generated several mutants that should impair AMP binding (see Table 4.3. The mutant 14-3-3 S47A, 14-3-3 K51A, 14-3-3 R58A and ChREBP W127A could be purified and all show impaired AMP binding when compared to *wt*. Interestingly, all these mutants also affected the binding of Glc6P (Figure 4.13B,C). A summary of the binding parameters of these experiments can be found in the Appendix Table 7.1. However, these parameters have to be taken with caution since protein-ligand concentrations have not been optimized for weak binding signals (e.g. S47A, K51A for AMP). Together with the data from the competition experiments, this is a strong indication that both metabolites interact with a related or overlapping bindingsite.

Mutation ChREBP	Mutation 14-3-3	Expression	Purification	Binding
N124A		yes	Aggregate during dial.	
W127A		yes	yes	No (AMP, G6P)
	S47A	yes	yes	No (dH -1 kcal/mol)
	K51A	yes	yes	Low and noisy signal only for AMP
	R129A	yes	Only 14-3-3	
	R58A	yes	yes	Very weak for AMP/ G6P
	K122A	yes	Only 14-3-3	
	Y130A	Only 14-3-3		

Table 4.3: Overview of generated mutants

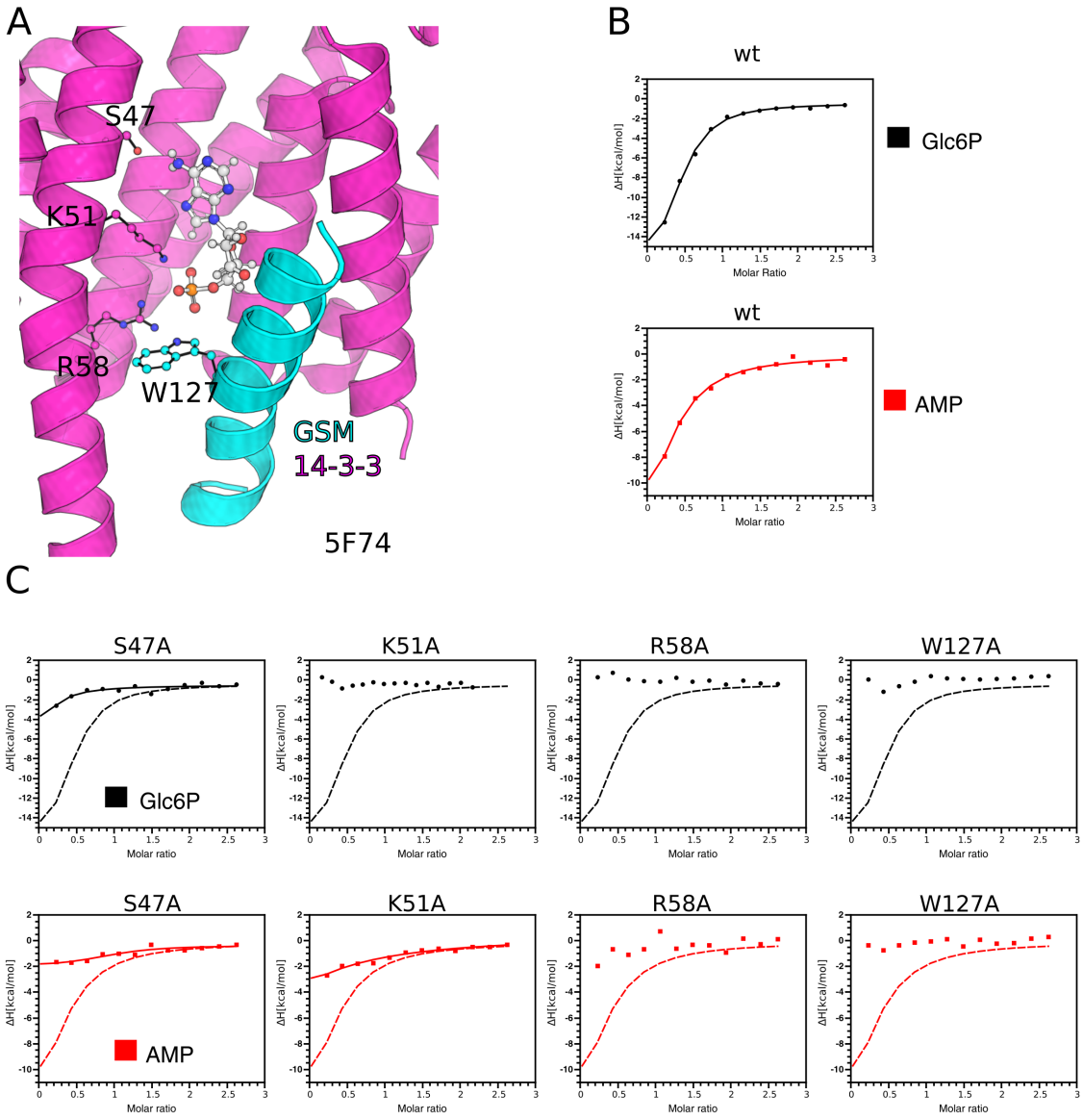

Figure 4.13: **Mutations of the AMP binding site affects metabolite binding**
A: Crystal structure of 14-3-3 (pink) and ChREBP α2- helix (cyan) with bound AMP, based on PDB 5F74. Mutated residues are represented as stick. B: Normalized heat graph of ITC experiments of *wt* 14-3-3/GSM for Glc6P (black) and AMP (red) binding. C: ITC experiments of mutants as indicated in A. AMP binding in red, Glc6P binding in black. Dashed lines represent *wt* binding as shown in B.

4.4.3 The SNP Q241H does not affect binding of Glc6P or AMP

In 2007 Kooner *et al.* identified the SNP Q241H and found an association to a reduction in triglycerides [Kooner et al., 2008]. Nakayama *et al.*[Nakayama et al., 2011] identified the single-nucleotide polymorphism (SNP) Q241H in a central-asian population and linked its presence to a protein rich lifestyle. We therefore speculated if this SNP could have an effect on metabolite binding, and therefore ChREBP activity. The SNP containing protein was expressed and purified as previously described and tested for AMP and Glc6P binding using ITC. However, this mutant behaves like wildtype in ITC binding experiments (Figure 4.14). Binding parameters can be found in Appendix Table 7.1. In support of this observation, Q241 is not conserved in MondoA or the *Drosophila* Mondo protein (Figure 1.7) and therefore might not be of functional importance.

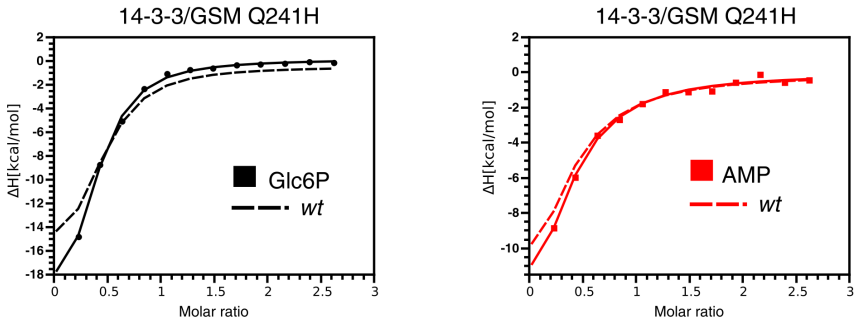

Syr	N	K_D [µM]	ΔH (kcal/mol)	ΔG (kcal/mol)	-TΔS (kcal/mol)
Glc6P	0.34± 2.2e-2	2.62 ± 0.5	-24.4± 2.42	-7.62	16.8
AMP	0.31± 8.4e-2	6.46 ± 2.5	-21.4± 8.13	-7.08	14.3

Figure 4.14: **SNP Q241H does not affect metabolite binding**
ITC experiments of the SNP Q241H show no difference in metabolite binding compared to *wt* (dashed line).

4.4.4 Mutants tested for metabolite binding were able to form a stable complex

Mutant complexes were expressed and purified successfully using the same protocol as for *wt*. The results of the final polishing step of this purifications is shown in Figure 3.11A. Although, based on the used purification protocol, purification of the complex is only possible by a stable interaction of 14-3-3 with the GSM, the characteristics of the mutant complexes were further investigated. To exclude the possibility, that mutants are not binding AMP and/or Glc6P be-

cause of dissociation of the 14-3-3/GSM complex, an analytical size exclusion chromatography was performed. An unstable complex is expected to cause a shift in the elution volume. However mutants behaved identical to *wt* (see Figure 4.15B). In a practical course, the student Rebecca Deutsch also performed thermal shift assays of *wt*, 14-3-3/GSM W127A, 14-3-3/GSM Q241H and 14-3-3 only. Also in this case no significant change was observed between the mutants and *wt* complexes (for data see [Deutsch, 2019].

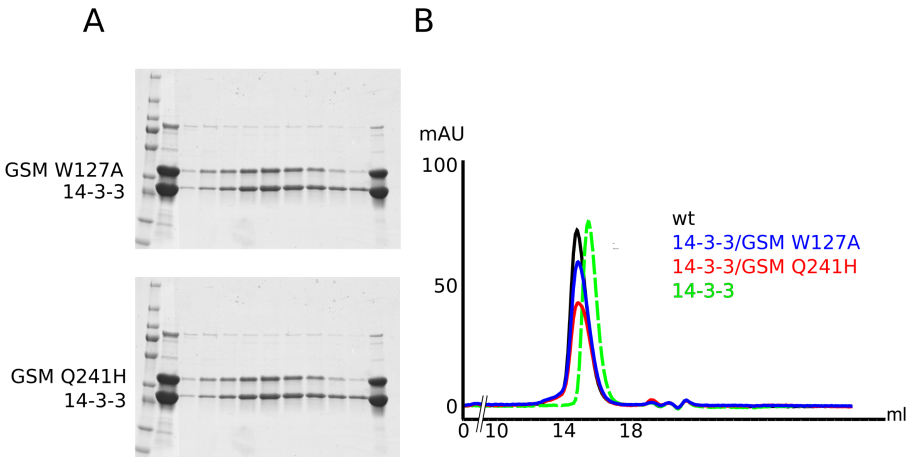

Figure 4.15: **Analytical size exclusion chromatography of mutants**
A: SDS-PAGE showing fractions of the final step of purification of mutants. B: Analytical size exclusion chromatography of *wt*, two GSM mutants and 14-3-3 show no dissociation of the 14-3-3/GSM complex.

4.5 Metabolite Specificity

4.5.1 Screening for the best scintillation-proximity assay conditions

As explained in Figure 4.16, the signal in a scintillation proximity assay is generated by close proximity of the radiolabeled ligand to the scintillation bead. This can either be caused by interaction with the target protein coupled to the beads, or through indirect effects, resulting in a background signal. Indirect effects are unspecific binding/interaction of the radioligand with the beads itself or high concentrations, resulting in large amounts of ligand in close proximity to the beads. To avoid these background signals, the experimental conditions had to be determined. First, it was tested if buffer-additives are needed

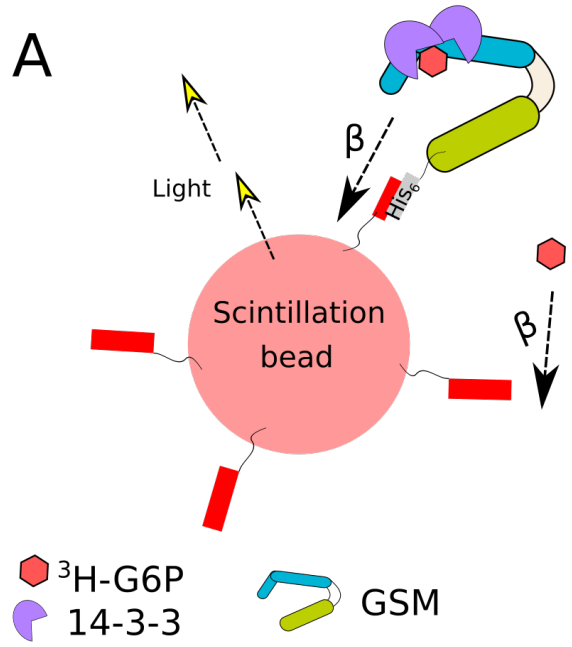

Figure 4.16: **Design of the scintillation proximity assay**
14-3-3/GSM binds via its C-terminal his-tag to the scintillation beads. Tritium labeled Glc6P (^{3}H-Glc6P) binding to the complex results in a luminescence signal.

to reduce unspecific background signals. Therefore constant amounts of tritium labeled Glucose-6-phosphate (^{3}H-Glc6P) and tritium labeled adenosine 5'-monophosphate (^{3}H-AMP) were incubated with SPA beads in presence and absence of 14-3-3/GSM. The use of standard buffer resulted in a high background signal (see Figure 4.17A), detergent did not significantly change this background intensity. Only the presence of ethylenediaminetetraacetic acid (EDTA) resulted in a significant reduction of background signal and a specific binding signal for ^{3}H-Glc6P and ^{3}H-AMP (see Figure 4.17A).

Next, the ligand concentration resulting in the strongest signal to noise ratio was determined. Therefore, different concentration of ^{3}H-Glc6P were added to a constant concentration of 14-3-3/GSM. To obtain the signal for specific binding, the background signal was determined for each ligand concentration (no 'protein samples' in Figure 4.17B) and subtracted from the signal in presence of protein. As expected the signal increases in dependence of the radioligand concentration. Figure 4.17C shows the quantification of the signal to noise ratio with an optimum between 0.125-0.5µCi/well.

The next parameter to control was the protein concentration itself. Therefore different concentrations of protein were added to a constant amount of SPA beads

and radioligand. As expected, at high concentrations the signal reaches a plateau because of ligand depletion and/or maximum binding of protein to SPA beads is reached (Figure 4.17D).

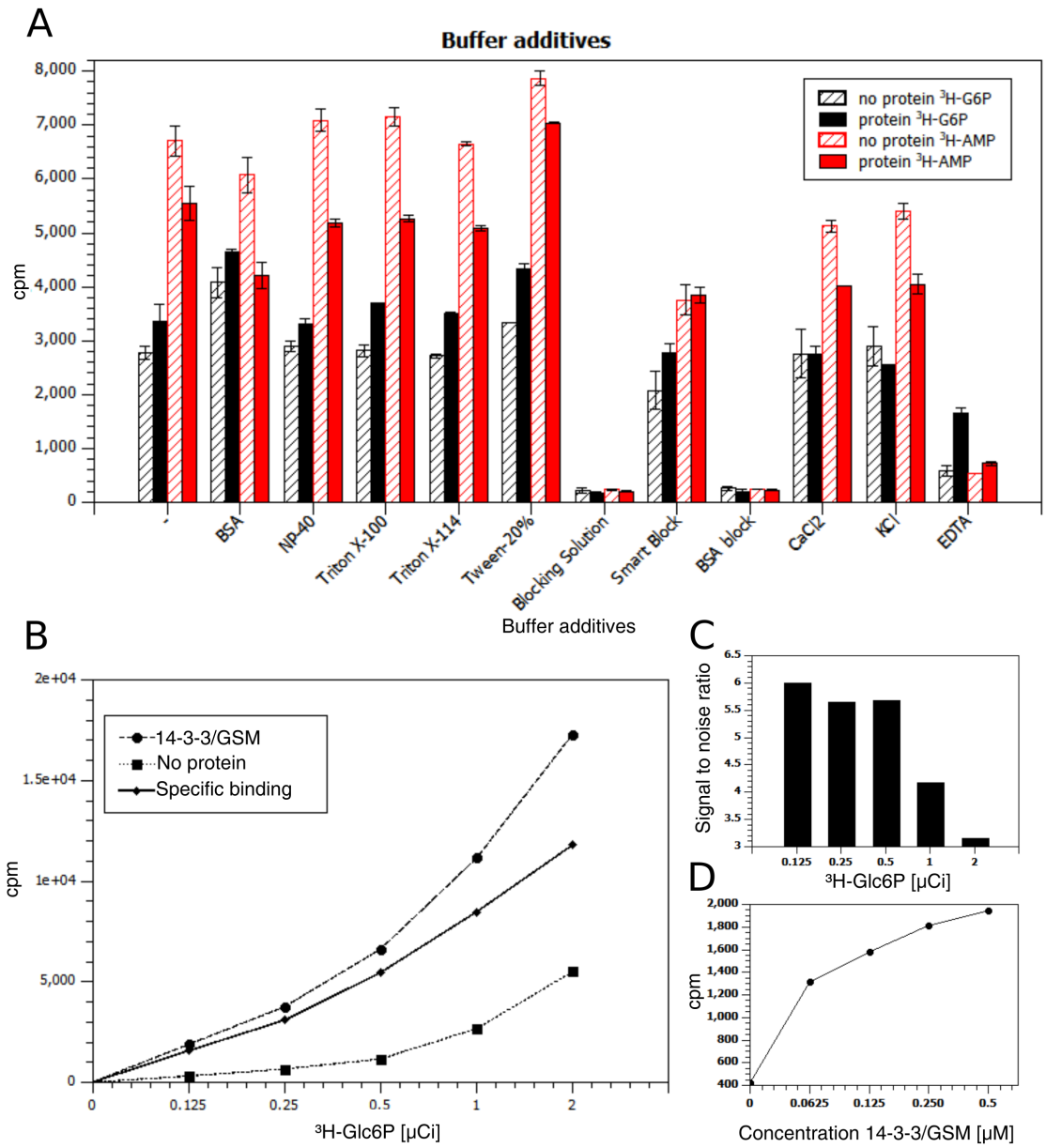

Figure 4.17: **Determination of SPA conditions**

A: Test of different buffer additives to reduce non-specific binding of ^{3}H-AMP (red) and ^{3}H-Glc6P (black) with (solid bars) and without (shaded bars) 14-3-3/GSM. Error is S.D. of duplicates (two wells/plate). B: Dilution series of ^{3}H-Glc6P with constant concentration of 14-3-3/GSM (0.5µM). C: Signal to noise ratio using different amounts of radioligand. D: Dilution series of 14-3-3/GSM complex and constant amounts of ^{3}H-Glc6P (0.2µCi/well).

4.5.2 Competition experiments are in line with previous binding assays

To confirm binding data obtained by ITC, 14-3-3/GSM was incubated together with a dilution series of the two known binders Glc6P and AMP together with a constant concentration of radiolabeled Glc6P (27 nM). In addition R5P also was tested, which showed binding in previous experiments (not shown). If binding takes place, the radiolabeled ligand is displaced from the binding site, resulting in a loss of signal (counts per minute (cpm)). As a negative control imidazole was included, which interferes with binding of the protein complex to the SPA-beads. To factor in non-specific binding of ^{3}H-Glc6P to SPA-beads, as well as potential quenching by the cold ligands itself, control samples containing no protein were included (see Figure 4.18A). In confirmation with ITC assays, Glc6P showed the highest affinity for binding, followed by R5P and AMP. As expected, addition of imidazole resulted in a loss of overall signal. This even was the case in the presence of low concentration of unlabeled Glc6P (see Figure 4.18A). The IC_{50} values were obtained by fitting to a sigmoidal Boltzmann function. Under the assumption ^{3}H-Glc6P has the same affinity as Glc6P the K_D was calculated [DeBlasi et al., 1989]. To calculate the Ki of heterologous ligands, such as AMP and R5P, the Cheng-Prusoff equation was used [Cheng and Prusoff, 1973]. The obtained values are very similar to those obtained by ITC (Figure 4.18B). The small differences might be an effect of different assay buffers used. The titration experiments again reflect the same difference in affinity as observed in the ligand screen, shown in Figure 4.19. Indicating the robustness of these binding events. The titration experiments were also used to choose the best competitor concentration for the screening assay, to see a strong signal change, as well as observe binding of metabolites with low affinities. In this particular case, 10µM were chosen to screen for ligands.

4.5.3 Scree of biological relevant metabolites for 14-3-3/GSM binding shows highest affinity for Glc6P

By testing a variety of sugar(-related) metabolites we can gain important insight about functional groups of the ligand itself, that are important for binding. Over the last decades several metabolites, such as F2,6bP, AMP, X5P and Glc6P were associated to ChREBP function (see Section 1.5.4). To test if these, and other metabolites are capable to compete with ^{3}H-Glc6P binding, purified 14-3-

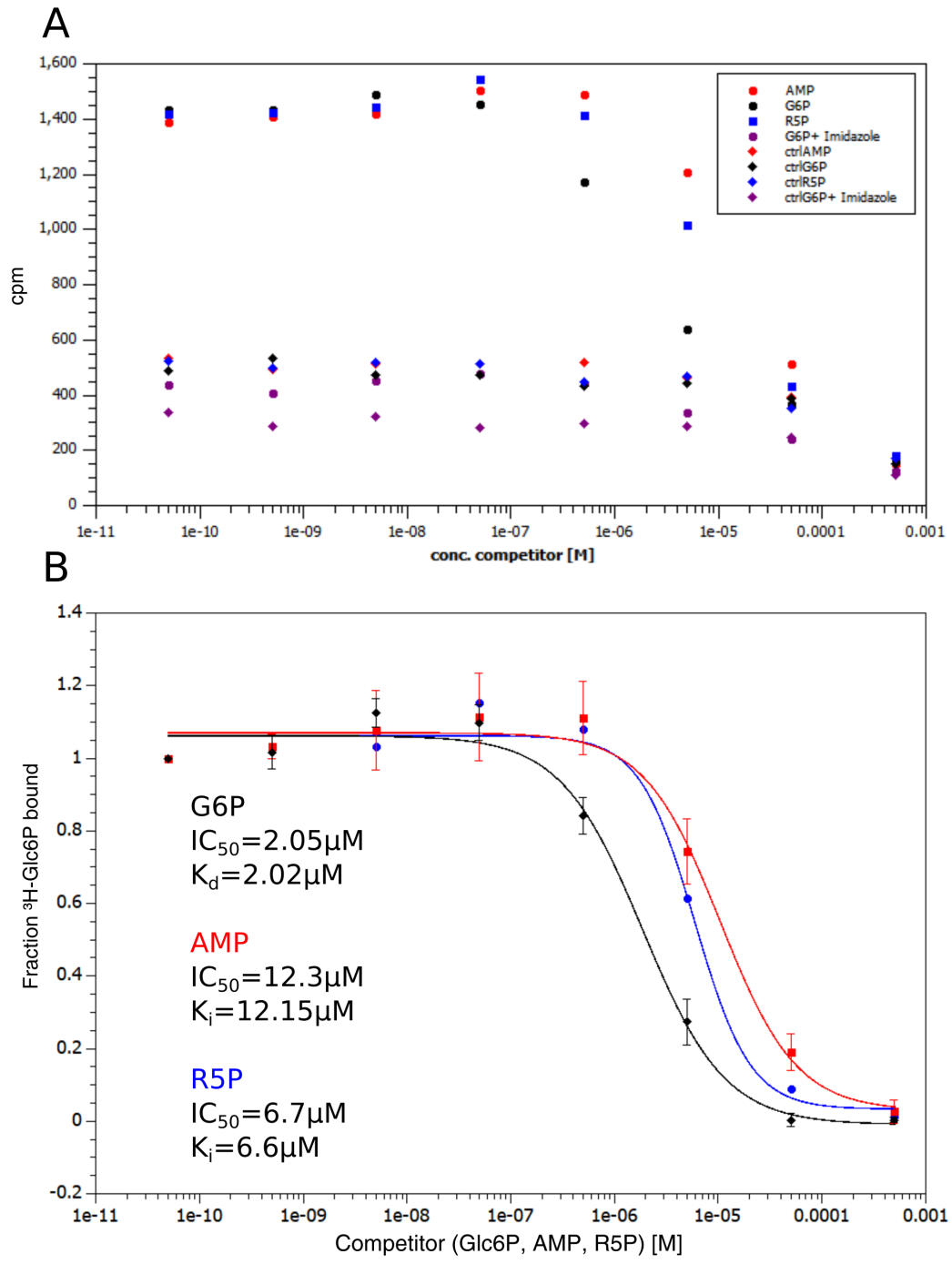

Figure 4.18: **SPA titration experiment**
A: Example of one replicate (plotted mean of 3wells/condition). Ctrl. samples do not contain 14-3-3/GSM. B: Normalized titration curve for Glc6P (black), AMP (red) and R5P (blue) against ^{3}H-Glc6P. For Glc6P and AMP n=3, for R5P one technical replicate. Error bars are S.D.

3/GSM was pre-incubated with 10µM of potential binders and SPA-beads. Afterwards tritium labeled Glucose-6-phosphate (^{3}H-Glc6P) was added. The binding of ^{3}H-Glc6P was measured by counts per minute (cpm) and normalized to a control containing no competing metabolite. Binding of a non radiolabeled ligand results in loss of ^{3}H-Glc6P binding. The results for the tested metabolites are shown in Figure 4.19. From the 27 tested metabolites Glc6P is the most potent binder. We and others showed previously that AMP is able to bind 14-3-3/GSM complex [Sato et al., 2016] (Section 4.4). Using this assay we were able to validate these findings. Interestingly GMP and R5P showed a stronger displacement of ^{3}H-Glc6P compared to AMP. Binding of dAMP and AMP are almost identical, suggesting the 2'-hydoxyl group of AMP is not involved in binding. Also weak binding of X5P and several fructose metabolites (F2,6bP, F6P, F1,6bP) is observed. These metabolites were reported in the past to regulate ChREBP activity [Arden et al., 2012, Kabashima et al., 2003, Kim et al., 2016], however the exact mechanism are not understood. The data suggests a K_D in the upper µM range for these metabolites, questioning the physiological relevance of these interactions. However, they still can give important information about the chemical space of the ligand and potential binding site.

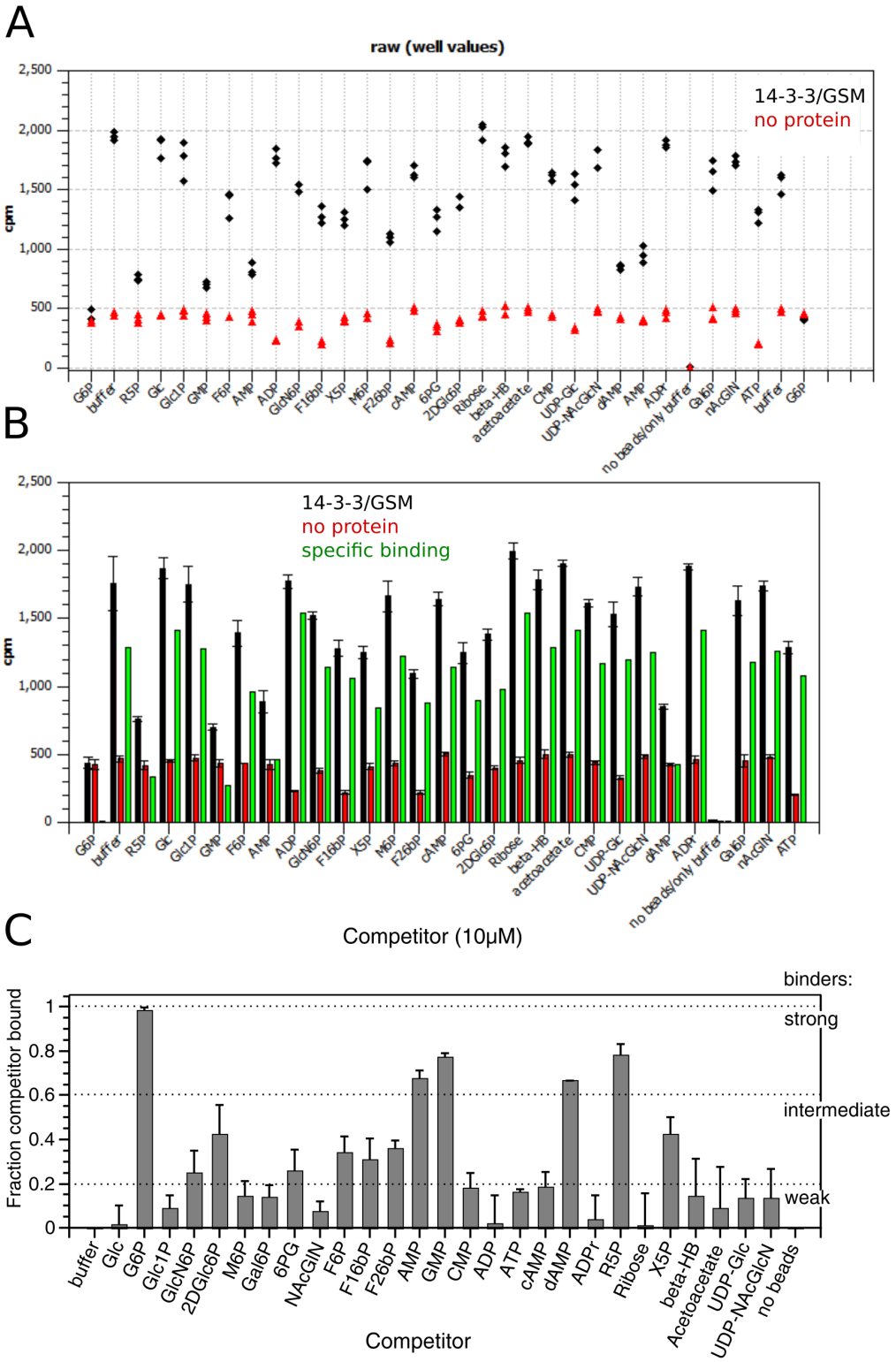

Figure 4.19: **Metabolite screen for ChREBP binding**

A: Graph showing the cpm of a representative plate. B: same experiment as in A, mean values and specific binding for each competitor. Error bars are S.D. of 3 tech. replicates (3 wells per plate). C: Normalized ^{3}H-Glc6P binding after addition of competing metabolites. Error bars show S.D. of 2-4 replicates for each metabolite with 3 technical replicates per plate. For abbreviations see list of metabolites (Table 3.10)

4.5.4 ITC experiments with different metabolites confirm findings of SPA

To verify our results obtained by SPA, some metabolites were also tested for binding by ITC (Figure 4.20) and the results are in line with the findings by SPA. Comparing the two assay approaches it has to be kept in mind that for SPA the metabolites are incubated for a long time with the target protein, allowing the binding and measuring of ligands with a low K_{on}. In addition, both binding assays are performed in different buffers, which could have an effect on binding. The K_D and binding parameters of metabolites showing a dose-response are shown in Table 4.4. Due to the standardized ITC conditions for each metabolite, ΔH and N hast to be taken with caution.

Ligand	K_D(µM)	N (sites)	ΔH (kcal/-mol)	ΔG (kcal/-mol)	-ΔS (kcal/-mol)
GMP	4.71	0.59	-10.7	-7.27	3.41
F2,6bP	7.39	0.99	-2.88	-7	-4.12
AMP	3.83	0.4	-12.5	-7.39	5.15
2DG6P	0.03	0.76	-2.1	-10.3	-8.23
GlcN6P	564	2.7E-03	-80	-4.43	75.6
Glc6P	3.11	0.25	-34	-7.51	26.5
R5P	1.20	0.48	-13.4	-8.08	5.36

Table 4.4: ITC Results for ligands that show binding

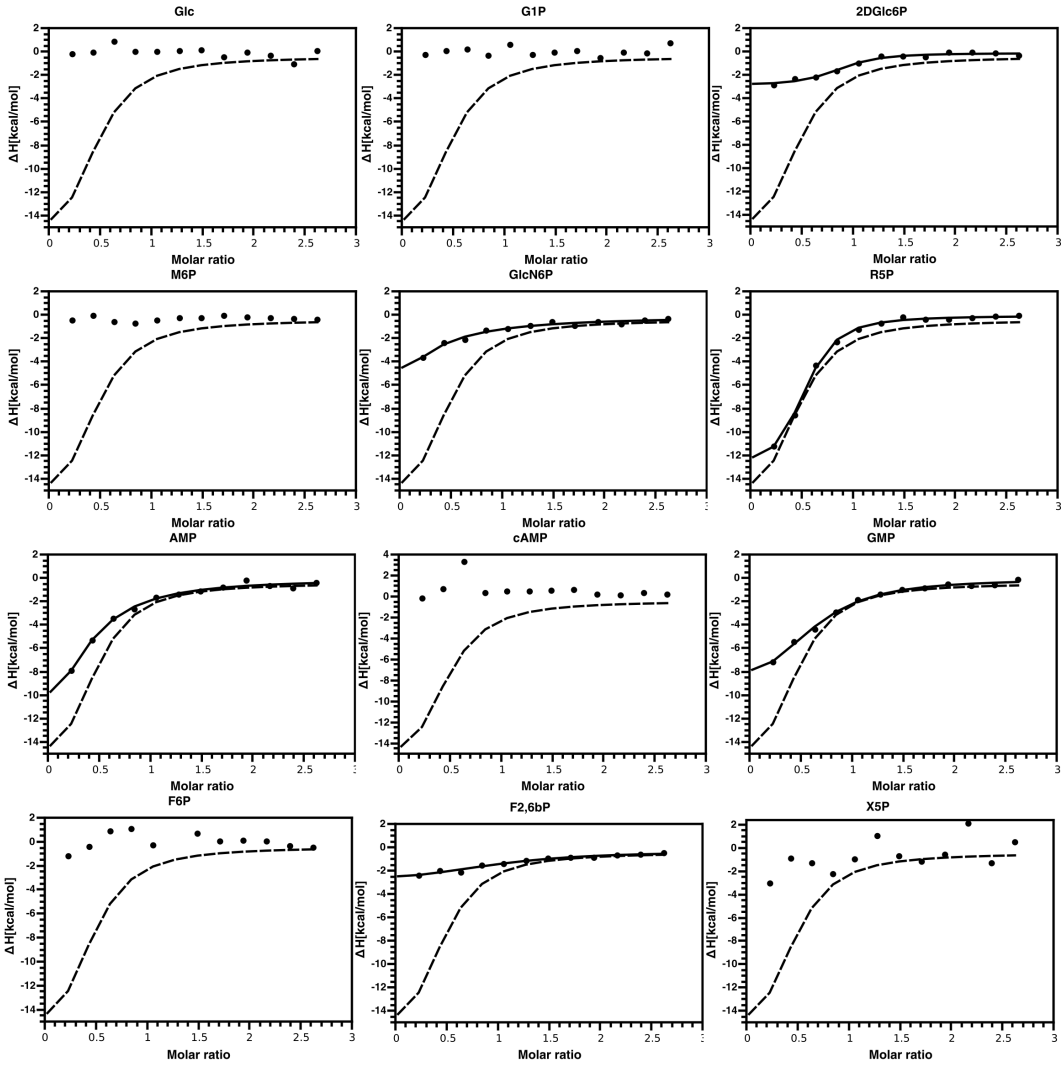

Figure 4.20: **ITC of 14-3-3/GSM and metabolites identified in SPA**
ITC experiment of different metabolites for 14-3-3/GSM binding. Cell loaded with 22 µM protein complex, syringe contained 300 µM of ligand. Dashed line represents binding of Glc6P.

4.5.5 Chemical space of ligands

Based on the results for metabolite binding by SPA and ITC, the chemical space of the ligands was analyzed in more detail to determine which groups and features might play a role in binding to the protein. Figure 4.21 shows the structure of all tested metabolites. Different regions (R) of glucose and ribose metabolites could be characterized for their importance in binding (Figure 4.22).

For Glc derived metabolites the most important region is R1. In order for Glc to bind, a phospho group has to be attached to C6. If this phospho-group is at R2, no binding can be observed (as for Glc1P). R3 allows some flexibility. The absence of the hydroxy-group does not abolish binding (2DGlc6P), also it can be replaced by an amine group (GlcN6P). However the highest affinity is observed with a hydroxy-group present. Interestingly, also the orientation of this group seems to be of sterical importance since mannose-6-phosphate failed to bind. The same was observed for the hydroxy-group in region 4, where Gal6P failed to bind.

For ribose derived metabolites it is also the phospho-group in region 1 which is the most important feature, since ribose itself and ADP failed to bind. R2 describes the base position for AMP or GMP. Strongest binding was observed in absence of any base (R5P), however the purines adenine and guanine are tolerated, with only a slight reduction in affinity. The pyrimidine cytosine failed to bind, most likely because of sterical hindrance at the binding site. The hydroxy-group at region R3 seems not to be involved in binding since dAMP and AMP bound with the same affinity.

The high throughput format of the SPA assay will allow to further characterize these regions in a robust, fast and economic fashion.

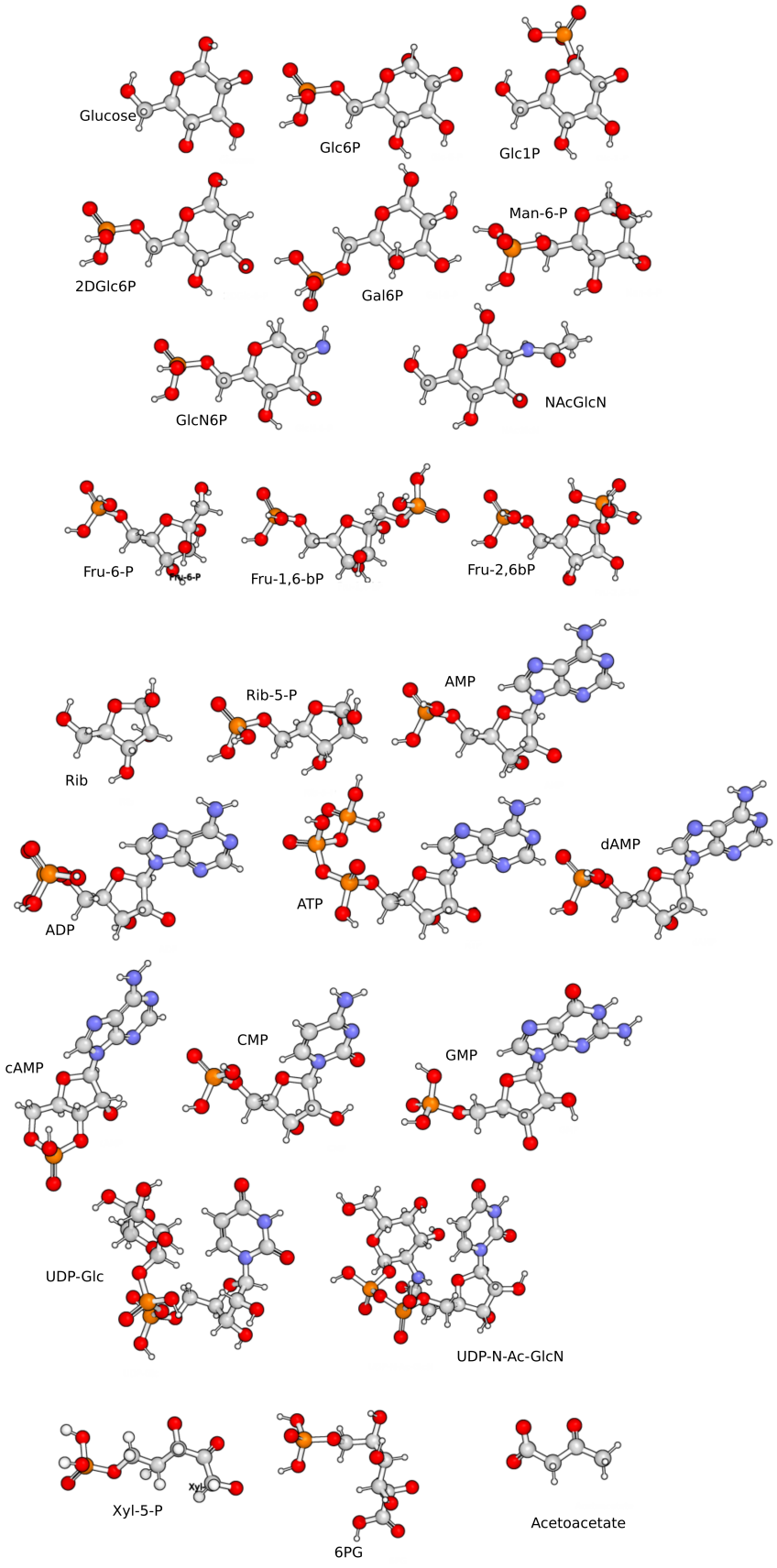

Figure 4.21: **Structure of tested metabolites in SPA and ITC**

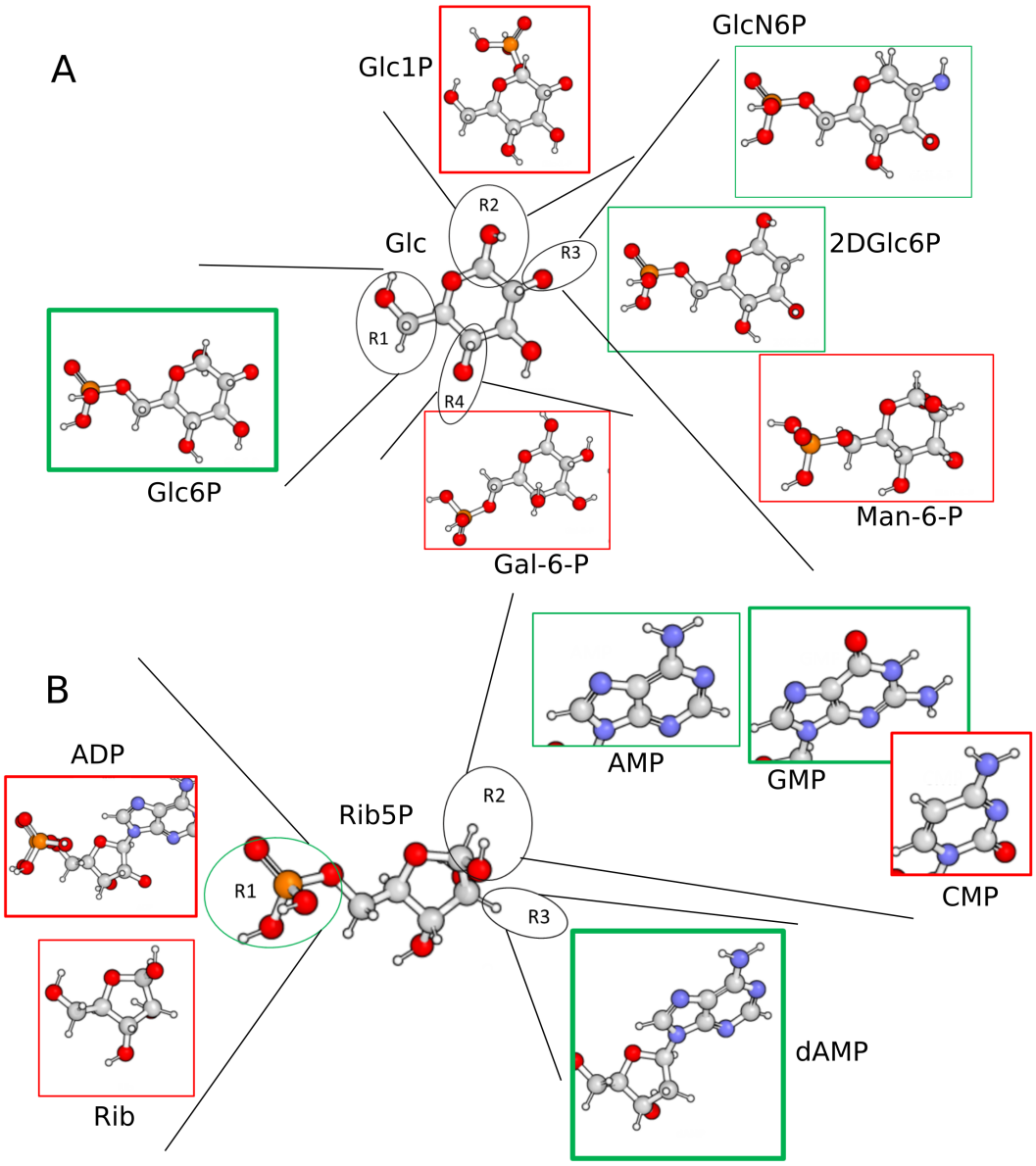

Figure 4.22: **Critical functional-groups and positions for binding**
A: Analysis of Glc derivatives B: Analysis of ribose based ligands. Green box indicates metabolites that can bind 14-3-3/GSM, red box indicates no binding. Stroke thickness is indication for affinity.

4.6 Binding of Glc6P causes distinct structural changes

Binding and competition studies, as well as mutation of the described AMP binding site, indicate that AMP and Glc6P compete for an overlapping region in the 14-3-3/GSM complex. This raises the important question which physiological role the binding of these metabolites play. AMP levels are high under starvation and were shown to inactivate ChREBP, however Glc and Glc6P are high under conditions where the cell is well fed and ChREBP is active. If ChREBP is regulated by these metabolites and they are binding to the same site, the difference in the physiological outcome could be explained by distinct changes in protein and/or complex conformations that are dependent on the bound ligand. This change in conformation would in this way result in a different physiological outcome.

To test this hypothesis and measure any differences between AMP and Glc6P biding on the level of protein structure, we employed a variety of methods, elucidated in this chapter.

4.6.1 Limited proteolysis to detect structural changes

Site specific proteases could be a useful tool to test for structural changes. If such changes occur, these could possibly reveal or hide cleavage sites, altering the digestion pattern by proteases.

Trypsin and chymotrypsin are sensitive for ligand induces structural changes

To find suitable site-specific proteases, a variety were tested at different concentrations. 14-3-3/GSM complex was incubated with and without Glc6P and protease was added. After 30 min incubation on ice the reaction was stopped and samples were analyzed by SDS-PAGE (see Figure 4.23). For most proteases no difference in digestion pattern was observed. However chymotrypsin (cuts at Trp, Tyr, Phe) and trypsin (cuts at Arg, Lys) showed a distinct digestion pattern for samples containing Glc6P compared to control samples. The experiments also showed that the GSM is quickly digested compared to 14-3-3 and other proteins which are not part of this thesis. This speaks for a more open, not very compact conformation. Based on this experiment, trypsin and chymotrypsin

were also used to test for distinct digestion patterns in presence of AMP and other potential metabolites.

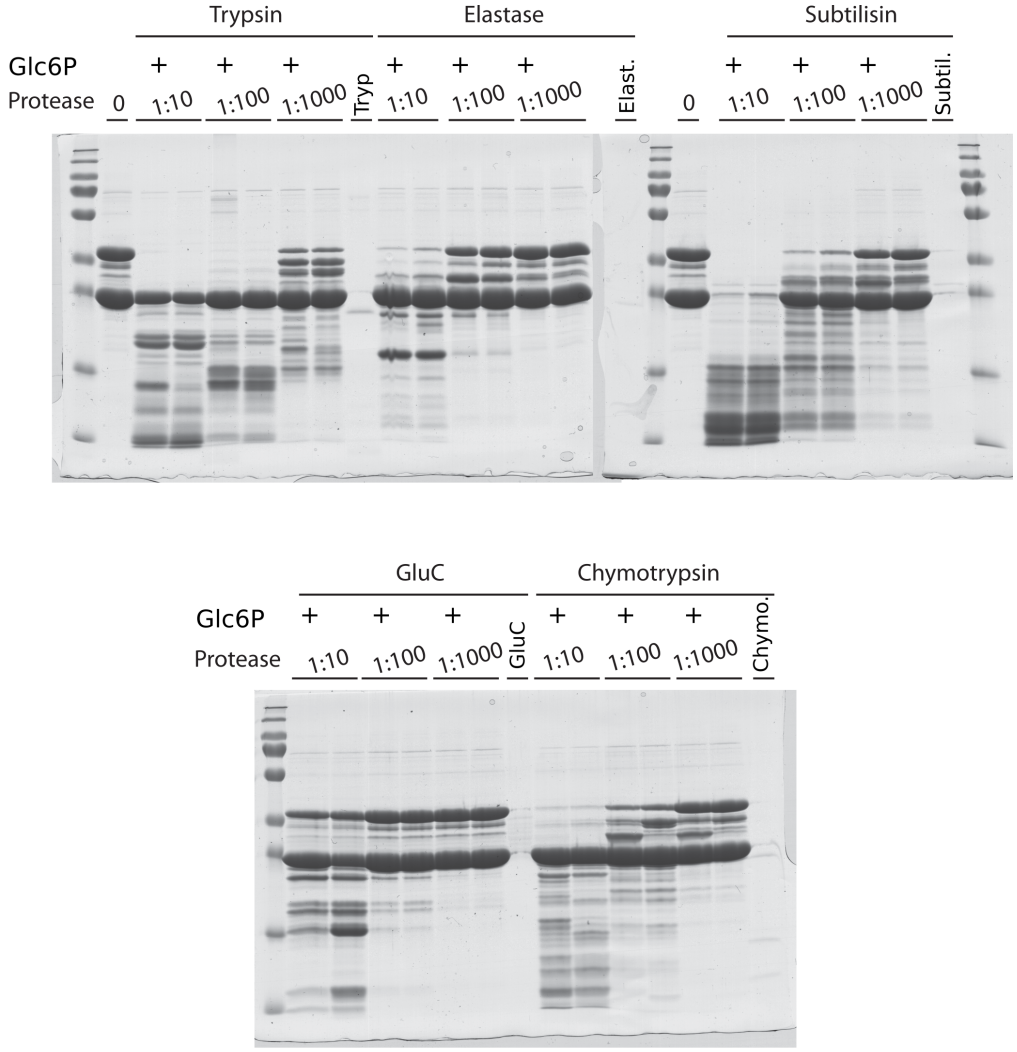

Figure 4.23: **Testing of different proteases for limited proteolysis**
Limited proteolysis of 14-3-3/GSM complex by a variety of proteases show for trypsin and chymotrypsin a distinct digestion pattern in presence of Glc6P, compared to non-ligand bound complex.

Titration of Glc6P and competition with AMP

To make sure the observed digestion pattern depends on Glc6P, a dilution series was generated and complex was added. After preincubation chymotrypsin was added. As described previously the digestion was analyzed on SDS-PAGE, showing a Glc6P dependence for the appearance and disappearance of specific

bands (marked with a red asterisk in Figure 4.24A). Since it was shown by ITC experiments (in Section 4.3.1) that AMP negatively influences the binding for Glc6P, we tested whether an increasing concentration of AMP would outcompete Glc6P. Resulting in a digestion pattern similar to the only AMP bound state. Although final AMP concentrations were 25times higher than Glc6P, the distinct fragment for Glc6P did not completely disappear. However its intensity slightly decreased (Figure 4.24B). Since limited proteolysis is a very dynamic assay, having a mixture of different peptide fragments and complexes (some might be able to bind only a specific metabolite) makes it difficult to interpret such competition assays.

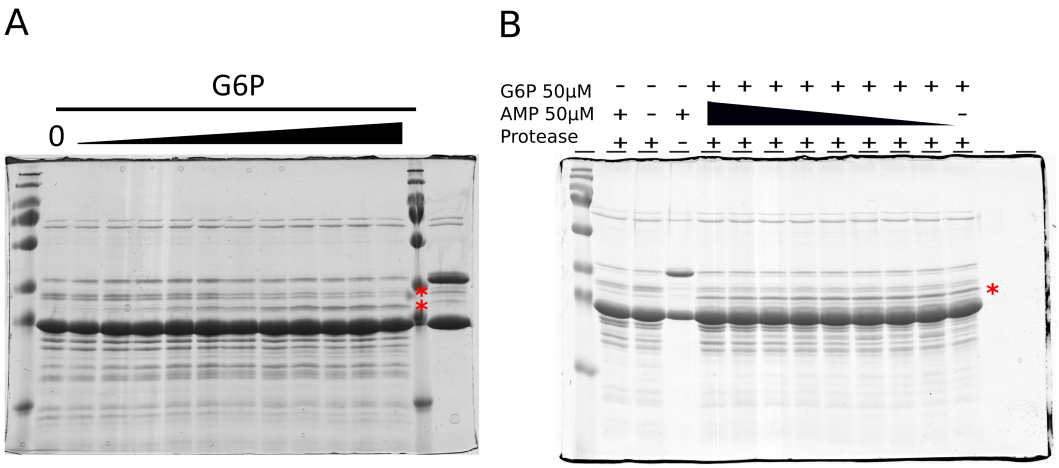

Figure 4.24: **Metabolite titrations for limited proteolysis**
A: The distinct digestion pattern for Glc6P is dependent on the concentration of Glc6P. Titration curve of Glc6P from 0 mM to 1.7 mM. B: SDS-PAGE of LiP using chymotrypsin and a constant concentration of Glc6P. AMP was added as a competitor in a range from 1.25 mM to 10 µM. Asterisks indicate protein fragments that are specific to the presence of Glc6P.

Tryptophan 127 mutant shows no specific digestion pattern in presence of Glc6P

One possibility for the stabilization of distinct bands is the protection of cleavage sites by the ligand itself. ITC experiments (Figure 4.13) showed that the W127A mutation in the GSM causes a Glc6P binding-deficiency. If this tryptophan is protected by Glc6P binding from chymotrypsin in the *wt*, the mutation of W127 to alanine should have the same effect on proteolysis as Glc6P binding (explained in Figure 4.25B). However, only *wt* in presence of Glc6P showed the distinct fragment (Figure 4.25A), excluding W127 as the relevant cleavage site.

This assay showed two additional important results. First, the digestion pattern is not caused by effects of Glc6P to chymotrypsin (e.g. altering activity). Second, the similarity between the digestions of W127A and *wt* in absence of Glc6P shows, that the mutant is most likely properly folded.

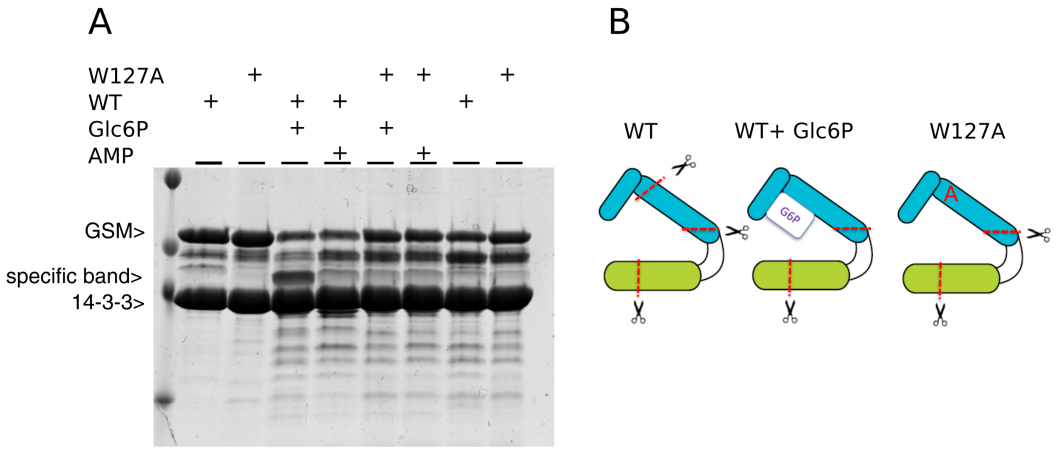

Figure 4.25: **LiP of W127A**
A: LiP of *wt* and W127A mutant with chymotrypsin in presence of AMP and Glc6P shows W127 is no chymotrypsin cleavage site. B: Schematic representation of the assay idea: Binding of Glc6P or mutation of W127 might block a chymotrypsin cleavage site (scissors), which is needed to generate the specific, Glc6P dependent, peptide.

Conformational changes are specific to Glc6P

To confirm the specificity of the limited proteolysis assay and also to better characterize binding of different metabolites and their potential influence on 14-3-3/GSM conformation, a series of metabolites were preincubated with the complex followed by proteolytic digest. Interestingly, it was possible to distinguish the 14-3-3/GSM digestion pattern in presence of Glc6P from those of other metabolites. Even though, the complex is able to bind those metabolites (such as GMP and R5P). This is the case for both tested proteases trypsin and chymotrypsin (Figure 4.26A and B), indicating that structural changes caused by Glc6P are specific to Glc6P and not to the binding event itself (Figure 4.26). Metabolites that are structurally very similar to Glc6P and were indicated as weak binders by the SPA (2DG6P, GlcN6P), show a digestion pattern that is a mixture between non-binders and Glc6P. However this effect is not very strong.

To analyze the fragment that is stabilized by Glc6P binding in the chymotrypsin digest (marked by asterisk in Figure 4.26B), the gel-band was cut out and ana-

lyzed by LC-MS/MS (Naga Nagaruna, MPI Martinsried). Comparing the peptide coverage to full-length GSM shows, that the C-terminal final ∼50aa are missing (Figure 4.26). These residues are part of the GRACE domain (from 198 to 297). Therefore it is intriguing to speculate, that upon Glc6P binding the GRACE domain becomes exposed (ChREBP is active) and therefore accessible to chymotrypsin in this assay.

Based on these experiments we can conclude that binding of Glc6P causes a distinct digestion pattern and therefore a distinct protein conformation when compared to AMP and other binders.

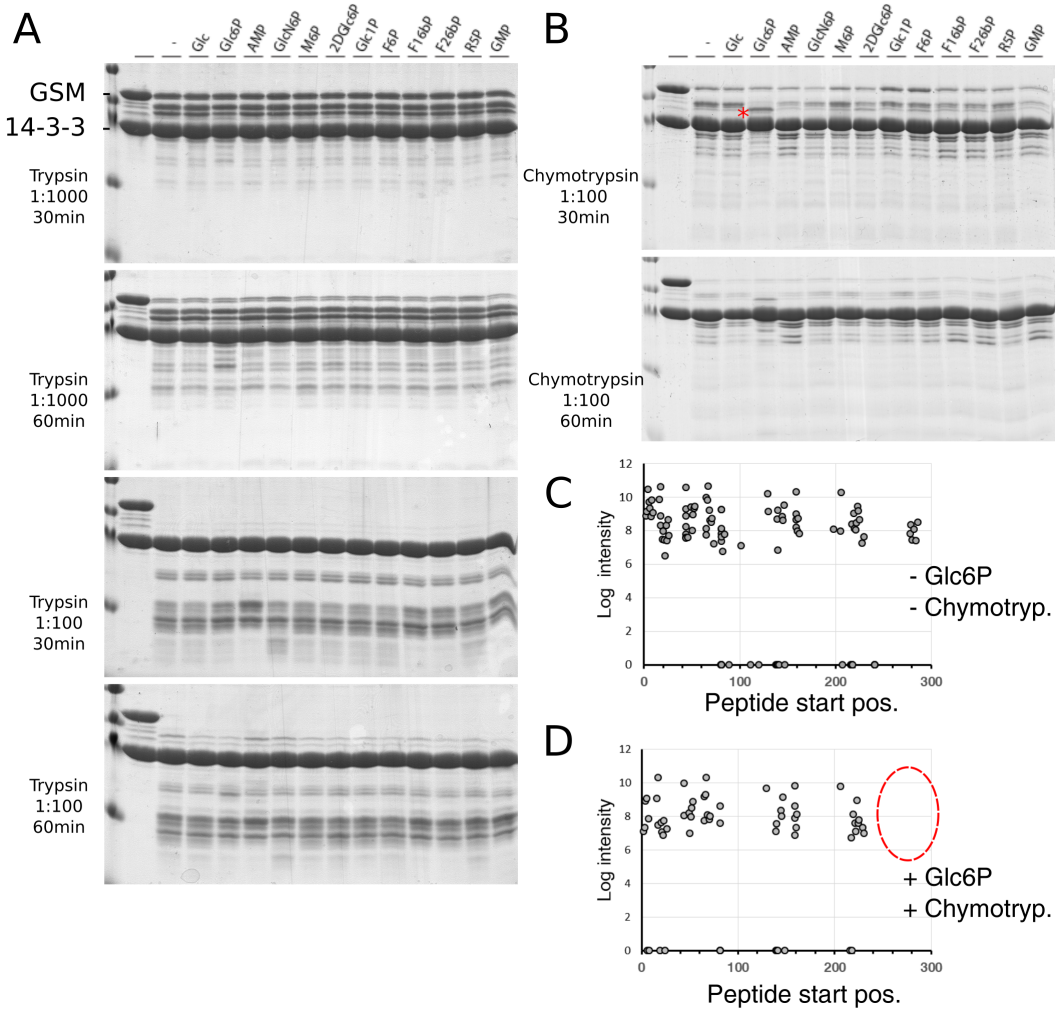

Figure 4.26: **Limited proteolysis of 14-3-3/GSM in presence of different metabolites** A: Trypsin digestion pattern of 14-3-3/GSM complex in presence of different metabolites. B: Digestion pattern of 14-3-3/GSM generated by chymotrypsin in presence of different metabolites. C: LC-MS/MS peptide coverage of full length GSM. D: LC-MS/MS peptide coverage of the band specific for Glc6P (marked with asterisk in B). No peptides could be detected in the last 50aa of the GRACE domain (red circle)

4.6.2 Secondary structure composition is not altered by Glc6P binding

Often the binding of a ligand to its target protein induces changes in the secondary structure. To test if this is the case for 14-3-3/GSM binding to Glc6P a circular dichroism experiment was performed and evaluated with Frits Kamp (DZNE, LMU Munich). These experiments showed that absence or presence of Glc6P does not have an effect on the secondary structure of the complex (Figure 4.27A). The measurements also revealed that the complex is 50% alpha-helical under the assumption of a 1:1 complex. For a 1:2 complex it would be 47%.

Based on the crystal structure 5wfx of 14-3-3, 173 of 246aa are helical (Figure 4.27C). Since only limited information about the secondary structure of the GSM is available, the structure was predicted using PSIPRED. For the GSM only 49 of 291aa are alpha-helical (Figure 4.27B). The only possibility to obtain a complex with around 50% alpha-helical residues is by having a 14-3-3dimer bound to one GSM (Table 4.5). These findings are in line with previous results discussed in Section 4.2 about the composition of the complex.

Complex	%α -helical Experimental	%α -helical Theoretical
14-3-3mono/GSM	50	41
14-3-3dimer/GSM	47	50

Table 4.5: Result table CD-spectroscopy

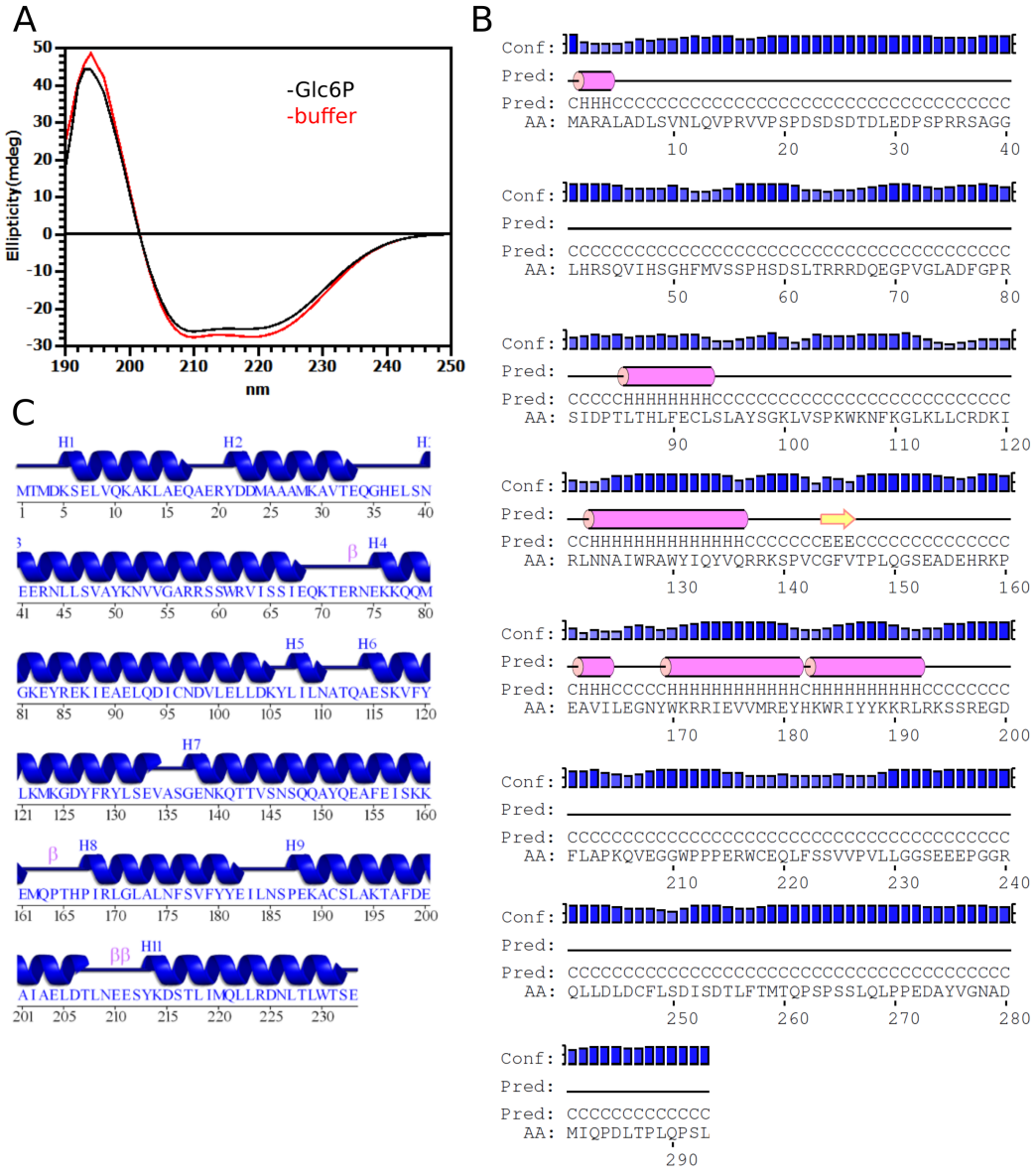

Figure 4.27: **CD-spectra of 14-3-3/GSM**

A: CD-spectra of 14-3-3/GSM with and without Glc6P show no change in secondary structure composition. B: Secondary structure prediction of the ChREBP-GSM region, using psipred-server. Blue columns indicate confidence of prediction. Pink columns represent alpha-helical regions. Yellow arrows beta-sheets. C: Representation of the 14-3-3 secondary structure derived from the crystal structure 5wfx.

4.6.3 Binding of metabolites does not affect tryptophan fluorescence

Binding of ligands often causes a re-arrangement or change in flexibility for specific amino acids in proteins. Since some amino acids have a strong intrinsic fluorescence (for example tryptophan) binding of ligands can change the fluorescence properties of target-proteins in a ligand dependent manner. Because at least one tryptophan (W127) is important for metabolite binding it was intriguing to test for intrinsic fluorescence in presence of different ligand concentrations. A dilution series of AMP and Glc6P was generated (1:2) ranging from 5 mM to 40 nM and a constant concentration of protein was added. The protein-ligand solution was excited at 280 nm and the emission was measured in a range from 300 nm to 450 nm (Figure 4.28A and B). On a first look, it seems that with increasing concentrations of AMP the emission is reduced. Where for Glc6P the signal stayed constant (Figure 4.28D). Interestingly, after preincubating 14-3-3/GSM with a fixed concentration of AMP (312.50 µM, black graph in Figure 4.28B) the signal can be brought back to normal by adding increasing amounts of Glc6P (Figure 4.28C and D). This would speak for a competition of Glc6P and AMP. To test if the reduction in fluorescence by increasing concentrations of AMP is really an effect of binding, the protein-complex was denatured (by SDS or incubation at 95°C) and the AMP binding experiments were repeated. As expected, the fluorescence signal increased compared to non-denatured protein. However, also in this case increasing amounts of AMP were able to reduce the fluorescence signal. Therefore It has to be assumed that AMP itself is quenching the fluorescence signal from proteins. Although this effect is only seen at very high concentrations it makes it difficult to interpret the results for the AMP – Glc6P titrations and competition experiments. Therefore it was decided to not use this assay for future binding experiments.

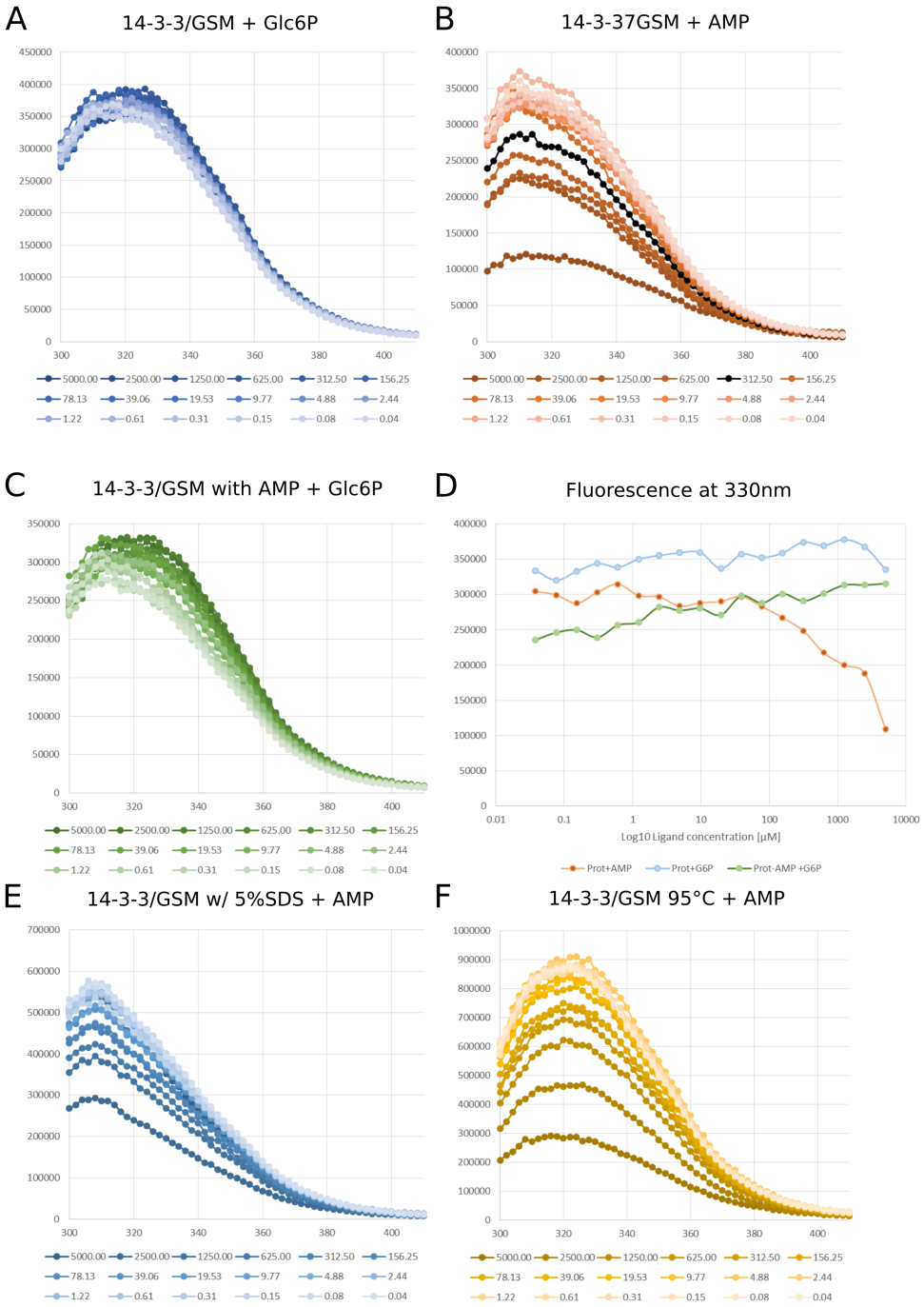

Figure 4.28: **Effect of ligand binding on intrinsic fluorescence**
Emission spectra of 14-3-3/GSM in presence of different metabolite(s)/ concentrations. Concentrations are shown in µM, fluorescence in AU. A: An increase of Glc6P concentration does not affect intrinsic fluorescence. B: High concentrations of AMP reduce the fluorescence signal. Black graph indicates concentration used for competition experiment in C. C: Competition of AMP (312.5 µM) with increasing concentrations of Glc6P. D: Fluorescence intensities at a fixed wavelength of 330 nm in dependence of ligand concentration (data from graphs A, B and C). E: Fluorescence intensities for protein denatured by 5% SDS. F: Fluorescence intensities for protein denatured by incubation at 95°C.

4.6.4 Hydrogen-Deuterium Exchange Mass Spectrometry

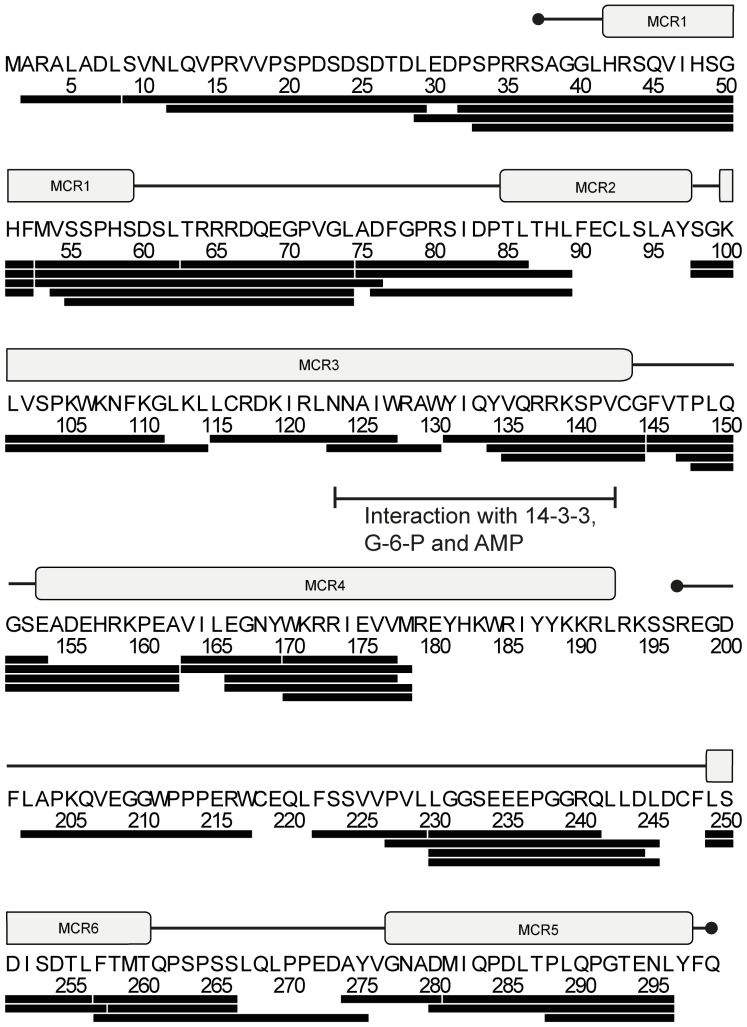

Figure 4.29: **Peptide coverage of the GSM oder HDX-MS conditions**
Black bars indicate detected peptides by LC-MS/MS of the GSM. Open bars indicate regions of the mondo conserved regions. Graph generated by Joana Veiga.

We showed that upon Glc6P binding the protein conformation differs from the unbound or AMP bound state. To define the structural changes, hydrogen-deuterium exchange mass-spectrometry (HDX-MS) was performed in collaboration with, and in the lab of Kasper Rand, University of Cophenhagen. The data was collected during two separate two week research stays in Copenhagen with the help of Joana Veiga. The data was then mainly analyzed and illustrated by

Joana Veiga and resulted in her Master-thesis [Veiga, 2019]. Since the findings are crucial for the overall understanding of ligand binding on ChREBP, they will be included in this thesis.

First, a peptide coverage map was generated. For this the 14-3-3/GSM complex was digested by pepsin and peptides were analyzed by LC-MS/MS under identical conditions as later for the labeled proteins in presence of metabolites. As shown in Figure 4.29, for most of the GSM one or more peptides could be detected. Regions no peptides were found are from amino acid positions 90-97, 179-201, 218-221, 246-248. The region of the detected peptides, also in context to the mondo conserved regions (MCR) is visualized in Figure Figure 4.29. In total 87% of the GSM sequence are covered. Next we wanted to investigate at which rate different regions/peptides exchange hydrogen with deuterium isotopes from the buffer solution in presence and absence of ligands. To do so, 14-3-3/GSM was incubated together with AMP or Glc6P or buffer only. After preincubation with ligand, labeling buffer was added containing deuterated water. The protein-ligand complex was then incubated for various timepoints. To stop labeling, ice cold quenching buffer was added and the sample was frozen at -80°C for analysis at a later timepoint by LC-MS.

Binding of AMP compared to control

First, the known 14-3-3/GSM ligand AMP was analyzed and compared to the control dataset (no ligand). We observed a significant difference for the peptide 115-127 as illustrated in Figure 4.30. This region showed a reduction in deuterium uptake. Interestingly, Sato and colleagues [Sato et al., 2016] described the same region interacting with AMP and 14-3-3. Therefore it can be assumed, that binding of AMP to the 14-3-3/GSM interface directly protects residues in uptake of deuterium compared to control. In addition, the peptide of the same region (123-130) shows potential Ex1 kinetics. The significant changes in deuterium uptake of this region is in support of published data by Sato *et al.* [Sato et al., 2016], as well as our own findings by *in vitro* mutation studies of this region, showing impaired binding of AMP (W127A, 4.4.2). Figure 4.30C shows the location of identified peptides in respect to their localization, deuterium exchange and conservation[3] of the amino acid conservation across organism. Showing that the significant peptides are highly conserved.

[3] using the ConSurf-server, standard settings

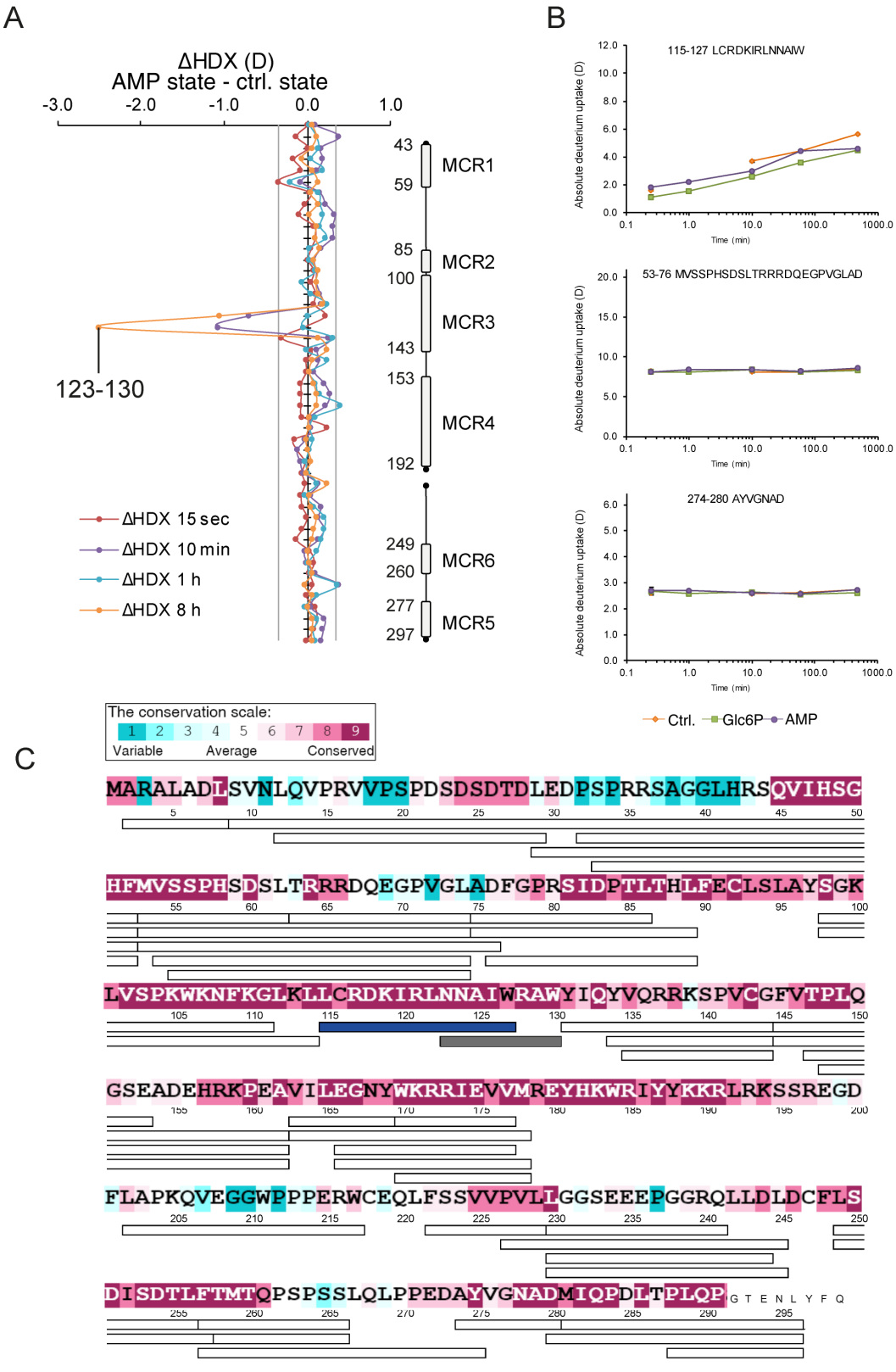

Figure 4.30: **Deuterium uptake in presence of AMP compared to control**
A: Butterfly plot comparing AMP bound state with control state in deuterium uptake. B: Example peptides and their absolute deuterium uptake shows a difference for peptide 115-127 (top panel). C: Overview of detected peptides (bars underneath sequence). Blue solid bars represent reduced deuterium uptake, compared to control. Grey solid bars represent peptides with potential Ex1 kinetics. Coloring of amino acid sequence reflects conservation across species. Figure was generated by Joana Veiga, modified by Thomas Pysik.

Binding of Glc6P compared to control

Since limited proteolysis indicated different conformations between Glc6P and AMP or the ligand free state, it was tested if this difference also can be detected by HDX-MS. As for AMP binding, a time course of deuterium uptake in presence of Glc6P was generated and compared to the control dataset (see Figure 4.31). Again, the region showing the strongest effect is 115-127, and Ex1 kinetics from 123-130 as seen for AMP binding. Interestingly, Glc6P binding significantly inhibited the deuterium uptake in additional regions: 9-52 (includes MCR1) and 98-114 (part of MCR3). Additional regions were detected that showed an increase in deuterium uptake (exposed to solvent): 163-178 (in MCR4 and part of the NLS) and 249-256 (MCR6, located in the GRACE domain). Since mutation studies showed, that Glc6P binding is lost or at least reduced for mutations in the 14-3-3/GSM interface (see Section 4.4.2) it can be assumed that the reduction in uptake of the region 115-127, as for AMP, can be explained by binding of Glc6P to this region. Interestingly, mutations in this region showed a reduced/inhibited response to Glc in *in vivo* experiments [Davies et al., 2008]. Compared to AMP, Glc6P binding causes additional structural changes in MCR3, and the N-terminal region of the GSM, involving the MCR1. The Exposure of the region 163-178, which is part of the NLS could explain binding of Importin and the increase in nuclear localization upon high Glc levels. This hypothesis is tested in chapter Section 4.7.1. MCR6 was described by McFerrin and colleagues [McFerrin and Atchley, 2012] as a potential Glc6P binding site based on sequence similarities. However, the fact that this region is exposed upon presence of Glc6P and ITC experiments with GSM fragments not containing this region that were still able to bind Glc6P (Section 4.1.1, and data by Nina Heppner [Heppner, 2016]) speaks against this hypothesis. Since MCR6 is located in the GRACE domain its conservation could be explained by interaction with other activator proteins in presence of Glc6P. Figure 4.30C shows the location of identified peptides in respect to their localization, deuterium exchange and conservation of the amino acid conservation across organism.

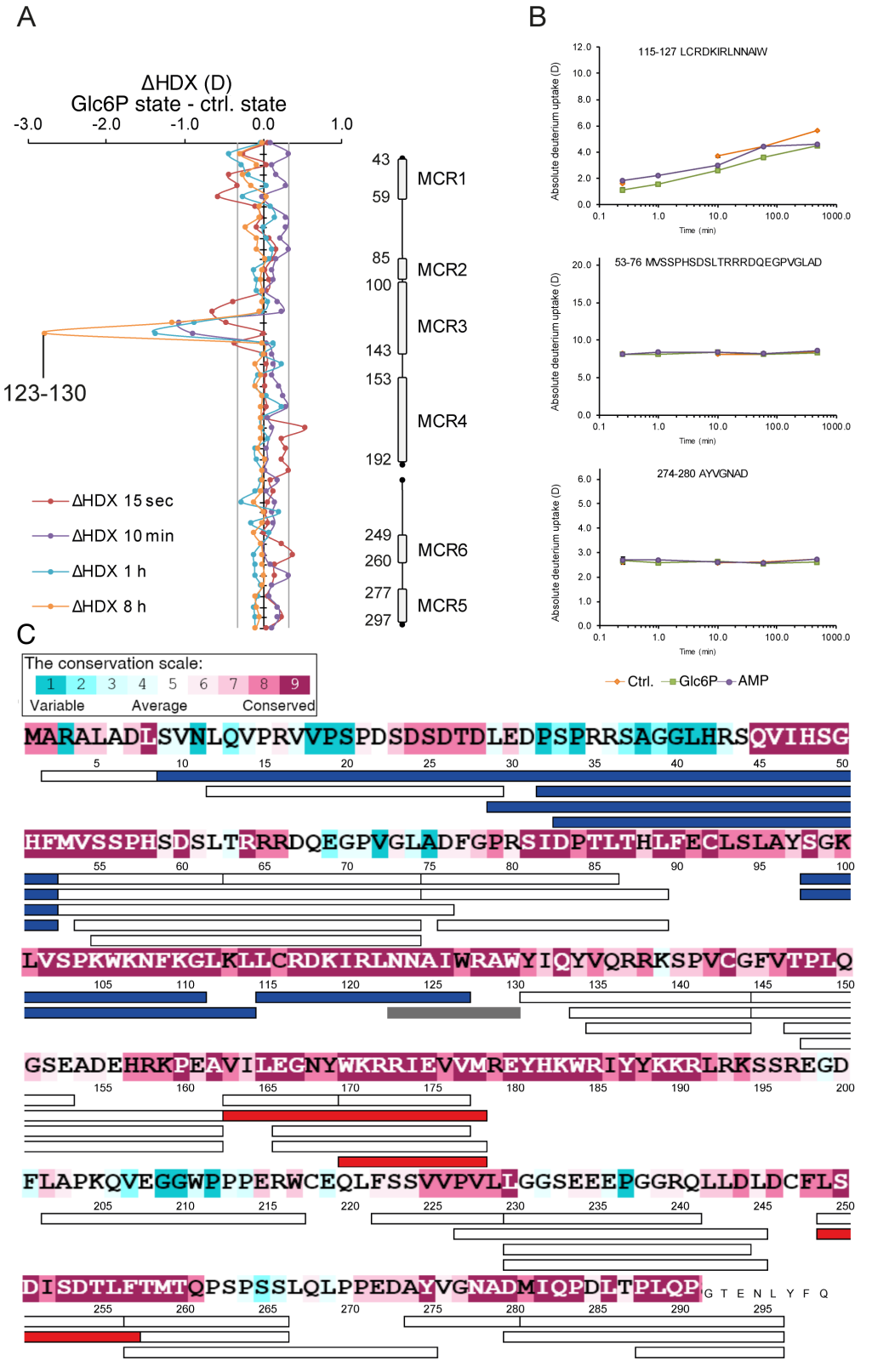

Figure 4.31: **Deuterium uptake in presence of Glc6P compared to control**
A: Butterfly plot comparing Glc6P bound state with control state in deuterium uptake. B: Example peptides and their absolute deuterium uptake shows a difference for peptide 115-127 (top panel). C: Overview of detected peptides (bars underneath sequence). Blue solid bars represent reduced deuterium uptake, compared to control. Grey solid bars represent peptides with potential Ex1 kinetics. Red solid bars represent peptides with increased deuterium uptake. Coloring of amino acid sequence reflects conservation across species. Figure was generated by Joana Veiga, modified by Thomas Pysik.

Sequence Start	Sequence End	ΔHDX Glc6P vs. Ctrl.	ΔHDX AMP vs. Ctrl.
1	29		
30	52	-	
53	89		
98	114	-	
115	127	- -	- -
123	130	- - -	- - -
131	169		
170	178	+	
179	201	/	/
202	245		
249	256	+	
257	295		

Table 4.6: Summary HDX experiments in presence of Glc6P and AMP.
- reduction in uptake, + increase in uptake compared to control. / no coverage. Modified from Joana Veiga

4.7 Potential protein interactions of the 14-3-3/GSM complex

4.7.1 Binding of Importin-α in dependence of Glc6P

An Importin binding site was characterized by Ge *et al.* in the region between 158-175 [Ge et al., 2011], in this thesis we showed by HDX (see Section 4.6.4) that this region becomes exposed by Glc6P binding to 14-3-3/GSM. Although Ge and colleagues did not specify the isoform of Importin-α binding to ChREBP, it can be assumed that the Importin-α1 was tested in their work. We decided to clone, express and purify Importin-α1. To test for interaction we performed an analytical size exclusion chromatography in presence of 1 mM Glc6P. As shown in Figure 4.32A, Importin-α1 does not bind to 14-3-3/GSM under these conditions. To exclude the possibility of Importin replacing the 14-3-3 dimer, resulting in a complex of similar size fractions were analyzed by SDS-PAGE (Figure 4.32B).

Importins contain an N-terminal IBB domain, which is interacting with Importin-β or, if not bound to the NLS of a target protein, is folding back into the substrate binding site of Importin-α. Since in the *in vitro* system used, no Importin-β is present, the IBB domain could be in direct competition with the NLS of

ChREBP. To exclude this possibility Δ70 Importin-α1 was purified, lacking the IBB domain. However, also in this case no interaction was observed (Figure 4.32C and D). Although our assay did not show an interaction with Importin, it can not be excluded that this is due to wrong buffer conditions or the interaction is too transient or weak to detect by size exclusion chromatography.

During the time the work for this thesis was conducted, the Importin-α1 crystal structure bound to the ChREBP-NLS peptide was published (PDB:6MJL). Therefore it has to be assumed that Importin indeed interacts with the ChREBP-NLS, if this interaction is regulated by Glc6P or other mechanism such as post-translational modifications is not known.

4.7.2 E.coli Glms contaminant or relevant interaction partner?

During purifications of 14-3-3/GSM we observed a contamination band on SDS-PAGE. The band was isolated and the protein identified as Glutamine-fructose-6-phosphate aminotransferase (Glms) by MS/MS. Since Glms, as well as its human homologue Gfat1, is involved in sugar metabolism the question was raised whether the co-purification of Glms from *E. coli* together with our target protein is a coincidence, or if it could be an interaction of physiological relevance.
In addition, due to the substrate and product similarity of Glms to Glc6P (Figure 4.33B) we had to control whether the binding signal for Glc6P in ITC and SPA could also come from a weak contamination of Glms in these assays. Glms was cloned, expressed and purified using the same buffers as for 14-3-3/GSM. Purified Glms was mixed with 14-3-3/GSM and the size was determined by size exclusion chromatography. Again no interaction was observed (4.33A). Due to the fact that Glms has a similar size as the 14-3-3/GSM complex as well as a similar isoelectric point it is assumed that it is not a physiological relevant protein-protein interaction and rather a contamination in the purification process. Additionally, Glms is also a known contaminant for Ni-NTA based purifications due to the presence of six surface histidines. To prevent such contaminations special engineered *E. coli* strains for protein expression were generated [Robichon et al., 2011].

To test whether Glms causes a false-positive binding signal in the binding assays ITC was performed using 30 µM pure Glms and 300 µM Glc6P or glucosamine-6-phosphate (GlcN6P), concentrations usually used for 14-3-3/GSM binding studies. As shown in Figure 4.33C no binding was observed for Glc6P and only a

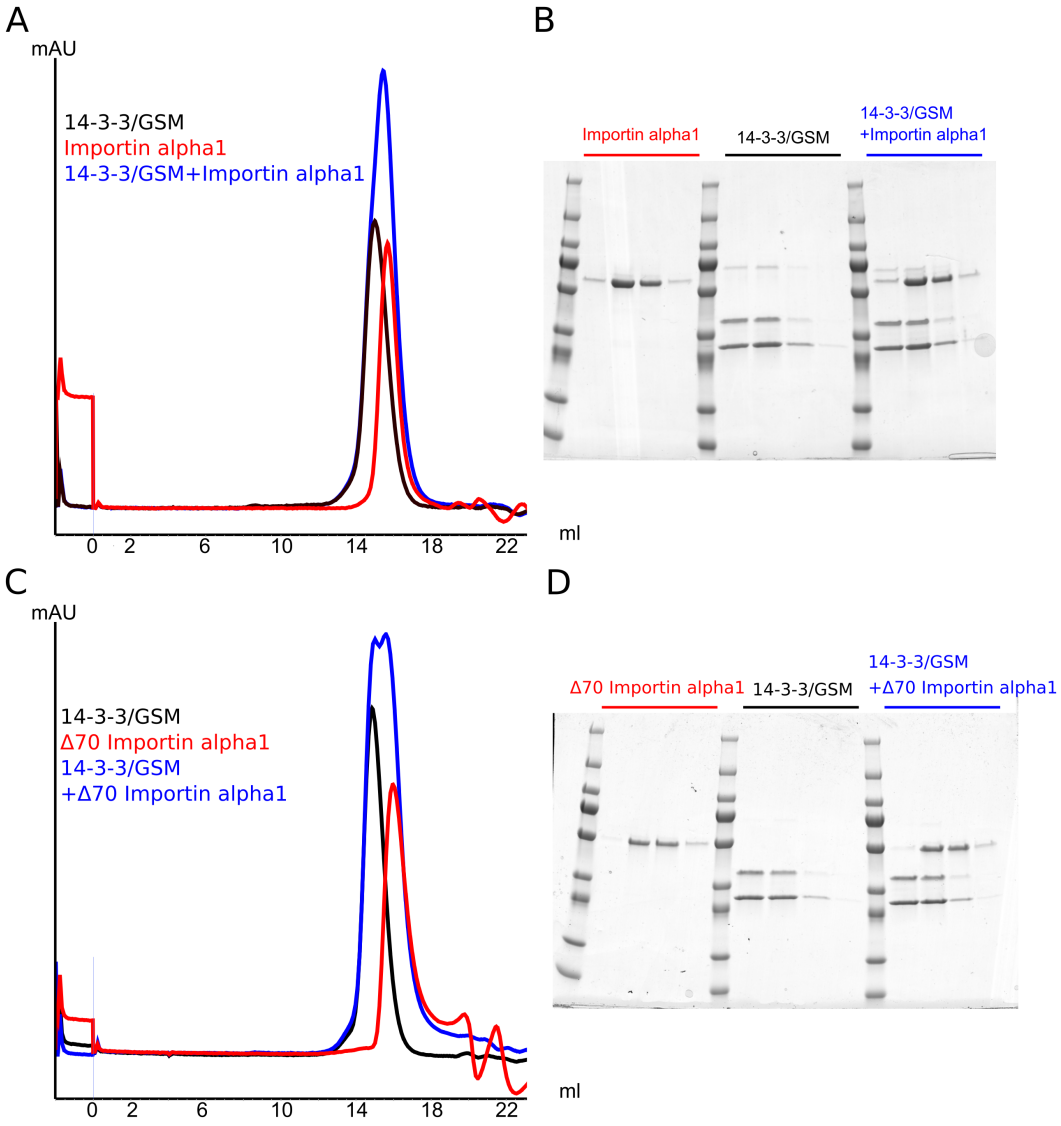

Figure 4.32: **Test for interaction between 14-3-3/GSM and Importin**
A: Size exclusion chromatography of 14-3-3/GSM (black), Importin-α1 (red) and a combination of both (blue) to test for Importin binding in presence of 1 mM Glc6P. B: SDS-PAGE of peak fractions from A. C: Analytical size exclusion, as performed in A, using an Importin-α1 IBB deletion (Δ70). D: Peak fractions of C.

very weak signal for GlcN6P. Due to the high concentration of Glms used in this assay, compared to Glms as a contaminant in 14-3-4/GSM samples, it can be concluded that the binding signals are true-positives and not caused by Glms. Describing 14-3-3/GSM as a sensor for intracellular Glc6P levels.

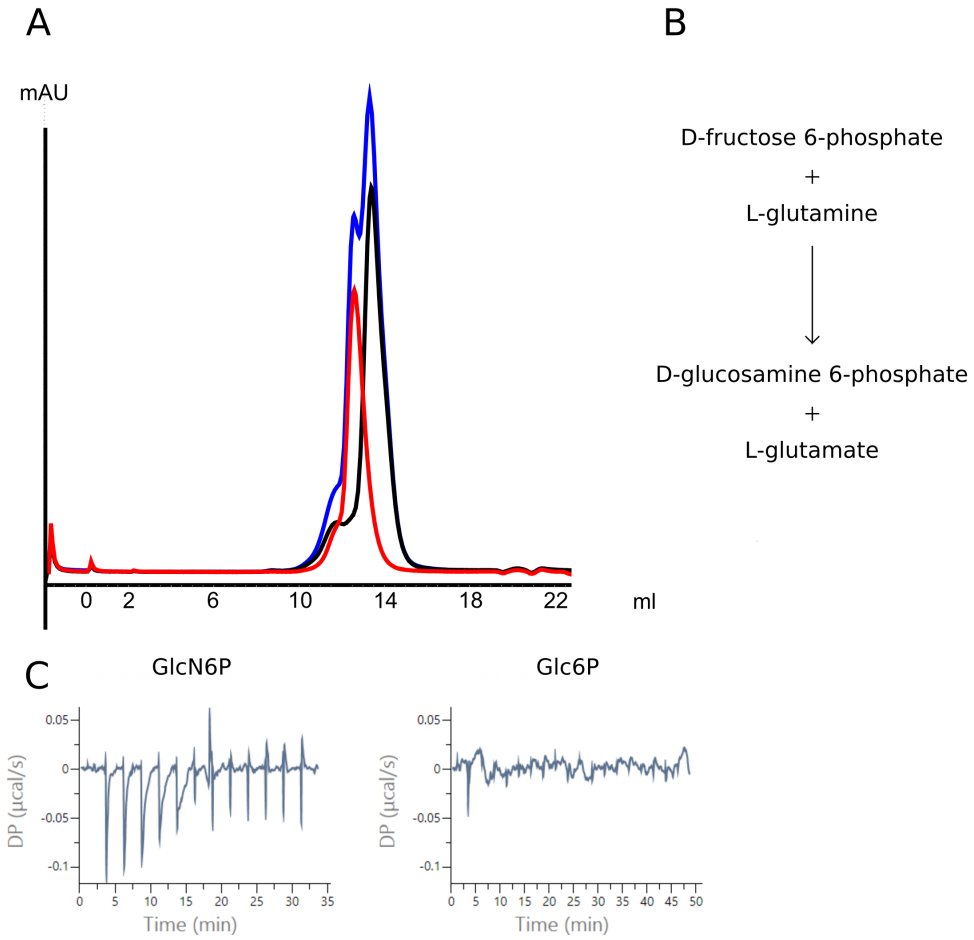

Figure 4.33: **Test for interaction of 14-3-3/GSM and Glms**
A: Size exclusion chromatography of 14-3-3/GSM (black), Glms (red) and a combination of both (blue), to test for Glms binding to 14-3-3/GSM. B: Enzymatic reaction catalyzed by Glms. C: ITC experiments of Glms with GlcN6P and Glc6P, to exclude false positive Glc6P binding of 14-3-3/GSM due to contamination with Glms.

5 Discussion

Already in 1992 Foufelle described the stimulatory effect of glucose on expression of lipogenic enzymes in white adipose tissue [Foufelle et al., 1992]. Already at this time a direct link between intracellular glucose-6-phosphate concentrations and mRNA levels of FAS and ACC were observed. However, the cause of the upregulation in expression was unknown. Three years later Shih and colleagues described the ChoRE motif as a regulatory element for glucose-responsive gene transcription [Shih et al., 1995]. It was until 2001 that ChREBP was discovered as the transcription factor binding to these motifs, regulating the expression of target genes in a glucose dependent manner [Yamashita et al., 2001]. Since then, the regulatory mechanisms acting on ChREBP are under investigation and debate. The most prominent mechanism is phospho-and dephosphorylation [Kabashima et al., 2003, Kawaguchi et al., 2001, Kawaguchi et al., 2002]. However, this model is questioned, since Tsatsos and others showed by mutation studies, as well as manipulation of phosphatase activities, ChREBP response to changing glucose level was still obtained [Li et al., 2006, Tsatsos and Towle, 2006]. Other post-translational modifications, such as acetylation and O-linked GlcNAcylation were described to regulate transactivity of ChREBP by affecting its turnover rate and affinity to target promotors [Bricambert et al., 2010, Guinez et al., 2011, Ido-Kitamura et al., 2012].

Over the last decade, the GSM evolved as an important domain for ChREBP activity. Several mutation studies showed the importance of multiple conserved regions in this module for response to glucose levels [Davies et al., 2010, Li et al., 2010, Li et al., 2006]. These studies also showed that the interaction with 14-3-3 is required for ChREBP activity under high glucose conditions [Li et al., 2008]. The mechanism how increasing glucose levels are affecting and sensed by the 14-3-3/GSM complex was the topic of this thesis. To interact with the environment, one of the most biological processes is to sense metabolites. Based on the current understanding in the field Wang and Lei described three criteria for biological sensors and receptors [Wang and Lei, 2018]:

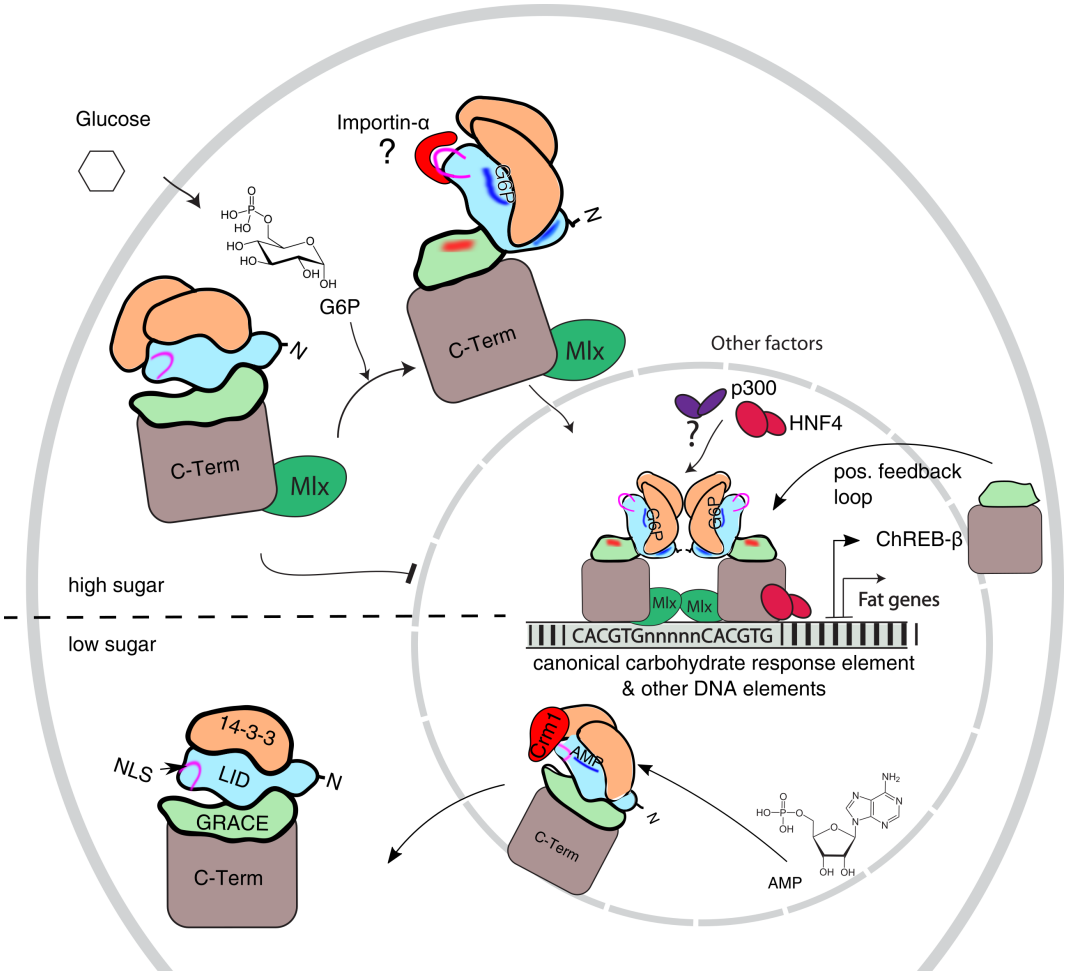

Figure 5.1: **Model of regulation of ChREBP activity by metabolite binding**
Under high glucose conditions Glc6P binds to the 14-3-3/ChREBP complex. Structural changes result in the exposure of the NLS (pink loop), as well as the GRACE domain (exposed peptides, as determined by HDX are indicated in red and pink). Binding of Importin to the NLS results in the nuclear import and subsequent binding to the ChoRE in the promotor region of target genes and ChREBP-β. ChREBP-β creates a positive feedback loop, further increasing expression of target genes. Under low glucose conditions, when AMP levels are high, AMP promotes the binding to 14-3-3 and reduces accessibility of the NLS, resulting in an Crm1 mediated export from the nucleus and retention in the cytoplasm. Blue loops indicate peptides with reduced deuterium uptake, red loops indicate increased deuterium uptake in HDX-MS.

Specificity: the sensor binds to the metabolite using a structurally recognizable domain. The binding of the sensor to the metabolite is highly specific to ensure accuracy.
Dynamicity: the binding of the sensor to the metabolite is reversible, meaning that the signal can be switched on and off. The dissociation constant of the binding is in the physiological range.
Functionality: In cells, the binding and dissociation of the metabolite modulate the activity/function of the sensor through modulating protein conformation or protein-protein interaction.

By testing a variety of structurally and biologically related metabolites to glucose-6-phosphate and AMP, we were able to demonstrate the specificity of the 14-3-3/GSM complex to Glc6P and its counterpart AMP. This was demonstrated using different biochemical and biophysical assays, such as ITC, MST and scintillation proximity assays. Mutation studies and existing crystal structures [Sato et al., 2016] pointed to the 14-3-3/GSM interface, mainly composed of the MCR3, as a critical region for metabolite binding. However, it has to be kept in mind that mutations in this region are also very critical for interactions between 14-3-3 and the GSM itself. The mutations shown in this thesis did not exhibit any different characteristics in expression, purification or elution volumes. Leading us to the conclusion that interaction between 14-3-3 and GSM is not, or only marginally affected. However, these mutants showed impaired binding to AMP and Glc6P, it has to be kept in mind the mutation of amino acids to alanine is, in most of the cases, a very drastic change. A high resolution structure in presence of Glc6P should be generated for the most in detail description of the binding-site. So far crystallization attempts for this thesis were not successful. In 2012 McFerrin [McFerrin and Atchley, 2012] suggested the newly described MCR6 as a potential binding site for Glc6P, based on bio-informatic analysis. However, in our tests fragments lacking this region were still able to bind Glc6P. This is in line with our mutation analysis of the MCR3, as well as HDX-MS. In which we had the strongest reduction in deuterium uptake for the MCR3 region in presence of ligand (AMP and Glc6P). Since HDX showed an exposure of MCR6 we think it might play a role in protein-protein interactions, which are not characterized to this timepoint.

For the dynamicity of 14-3-3/GSM we could demonstrate by competition experiments (ITC and SPA), that the binding event is reversible and therefore ChREBP can be turned on and off. To determine the physiological range of free

Glc6p is very difficult, since this can differ strongly between cell types and media conditions. However, it is well known that Glc6P levels increase significantly upon dosage of high glucose [Girard et al., 1997, Kang et al., 1996].

Second, hexokinases are allosteric inhibited by Glc6P itself (feedback-inhibition). Dependent on the isoform, the Ki for this inhibition is between 20 and 100 µM [Wilson, 2003]. Therefore, it has to be assumed the K_D for Glc6P of 2 µM (in an *in vitro* system) is within the physiological range. The competition with AMP for binding might be an important feedback mechanism for the regulation of ChREBP. Since Glc6P is in the center of many catabolic and anabolic pathways it has to be ascertained that Glc6P activates ChREBP and its lipogenic target genes in energy rich states only. For example, under starving conditions the glycogenolytic pathway is activated and glycogen broken down to Glc1P and transformed to Glc6P to enter glycolysis. To inhibit ChREBP, high levels of AMP might prevent the activation of ChREBP under these conditions, allowing the upregulation of ATP producing pathways. A prominent example for such regulatory mechanisms between two opposing metabolites is AMPK, which is regulated by the ratio between AMP/ATP. Sato *et al.* showed an 1.3 fold increase of free and total cellular AMP under low glucose conditions, when compared to high glucose conditions (free AMP 5.6µM, total AMP 157µM under low glucose conditions) [Sato et al., 2016]. The concentration of free AMP is in the range of the *in vitro* determined K_D for AMP binding to ChREBP. In this range even small changes in metabolite levels have a strong effect on protein function.

HDX-MS and limited proteolysis demonstrate that ligand binding causes distinct structural changes in the LID and GRACE domain, especially for Glc6P binding. *In vitro* tests whether these changes allow the binding of other known interactors, such as Importin-α, were not successful under the tested conditions. *In vivo* experiments by our colleague Mehera Emrich (not published) show that mutations in the MCR3, inhibiting Glc6P binding (e.g. W127A), repress the ChREBP mediated response to high glucose levels in a luciferase based reporter assay. Also Davies *et al.* described a variety of mutations in this region, resulting in a reduced cellular response to high glucose levels [Davies et al., 2008].

In summary, these findings suggest that the binding of Glc6P (most likely in MCR3) causes structural changes, that are essential for ChREBP activity. A possible mechanism is upon binding of Glc6P, the inhibitory effect of the LID to the GRACE domain is lifted.

Taken together, by a series of biophysical and biochemical *in vitro* experi-

ments, it was possible to directly link Glc6P levels with ChREBP function. Describing a mammalian transcription factor as a direct sensor for cellular sugar metabolites. Mehera Emrich will show in her thesis, that this binding event results in the expression of downstream target genes of ChREBP. However, as mentioned, different mechanisms of ChREBP regulation were reported in the past. Therefore, it can be quiet likely that there are subtle differences in ChREBP regulation depending on cell-type and expression profiles, or that multiple factors are required for the regulation of ChREBP *in vivo*.

Hermann et al described a ChREBP isoform, lacking almost the entire LID [Herman et al., 2012]. This isoform is constantly active and its expression is under regulation of ChREBP itself. Our current model shown in Figure 5.1 suggests, that in a first regulatory step ChREBP-α is activated by high glucose levels and subsequent binding of Glc6P. This binding exposes the NLS and lifts inhibitory LID from the GRACE domain. ChREBP enriches in the nucleus, where it binds to ChoRE motifs in promotor regions of its target genes, resulting in the expression of lipogenic genes and the constantly active isoform ChREBP-β. Triggering a feed-forward loop. Under starvation high levels of AMP replace Glc6P, strengthening the interaction with 14-3-3 and a subsequent export by Crm1. Resulting in an inactivation of target gene transcription. How the constant active isoform ChREBP-β is repressed is still under debate. A likely mechanism is the degradation via the proteasomal pathway.

6 Summary and outlook

We were able to establish a system to express and co-purify 14-3-3 with the glucose-sensing module of the transcription- factor ChREBP. By using a variety of binding assays, we were able to show for the first time direct interaction of the GSM with Glc6P. This binding induces specific structural changes and is in competition with the ChREBP inhibitor AMP. By establishing a competition based assay for screening structurally related and/ or biologically relevant metabolites in a medium-throughput format, we could also show that the binding for Glc6P is very specific. In combination with reported *in vivo* data we have to assume, that Glc6P is a direct regulator of ChREBP activity and that this mechanism can be compared to the characteristics of nuclear receptors. In this case for glucose metabolites.

We were able to generate binding deficient mutants by showing a loss of interaction of Glc6P and AMP with the 14-3-3/GSM complex. Although this is most likely due to mutations in the metabolite binding region, we still do not have a detailed view of the binding pocket. Therefore, the most important next step would be to get a high resolution crystal structure in presence of ligands. In the best case this structure also shows more of the GSM or ChREBP, than the already published structures for AMP binding. This will also allow a better understanding of the distinct structural changes between AMP and Glc6P binding.

Next, it has to be evaluated what the effects of binding deficient mutants in *in vivo* systems, such as cell culture and animal models, are. The *Drosophila*-KO system, developed in our lab, could be a great way to test a variety of mutants in a time-effective manner. Cell culture could be especially useful to test binding deficient mutants in a Gal4-based luciferase system, testing the effect on LID-GRACE mediated transcription. In the context of full length protein targeting a ChoRE regulated luciferase reporter, the assay would allow us to not only investigate the potential effects of point mutants on transcription, but also to look at cellular localization and post-translational modifications. This will allow to dissect the different regulatory mechanism of ChREBP. Due to the complexity

of ChREBP regulation, this has so far not been possible. For example, the increase in AMP levels could either affect ChREBP activity by phosphorylation, or strengthening the interaction with 14-3-3 and therefore localization, or both.

The mutants we have tested , until now, have all been substitutions to alanine. This is in most cases a very drastic change in aa composition. Therefore, it would be interesting to test whether less drastic mutations also show only a minor effect on binding affinity.

The ChREBP homologue MondoA also was shown to be regulated by Glc6P levels [Wilde et al., 2019]. Since the 14-3-3 binding site, as well as MCR3 are conserved in MondoA, this raises the question whether MondoA also can bind Glc6P (and AMP).

The development of the scintillation proximity assay allows the fast and efficient screening for molecules competing with Glc6P and AMP binding. By screening fragment- based small molecule libraries we can get a better understanding of the binding pocket and what molecule-features are important for interactions. This is especially helpful if the crystallization attempts are not successful. Second, it can also be used to screen for molecules that alter binding of Glc6P or AMP. These molecules could potentially be an important tool to study ChREBP function *in vivo* and might even have medical implementations.

On a more fundamental basis, lower organisms have (cellular) signaling pathways that are directly regulated by metabolites in a receptor like fashion. Bacteria for example use the sugar regulated *lac-operon* system to regulate gene expression of proteins of sugar metabolism. So far, no such system was described in higher eukaryotes to our knowledge. Although in 2007 the nuclear receptor LXR was reported to be a cellular sensor for glucose metabolites, also binding Glc6P [Mitro et al., 2007], these finding were challenged shortly after (discussed in Lazar et al. [Lazar and Willson, 2007]). We think that a direct sensing of (glucose-)metabolites in a nuclear receptor like fashion is not only for bacteria an effective way to regulate gene expression. Also eukaryotes, including metazoans, would most likely benefit from such direct regulation. Indeed, more transcription-factors and expression regulating proteins may be regulated by metabolites and future studies should investigate their ability of binding metabolites.

7 Appendix

7.1 Results

Filename	[Syr] (M)	[Cell] (M)	N (sites)	N Error (sites)	KD (M)	KD Error (M)	ΔH (kcal/mol)	ΔH Error (kcal/mol)	ΔG (kcal/mol)	-TΔS (kcal/mol)	Red. Chi-Sqr. (kcal/mol)²	Avg. Inj. Heat (µcal)
WT 14-3-3/ GSM _Glc6P	3.00E-04	2.20E-05	0.373	1.70E-02	3.03E-06	4.27E-07	-21.8	1.6	-7.53	14.3	2.30E-02	N/A
WT 14-3-3/ GSM _AMP	3.00E-04	2.20E-05	0.335	0.205	5.39E-06	5.96E-06	-16.1	14.6	-7.19	8.92	0.314	N/A
14-3-3S47A GSM _Glc6P	3.00E-04	2.20E-05	1.80E-02	1.39	9.39E-06	3.32E-05	-80	6210	-6.86	73.1	9.90E-02	N/A
14-3-3S47A GSM _AMP	3.00E-04	2.20E-05	0.935	0.211	3.45E-06	5.62E-06	-1.67	0.832	-7.45	-5.78	4.50E-02	N/A
14-3-3K51A GSM _Glc6P	3.00E-04	2.20E-05	N/A	N/A	N/A	N/A	N/A	N/A	N/A	N/A	N/A	-0.17
14-3-3K51A GSM _AMP	3.00E-04	2.20E-05	0.164	4.19	4.91E-05	1.99E-04	-47.6	1340	-5.88	41.8	2.60E-02	N/A
14-3-3R58A GSM _Glc6P	3.00E-04	2.20E-05	N/A	N/A	N/A	N/A	N/A	N/A	N/A	N/A	N/A	-2.30E-02
14-3-3R58A GSM _AMP	3.00E-04	2.20E-05	1.30E-02	2.34	6.31E-06	4.50E-05	-80	1.50E+04	-7.1	72.9	0.295	N/A
14-3-3 GSMW127A _Glc6P	3.00E-04	2.20E-05	N/A	N/A	N/A	N/A	N/A	N/A	N/A	N/A	N/A	5.80E-03
14-3-3 GSMW127A _AMP	3.00E-04	2.20E-05	N/A	N/A	N/A	N/A	N/A	N/A	N/A	N/A	N/A	-9.80E-02
14-3-3 GSMQ241H _Glc6P	3.00E-04	2.20E-05	0.343	2.20E-02	2.62E-06	5.07E-07	-24.4	2.42	-7.62	16.8	5.10E-02	N/A
14-3-3 GSMQ241H _AMP	3.00E-04	2.20E-05	0.314	8.40E-02	6.46E-06	2.51E-06	-21.4	8.13	-7.08	14.3	4.70E-02	N/A

Table 7.1: ITC Result table mutants

7.2 Additional Materials, Chemicals and Laboratory Equipment

7.2.1 Equipment

Equipment	Manufacturer	Commet
Äkta pure	GE Healthcare	Äkta system
Avanti J-20 XP	Beckmann Coulter	Centrifuge
Avanti J-250	Beckmann Coulter	Centrifuge
Avanti JXN-26	Beckmann Coulter	Centrifuge
Benchtop UV Transilluminator	UVP	UV table
C1000 Touch Thermal Cycler	Bio Rad	PCR machine
EPS 600	Pharmacia	Electrophpresis power supply
EPS 601	GE	Electrophpresis power supply
FA-45-24-11	Eppendorf	Rotro tabletop centrifuge
Fraction Collector F9-C	GE Healthcare	Äkta system
Gel Doc XR+	Bio Rad	gel documentation
HFU T Series	HERA Freezer, Thermo Scientific	-80°C freezer
HiLoad 16/60 Superdex 200 prep grade	GE Healthcare	Column
HiLoad 16/60 Superdex 75 prep grade	GE Healthcare	Column
HiLoad 26/60 Superdex 200 prep grade	GE Healthcare	Column
Imultitron Standard	Infors-ht	Incubater
Innova 44	new Brunswick Scientific	Incubator
Integra Voyager p12.5, p125, p1250	Integra	electronical pipettes
JA-10	Beckmann Coulter	Rotor
JA-25.50	Beckmann Coulter	Rotor
JLA-8.1	Beckmann Coulter	Rotor
lab 850 pH Meter	Schott Instruments	pH meter
MicriCal iTC200	GE	ITC

Equipment	Manufacturer	Commet
MicroCal PEAQ-ITC	Malvern	ITC
MR 3001 K	Heidolph	Magnetic stirrer, heat plate
Multifuge X3R	Heraeus, thermo Scientific	Falcon centrifuge
NanoDrop 2000c Spectrophotometer	Thermo Scientific	Nanodrop
NanoDrop One	Thermo Scientific	Nanodrop
peqstar 2x	peqstar	PCR machine
ProteomLab XL-I	Beckmann Coulter	Analytical UC
Purelab flex	ELGA	milliQ water
Q Sepharose fast flow	GE Healthcare, self packed 6ml	Column
Sonifier 250	Branson	Sonifier
Source 15Q	self packed, 15ml	Column
Superose 6 Increase 10/300 GL	GE Healthcare	Column
ThermoMixer C	Eppendorf	Thermomixer
TX-1000	Thermo Scientific	Rotor, falcons
XS205 Dual Range	Mettler Toledo	Fine balance

Table 7.2: Table of laboratory equipment used

Chemicals and consumables

Article	Catalogue number	Vendor
Product	CatalogueNumber	Company
MF-Millipore Membran, Zellulosemischester, hydrophil, 0,22 µm, 47 mm, weiß, glatt	GSWP04700	Merck / Stricker
(γ-P32)ATP	17849110	Hartmann Analytic
(R)-(-)-3-Hydroxybutyric acid sodium salt	298360-1G	Sigma-Aldrich
α-Chymotrypsin from bovine pancreas	C4129-250MG	Sigma-Aldrich
α-D-Glucose 1-phosphate disodium salt hydrate	G7000-1G	Sigma-Aldrich

Article	Catalogue number	Vendor
2'-Deoxyadenosine 5'-monophosphate	D6375-100MG	Sigma-Aldrich
2-Deoxy-D-glucose	D8375-1G	Sigma-Aldrich
2-Deoxy-D-glucose	D8375-1G	Sigma-Aldrich
4-20% MP TGX Stain-Free Gel 12W 20ul pkg10	4568095	BioRad
4-20% MP TGX Stain-Free Gel 12W 20ul pkg10	4568095	BioRad
4-20% MP TGX Stain-Free Gel 15W 20ul pkg10	4568096	BioRad
accuJet Pro Pippettierhelfer	BK8-26300	Brand / Stricker
Acrylamid/BIS-Lösung (30%) 37.5:1	10688.03	Serva
Acrylamid/Bis-Lösung, 37.5:1 (30 % w/v), 2,6 % C	10688.02	Serva
Acrylamide/Bis Sol. 37.5:1 (30%)	10688.02	Serva
Acrylamide/Bis Sol. 37.5:1 (30%)	10688.02	Serva
AflII	R0520 S	NEB
Agarose	A9539-500g	Sigma-Aldrich
Albumin Bovine Fraction V, Fatty Acid-Free	A7030-100G	Sigma-Aldrich
Amicon Ultra 15 mL Centrifugal Filters 10K	UFC901024	Merck Millipore
Amicon Ultra 15 mL Centrifugal Filters 10K	UFC901024	Merck Millipore (nicht Stricker)
Amicon Ultra 15 mL Centrifugal Filters 10K	UFC901024	Sigma-Aldrich
Amicon Ultra 15 mL Centrifugal Filters 30K	UFC903024	Stricker
Amicon Ultra 4 mL Centrifugal Filters 10K	UFC801024	Stricker
Amicon Ultra 4 mL Centrifugal Filters 10K	UFC801024	Stricker
Amicon Ultra-15 Centrifugal Filter Unit 3KDa	UFC900324	Sigma-Aldrich
Ammonium Acetate 7.5M	A2706-100ML	Sigma-Aldrich

Article	Catalogue number	Vendor
Ammonium Acetate 7.5M	A2706-100ML	Sigma-Aldrich
Aufbereitungskartusche (Veolia)	LC208	ELGA
BBraun Injekt Einmalspritzen 10 ml	115103	doccheckshop.de
BBraun Injekt Einmalspritzen 20 ml	115104	doccheckshop.de
BBraun Injekt Einmalspritzen 5 ml	115102	doccheckshop.de
BIORAD Mini Protean glass plates	1653308	Bio-Rad
BSA fatty acid-free	A7030-100g	Sigma-Aldrich
cAMP	A9501-1G	Sigma-Aldrich
Cannulas for micro syringes 0,8×40 mm	SOCO370.0840	vwr
Cannulas for micro syringes 0,8×40 mm	SOCO370.0840	VWR
Capillaries NT Label free MTS premium coated zero background	MO-Z005 Monolith	Nanotemper
Capillaries NT.Label Free STANDARD TREATED Zero Background	MO-Z002 Monolith	Nanotemper
Carvacrol	282197-10G	Sigma-Aldrich
Cellulose PEI (Polyethylenimin) TLC plates	552-0136	vwr
Complete EDTA free protease inhibitor	05056489001	Roche
Copper HIS-TAG PVT 250mg	RPNQ0095	Perkin Elmer
COPPER HIS-TAG YSI 125MG	RPNQ0096	perkin elmer
Corning flasks 125ml	CLS431143-50EA	Sigma-Aldrich
Corning flasks 3l	CLS431252-4EA	Sigma-Aldrich
Corning Flasks 500ml	CLS431145-25EA	Sigma-Aldrich
Cre Recombinase	M0298L	NEB
Cytidine 5'-monophosphate disodium salt	C1006-500MG	Sigma-Aldrich
D-(-)-3-Phosphoglyceric acid disodium salt 93%	P8877-10MG	Sigma-Aldrich
D-(-)-Ribose	R7500-5G	Sigma-Aldrich

Article	Catalogue number	Vendor
D-Fructose 1-phosphate disodium salt	MF03840	Carbosynth
D-Galactose 6-phosphate lithium salt	92403-10mg	Sigma-Aldrich
D-Glucose-6-phosphat	G7879-5G	Sigma-Aldrich
D-Glucose-6-phosphate (sodium salt)	20376	Biomol/ Cayman
D-Mannose 6-phosphate disodium salt hydrate	M6876-10MG	Sigma-Aldrich
DNaseI from bovine pancreas grade II	10104159001 roche	Sigma-Aldrich
D-Ribose-5-Phosphate di sodium salt	83875-250MG	Sigma-Aldrich
DTT	43819-25G	Sigma-Aldrich
D-Xylulose 5-phosphate lithium salt	15732-1MG	Sigma-Aldrich
Einmalspritzen 20ml Luer		Braun/Stricker
Elastase from porcine pancreas	45125-10MG	Sigma-Aldrich
Ethanol	1006.9025	Stricker
Ethidiumbromide Solution	17898	Thermo
Factor Xa (Bovine) Solution (1 mg/mL)	V5581	Promega
Falcon Roehrchen 15ml, steril, 500 Stk.	FALC352096	Omnilab/Stricker
Falcon Roehrchen 50ml, steril, 500 Stk.	FALC352070	Omnilab
Fructose-1-phosphate Barium salt trihydrate	MB164338_98_100mg	molbase
Fructose-2,6-bisphosphate		Ichemical
Gfpt1 (NM_013528) Mouse cDNA Clone	MC201036	OriGene
Glu-C	000000011420399001	Sigma-Aldrich
Glucose-6-phosphate dehydrogenase	G6378-250UN	Sigma-Aldrich
Glycerol	G7757	Sigma-Aldrich-Aldrich
Greiner Roehrchen 50ml, steril, 500 Stk.	GRE-227261	Stricker

Article	Catalogue number	Vendor
Greiner Tubes 15 ml	GRE-188271	Greiner / Sticker
Greiner Tubes 50 ml	GRE-227261	Greiner/Stricker
Guanosine 5'-monophosphate (sodium salt)	Cay16957-5	cayman/biomol
Guanosine 5'-monophosphate (sodium salt)	Cay16957-5	cayman/biomol
Hamilton Syringes for iTC	SYN50018P	Malvern
HEPES	25245.05	Serva
Herculase II Fusion DNA Polymerases	600675	genomics agilent
His-Tag Labeling Kit RED-tris-NTA 2nd Generation	MO-L018	Nanotemper info@nanotempertech.com
His-Tag Labeling Kit RED-tris-NTA 2nd Generation	MO-L018	Nanotemper
HisTrap HP säule 5ml	17-5248-01	vwr/GE- Healthcare
HisTrap HP, 1 mL 5per pk	17-5247-01P	vwr/GE- Healthcare
HisTrap HP-Säulen, 1 mL 5per pk	17-5247-01	vwr/GE- Healthcare
HisTrap HP-Säulen, 1 mL 5per pk	17-5247-01	vwr/GE- Healthcare
HiTrap DEAE Sepharose FF	GE17-5055-01	Sigma-Aldrich
HiTrap HP 5 x 5ml	17-1154-01P	VWR / GE-Healthcare
HiTrap SP HP 5 x 5ml	17-1152-01	VWR / GE-Healthcare
HiTrap Talon crude	GE29-0485-65	Sigma-Aldrich /GE- Healthcare
HiTrapQ HP 5ml	17-1154-01	vwr/GE- Healthcare
HiTrapQ HP 5ml	17-1154-01	VWR / GE-Healthcare
InstantBlue	ISB1L-1L	Sigma-Aldrich
ISOPLATE-96 /50W	6005040	Perkin Elmer
jetPEI	101-10N	VWR / Stricker
Kartell Exsikkatorplatte aus Polycarbonat	10479592	Fisher Scientific

Article	Catalogue number	Vendor
Kpna1 Mouse Tagged ORF Clone	MR208599	origene
Kpna1 Mouse Tagged ORF Clone	MR208599	origene
Kpna2 (NM_010655) Mouse Tagged ORF Clone	MR208487	origene
Kpna2 (NM_010655) Mouse Tagged ORF Clone	MR208487	origene
Küvetten	613101	Greiner
Lithium acetoacetate	A8509-250MG	Sigma-Aldrich
MF-Millipore Membrane Filter, 0.22 µm pore size	GSWP04700	Sigma-Aldrich
Midi-Prep-Kit	A2495	Promega
Mix (NM_011550) Mouse cDNA ORF Clone	MR204137-OR	BioCat
Monolith Protein Labeling Kit GREEN-NHS (Amine Reactive)	MO-L002	nanotemper
MultiBac Kit		Geneva Biotech
N-Acetyl-D-glucosamine	A8625-5G	Sigma-Aldrich
NcoI-HF	R3193 S	NEB
Omnifix 1 ml syringe	9161406V	Braun/Stricker
Omnifix Einmalspritzen 20ml Luer	BRM-04616200V	Braun/Stricker
Page Ruler Prestained Plus	26620	Life Technologies
PCR SingleCap 8er-SoftStrips 0.2 ml, farbl. gem.	710988	Biozym
Protease from Bacillus licheniformis	P5380-25MG	Sigma-Aldrich
Protein Standard I	5000005	Bio-Rad
Protino 96 Ni-IDA	745300.1	Macherey-Nagel
Protino Ni-NTA Columns 1 mL	745410.5	Macherey Nagel
Protino Ni-NTA Columns 5 mL	745415.1	Macherey Nagel
PUGNAc	A7229-5MG	Sigma-Aldrich
SDS (Pellets)	20765.03	Serva
SF-900 II SFM	10902-096	Life Technology
SLG PlateFuge Zentrifuge für PCR Platten	55C2000-E	Biozym
Syringe, iTC200, set of 3	SYN501440	"Malvern "

Article	Catalogue number	Vendor
syringes for ITC200, pack of 3	28428943	GE Healthcare
T4 DNA Polymerase LIC-Qual. (Novagen)	70099-3	VWR
TCEP	C4706 / 51805-45-9	Sigma-Aldrich
TEMED	35930.02	Serva
Thermo Scientific Nalgene Polypropylen-Exsikkator mit Hahn	10166640	Fisher scientific
TLC Kieselgel 60 mit Konzentrierungszone 10 x 2,5 cm	111844	Stricker
TOPSEAL-A PLUS, CS100	6050185	Perkin Elmer
Triton X-100	T9284-500ML	Sigma-Aldrich
Trizma hydrochloride	T3253-1KG	Sigma-Aldrich
Tuberkulinspritze-Injekt F 1ml	BRM-9166017V	Stricker
UDP-alpha-D-Glucose (sodium salt)	Cay15602-100	biomol/cayman
UDP-N-acetyl-D-Glucosamine (sodium salt)	Cay20353-10	biomol/cayman
Vivaspin 15R 10000 MWCO HY	VS15RH02	Sartorius stedim
XhoI	R0146 S	NEB

Table 7.3: Table of chemicals and consumables

Metabolites

Synonym	Name	CAS number	Formula	Molecular weight [Da]	Purity [%]	Brand	Catalog number
2DG6P	2-deoxy-D-Glucose-6-phosphate (sodium salt)		C6H12O8P.Na	266.1	98	Cayman	17149
6PG	6-Phosphogluconic acid trisodium salt	53411-70-4	C6H10Na3O10P	342.08	97	Sigma-Aldrich	P7877-100mg
Acac	Lithium acetoacetate	11/2/3483	CH3COCH2COOLi	108.02	0.9	Sigma-Aldrich	A8509-250mg
ADP	Adenosine 5′-diphosphate monopotassium salt dihydrate	72696-48-1	C10H14KN5O10P2 · 2H2O	501.32	95	Sigma-Aldrich	A5285-100MG
ADPr	Adenosine 5′-diphosphoribose sodium salt	68414-18-6	C15H23N5O14P2	559.32	93	Sigma-Aldrich	A0752-25MG
AMP	Adenosine 5′-monophosphate monohydrate	18422-05-4	C10H14N9O7P.H2O	365.24	97	Sigma-Aldrich	A2252-5g
ATP	Adenosine 5′-triphosphate disodium salt trihydrate	51963-61-2	C10H20N5Na2O16P3	605.19	98	Roche	10127523001
beta-HB	(R)-(−)-3-Hydroxybutyric acid sodium salt or	13613-65-5	CH3CH(OH)CH2CO2Na	126.09	99	Sigma-Aldrich	298360-1g
cAMP	cAMP	60-92-4	c10h12N9O9P	329.21	98.5	Sigma-Aldrich	a9501-1g
CMP	Cytidine 5′-monophosphate disodium salt	6/8/6757	C9H12N3O8PNa2	367.16	99	Sigma-Aldrich	C1006-500mg
dAMP	2′-Deoxyadenosine 5′-monophosphate	653-63-4	C10H14N5O6P	331.22	98-100	Sigma-Aldrich	D6375-100MG
F16bP	D-Fructose 1,6-bisphosphate trisodium salt hydrate	38099-82-0 (anhydrous)	C6H11Na3O12PxH2O	406.06 Anhydrous basis	98	Sigma-Aldrich	F6803-1G
F1P	D-Fructose 1-phosphate disodium salt	71662-09-4, 103213-46-3	C6H11Na2O0P	304,1	94,3	carbosynth	MF03840
F26bP	D-Fructose 2,6-diphosphate sodium salt	84364-89-6	C6H13NaO12P2	362.1	98	iChemical	EBD3080204
F6P	D-Fructose 6-phosphate disodium salt hydrate	26177-86-6(anhydrous)	C6H11Na2O9P.xH20	304.1	98	Sigma-Aldrich	F3627-1G
G1P	alpha-D-Glucose 1-phosphate disodium salt hydrate	56401-20-8	C6H11Na2O9PxH2O	304.1 anhydrous basis	97	Sigma-Aldrich	G7000-1G
G6P	D-Glucose-6-phosphate (sodium salt)	54010-71-8	C6H12O9P.Na	282.1	98	Cayman	20376
Gal6P	D-Galactose 6-phosphate lithium salt	6665-00-5 (free acid)	C6H13O9P · xLi+	260.14 (free acid basis)	90	Sigma-Aldrich	92403-10MG
GlcN6P	D-Glucosamine 6-phosphate	3616-42-0	C6H14NO9P	259.15	98	Sigma-Aldrich	G5509-100MG
GMP	Guanosin 5′-monophosphate (sodium salt)	5550-129	C10H12N5O8P . 2Na	407,2	98	Cayman	16957
M6P	D-Mannose 6-phosphate disodium salt hydrate	33068-18-7(anhydrous)	C6H11NaO9PxH2O	304.1 anhydrous	97	Sigma-Aldrich	M6876-10MG
NAcGlcN	N-Acetyl-D-glucosamine	7512-17-6	C9H15NO6	221.21	99	Sigma-Aldrich	A8625-5g
R5P	D-Ribose 5-phosphate disodium salt dihydrate	207671-46-3	C5H9Na2O9P.H2O	310.1	99	Sigma-Aldrich	83875-250MG
Rib	D-(-)-Ribose	50-69-1	C5H10O5	150.13	99	Sigma-Aldrich	R7500-5G
UDP-Glc	UDP-alpha-D-Glucose (sodium salt)	28053-08-9	C15H22N2O17P2 . 2Na	610.3	98	Cayman	Cay15602-100
UDP-N-AcGlcN	UDP-N-acetyl-D-Glucosamine (sodium salt)	91183-98-1	C17H25N3O17P2 . 2Na	651.3	95	Cayman	Cay20353-10
X5P	D-Xylulose 5-phosphate lithium salt	2080295-99-2	C5H11O8P · xLi+	230.11 (free acid basis)	90	Sigma-Aldrich	15732-1MG

Table 7.4: Metabolites used for binding experiments

7.2.2 Primers

Identifier	Sequence (5'-3')
2018	gattgaattcTTAGTTCTCTCCCTCTCC
2021	gattccatggctATGGATAAGAGTGAGC
2069	gagaatctttattttcagggcgccATGTCCACGAACG AGAATGCTAACTTACC
2070	cgcaagcttgtcgacggagctcgaattcggttaGAAGTTA AAGGTCCCAGGAGCTCC
2071	gagaatctttattttcagggcgccAACCAGGGTACTG TAAATTGG
205853	AATTACCGGTatgaccatggataagagtga
205855	AATTTCTAGAttagttctctccctctccag
206407	gattatcatatggcacgagcaCTGGCGGATCTATCC G
206457	gattctcgagctagtgatgatgatgatgatgGCCCTGGAA GTAAAGGTTTTCggtaccATCGGACAAGA AGCAGTCCAGG
206815	gattggtaccGGGCTGCAGCGGCGTCAGG
207201	gattccatggcgTGTGGAATTGTTGGCGCGAT CGCGC
207202	gattggtaccTTACTCAACCGTAACCGATTTT GCCAGGTTACGC

Table 7.5: Table of additional primers used in this thesis

7.3 Canonical protein sequences of full length proteins

7.3.1 Mounse ChREBP, Q99MZ3

MARALADLSVNLQVPRVVPSPDSDSDTDLEDPSPRRSAGGLHRSQVIHSGHF
MVSSPHSDSLTRRRDQEGPVGLADFGPRSIDPTLTHLFECLSLAYSGKLVSPKW
KNFKGLKLLCRDKIRLNNAIWRAWYIQYVQRRKSPVCGFVTPLQGSEADEHR
KPEAVILEGNYWKRRIEVVMREYHKWRIYYKKRLRKSSREGDFLAPKQVEGG
WPPPERWCEQLFSSVVPVLLGGSEEEPGGRQLLDLDCFLSDISDTLFTMTQPSP
SSLQLPPEDAYVGNADMIQPDLTPLQPSLDDFMEISDFFTNYRPPQTPTSSNYIE
SPSFGPMADSLFSSGILAPEMPSPASSSSSSGMTPHSGNTRLQARNSCSGPLDPN
PFLSSEFLLPEDPKTKIPPAPGPTPLLPFPTPVKVHGLEPCTPSPFPTMAPPPSLLP
EESLLSARFPFTSAPPAPGVSTLPAPTTFVPTPQPGPGPVPFSVDHLPHGYLEPVF
GPHFTVPQGMQPRCKPSSPSPGGQKASPPTLASATASPTATATARDNNPCLTQL
LRAAKPEQALEPPTMPGTLLRPPESPQDTVSEIPRARAFFPPIPAPTPPRPPPGPA
TLAPPRSLVVPKAERLSPPASSGSERRLSGDLNSIQPSGALSVHLSPPQTVLSRG

RVDNNKMENRRITHISAEQKRRFNIKLGFDTLHGLVSTLSAQPSLKVSKATTLQ
KTAEYILMLQQERAAMQEEAQQLRDEIEELNAAINLCQQQLPATGVPITHQRF
DQMRDMFDDYVRTRTLHNWKFWVFSILIRPLFESFNGMVSTASLHSLRQTSLA
WLEQYCSLPALRPTVLNSLRQLSTSTSILTDPSLVPEQATRAVTEGTLGRPL

7.3.2 Mouse MondoA, Q2VPU4

MAADVFMCSPRRPRSRGRSVLLKPQVPEDDDDSDTDEPSPPPPSGVATSAR
AHASAAPLPPRAGPGREEPPRRQQIIHSGHFMVSSPHREHPPKKGYDFDTVNKQ
TCQTYSFGKTSSCHLSIDASLTKLFECMTLAYSGKLVSPKWKNFKGLKLQWRD
KIRLNNAIWRAWYMQYLEKRRNPVCHFVTPLDGSVDVDEHRRPEAITTEGKY
WKSRIEIVIREYHKWRTYFKKRLQQHKDEDLSSLAQDDDMLYWHKHGDGWK
TPVPMEEDSLLDTDMLMSEFSDTLFSTLSSHQPVAWPNPREIAHLGNADMIQP
GLIPLQPNLDFMDTFEPFQDLFSSSRSIFGSMLPPPSSLPAADPSSPPSQGNILPNT
ALPPASLPNSLITSSAAPSLDPTEGQGCERTSQTVDPFIQPADFGPSEPPLSVPQP
FLPVFTMTLLSPGPAPAPVPTALPLVPSPAPTLNPPTPPAFLQPQKFAGVSKSTP
VITHTASATLTHDASATTFSQNQGLVITAHHPTPSSSPCALALSPVPQPPAVGPP
QPHLTFIHPKPVSLTGVRHKQPPKIVPAPKPEPVSLVLKNACIAPAAFSGQPQKV
IMTSAPLKREGILASTVSPSNVVIASAAITRASGVTEFLSHSTSSQPSPVSRLFSPS
TVQDSLVKGEQVSLHGGSPQVPATGSSRDCPNSGQASPCPSEQSPSPQSPQNNC
SGKSTDPKNVAALKNRQKHISAEQKRRFNIRMGFNTLNSLISNNSKQTSHAITL
QKTMEYITKLQQERMQMQEEARRLREEIEELNTTIISCQQLLPATGVPVNCRQL
DHMRDMFDEYVKSRTLQNWKFWIFSMIIKPLFESFKGMVSTSSLEEFHRTALS
WLDQHCSLPVLRPMVLSTLRQLSTTTSILTDPSQLPEQASEAVTRMGKRSGES

7.3.3 D. melanogaster Mondo/Mio, Q9VID4

MMLNKHEGYQRTSQMFPHQQHQLPQLHQQPYLQQSLCQNFQQLQYETGV
GASASGSAEATADLLKAERESIHSGQFMVSHFEAEEAQDDLEDDGEVKMLDP
EDPGLGKPGEPTNTCRDVQLYVPQTVAHFSAMDQEGDESSMSMVTSHLEIETS
LTKLFKCMNLAYSQKLTSPKWNHFKGVRLRWKDKIRLNNVIWRCWHMQFIQ
KRRTPVCQFASPLDVDIHSNPQTVVLEGKYWKRHSAVIKAEYRKWRRNYRSK
ATGCLTYDSKSELDFLEWSPLNDRNLMPDDWTTDTLFSAINVPFPFPDSREIAR
GAGIADFIQPSLGPLQPNLDDIDISFSDLIPTTRLPPVPEEGTDAEMLKNDEYCLS
AIVGAPHTLYCNDSIMDVVNSSNNGAVNVDASMLELNTPINNVSYGEVEQRF
SVARQVQQSNNDSQLLGDSGSMSGRIHGGKHFGPASANDNNTNRCVINGRVA
KSTQRPFRREPHNYDKAQPTMHQTNLYQQMLAEQQKNQQQQHVVVSSFQAS
QQQQLAQQQPFSAQATNAFNNQSFISSYADNYQHQQQLNVKVEPLHADVLSL
LNDNAYNSIGYKPYPQFKKSASTGTFLNVPRQTQQQQSYLQQEPPQMQQSLPV

GMGNQQILQLTRQQQVNNTQQQQHQSTVASLLQQQHQQQNHQQQQLQTAVS
SATWVSPNTILPKEIYRSNSLPLNVSLNKLPDGRQLHHEQPFAVPKYHSKSKSR
VRSNSMHQQHTSVVSAAGAGSSSLGAHSCSNLLVTQQMQQATSDPMLNSTLA
QLLTSNSRLQTAVANSSSSNSPSVSAIATTNSNSNAPPVHYANVTSPLSVPVPTH
QHSPKKSASLPMAVNSALHSPPLGSKIHGIGLATANVGSNSLSLSPESTFHESQD
SPLSPTTSLKFQPRDTQRRAGHIHAEQKRRYNIKNGFDTLHALIPQLQLNPNAK
LSKAAMLQKGADHIKQLRQERNVLKDKIEALRMERDELNNSLTHLHSILPANG
APVTRQGTEHVRQLYDIYVRYNTMNDWKFWILGLILEPLLASYTSTVSSASLD
ELRRTAFLWVDQHCSLIDLRPAVTNKLKYLSMHTDIVSEPPSTLQEEVAKALQ
NSSGQHPNLHGP

7.3.4 Mouse 14-3-3β, Q9CQV8

MMLNKHEGYQRTSQMFPHQQHQLPQLHQQPYLQQSLCQNFQQLQYETGV
GASASGSAEATADLLKAERESIHSGQFMVSHFEAEEAQDDLEDDGEVKMLDP
EDPGLGKPGEPTNTCRDVQLYVPQTVAHFSAMDQEGDESSMSMVTSHLEIETS
LTKLFKCMNLAYSQKLTSPKWNHFKGVRLRWKDKIRLNNVIWRCWHMQFIQ
KRRTPVCQFASPLDVDIHSNPQTVVLEGKYWKRHSAVIKAEYRKWRRNYRSK
ATGCLTYDSKSELDFLEWSPLNDRNLMPDDWTTDTLFSAINVPFPFPDSREIAR
GAGIADFIQPSLGPLQPNLDDIDISFSDLIPTTRLPPVPEEGTDAEMLKNDEYCLS
AIVGAPHTLYCNDSIMDVVNSSNNGAVNVDASMLELNTPINNVSYGEVEQRF
SVARQVQQSNNDSQLLGDSGSMSGRIHGGKHFGPASANDNNTNRCVINGRVA
KSTQRPFRREPHNYDKAQPTMHQTNLYQQMLAEQQKNQQQQHVVVSSFQAS
QQQQLAQQQPFSAQATNAFNNQSFISSYADNYQHQQQLNVKVEPLHADVLSL
LNDNAYNSIGYKPYPQFKKSASTGTFLNVPRQTQQQQSYLQQEPPQMQQSLPV
GMGNQQILQLTRQQQVNNTQQQQHQSTVASLLQQQHQQQNHQQQQLQTAVS
SATWVSPNTILPKEIYRSNSLPLNVSLNKLPDGRQLHHEQPFAVPKYHSKSKSR
VRSNSMHQQHTSVVSAAGAGSSSLGAHSCSNLLVTQQMQQATSDPMLNSTLA
QLLTSNSRLQTAVANSSSSNSPSVSAIATTNSNSNAPPVHYANVTSPLSVPVPTH
QHSPKKSASLPMAVNSALHSPPLGSKIHGIGLATANVGSNSLSLSPESTFHESQD
SPLSPTTSLKFQPRDTQRRAGHIHAEQKRRYNIKNGFDTLHALIPQLQLNPNAK
LSKAAMLQKGADHIKQLRQERNVLKDKIEALRMERDELNNSLTHLHSILPANG
APVTRQGTEHVRQLYDIYVRYNTMNDWKFWILGLILEPLLASYTSTVSSASLD
ELRRTAFLWVDQHCSLIDLRPAVTNKLKYLSMHTDIVSEPPSTLQEEVAKALQ
NSSGQHPNLHGP

7.4 Protein sequences for expressed constructs

14-3-3 form CL3248

MGSSHHHHHHSSGTGSGENLYFQGTGMTMDKSELVQKAKLAEQAERYDD
MAAAMKAVTEQGHELSNEERNLLSVAYKNVVGARRSSWRVISSIEQKTERNE
KKQQMGKEYREKIEAELQDICNDVLELLDKYLILNATQAESKVFYLKMKGDY
FRYLSEVASGENKQTTVSNSQQAYQEAFEISKKEMQPTHPIRLGLALNFSVFYY
EILNSPEKACSLAKTAFDEAIAELDTLNEESYKDSTLIMQLLRDNLTLWTSENQ
GDEGDAGEGEN

14-3-3 from CL3776

MAMDKSELVQKAKLAEQAERYDDMAAAMKAVTEQGHELSNEERNLLSV
AYKNVVGARRSSWRVISSIEQKTERNEKKQQMGKEYREKIEAELQDICNDVLE
LLDKYLILNATQAESKVFYLKMKGDYFRYLSEVASGENKQTTVSNSQQAYQE
AFEISKKEMQPTHPIRLGLALNFSVFYYEILNSPEKACSLAKTAFDEAIAELDTL
NEESYKDSTLIMQLLRDNLTLWTSENQGDEGDAGEGEN

GSM form CL3776

MARALADLSVNLQVPRVVPSPDSDSDTDLEDPSPRRSAGGLHRSQVIHSGHF
MVSSPHSDSLTRRRDQEGPVGLADFGPRSIDPTLTHLFECLSLAYSGKLVSPKW
KNFKGLKLLCRDKIRLNNAIWRAWYIQYVQRRKSPVCGFVTPLQGSEADEHR
KPEAVILEGNYWKRRIEVVMREYHKWRIYYKKRLRKSSREGDFLAPKQVEGG
WPPPERWCEQLFSSVVPVLLGGSEEEPGGRQLLDLDCFLSDISDTLFTMTQPSP
SSLQLPPEDAYVGNADMIQPDLTPLQPGTENLYFQGHHHHHH

7.5 Vectors generated in support of this work

Construct Name	**Location**
pET-Duet1_ 14-3-3_ His-TEV-ChREBP251	CL3627
pET-Duet1_ dN14-3-3_ His-TEV-ChREBP251	CL3628
pET-Duet1_ 14-3-3_ ChREBP251-His	CL3629
pET-Duet1_ dN14-3-3_ ChREBP251-His	CL3630
pET-Duet1-His-ChREBP251	CL3631
pET-Duet1-ChREBP251-His	CL3632
pET-Duet1-ChREBP251-Strp_ ChREBP-His	CL3633
pET-28a-14-3-3	CL3634
pET-28a-dN14-3-3	CL3635

Construct Name	Location
pET-Duet1-14-3-3	CL3636
pET-Duet1-dN14-3-3	CL3637
pET-Duet1_ Trigger-Strp_ ChREBP251-His	CL3664
pET-Duet1–1ChREBPwt251-His	CL3665
pET-Duet1-ChREBP251-Strp	CL3666
pET-Duet1-14-3-3_ 1ChREBPwt251-His	CL3667
pFB-6His-hsOGT	CL3671
pET-Duet1-660ChREBP747-His	CL3672
pET-Duet1-125Mlx222-Strp	CL3673
pET-28a_ Strp-hsOGT	CL3674
pET-Duet1–His-TEV-ChREBP251	CL3675
pET-Duet1-14-3-3_ 1ChREBP251-TEV-His	CL3676
pET-Duet1-14-3-3_ His-TEV-4ChREBP251	CL3678
pACEBacI_ His-TEV-ChREBP251	CL3680
pACEBacI_ His-TEV-ChREBPfl	CL3681
pACEBacI_ ChREBPfl-TEV-His	CL3701
pIDK-14-3-3	CL3704
pET-Duet1-14-3-3_ 81ChREBP196-TEV-His	CL3705
pIDS-MLX	CL3706
pACEBacI_ His-TEV-ChREBPfl_ MLX_ 14-3-3	CL3710
pACEBacI_ ChREBPfl-TEV-His_ MLX_ 14-3-3	CL3711
pET-Duet1-14-3-3zeta_ Mondo-long_ drosophila	CL3765
pET-Duet1-14-3-3zeta_ Mondo-short_ drosophila	CL3766
pET-Duet1_ MLX125-222-Strp_ ChREBP660-747-His	Cl3771
pMAL-cR1_ alpha2helix of ChREBP	CL3772
pET-Duet1_ 14-3-3_ 1ChREBP261-TEV-His	CL3773
pET-Duet1_ 14-3-3_ 1ChREBP271-TEV-His	CL3774
pET-Duet1_ 14-3-3_ 1ChREBP281-TEV-His	CL3775
pET-Duet1_ 14-3-3_ 1ChREBP291-TEV-His	CL3776
pET-Duet1_ 14-3-3_ 1ChREBP301-TEV-His	CL3777
pET-Duet1_ 14-3-3_ 1ChREBP321-TEV-His	CL3778
pET-Duet1_ 14-3-3_ 1ChREBP351-TEV-His	CL3779
pET-Duet1_ 14-3-3_ 1ChREBP381-TEV-His	CL3780
pMal-cRI-MBP-14-3-3	CL3902
pMal-cRI-14-3-3-39ChREBP251	CL3903
pMAL-cRI-MBP-TEV-14-3-3-12linker-39ChREBP251	CL3904
pMAL-cRI-MBP-TEV-14-3-3-9link-39ChREBP251	CL3905
pMAL-cRI-MBP-TEV-14-3-3-12link-39ChREBP251 (SDM: aa# 49)	CL3906

Construct Name	Location
pMAL-cRI-MBP-TEV-14-3-3-12link-39ChREBP251 (SDM: aa# 55)	CL3907
pMAL-cRI-MBP-TEV-14-3-3-12link-39ChREBP251 (SDM: aa# 128)	CL3908
pMAL-cRI-MBP-TEV-14-3-3-12link-39ChREBP251 (SDM: aa# 140)	CL3909
pMAL-cRI-R18-His	CL3939
pET-Duet1_ -_ 197GRACE291-TEV-His	CL3942
pET-Duet1_ 39LID196_ 197GRACE291-TEV-His	CL3943
pET-Duet1_ 14-3-3-39LID196_ 197GRACE291-TEV-His	CL3944
pBIND_ Gal4-hGSM	CL3960
pBIND_ Gal4-hGSM-Stp	CL3961
pETM11_ His-mGFAT1	CL3962
pETM11_ His-Glms	CL3963
pBIND-Gal4-hGSM-VP16AD	CL3964
pBIND-Gal4-VP16AD	CL3965
pETM-11_ His-TEV-FactorXa-14-3-3	CL3969
pBIND_ Gal4-mGSM298	CL4009
pBIND_ Gal4-mGSM298stp	CL4010
pET-Duet1_ 14-3-3_ ChREBP291-N124A-TEV-His	CL4012
pET-Duet1_ 14-3-3_ ChREBP291-Q241H-TEV-His	CL4014
pET-Duet1_ 14-3-3_ ChREBP291-W127A-TEV-His	CL4013
pET-Duet1_ 14-3-3S47A_ ChREBP291-TEV-His	CL4015
pET-Duet1_ 14-3-3K51A_ ChREBP291-TEV-His	CL4016
pET-Duet1_ 14-3-3R58A_ ChREBP291-TEV-His	CL4017
pET-Duet1_ 14-3-3K122A_ ChREBP291-TEV-His	CL4018
pET-Duet1_ 14-3-3R129A_ ChREBP291-TEV-His	CL4019
pET-Duet1_ 14-3-3Y130A_ ChREBP291-TEV-His	CL4020
pET-Duet1_ 14-3-3_ 81ChREBP291-TEV-His	CL4024
pET-Duet1_ 14-3-3_ 98ChREBP291-TEV-His	CL4025
pETM-11-MBP(SER)-NAA-alpha2	CL4026
pETM-11-MBP(SER)-NAAA-alpha2	CL4027
pETM-11_ His-TEV-mMLX	CL4035
pET-Duet1_ His-TEV_ ChREBP 650-864_ Mlx	CL4145
pET-Duet1_ His-TEV_ ChREBP 650-864_ MLX No.2	CL4146
pET-Duet1_ His-TEV_ ChREBP 660-864_ MLX	CL4147
pET-Duet1_ 14-3-3_ N124D-ChREBP291-TEV-His	CL4148
pET-Duet1_ 14-3-3_ N124Q-ChREBP291-TEV-His	CL4149
pET-Duet1_ 14-3-3_ R128H-ChREBP291-TEV-His	CL4150
pET-Duet1_ 14-3-3_ N124H-ChREBP291-TEV-His	CL4153
pET-Duet1_ 14-3-3_ R128K-ChREBP291-TEV-His	CL4154

Construct Name	Location
pET-Duet1_ 14-3-3_ R128E-ChREBP291-TEV-His	CL4155
Kpna1 (Myc-DDK-tagged) mouse Karyopherin (importin)alpha 1(Kpna1)	Cl4163
Kpna2 (Myc-DDK-tagged)- Mouse Karyopherin (importin) alpha2 (Kpna2)	Cl4164
pEt-M11_ His-TEV-Importin alpha	CL4165
pcDNA3_ MondoA v5 (Ayer lab)	CL4179
pcDNA3_ MondoA v5	CL4180
pET-M11_ His-TEV-70Importin-alpha (Kpna2)	CL4192
pET-Duet1_ 70Importin-alpha_ ChREBP291-TEV-His	Cl4198

Table 7.6: Table of vectors created during this PhD

Bibliography

[Abdul-Wahed et al., 2017] Abdul-Wahed, A., Guilmeau, S., and Postic, C. (2017). Sweet Sixteenth for ChREBP: Established Roles and Future Goals. *Cell Metabolism*, 26(2):324–341.

[Arden et al., 2012] Arden, C., Tudhope, S., Petrie, J., Al-Oanzi, Z., Cullen, K., Lange, A., Towle, H., and Agius, L. (2012). Fructose 2,6-bisphosphate is essential for glucose-regulated gene transcription of glucose-6-phosphatase and other ChREBP target genes in hepatocytes. *Biochemical Journal*, 443(1):111–123.

[Atchley and Fitch, 1997] Atchley, W. R. and Fitch, W. M. (1997). A natural classification of the basic helix–loop–helix class of transcription0xE2factors. *Proceedings of the National Academy of Sciences of the United States of America*, 94(10):5172–5176.

[Bergot et al., 1992] Bergot, M.-O., Diaz-Guerra, M.-J. M., Puzenat, N., Raymondjean, M., and Kahn, A. (1992). Cis -regulation of the L-type pyruvate kinase gene promoter by glucose, insulin and cyclic AMP. *Nucleic Acids Research*, 20(8):1871–1878.

[Bien and Espenshade, 2010] Bien, C. M. and Espenshade, P. J. (2010). Sterol Regulatory Element Binding Proteins in Fungi: Hypoxic Transcription Factors Linked to Pathogenesis. *Eukaryotic Cell*, 9(3):352–359.

[Billin et al., 1999] Billin, A. N., Eilers, A. L., Queva, C., and Ayer, D. E. (1999). Mlx, a Novel Max-like BHLHZip Protein That Interacts with the Max Network of Transcription Factors. *Journal of Biological Chemistry*, 274(51):36344–36350.

[Bricambert et al., 2010] Bricambert, J., Miranda, J., Benhamed, F., Girard, J., Postic, C., and Dentin, R. (2010). Salt-inducible kinase 2 links transcriptional coactivator p300 phosphorylation to the prevention of ChREBP-dependent hepatic steatosis in mice. *The Journal of Clinical Investigation*, 120(12):4316–4331.

[Brown and Goldstein, 1997] Brown, M. S. and Goldstein, J. L. (1997). The SREBP Pathway: Regulation of Cholesterol Metabolism by Proteolysis of a Membrane-Bound Transcription Factor. *Cell*, 89(3):331–340.

[Burke et al., 2009] Burke, S. J., Collier, J. J., and Scott, D. K. (2009). cAMP opposes the glucose-mediated induction of the L-PK gene by preventing the recruitment of a complex containing ChREBP, HNF4α, and CBP. *The FASEB Journal*, 23(9):2855–2865.

[Burley, 1996] Burley, S. K. (1996). The TATA box binding protein. *Current Opinion in Structural Biology*, 6(1):69–75.

[Burnouf et al., 2012] Burnouf, D., Ennifar, E., Guedich, S., Puffer, B., Hoffmann, G., Bec, G., Disdier, F., Baltzinger, M., and Dumas, P. (2012). kinITC: A New Method for Obtaining

Joint Thermodynamic and Kinetic Data by Isothermal Titration Calorimetry. *Journal of the American Chemical Society*, 134(1):559–565.

[Cairo et al., 2001] Cairo, S., Merla, G., Urbinati, F., Ballabio, A., and Reymond, A. (2001). WBSCR14, a gene mapping to the Williams–Beuren syndrome deleted region, is a new member of the Mlx transcription factor network. *Human Molecular Genetics*, 10(6):617–627.

[Cha-Molstad et al., 2009] Cha-Molstad, H., Saxena, G., Chen, J., and Shalev, A. (2009). Glucose-stimulated Expression of Txnip Is Mediated by Carbohydrate Response Element-binding Protein, p300, and Histone H4 Acetylation in Pancreatic Beta Cells. *Journal of Biological Chemistry*, 284(25):16898–16905.

[Chaudhri et al., 2003] Chaudhri, M., Scarabel, M., and Aitken, A. (2003). Mammalian and yeast 14-3-3 isoforms form distinct patterns of dimers in vivo. *Biochemical and Biophysical Research Communications*, 300(3):679–685.

[Chen et al., 2007] Chen, W., Chen, G., Head, D. L., Mangelsdorf, D. J., and Russell, D. W. (2007). Enzymatic Reduction of Oxysterols Impairs LXR Signaling in Cultured Cells and the Livers of Mice. *Cell metabolism*, 5(1):73–79.

[Cheng and Prusoff, 1973] Cheng, Y.-C. and Prusoff, W. H. (1973). Relationship between the inhibition constant (KI) and the concentration of inhibitor which causes 50 per cent inhibition (I50) of an enzymatic reaction. *Biochemical Pharmacology*, 22(23):3099–3108.

[Cramer, 2019] Cramer, P. (2019). Organization and regulation of gene transcription. *Nature*, 573(7772):45–54.

[da Silva et al., 2006] da Silva, X. G., Rutter, G. A., Diraison, F., Andreolas, C., and Leclerc, I. (2006). ChREBP binding to fatty acid synthase and L-type pyruvate kinase genes is stimulated by glucose in pancreatic β-cells. *Journal of Lipid Research*, 47(11):2482–2491.

[Davies et al., 2008] Davies, M. N., O'Callaghan, B. L., and Towle, H. C. (2008). Glucose Activates ChREBP by Increasing Its Rate of Nuclear Entry and Relieving Repression of Its Transcriptional Activity. *The Journal of Biological Chemistry*, 283(35):24029–24038.

[Davies et al., 2010] Davies, M. N., O'Callaghan, B. L., and Towle, H. C. (2010). Activation and repression of glucose-stimulated ChREBP requires the concerted action of multiple domains within the MondoA conserved region. *American Journal of Physiology - Endocrinology and Metabolism*, 299(4):E665–E674.

[Deaton and Bird, 2011] Deaton, A. M. and Bird, A. (2011). CpG islands and the regulation of transcription. *Genes & Development*, 25(10):1010–1022.

[DeBlasi et al., 1989] DeBlasi, A., O'Reilly, K., and Motulsky, H. J. (1989). Calculating receptor number from binding experiments using same compound as radioligand and competitor. *Trends in Pharmacological Sciences*, 10(6):227–229.

[DeBose-Boyd and Ye, 2018] DeBose-Boyd, R. A. and Ye, J. (2018). SREBPs in Lipid Metabolism, Insulin Signaling, and Beyond. *Trends in Biochemical Sciences*, 43(5):358–368.

[Dentin et al., 2005] Dentin, R., Benhamed, F., Pégorier, J.-P., Foufelle, F., Viollet, B., Vaulont, S., Girard, J., and Postic, C. (2005). Polyunsaturated fatty acids suppress glycolytic and lipogenic genes through the inhibition of ChREBP nuclear protein translocation. *Journal of Clinical Investigation*, 115(10):2843–2854.

[Dentin et al., 2012] Dentin, R., Tomas-Cobos, L., Foufelle, F., Leopold, J., Girard, J., Postic, C., and Ferré, P. (2012). Glucose 6-phosphate, rather than xylulose 5-phosphate, is required for the activation of ChREBP in response to glucose in the liver. *Journal of Hepatology*, 56(1):199–209.

[Deutsch, 2019] Deutsch, R. (2019). *Report Methods in Life Sciences Practical Course*. PhD thesis, Ludwig-Maximilians-Universität München.

[Docherty et al., 2015] Docherty, J. E., Manno, J. E., McDermott, J. E., and DiAngelo, J. R. (2015). Mio acts in the Drosophila brain to control nutrient storage and feeding. *Gene*.

[Doiron et al., 1996] Doiron, B., Cuif, M.-H., Chen, R., and Kahn, A. (1996). Transcriptional Glucose Signaling through The Glucose Response Element Is Mediated by the Pentose Phosphate Pathway. *Journal of Biological Chemistry*, 271(10):5321–5324.

[Duncan et al., 1997] Duncan, E. A., Brown, M. S., Goldstein, J. L., and Sakai, J. (1997). Cleavage Site for Sterol-regulated Protease Localized to a Leu-Ser Bond in the Lumenal Loop of Sterol Regulatory Element-binding Protein-2. *Journal of Biological Chemistry*, 272(19):12778–12785.

[Duncan et al., 1998] Duncan, E. A., Davé, U. P., Sakai, J., Goldstein, J. L., and Brown, M. S. (1998). Second-site Cleavage in Sterol Regulatory Element-binding Protein Occurs at Transmembrane Junction as Determined by Cysteine Panning. *Journal of Biological Chemistry*, 273(28):17801–17809.

[Dynan and Tjian, 1983] Dynan, W. S. and Tjian, R. (1983). The promoter-specific transcription factor Sp1 binds to upstream sequences in the SV40 early promoter. *Cell*, 35(1):79–87.

[Eilers et al., 2002] Eilers, A. L., Sundwall, E., Lin, M., Sullivan, A. A., and Ayer, D. E. (2002). A Novel Heterodimerization Domain, CRM1, and 14-3-3 Control Subcellular Localization of the MondoA-Mlx Heterocomplex. *Molecular and Cellular Biology*, 22(24):8514–8526.

[Fenouil et al., 2012] Fenouil, R., Cauchy, P., Koch, F., Descostes, N., Cabeza, J. Z., Innocenti, C., Ferrier, P., Spicuglia, S., Gut, M., Gut, I., and Andrau, J.-C. (2012). CpG islands and GC content dictate nucleosome depletion in a transcription-independent manner at mammalian promoters. *Genome Research*, 22(12):2399–2408.

[Ferré-D'Amaré et al., 1993] Ferré-D'Amaré, A. R., Prendergast, G. C., Ziff, E. B., and Burley, S. K. (1993). Recognition by Max of its cognate DNA through a dimeric b/HLH/Z domain. *Nature*, 363(6424):38–45.

[Filtz et al., 2014] Filtz, T. M., Vogel, W. K., and Leid, M. (2014). Regulation of transcription factor activity by interconnected post-translational modifications. *Trends in Pharmacological Sciences*, 35(2):76–85.

[Foufelle et al., 1992] Foufelle, F., Gouhot, B., Pégorier, J. P., Perdereau, D., Girard, J., and Ferré, P. (1992). Glucose stimulation of lipogenic enzyme gene expression in cultured white adipose tissue. A role for glucose 6-phosphate. *Journal of Biological Chemistry*, 267(29):20543–20546.

[Fuda et al., 2009] Fuda, N. J., Ardehali, M. B., and Lis, J. T. (2009). Defining mechanisms that regulate RNA polymerase II transcription in vivo. *Nature*, 461(7261):186–192.

[Fukasawa et al., 2010] Fukasawa, M., Ge, Q., Wynn, R. M., Ishii, S., and Uyeda, K. (2010). Coordinate regulation/localization of the carbohydrate responsive binding protein (ChREBP) by two nuclear export signal sites: Discovery of a new leucine-rich nuclear export signal site. *Biochemical and Biophysical Research Communications*, 391(2):1166–1169.

[Ge et al., 2012] Ge, Q., Huang, N., Wynn, R. M., Li, Y., Du, X., Miller, B., Zhang, H., and Uyeda, K. (2012). Structural Characterization of a Unique Interface between Carbohydrate Response Element-binding Protein (ChREBP) and 14-3-3β Protein. *Journal of Biological Chemistry*, 287(50):41914–41921.

[Ge et al., 2011] Ge, Q., Nakagawa, T., Wynn, R. M., Chook, Y. M., Miller, B. C., and Uyeda, K. (2011). Importin-α Protein Binding to a Nuclear Localization Signal of Carbohydrate Response Element-Binding Protein (ChREBP). *Journal of Biological Chemistry*, 286(32):28119–28127.

[Girard et al., 1997] Girard, J., Ferré, P., and Foufelle, F. (1997). Mechanisms by Which Carbohydrates Regulate Expression of Genes for Glycolytic and Lipogenic Enzymes. *Annual Review of Nutrition*, 17(1):325–352.

[Guinez et al., 2011] Guinez, C., Filhoulaud, G., Rayah-Benhamed, F., Marmier, S., Dubuquoy, C., Dentin, R., Moldes, M., Burnol, A.-F., Yang, X., Lefebvre, T., Girard, J., and Postic, C. (2011). O-GlcNAcylation Increases ChREBP Protein Content and Transcriptional Activity in the Liver. *Diabetes*, 60(5):1399–1413.

[Hart, 2019] Hart, G. W. (2019). Nutrient regulation of signaling and transcription. *Journal of Biological Chemistry*, 294(7):2211–2231.

[Havula et al., 2013] Havula, E., Teesalu, M., Hyötyläinen, T., Seppälä, H., Hasygar, K., Auvinen, P., Orešič, M., Sandmann, T., and Hietakangas, V. (2013). Mondo/ChREBP-Mlx-Regulated Transcriptional Network Is Essential for Dietary Sugar Tolerance in Drosophila. *PLoS Genetics*, 9(4):e1003438.

[Heppner, 2016] Heppner, N. (2016). Interaction of Transcription Factor ChREBP with Glucose Metabolites. Master's thesis, LMU Munich.

[Herman et al., 2012] Herman, M. A., Peroni, O. D., Villoria, J., Schön, M. R., Abumrad, N. A., Blüher, M., Klein, S., and Kahn, B. B. (2012). A novel ChREBP isoform in adipose tissue regulates systemic glucose metabolism. *Nature*, 484(7394):333–338.

[Hong and Tontonoz, 2014] Hong, C. and Tontonoz, P. (2014). Liver X receptors in lipid metabolism: opportunities for drug discovery. *Nature Reviews Drug Discovery*, 13(6):433–444.

[Hoogerland et al., 2019] Hoogerland, J. A., Lei, Y., Wolters, J. C., de Boer, J. F., Bos, T., Bleeker, A., Mulder, N. L., van Dijk, T. H., Kuivenhoven, J. A., Rajas, F., Mithieux, G., Haeusler, R. A., Verkade, H. J., Bloks, V. W., Kuipers, F., and Oosterveer, M. H. (2019). Glucose-6-phosphate regulates hepatic bile acid synthesis in mice. *Hepatology*, page hep.30778.

[Horbach et al., 2015] Horbach, T., Götz, C., Kietzmann, T., and Dimova, E. Y. (2015). Protein kinases as switches for the function of upstream stimulatory factors: implications for tissue injury and cancer. *Frontiers in Pharmacology*, 6.

[Hua et al., 1996] Hua, X., Nohturfft, A., Goldstein, J. L., and Brown, M. S. (1996). Sterol Resistance in CHO Cells Traced to Point Mutation in SREBP Cleavage–Activating Protein. *Cell*, 87(3):415–426.

[Hua et al., 1993] Hua, X., Yokoyama, C., Wu, J., Briggs, M. R., Brown, M. S., Goldstein, J. L., and Wang, X. (1993). SREBP-2, a second basic-helix-loop-helix-leucine zipper protein that stimulates transcription by binding to a sterol regulatory element. *Proceedings of the National Academy of Sciences*, 90(24):11603–11607.

[Ido-Kitamura et al., 2012] Ido-Kitamura, Y., Sasaki, T., Kobayashi, M., Kim, H.-J., Lee, Y.-S., Kikuchi, O., Yokota-Hashimoto, H., Iizuka, K., Accili, D., and Kitamura, T. (2012). Hepatic FoxO1 Integrates Glucose Utilization and Lipid Synthesis through Regulation of Chrebp O-Glycosylation. *PLOS ONE*, 7(10):e47231.

[Iizuka et al., 2004] Iizuka, K., Bruick, R. K., Liang, G., Horton, J. D., and Uyeda, K. (2004). Deficiency of carbohydrate response element-binding protein (ChREBP) reduces lipogenesis as well as glycolysis. *Proceedings of the National Academy of Sciences of the United States of America*, 101(19):7281–7286.

[Iizuka et al., 2013] Iizuka, K., Wu, W., Horikawa, Y., and Takeda, J. (2013). Role of glucose-6-phosphate and xylulose-5-phosphate in the regulation of glucose-stimulated gene expression in the pancreatic β cell line, INS-1E. *Endocrine Journal*, 60(4):473–482.

[Janowski et al., 1996] Janowski, B. A., Willy, P. J., Devi, T. R., Falck, J. R., and Mangelsdorf, D. J. (1996). An oxysterol signalling pathway mediated by the nuclear receptor LXRα. *Nature*, 383(6602):728–731.

[Johnson et al., 2014] Johnson, D. W., Llop, J. R., Farrell, S. F., Yuan, J., Stolzenburg, L. R., and Samuelson, A. V. (2014). The Caenorhabditis elegans Myc-Mondo/Mad Complexes Integrate Diverse Longevity Signals. *PLOS Genetics*, 10(4):e1004278.

[Jois et al., 2017] Jois, T., Chen, W., Howard, V., Harvey, R., Youngs, K., Thalmann, C., Saha, P., Chan, L., Cowley, M. A., and Sleeman, M. W. (2017). Deletion of hepatic carbohydrate response element binding protein (ChREBP) impairs glucose homeostasis and hepatic insulin sensitivity in mice. *Molecular Metabolism*, 6(11):1381–1394.

[Jones et al., 1995] Jones, D. H., Ley, S., and Aitken, A. (1995). Isoforms of 14-3-3 protein can form homo- and heterodimers in vivo and in vitro: implications for function as adapter proteins. *FEBS Letters*, 368(1):55–58.

[Joseph et al., 2002] Joseph, S. B., Laffitte, B. A., Patel, P. H., Watson, M. A., Matsukuma, K. E., Walczak, R., Collins, J. L., Osborne, T. F., and Tontonoz, P. (2002). Direct and Indirect Mechanisms for Regulation of Fatty Acid Synthase Gene Expression by Liver X Receptors. *Journal of Biological Chemistry*, 277(13):11019–11025.

[Kabashima et al., 2003] Kabashima, T., Kawaguchi, T., Wadzinski, B. E., and Uyeda, K. (2003). Xylulose 5-phosphate mediates glucose-induced lipogenesis by xylulose 5-phosphate-activated protein phosphatase in rat liver. *Proceedings of the National Academy of Sciences of the United States of America*, 100(9):5107–5112.

[Kadonaga et al., 1988] Kadonaga, J. T., Courey, A. J., and Tjian, R. (1988). Distinct Regions of Spl Modulate DNA Binding and Transcriptional Activation. *Science*, 242:6.

[Kahn et al., 2005] Kahn, B. B., Alquier, T., Carling, D., and Hardie, D. G. (2005). AMP-activated protein kinase: Ancient energy gauge provides clues to modern understanding of metabolism. *Cell Metabolism*, 1(1):15–25.

[Kang et al., 1996] Kang, R., Yamada, K., Tanaka, T., Lu, T., and Noguchi, T. (1996). Relationship between the Concentrations of Glycolytic Intermediates and Expression of the L-Type Pyruvate Kinase Gene in Cultured Hepatocytes. *Journal of Biochemistry*, 119(1):162–166.

[Kawaguchi et al., 2002] Kawaguchi, T., Osatomi, K., Yamashita, H., Kabashima, T., and Uyeda, K. (2002). Mechanism for Fatty Acid "Sparing" Effect on Glucose-induced Transcription REGULATION OF CARBOHYDRATE-RESPONSIVE ELEMENT-BINDING PROTEIN BY AMP-ACTIVATED PROTEIN KINASE. *Journal of Biological Chemistry*, 277(6):3829–3835.

[Kawaguchi et al., 2001] Kawaguchi, T., Takenoshita, M., Kabashima, T., and Uyeda, K. (2001). Glucose and cAMP regulate the L-type pyruvate kinase gene by phosphorylation/dephosphorylation of the carbohydrate response element binding protein. *Proceedings of the National Academy of Sciences of the United States of America*, 98(24):13710–13715.

[Kim et al., 2017] Kim, M., Astapova, I. I., Flier, S. N., Hannou, S. A., Doridot, L., Sargsyan, A., Kou, H. H., Fowler, A. J., Liang, G., and Herman, M. A. (2017). Intestinal, but not hepatic, ChREBP is required for fructose tolerance. *JCI Insight*, 2(24).

[Kim et al., 2016] Kim, M.-S., Krawczyk, S. A., Doridot, L., Fowler, A. J., Wang, J. X., Trauger, S. A., Noh, H.-L., Kang, H. J., Meissen, J. K., Blatnik, M., Kim, J. K., Lai, M., and Herman, M. A. (2016). ChREBP regulates fructose-induced glucose production independently of insulin signaling. *The Journal of Clinical Investigation*, 126(11):4372–4386.

[Knezetic and Luse, 1986] Knezetic, J. A. and Luse, D. S. (1986). The presence of nucleosomes on a DNA template prevents initiation by RNA polymerase II in vitro. *Cell*, 45(1):95–104.

[Kooner et al., 2008] Kooner, J. S., Chambers, J. C., Aguilar-Salinas, C. A., Hinds, D. A., Hyde, C. L., Warnes, G. R., Gómez Pérez, F. J., Frazer, K. A., Elliott, P., Scott, J., Milos, P. M., Cox, D. R., and Thompson, J. F. (2008). Genome-wide scan identifies variation in MLXIPL associated with plasma triglycerides. *Nature Genetics*, 40(2):149–151.

[Laemmli, 1970] Laemmli, U. K. (1970). Cleavage of Structural Proteins during the Assembly of the Head of Bacteriophage T4. *Nature*, 227(5259):680–685.

[Lazar and Willson, 2007] Lazar, M. A. and Willson, T. M. (2007). Sweet Dreams for LXR. *Cell Metabolism*, 5(3):159–161.

[Lee et al., 2008] Lee, S., Lee, J., Lee, S.-K., and Lee, J. W. (2008). Activating Signal Cointegrator-2 Is an Essential Adaptor to Recruit Histone H3 Lysine 4 Methyltransferases MLL3 and MLL4 to the Liver X Receptors. *Molecular Endocrinology*, 22(6):1312–1319.

[Li et al., 2006] Li, M. V., Chang, B., Imamura, M., Poungvarin, N., and Chan, L. (2006). Glucose-Dependent Transcriptional Regulation by an Evolutionarily Conserved Glucose-Sensing Module. *Diabetes*, 55(5):1179–1189.

[Li et al., 2010] Li, M. V., Chen, W., Harmancey, R. N., Nuotio-Antar, A. M., Imamura, M., Saha, P., Taegtmeyer, H., and Chan, L. (2010). Glucose-6-phosphate mediates activation of the carbohydrate responsive binding protein (ChREBP). *Biochemical and Biophysical Research Communications*, 395(3):395–400.

[Li et al., 2008] Li, M. V., Chen, W., Poungvarin, N., Imamura, M., and Chan, L. (2008). Glucose-Mediated Transactivation of Carbohydrate Response Element-Binding Protein Requires Cooperative Actions from Mondo Conserved Regions and Essential *Trans* -Acting Factor 14-3-3. *Molecular Endocrinology*, 22(7):1658–1672.

[Linden et al., 2018] Linden, A. G., Li, S., Choi, H. Y., Fang, F., Fukasawa, M., Uyeda, K., Hammer, R. E., Horton, J. D., Engelking, L. J., and Liang, G. (2018). Interplay between ChREBP and SREBP-1c coordinates postprandial glycolysis and lipogenesis in livers of mice. *Journal of Lipid Research*, 59(3):475–487.

[Lorch and Kornberg, 2015] Lorch, Y. and Kornberg, R. D. (2015). Chromatin-remodeling and the initiation of transcription. *Quarterly Reviews of Biophysics*, 48(4):465–470.

[Lorch et al., 1987] Lorch, Y., LaPointe, J. W., and Kornberg, R. D. (1987). Nucleosomes inhibit the initiation of transcription but allow chain elongation with the displacement of histones. *Cell*, 49(2):203–210.

[Ma et al., 2007] Ma, L., Sham, Y. Y., Walters, K. J., and Towle, H. C. (2007). A critical role for the loop region of the basic helix–loop–helix/leucine zipper protein Mlx in DNA binding and glucose-regulated transcription. *Nucleic Acids Research*, 35(1):35–44.

[Ma et al., 2005] Ma, L., Tsatsos, N. G., and Towle, H. C. (2005). Direct Role of ChREBP·Mlx in Regulating Hepatic Glucose-responsive Genes. *Journal of Biological Chemistry*, 280(12):12019–12027.

[McFerrin and Atchley, 2012] McFerrin, L. G. and Atchley, W. R. (2012). A Novel N-Terminal Domain May Dictate the Glucose Response of Mondo Proteins. *PLoS ONE*, 7(4):e34803.

[Meng et al., 2016] Meng, J., Feng, M., Dong, W., Zhu, Y., Li, Y., Zhang, P., Wu, L., Li, M., Lu, Y., Chen, H., Liu, X., Lu, Y., Sun, H., and Tong, X. (2016). Identification of HNF-4α as a key transcription factor to promote ChREBP expression in response to glucose. *Scientific Reports*, 6:23944.

[Merla, 2004] Merla, G. (2004). The subcellular localization of the ChoRE-binding protein, encoded by the Williams-Beuren syndrome critical region gene 14, is regulated by 14-3-3. *Human Molecular Genetics*, 13(14):1505–1514.

[Mitro et al., 2007] Mitro, N., Mak, P. A., Vargas, L., Godio, C., Hampton, E., Molteni, V., Kreusch, A., and Saez, E. (2007). The nuclear receptor LXR is a glucose sensor. *Nature*, 445(7124):219–223.

[Mouchiroud et al., 2014] Mouchiroud, L., Eichner, L. J., Shaw, R., and Auwerx, J. (2014). Transcriptional coregulators: fine-tuning metabolism. *Cell metabolism*, 20(1):26–40.

[Nakamura et al., 2016] Nakamura, S., Karalay, z., Jäger, P. S., Horikawa, M., Klein, C., Nakamura, K., Latza, C., Templer, S. E., Dieterich, C., and Antebi, A. (2016). Mondo complexes regulate TFEB via TOR inhibition to promote longevity in response to gonadal signals. *Nature Communications*, 7(1):1–15.

[Nakayama et al., 2011] Nakayama, K., Yanagisawa, Y., Ogawa, A., Ishizuka, Y., Munkhtulga, L., Charupoonphol, P., Supannnatas, S., Kuartei, S., Chimedregzen, U., Koda, Y., Ishida, T., Kagawa, Y., and Iwamoto, S. (2011). High prevalence of an anti-hypertriglyceridemic variant of the MLXIPL gene in Central Asia. *Journal of Human Genetics*, 56(12):828–833.

[Nishimura and Uyeda, 1995] Nishimura, M. and Uyeda, K. (1995). Purification and Characterization of a Novel Xylulose 5-Phosphate-activated Protein Phosphatase Catalyzing Dephosphorylation of Fructose-6-phosphate,2-kinase:Fructose-2,6-bisphosphatase. *Journal of Biological Chemistry*, 270(44):26341–26346.

[Noordeen et al., 2012] Noordeen, N. A., Meur, G., Rutter, G. A., and Leclerc, I. (2012). Glucose-Induced Nuclear Shuttling of ChREBP Is Mediated by Sorcin and Ca2+ Ions in Pancreatic β-Cells. *Diabetes*, 61(3):574–585.

[Ortega-Prieto and Postic, 2019] Ortega-Prieto, P. and Postic, C. (2019). Carbohydrate Sensing Through the Transcription Factor ChREBP. *Frontiers in Genetics*, 10.

[Payvar et al., 1981] Payvar, F., Wrange, O., Carlstedt-Duke, J., Okret, S., Gustafsson, J. A., and Yamamoto, K. R. (1981). Purified glucocorticoid receptors bind selectively in vitro to a cloned DNA fragment whose transcription is regulated by glucocorticoids in vivo. *Proceedings of the National Academy of Sciences of the United States of America*, 78(11):6628–6632.

[Peet et al., 1998] Peet, D. J., Turley, S. D., Ma, W., Janowski, B. A., Lobaccaro, J. M., Hammer, R. E., and Mangelsdorf, D. J. (1998). Cholesterol and bile acid metabolism are impaired in mice lacking the nuclear oxysterol receptor LXR alpha. *Cell*, 93(5):693–704.

[Poupeau and Postic, 2011] Poupeau, A. and Postic, C. (2011). Cross-regulation of hepatic glucose metabolism via ChREBP and nuclear receptors. *Biochimica et Biophysica Acta (BBA) - Molecular Basis of Disease*, 1812(8):995–1006.

[Prip-Buus et al., 1995] Prip-Buus, C., Perdereau, D., Foufelle, F., Maury, J., Ferré, P., and Girard, J. (1995). Induction of Fatty-Acid-Synthase Gene Expression by Glucose in Primary Culture of Rat Hepatocytes. *European Journal of Biochemistry*, 230(1):309–315.

[Radhakrishnan et al., 2004] Radhakrishnan, A., Sun, L.-P., Kwon, H. J., Brown, M. S., and Goldstein, J. L. (2004). Direct Binding of Cholesterol to the Purified Membrane Region of SCAP: Mechanism for a Sterol-Sensing Domain. *Molecular Cell*, 15(2):259–268.

[Robichon et al., 2011] Robichon, C., Luo, J., Causey, T. B., Benner, J. S., and Samuelson, J. C. (2011). Engineering Escherichia coli BL21(DE3) Derivative Strains To Minimize E. coli Protein Contamination after Purification by Immobilized Metal Affinity Chromatography E296BF. *Applied and Environmental Microbiology*, 77(13):4634–4646.

[Sabatini et al., 2019] Sabatini, P. V., Speckmann, T., and Lynn, F. C. (2019). Friend and foe: β-cell Ca2+ signaling and the development of diabetes. *Molecular Metabolism*, 21:1–12.

[Sakiyama et al., 2010] Sakiyama, H., Fujiwara, N., Noguchi, T., Eguchi, H., Yoshihara, D., Uyeda, K., and Suzuki, K. (2010). The role of O-linked GlcNAc modification on the glucose response of ChREBP. *Biochemical and Biophysical Research Communications*, 402(4):784–789.

[Sakiyama et al., 2008] Sakiyama, H., Wynn, R. M., Lee, W.-R., Fukasawa, M., Mizuguchi, H., Gardner, K. H., Repa, J. J., and Uyeda, K. (2008). Regulation of Nuclear Import/Export of Carbohydrate Response Element-binding Protein (ChREBP): INTERACTION OF AN - HELIX OF ChREBP WITH THE 14-3-3 PROTEINS AND REGULATION BY PHOSPHORYLATION. *Journal of Biological Chemistry*, 283(36):24899–24908.

[Sans et al., 2006] Sans, C. L., Satterwhite, D. J., Stoltzman, C. A., Breen, K. T., and Ayer, D. E. (2006). MondoA-Mlx Heterodimers Are Candidate Sensors of Cellular Energy Status: Mitochondrial Localization and Direct Regulation of Glycolysis. *Molecular and Cellular Biology*, 26(13):4863–4871.

[Sato et al., 2016] Sato, S., Jung, H., Nakagawa, T., Pawlosky, R., Takeshima, T., Lee, W.-R., Sakiyama, H., Laxman, S., Wynn, R. M., Tu, B. P., MacMillan, J. B., Brabander, J. K. D., Veech, R. L., and Uyeda, K. (2016). Metabolite Regulation of Nuclear Localization of Carbohydrate-response Element-binding Protein (ChREBP) ROLE OF AMP AS AN ALLOSTERIC INHIBITOR. *Journal of Biological Chemistry*, 291(20):10515–10527.

[Scholtz et al., 1991] Scholtz, J. M., Qian, H., York, E. J., Stewart, J. M., and Baldwin, R. L. (1991). Parameters of helix-coil transition theory for alanine-based peptides of varying chain lengths in water. *Biopolymers*, 31(13):1463–1470.

[Schultz et al., 2000] Schultz, J. R., Tu, H., Luk, A., Repa, J. J., Medina, J. C., Li, L., Schwendner, S., Wang, S., Thoolen, M., Mangelsdorf, D. J., Lustig, K. D., and Shan, B. (2000). Role of LXRs in control of lipogenesis. *Genes & Development*, 14(22):2831–2838.

[Shih et al., 1995] Shih, H.-M., Liu, Z., and Towle, H. C. (1995). Two CACGTG Motifs with Proper Spacing Dictate the Carbohydrate Regulation of Hepatic Gene Transcription. *Journal of Biological Chemistry*, 270(37):21991–21997.

[Sirito et al., 1992] Sirito, M., Walker, S., Lin, Q., Kozlowski, M. T., Klein, W. H., and Sawadogo, M. (1992). Members of the USF family of helix-loop-helix proteins bind DNA as homo- as well as heterodimers.

[Sluchanko and Gusev, 2012] Sluchanko, N. N. and Gusev, N. B. (2012). Oligomeric structure of 14-3-3 protein: What do we know about monomers? *FEBS Letters*, 586(24):4249–4256.

[Stoeckman et al., 2004] Stoeckman, A. K., Ma, L., and Towle, H. C. (2004). Mlx Is the Functional Heteromeric Partner of the Carbohydrate Response Element-binding Protein in Glucose Regulation of Lipogenic Enzyme Genes. *Journal of Biological Chemistry*, 279(15):15662–15669.

[Sun et al., 2005] Sun, L.-P., Li, L., Goldstein, J. L., and Brown, M. S. (2005). Insig Required for Sterol-mediated Inhibition of Scap/SREBP Binding to COPII Proteins in Vitro. *Journal of Biological Chemistry*, 280(28):26483–26490.

[Svensson et al., 2003] Svensson, S., Östberg, T., Jacobsson, M., Norström, C., Stefansson, K., Hallén, D., Johansson, I. C., Zachrisson, K., Ogg, D., and Jendeberg, L. (2003). Crystal structure of the heterodimeric complex of LXRα and RXRβ ligand-binding domains in a fully agonistic conformation. *The EMBO Journal*, 22(18):4625–4633.

[Tsatsos and Towle, 2006] Tsatsos, N. G. and Towle, H. C. (2006). Glucose activation of ChREBP in hepatocytes occurs via a two-step mechanism. *Biochemical and Biophysical Research Communications*, 340(2):449–456.

[Veiga, 2019] Veiga, J. (2019). *Investigating the conformational changes of the ChREBP/Protein 14-3-3 complex upon binding to Glucose-6-Phosphate and AMP by Hydrogen/Deuterium Exchange Mass Spectrometry*. PhD thesis.

[Wagner et al., 2003] Wagner, B. L., Valledor, A. F., Shao, G., Daige, C. L., Bischoff, E. D., Petrowski, M., Jepsen, K., Baek, S. H., Heyman, R. A., Rosenfeld, M. G., Schulman, I. G., and Glass, C. K. (2003). Promoter-Specific Roles for Liver X Receptor/Corepressor Complexes in the Regulation of ABCA1 and SREBP1 Gene Expression. *Molecular and Cellular Biology*, 23(16):5780–5789.

[Wang et al., 1994] Wang, X., Sato, R., Brown, M. S., Hua, X., and Goldstein, J. L. (1994). SREBP-1, a membrane-bound transcription factor released by sterol-regulated proteolysis. *Cell*, 77(1):53–62.

[Wang et al., 2015] Wang, Y., Viscarra, J., Kim, S.-J., and Sul, H. S. (2015). Transcriptional regulation of hepatic lipogenesis. *Nature Reviews Molecular Cell Biology*, 16(11):678–689.

[Wang and Lei, 2018] Wang, Y.-P. and Lei, Q.-Y. (2018). Metabolite sensing and signaling in cell metabolism. *Signal Transduction and Targeted Therapy*, 3(1):30.

[Wilde et al., 2019] Wilde, B. R., Ye, Z., Lim, T.-Y., and Ayer, D. E. (2019). Cellular acidosis triggers human MondoA transcriptional activity by driving mitochondrial ATP production. *eLife*, 8:e40199.

[Willy et al., 1995] Willy, P. J., Umesono, K., Ong, E. S., Evans, R. M., Heyman, R. A., and Mangelsdorf, D. J. (1995). LXR, a nuclear receptor that defines a distinct retinoid response pathway. *Genes & Development*, 9(9):1033–1045.

[Wilson, 2003] Wilson, J. E. (2003). Isozymes of mammalian hexokinase: structure, subcellular localization and metabolic function. *Journal of Experimental Biology*, 206(12):2049–2057.

[Wong et al., 2009] Wong, R. H. F., Chang, I., Hudak, C. S. S., Hyun, S., Kwan, H.-Y., and Sul, H. S. (2009). A Role of DNA-PK for the Metabolic Gene Regulation in Response to Insulin. *Cell*, 136(6):1056–1072.

[Woodcock et al., 2017] Woodcock, J., Goodwin, K., J. Sandow, J., Coolen, C., Perugini, M., I. Webb, A., Pitson, S., F. Lopez, A., and Carver, J. (2017). Role of salt bridges in the dimer interface of 14-3-3ζ in dimer dynamics, N-terminal α-helical order and molecular chaperone activity. *Journal of Biological Chemistry*, 293:jbc.M117.801019.

[Yamashita et al., 2001] Yamashita, H., Takenoshita, M., Sakurai, M., Bruick, R. K., Henzel, W. J., Shillinglaw, W., Arnot, D., and Uyeda, K. (2001). A glucose-responsive transcription factor that regulates carbohydrate metabolism in the liver. *Proceedings of the National Academy of Sciences*, 98(16):9116–9121.

[Yang et al., 2017] Yang, A.-Q., Li, D., Chi, L., and Ye, X.-S. (2017). Validation, identification and biological consequences of the site-specific O-GlcNAcylation dynamics of ChREBP. *Molecular & Cellular Proteomics*, page mcp.M116.061416.

[Ye and DeBose-Boyd, 2011] Ye, J. and DeBose-Boyd, R. A. (2011). Regulation of cholesterol and fatty acid synthesis. *Cold Spring Harbor perspectives in biology*, 3(7).

[Yellaturu et al., 2009] Yellaturu, C. R., Deng, X., Cagen, L. M., Wilcox, H. G., Mansbach, C. M., Siddiqi, S. A., Park, E. A., Raghow, R., and Elam, M. B. (2009). Insulin Enhances Post-translational Processing of Nascent SREBP-1c by Promoting Its Phosphorylation and Association with COPII Vesicles. *The Journal of Biological Chemistry*, 284(12):7518–7532.

[Yokoyama et al., 1993] Yokoyama, C., Wang, X., Briggs, M. R., Admon, A., Wu, J., Hua, X., Goldstein, J. L., and Brown, M. S. (1993). SREBP-1, a basic-helix-loop-helix-leucine zipper protein that controls transcription of the low density lipoprotein receptor gene. *Cell*, 75(1):187–197.

[Zhang et al., 2016] Zhang, P., Li, L., Bao, Z., and Huang, F. (2016). Role of BAF60a/BAF60c in chromatin remodeling and hepatic lipid metabolism. *Nutrition & Metabolism*, 13(1):30.

Cross-regulation of hepatic glucose metabolism via ChREBP and nuclear receptors

Author: Audrey Poupeau,Catherine Postic
Publication: Biochimica et Biophysica Acta (BBA) - Molecular Basis of Disease
Publisher: Elsevier
Date: August 2011

Order Completed

Thank you for your order.

This Agreement between Biomedical Center Munich Faculty of Medicine Ludwig-Maximilians-Universität München -- Thomas Pysik ("You") and Elsevier ("Elsevier") consists of your license details and the terms and conditions provided by Elsevier and Copyright Clearance Center.

Your confirmation email will contain your order number for future reference.

License Number	4702070700114
License date	Nov 04, 2019

Printable Details

Licensed Content

Licensed Content Publisher	Elsevier
Licensed Content Publication	Biochimica et Biophysica Acta (BBA) - Molecular Basis of Disease
Licensed Content Title	Cross-regulation of hepatic glucose metabolism via ChREBP and nuclear receptors
Licensed Content Author	Audrey Poupeau,Catherine Postic
Licensed Content Date	Aug 1, 2011
Licensed Content Volume	1812
Licensed Content Issue	8
Licensed Content Pages	12
Journal Type	S&T

Order Details

Type of Use	reuse in a thesis/dissertation
Portion	figures/tables/illustrations
Number of figures/tables/illustrations	1
Format	both print and electronic
Are you the author of this Elsevier article?	No
Will you be translating?	No

About Your Work

Title	The Regulatory Effects of Glucose Metabolites on the Transcription Factor ChREBP
Institution name	LMU Munich, BMC, AG Ladurner
Expected presentation date	Dec 2019

Additional Data

Portions	Fiure 2

Requestor Location

Requestor Location	Biomedical Center Munich Faculty of Medicine Ludwig-Maximilians-Universität München Großhaderner Str. 9 Planegg-Martinsried, Bavaria 82152 Germany Attn: Biomedical Center Munich Faculty of Medicine Ludwig-Maximilians-Universität München

Tax Details

Publisher Tax ID	GB 494 6272 12

Price

Total	0.00 EUR

Total: 0.00 EUR

CLOSE WINDOW | ORDER MORE

Copyright Clearance Center RightsLink®

License Details

This Agreement between Biomedical Center Munich Faculty of Medicine Ludwig-Maximilians-Universität München -- Thomas Pysik ("You") and Springer Nature ("Springer Nature") consists of your license details and the terms and conditions provided by Springer Nature and Copyright Clearance Center.

Print Copy

License Number	4699460923367
License date	Oct 31, 2019
Licensed Content Publisher	Springer Nature
Licensed Content Publication	Journal of Human Genetics
Licensed Content Title	High prevalence of an anti-hypertriglyceridemic variant of the MLXIPL gene in Central Asia
Licensed Content Author	Kazuhiro Nakayama et al
Licensed Content Date	Sep 22, 2011
Type of Use	Thesis/Dissertation
Requestor type	academic/university or research institute
Format	print and electronic
Portion	figures/tables/illustrations
Number of figures/tables/illustrations	1
High-res required	no
Will you be translating?	no
Circulation/distribution	1 - 29
Author of this Springer Nature content	no
Title	The Regulatory Effects of Glucose Metabolites on the Transcription Factor ChREBP
Institution name	LMU Munich, BMC, AG Ladurner
Expected presentation date	Dec 2019
Portions	Figure 1a
Requestor Location	Biomedical Center Munich Faculty of Medicine Ludwig-Maximilians-Universität München Großhaderner Str. 9 Planegg-Martinsried, Bavaria 82152 Germany Attn: Biomedical Center Munich Faculty of Medicine Ludwig-Maximilians-Universität München
Total	**0.00 EUR**

BACK

Copyright Clearance Center RightsLink®

License Details

This Agreement between Biomedical Center Munich Faculty of Medicine Ludwig-Maximilians-Universität München -- Thomas Pysik ("You") and Springer Nature ("Springer Nature") consists of your license details and the terms and conditions provided by Springer Nature and Copyright Clearance Center.

Print Copy

License Number	4700230335837
License date	Nov 01, 2019
Licensed Content Publisher	Springer Nature
Licensed Content Publication	Nature
Licensed Content Title	Organization and regulation of gene transcription
Licensed Content Author	Patrick Cramer
Licensed Content Date	Aug 28, 2019
Type of Use	Thesis/Dissertation
Requestor type	academic/university or research institute
Format	print and electronic
Portion	figures/tables/illustrations
Number of figures/tables/illustrations	2
High-res required	no
Will you be translating?	no
Circulation/distribution	1 - 29
Author of this Springer Nature content	no
Title	The Regulatory Effects of Glucose Metabolites on the Transcription Factor ChREBP
Institution name	LMU Munich, BMC, AG Ladurner
Expected presentation date	Dec 2019
Portions	Figure 1, Table1
Requestor Location	Biomedical Center Faculty of Medicine LMU München Großhaderner Str.9 Planegg-Martinsried, Bavaria 82152 Germany Attn: Biomedical Center Munich Faculty of Medicine Ludwig-Maximilians-Universität München
Total	**0.00 EUR**

BACK

Sterol Regulatory Element Binding Proteins in Fungi: Hypoxic Transcription Factors Linked to Pathogenesis

Author: Clara M. Bien,Peter J. Espenshade

Publication: Eukaryotic Cell

Publisher: American Society for Microbiology

Date: Mar 2, 2010

Permissions Request

ASM authorizes an advanced degree candidate to republish the requested material in his/her doctoral thesis or dissertation. If your thesis, or dissertation, is to be published commercially, then you must reapply for permission.

BACK CLOSE WINDOW

SPRINGER NATURE

Transcriptional regulation of hepatic lipogenesis

Author: Yuhui Wang, Jose Viscarra, Sun-Joong Kim, Hei Sook Sul
Publication: Nature Reviews Molecular Cell Biology
Publisher: Springer Nature
Date: Oct 22, 2015

Order Completed

Thank you for your order.

This Agreement between Biomedical Center Munich Faculty of Medicine Ludwig-Maximilians-Universität München -- Thomas Pysik ("You") and Springer Nature ("Springer Nature") consists of your license details and the terms and conditions provided by Springer Nature and Copyright Clearance Center.

Your confirmation email will contain your order number for future reference.

License Number	4701880028813
License date	Nov 04, 2019

Printable Details

Licensed Content

Licensed Content Publisher	Springer Nature
Licensed Content Publication	Nature Reviews Molecular Cell Biology
Licensed Content Title	Transcriptional regulation of hepatic lipogenesis
Licensed Content Author	Yuhui Wang, Jose Viscarra, Sun-Joong Kim, Hei Sook Sul
Licensed Content Date	Oct 22, 2015
Licensed Content Volume	16
Licensed Content Issue	11

Order Details

Type of Use	Thesis/Dissertation
Requestor type	academic/university or research institute
Format	print and electronic
Portion	figures/tables/illustrations
Number of figures/tables/illustrations	1
High-res required	no
Will you be translating?	no
Circulation/distribution	1 - 29
Author of this Springer Nature content	no

About Your Work

Title	The Regulatory Effects of Glucose Metabolites on the Transcription Factor ChREBP
Institution name	LMU Munich, BMC, AG Ladurner
Expected presentation date	Dec 2019

Additional Data

Portions	Figure 1

Requestor Location

Requestor Location	Biomedical Center Munich Faculty of Medicine Ludwig-Maximilians-Universität München Großhaderner Str. 9 Planegg-Martinsried, Bavaria 82152 Germany Attn: Biomedical Center Munich Faculty of Medicine Ludwig-Maximilians-Universität München

Tax Details

Price

Total	0.00 EUR

Total: 0.00 EUR

CLOSE WINDOW | ORDER MORE